“Innate regulation of B cell responses to pathogens”

Mauro Nicolás Gaya

University College London

Cancer Research UK - London Research Institute

PhD supervisor: Facundo D. Batista

A thesis submitted for the degree of

Doctor of Philosophy

University College London

September 2015

To my parents and Virginia, my biology teacher at school.

Declaration

I, Mauro Nicolás Gaya confirm that the work presented in this thesis is my own. Where information has been derived from other sources, I confirm that this has been indicated in the thesis.

Mauro Nicolás Gaya

September 2015, London

Abstract

B cells are a group of lymphocytes that contribute to the adaptive immune response by producing highly specific antibodies against pathogenic antigens. In vivo, B cells get activated when they recognise a specific antigen on the surface of presenting cells through their B cell receptor. Among these cells, a population of macrophages at the lymph node subcapsular sinus has recently emerged as a key player in the presentation of antigen to B cells. Following antigenic stimulation, B cells process and present pathogen-derived peptides to specific $CD4^+$ T cells, what induces B cell proliferation and differentiation into antibody secreting cells. Moreover, it was recently found that an innate-like population of T cells named natural killer T cells could also provide cognate help to B cells in response to lipid antigens.

The aim of this thesis is to investigate the functional role of subcapsular sinus macrophages and natural killer T cells in the B cell response to infectious pathogens. To this end, I combined a number of innovative imaging approaches with the generation of a new series of transgenic mouse strains and infectious models. I found, in short, that virus and bacteria-induced inflammation triggers a temporary disruption of the subcapsular sinus macrophage organisation, resulting in diminished antigen capture and B cell responses to secondary infections. Furthermore, I unveiled a new way in which iNKT cells get activated and regulate germinal centre responses during respiratory viral infections. These findings are important as they shed light on some of the regulatory mechanisms for antigen encounter and B cell response during infection.

Acknowledgements

Thanks Facundo for giving me the opportunity to do my PhD in your lab, for being enthusiastic and critical about my projects and for having the time not only to discuss about science but also personal things. I am convinced that I could not have chosen a better lab to do my PhD. Thanks to my second supervisor Caetano, for all your suggestions and pushing me to think harder. Thanks to all the past and present members of the lymphocyte interaction laboratory for these wonderful four years and for your help in developing the projects and reading my thesis: Patricia (my guide during my first year), Nuria, Francesca and Shweta (my elder sisters in the lab), Pieta, Bruno, Selina, Lola, Carol, Cecilia, Andreas, Angelo, Christoph, Carlson, Paula, Andreas, Irene, David, Naomi and Julia. Special thanks to the lab manager Beatriz for helping me as no one else could have done and for bringing the happiness to the lab. Super special thanks to my PhD sister Marianne, because I'm sure I would not have arrived to this point without all your deadline reminders, for being such a nice person, for teaching me French, for our internal jokes, but most importantly, for your crêpes and apple compote.

Thanks to all the people that made these 4 years in London amazing: our PhD student group, especially Yaiza for all our *cafelitos* and my first non-Argentinean wedding experience. Thanks Dario and Ruben for making me feel like living at home. Merci Rémi pour ta courgette gratin, pour cette dernière année incroyable et pour celles à venir.

Finalmente, gracias a mis amigos de Buenos Aires: Cristian, Santi, Nico, Mayra, Cami, Naty, Fabi, Agus y Juanjo por ser el apoyo moral y no olvidarse que tienen un amigo a 11.102 km de distancia. Gracias Pablo, por nuestros años juntos y tu compañía incondicional. Gracias a mi familia, porque son lo mas importante que tengo: a mis viejos, Elida y Carlos, que no faltaron ningún año a visitarme, a mis hermanos, Hernán, Rodrigo y Belén y a Romi y Renzo. Los amo.

Table of contents

Table of figures

List of tables

Abbreviations

Abbreviations	Meaning
ADCC	Antibody-dependent cell-mediated cytotoxicity
AID	Activation-induced cytidine deaminase
AIDS	Acquired immunodeficiency syndrome
APRIL	A proliferation inducing ligand
ASC	Apoptosis-associated speck-like protein containing a CARD
ASCs	Antibody-secreting cells
Atg	Autophagy-related genes
BAFF	B cell activation factor
BCAP	B cell adaptor protein
Bcl6	B cell lymphoma 6 protein
BCR	B cell receptor
Blimp-1	B lymphocyte-induced maturation protein-1
BM-DC	Bone marrow-derived DCs
BSA	Bovine serum albumin
CARD	Caspase activation and recruitment domain
CCL	C-C motif chemokine ligand
CCR	C-C chemokine receptor
CFU	Colony-forming units
C_H	Constant region of the heavy chain
C_L	Constant region of the light chain
CLL	Clodronate
CLP	Common lymphoid progenitor
CLR	C-type lectin receptor
CPH	Carboxypeptidase-H

CXCL	C-X-C motif chemokine ligand
CXCR	C-X-C chemokine receptor
DAG	Diacylglycerol
DAMP	Damage-associated molecular pattern molecules
DC	Dendritic cell
DC-SIGN	DC-specific Intercellular adhesion molecule-3-grabbing non-integrin
DFCP1	Double FYVE-containing protein 1
DIG	Digoxigenin
DMSO	Dimethyl sulfoxide
DNA	Deoxyribonucleic acid
dNTP	Deoxynucleotide triphosphate
DT	Diphtheria toxin
E4BP4	E4 promoter-binding proteins
Egr	Early growth response
ELISA	Enzyme-linked immunosorbent assay
ELISPOT	Enzyme-linked immunosorbent spot
ER	Endoplasmic reticulum
ES	Embryonic stem
FACS	Fluorescence activated cell sorting
FCS	Foetal calf serum
FDC	Follicular DCs
Foxp3	Forkhead box P3
FRC	Fibroblastic reticular cells
GBS	Group B Streptococcus
GC	Germinal centre
GEF	Guanine-exchange factors

GM-CSF	Granulocyte-macrophage colony-stimulating factor
HEL	Hen egg lysozyme
HEPES	4-2-hydroxyethyl-1-piperazineethanesulfonic acid
HEV	High endothelial venules
HIV	Human immunodeficiency virus
HPLC	High-performance liquid chromatography
HSC	Hematopoietic stem cells
HSV	Herpes simplex virus
ICAM-1	Intercellular Adhesion Molecule 1
ICG	Indocyanine green
IFN	Interferon
Ig	Immunoglobulin
iGb3	Isoglobotriosylceramide
iGb3s	Isoglobotriosylceramide synthase
IL	Interleukin
ILC	Innate lymphoid cell
iNOS	Inducible nitric oxide synthase
IP3	Inositol 3-phosphate
LC3	Microtubule-associated protein light chain 3
LCMV	Lymphocytic choriomeningitis virus
LEC	Lymphatic endothelial cells
LFA-1	Lymphocyte function-associated antigen 1
LN	Lymph node
LPS	Lipopolysaccharide
LRR	Leucine-rich repeat
MAIT	Mucosal-associated invariant T cells
MAPK	Mitogen-activated protein kinases

MCMV	Mouse cytomegalovirus
MDSC	Myeloid-derived suppressor cells
MFI	Mean fluorescence intensity
MHC	Major histocompatibility complex
MS	Mass spectrometry
MTOC	Microtubule organising centre
mTOR	Mammalian target of rapamycin
MyD88	Myeloid differentiation primary response protein
NBD	Nucleotide binding domain
NEAA	Non essential amino acids
NF-kB	Nuclear factor kappa-light-chain-enhancer of activated B cells
NFAT	Nuclear factor of activated T cells
NK	Natural Killer
NLR	NOD-like receptors
NOD	Nucleotide-binding oligomerisation domain
NP	Nucleoprotein
OVA	Ovalbumin
PAMP	Pathogen-associated molecular patterns
PAX5	Paired box 5
PBS	Phosphate-buffered saline
PC	Plasma cell
PCR	Polymerase chain reaction
PD-1	Programmed cell death 1
PFU	Plaque-forming units
PGE2	Prostaglandin E2
PI3K	Phosphatidylinositol 3-phosphate kinase

PIP2	Phosphatidylinositol 4,5-biphosphate
PKC	Protein kinase C
PLCγ2	Phospholipase C γ2
PLVAP	Plasmalemma vesicle-associated protein
PLZF	Promyelocytic leukaemia zinc finger protein
PMA	Phorbol 12-myristate 13-acetate
PRR	Pattern recognition receptors
PtdIns3P	Phosphatidylinositol 3-phosphates
RAG	Recombination-activating genes
RIG-I	Retinoic acid-inducible gene 1
RLR	RIG-I-like receptors
Rm	Recombinant mouse
RNA	Ribonucleic acid
RSV	Respiratory syncytial virus
SAA-1	Serum amyloid A 1
SCS	Subcapsular sinus
SDS	Sodium dodecyl sulphate
SIGN-R1	Specific Icam-3 grabbing nonintegrin-related 1
SLE	Systemic lupus erythematous
SR	Scavenger receptor
TCR	T cell receptor
TfH	T follicular helper
TIR	Toll-interleukin receptor
TLR	Toll-like receptors
TRIF	TIR domain-containing adaptor protein-inducing IFN-β
ULK	Unc-51 like kinases
VACV	Vaccinia virus

VCAM-1	Vascular cell adhesion protein 1
VDJ	Variable Diverse Joining
V_H	Variable region of the heavy chain
V_L	Variable region of the light chain
VLA-4	Very late antigen
VSV	Vesicular stomatitis virus
WIPI	WD-repeat protein interacting with phosphoinoside
XBP1	X-box binding protein 1

Chapter 1. Introduction

1.1 The immune system: past, present and future challenges

Despite living in an environment full of potential pathogens, on only few occasions do we suffer relevant infectious processes; moreover, when infection does happen, it is usually resolved within a few days. The reason why we are protected from a full range of potential microbes is because of our ability to mount an immune response against them. Our immune system integrates mechanisms from both the innate and the adaptive immunity to counteract the infection process. Moreover, the latter generates a phenomenon called “immune memory”, which allows us to stay protected from future reinfections with the same pathogens for years, or even for life.

However, the immune response has several limitations against certain pathogens. For example, once HIV (human immunodeficiency virus) is acquired, the organism is not able to eliminate it in most cases. For years, the immune system of the infected patient fights against HIV and their immune system manages to partially control the dissemination of the virus and the harmful effects that the virus produces. However, in the absence of antiretroviral therapy, the host finally succumbs and develops AIDS (acquired immune deficiency syndrome) (Maartens, Celum and Lewin, 2014). Moreover, humans cannot resolve infections with *Trypanozoma cruzi*, the etiologic agent of Chagas disease. Although the immune system manages to raise a sufficient response to control dissemination of the parasite, and partially control its harmful effects, affected people may die from heart failure after several years (Dias, 2006). Another example is infection with *Mycobacterium tuberculosis*, the causative agent of tuberculosis, which affects 10 million people each year. Even though the immune system efficiently controls the course of the infection by decreasing the bacterial load in the lung parenchyma, it does not manage to eradicate the pathogen. If the patient subsequently suffers from a condition that compromises the function of the immune system, the tuberculosis infection will expand rapidly (Sasindran and Torrelles, 2011).

Currently, we have an overall picture of the physiopathology of the immune response during infection. However, it is undeniable that we still have much to understand. For instance, not much is known about the mechanisms that pathogens use to evade the immune response that they themselves triggered. Moreover, we do not know how the immune system works during co-infections with different pathogens or why we are more vulnerable to contracting new infections when there is a previous infection on going in our bodies. Furthermore, even though completely new subsets of innate or innate-like lymphoid cells, such as ILCs (innate lymphoid cells), NK (natural killer) T cells or γδ T cells, have been discovered in recent years, their activation processes and roles during infection are still far from being understood. This lack of knowledge is reflected in our incapacity to create therapeutic tools that could prevent certain infectious processes or contribute towards the eradication of infections.

We have developed successful vaccines against numerous pathogens causing diseases like smallpox, poliomyelitis, measles, diphtheria, tetanus and hepatitis B, among others. Importantly, in some cases, complete eradication of the disease was achieved through vaccination (Table 1.1). However, we still do not have vaccines against the great majority of parasitic diseases such as malaria, leishmaniasis or Chagas disease or for the prevention and treatment of HIV infection. Moreover, even though seasonal vaccines against influenza protect us against circulating viral strains for a few years, a universal flu vaccine has still not been generated. In consequence, every year around 1 million people die because of parasitic infections, 1 to 2 million people die of AIDS and 500,000 people die from influenza infection (Pica and Palese, 2013, Maartens, Celum and Lewin, 2014, Sacks, 2014). It is therefore essential to understand how the immune system operates during infection to generate new therapeutic tools to protect against pathogenic threats.

Table 1.1 Estimated annual morbidity in the United States pre and post-vaccination era.

Disease	Pre-vaccine era	2010
Smallpox	29,005	0
Diphtheria	21,053	0
Polio	16,316	0
Rubella	47,745	4
Tetanus	580	14
Measles	530,217	61
Mumps	162,344	982
Hepatitis B	66,232	11,269
Pertussis	200,752	13,506
Chickenpox	4,085,120	449,363

Adapted from Centres for Disease, Control and Prevention.

1.2 Innate and adaptive immunity

Immunity can generally be defined as the capacity to successfully prevent or overcome a pathogenic infection. This is dependent on the ability of immune cells to recognise foreign threats though the expression of specialised receptors. Depending on the type of the receptors they express, immune cells have been historically divided into two groups: innate immunity and adaptive immunity (Iwasaki and Medzhitov, 2010).

1.2.1 Innate immunity

The innate immune system is our first line of defence and it provides immediate protection against infection. The innate branch is mainly composed of the body surface barriers and a broad range of leukocytes. The surface barriers include the skin and other epithelia such as the respiratory, digestive and genitourinary tracts. As most infective pathogens enter the organism through these surfaces, these epithelia represent a protective, constitutive, efficient and common

physical barrier to prevent infection. If these barriers are breached, the innate immune system will respond by activating different mechanisms according to the infectious pathogen. Broadly speaking, neutrophils and macrophages are essential for fighting extracellular bacteria; plasmacytoid DCs (dendritic cells) and NK cells are important during viral infection; and mast cells, basophils and eosinophils are key during helminthic parasite infection. These innate immune cells participate in the immune response by exerting antimicrobial activity (phagocytosis of pathogens and production of antimicrobial peptides) and by producing chemical mediators (chemokines and cytokines) that recruit immune cells to sites of infection and orientate the course of the innate and adaptive immune response (Charles A Janeway et al., 2001) .

All the cells of the innate branch of the immune system share a conserved tool to recognise microorganisms: the PRRs (pattern recognition receptors). PRRs are germline-encoded receptors that recognise PAMPs (pathogen associated molecular patterns). These PAMPs are conserved molecular sequences present in microorganisms, but not in the host, which are essential for their survival and pathogenicity. For instance, cell wall components or even genetic material can be detected by PRRs. PRRs can be classified in five different families: 1) TLRs (Toll-like receptors), 2) NLRs (NOD (nucleotide binding and oligomerisation domain)-like receptors), 3) RLRs (RIG (retinoic acid-inducible gene)-I-like receptors), 4) CLRs (C-type lectin receptors) and 5) SRs (scavenger receptors) (Kumar, Kawai and Akira, 2011).

TLRs, which are the most characterised PRRs, were first identified in *Drosophila* and so far 13 members of this family have been described in mammals. They are expressed on the plasmatic and endosomal membranes of the cells and they contain an extracellular domain in charge of recognising the PAMPs and an intracellular domain involved in signalling transduction. The cytoplasmic domain of the TLRs is similar to that expressed by the family of IL (interleukin)-1 receptors, IL-1R and IL-18R, and is called TIR (Toll-IL-1 receptor). Signalling through TLRs upon recognition of their ligands recruits MyD88 (myeloid differentiation primary response protein 88) and/or TRIF (TIR domain-containing adaptor protein-inducing IFN (intereferon)-β) adaptors to the intracellular domain (Figure 1.1A). This

recruitment induces signalling through NF-κB (nuclear factor kappa-light-chain-enhancer of activated B cells) and the production of cytokines, chemokines and antimicrobial molecules. Three of the most studied TLRs are TLR4, which recognises LPS (lipopolysaccharide) present in the surface of gram-negative bacteria, TLR9, which recognises microbial nucleic acids rich in unmethylated CpG sequences and TLR7, which recognises viral single-stranded RNAs (ribonucleic acids) (Kawai and Akira, 2011).

NLRs are the cytoplasmic counterpart of TLRs and so far 23 members have been described. They recognise microbial components that have gained access to the cytoplasm and also cell damage signals. NLRs contain three different domains: a C-terminal domain able to recognise PAMPs, a central domain that binds nucleotides and regulates auto-oligomerisation of the receptors following activation, and a N-terminal effector domain, in charge of recruiting effector proteins. Signalling through NLRs induces auto-oligomerisation and the formation of protein complexes that act as scaffolds to recruit the adaptor protein ASC (apoptosis-associated speck-like protein containing a CARD (caspase activation and recruitment domain)) and Caspase-1. These high molecular weight complexes containing NLRs, ASC and Caspase-1 are called inflammasomes. Once inflammasomes are assembled, Caspase-1 is activated and mediates the cleavage of pro-IL-1β and pro-IL-18 to their active forms. These cytokines are then released from the cell to mediate the initiation of the inflammatory response (Figure 1.1B) (Chen et al., 2009).

In most cases, the innate immunity manages to eradicate the emerging infection. However, if not, the innate immune system will contain the infection until the mechanisms of the adaptive immunity are operative; a process that can take up to a week.

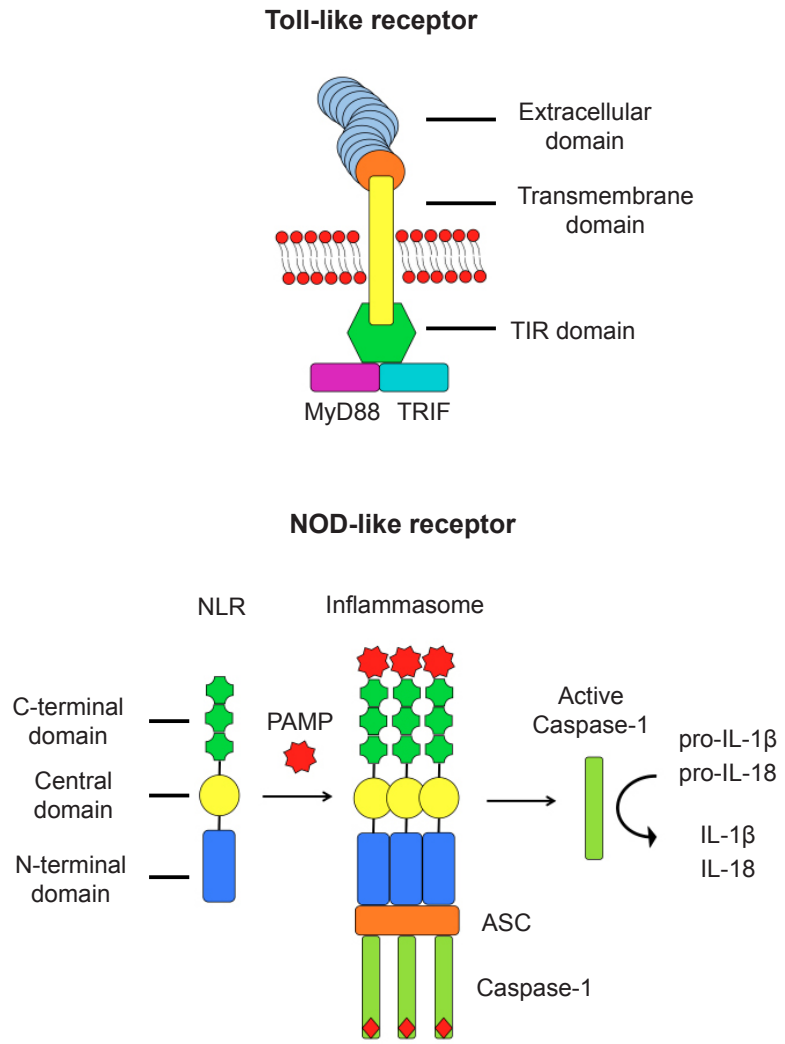

Figure 1.1 Schematic structures of Toll and NOD-like receptors

(A) General structure of a TLR showing the extracellular domain containing LRRs (leucine rich repetitive motifs) that recognise PAMPs, a transmembrane domain and an intracellular domain called TIR that mediates TLR signalling. TLR activation induces recruitment of the adaptor molecules MyD88 and/or TRIF. (B) Structure of a NOD like receptor containing a C-terminal domain containing LRRs that recognise PAMPs, a central NBD (nucleotide binding domain) that mediates receptor oligomerisation and the N-terminal effector domain that recruits the ASC adaptor and Caspase-1 to form the inflammasome after activation. The assembly of the inflammasome induces the cleavage of pro-IL-1β and pro-IL-18 to active IL-1β and IL-18.

1.2.2 Adaptive immunity

The adaptive immune system is our second line of defence and unlike innate immunity, it is highly specific and generates immune memory, providing long-lasting protection from future re-infections with the same pathogen. The cells that carry out the adaptive immune response are the white blood cells known as lymphocytes, of which there are two main types: B cells and T cells. B cells mediate the humoral response and T cells lead the cell-mediated response. In humoral immunity, B cells produce specific antibodies against infectious pathogens to inactivate them and mediate their clearance. In contrast, in cell-mediated immunity, T cells produce inflammatory cytokines and enable the destruction of infected cells (Iwasaki and Medzhitov, 2010).

B cells and T cells express pathogen-specific receptors generated *de novo* during the lifetime of the host. These receptors, known as the BCR (B cell receptor) and the TCR (T cell receptor), recognise particular motifs present in the pathogens known as antigens. While B cells recognise antigens in their native form, T cells recognise antigen-derived peptides in the context of MHC (major histocompatibility complex) molecules in the surface of other immune cells (Janeway et al., 2001).

The BCR comprises a membrane-bound Ig (immunoglobulin), which associates with the signalling components Igα and Igβ (also known as CD79A and CD79B) to form a BCR complex. Four proteins constitute the membrane-bound Ig: two identical copies of a heavy chain and two identical copies of a light chain, all covalently linked through disulphide bonds. The Ig domains closest to the N-terminal, from both heavy and light chains, are known as the variable regions (V_H and V_L respectively). Both V_H and V_L contribute to the antigen-binding region, which defines the binding specificity of the BCR. The remaining immunoglobulin domains of the heavy and light chains are known as the constant regions (C_H and C_L respectively) (Figure 1.2A). There are two different types of light chains called kappa (κ) and lambda (λ) and five different types of heavy chains γ, δ, α, μ and ε that define the different classes of immunoglobulins: IgG, IgD, IgA, IgM and IgE (Harwood and Batista, 2009).

The TCR is formed by two different protein chains anchored to the membrane. There are two main different varieties of TCR: one is formed by an α and a β chain (TCR αβ), present in most T cells, and one by a γ and a δ chain (TCR γδ) present in a minor population of T cells known as γδ T cells. The TCR chains also contain variable regions (V_α and V_β or V_γ and V_δ) that determine the antigen-binding site, and constant regions (C_α and C_β or C_γ and C_δ), which are conserved in the different individual T cells. The TCR chains are bound by disulphide bonds. The TCR is associated with the CD3 complex, which controls signal transduction after antigen recognition and assembly of the TCR. The CD3 complex is formed by a CD3ε chain in a heterodimer with CD3γ or CD3δ associated, along with the TCR, with a fourth component known as the ζ chain (Wucherpfennig et al., 2010) (Figure 1.2B).

Importantly, both the BCR and TCR are not genetically pre-determined as are PRRs, rather, they arise by random rearrangement of genetic segments; a mechanism that allows a small number of genes to generate a vast number of antigen receptors uniquely expressed on each individual lymphocyte (Iwasaki and Medzhitov, 2010).

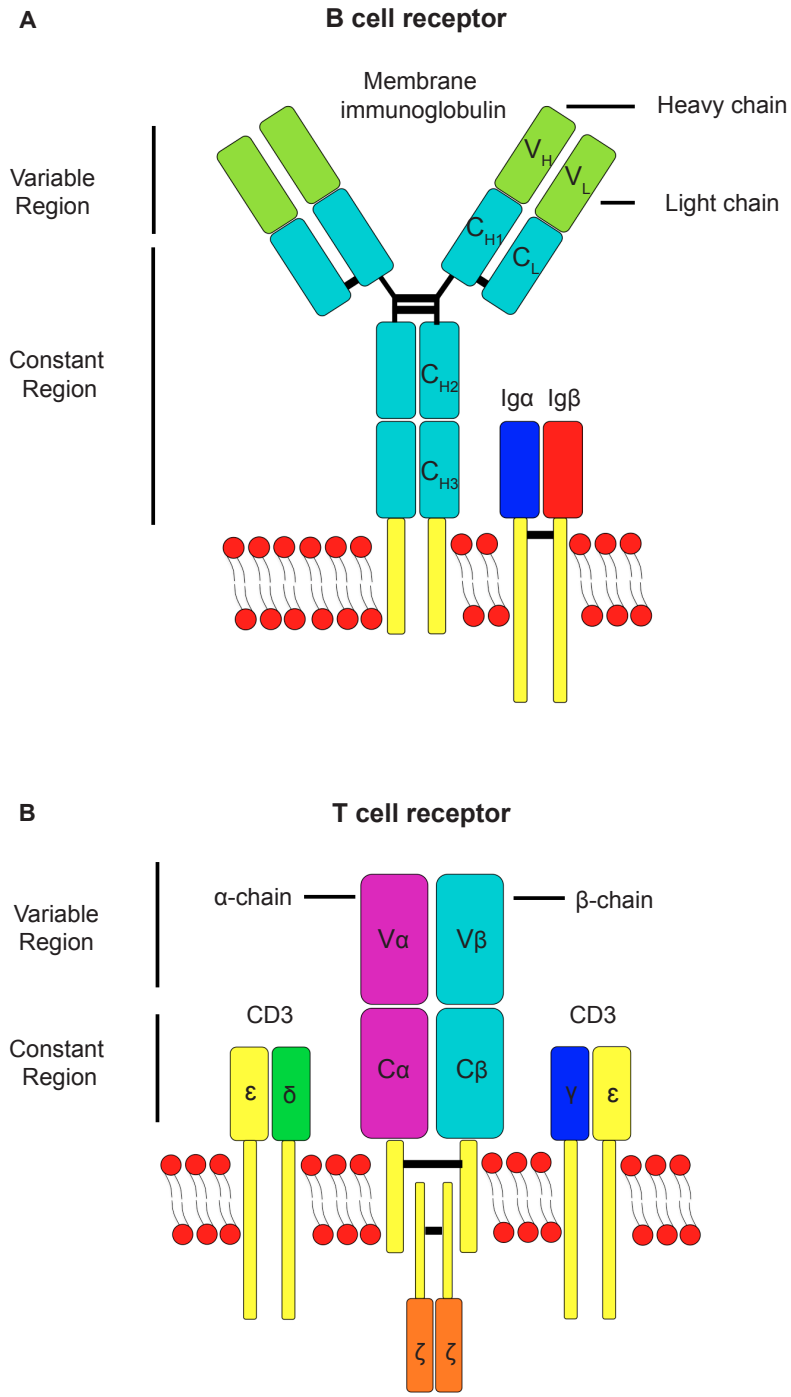

Figure 1.2 Structures of a BCR and a TCRαβ complex

Schematic diagrams of a BCR and a TCRαβ complex. (**A**) The BCR is composed by a membrane-bound Ig and the signalling components Igα and Igβ. The membrane-bound Ig contains two identical heavy chains and two identical light chains bound by disulphide bonds. (**B**) The TCRαβ is composed by two different chains named TCRα and TCRβ bound by disulphide bonds and the signalling complex CD3. Both the BCR and TCR have variable regions controlling antigen recognition, and constant regions that remain conserved among the different lymphocytes.

As thousands of antigens exist in the microbial world, we need many different B cell and T cell clones to recognise them. This implies that only 1 out of 10^5 or 10^6 lymphocytes in our body will be specific for a certain antigen (Moon et al., 2007). This strategy gives rise to two different problems: firstly, the probability that such a reduced number of lymphocytes would encounter a specific antigen in the body just by random search is quite remote, and secondly, that even if the encounter happened, this reduced number of lymphocytes would not be able to mediate an efficient antimicrobial response against millions of microorganisms and infected cells. Interestingly, adaptive immunity has managed to solve these central problems by restricting the area of antigen encounter and developing fast proliferation of specific lymphocytes. In order to encounter specific antigens, naïve lymphocytes do not have to patrol for antigens around the whole organism but only in specialised regions called secondary lymphoid organs, to which all the pathogens that have crossed the natural barriers of our body are drained. Moreover, the B cells and T cells that recognise these antigens undergo a process called clonal expansion that rapidly generates thousands of lymphocytes with identical antigen specificity. Once expanded, most of the specific lymphocytes will mediate effector functions to clear the pathogen and infected cells and a minor fraction will differentiate into memory cells to mediate a fast response against future reinfections with the same pathogen. These factors together; the recirculation of B and T cells though secondary lymphoid organs in search of antigen, the clonal expansion and the development of immune memory, make adaptive immunity a unique and effective system to control and clear pathogens during infection and avoid future challenges with similar pathogens (Janeway et al., 2001).

The activation of the adaptive immune system is highly reliant on innate immunity. During an infection, DCs and macrophages are in charge of presenting pathogens to B cells and T cells through a process known as antigen presentation. DCs, which are mainly located in the body surface barriers such as the skin and other epithelia, capture pathogens in the periphery and migrate to secondary lymphoid organs (Randolph, Angeli and Swartz, 2005). Once there, they present captured pathogens to specific B cells and T cells to mediate their activation. Moreover, as explained later in more detail, a population of macrophages in the border of secondary lymphoid organs also mediates the retention of pathogens and

their presentation to specific B cells (Carrasco and Batista, 2007, Junt et al., 2007, Phan et al., 2007). Therefore, innate immunity is not only foremost in containing the nascent infection but also in control of activating the specific mechanisms of adaptive immunity.

1.2.3 Innate-like lymphocytes: the inbetweeners

Interestingly, not all B cells and T cells behave according to the simplified schema mentioned above. There are some subsets of lymphocytes known as innate B cells and T cells that bear certain characteristics resembling those of innate immunity. Unlike conventional lymphocytes, innate B cells and T cells possess a relatively restricted repertoire of antigen receptors and are enriched in mucosal tissues, where pathogens are first encountered. Moreover, they rapidly respond after infection by secreting natural antibodies, cytokines and cytotoxic effectors (Lanier, 2013).

B cells with “innate-like” functions include B-1 cells, localised at epithelial barriers and peritoneal and pleural cavities, and marginal zone B cells, which are a sessile population found exclusively in the spleen. They differ from the conventional B cells because of a more restricted BCR repertoire strongly biased towards the recognition of pathogen-associated repetitive antigens. Moreover, they express high levels of TLRs, allowing them to be activated by a broad array of microbial ligands, and they can respond independently of co-stimulatory signals, in a manner reminiscent of innate immune cells. These B cell populations make so-called natural antibodies that recognise conserved features of bacterial carbohydrates and phospholipids. Although natural antibodies often have a lower affinity than antibodies generated by conventional B cells, they can protect the host against bacterial pathogens soon after infection (Cerutti, Cols and Puga, 2013).

T cell populations also include subsets with innate-like properties: NKT cells, γδ T cells and MAIT (mucosa-associated invariant T) cells. NKT cells express a αβ TCR that preferentially uses a single TCRα gene and a very restricted set of TCRβ genes. Unlike conventional T cells, which recognise peptide antigens bound to

MHC molecules, NKT cells recognise lipids displayed on CD1d molecules. NKT cells produce cytokines more rapidly than conventional naïve T cells and do not possess memory after their encounter with an antigen (Brennan, Brigl and Brenner, 2013). MAIT cells also have restricted TCR chain usage and they recognise riboflavin metabolites from bacteria and fungi presented on the MHC-related molecule MR1 (Kjer-Nielsen et al., 2012). MAIT cells are preferentially localised in mucosal tissues and respond to microbial infection by rapidly producing cytokines and cytotoxic effectors (Kurioka et al., 2015). γδ T cells constitute another population of T cells with innate properties. These T cells, express an atypical TCR composed of two chains, TCRγ and TCRδ, which differ from the TCRα and TCRβ chains comprising the canonical TCR. They have a very limited receptor repertoire: all peripheral γδ T cells express the same TCRγ chain combined with TCRδ chains that differ depending on the tissue localisation. γδ T cells can recognise a wide range of antigens, from phospho-antigens to molecules expressed on stressed cells, although the ligands for most γδ T cells remain elusive. When activated, γδ T cells display rapid secretion of cytokines and cytolytic activity, in part due to their pre-activated phenotype (Vantourout and Hayday, 2013). In the case of MAIT cells and γδ T cells, it is not clear if they can induce immunological memory.

More than two thousand years have passed since Thucydides first wrote about immunity in reference to patients who had survived the plague of Athens and who could nurse the sick people without contracting the illness a second time (Habs, 1982). Yet we are still attempting today to fully understand the complexity of our immune system. Expanding our knowledge in this field is key for the development of better vaccines to protect us against potential pathogenic threats. Most currently available vaccines have been empirically designed. However, in most cases the success of these vaccines has been associated with the induction of high-titres of antibodies in vaccinated people (Siegrist, 2008). Therefore, to improve the rational design of future vaccines it is essential to understand how B cells, the immune cells producing these antibodies, work *in vivo* during pathogenic challenges. During my thesis I have focussed on discovering how different cells from the innate immune system assist B cells to develop a robust response during infection.

1.3 B cell ontogeny and distribution

B cells, as with other cells of the immune system, originate in the bone marrow from a common precursor. During development, B cells acquire their antigen receptor, the BCR, which is necessary for the recognition of potential pathogens. As each B cell expresses a particular BCR with a unique specificity, the B cell repertoire of each individual allows the mounting of an adaptive immune response to the thousands of different antigens present in the environment.

1.3.1 B cell development

B cells originate in the bone marrow from HSCs (hematopoietic stem cells). These HSCs generate two different progenitors: a myeloid progenitor, that gives rise to myeloid cells, such as DCs and macrophages, and a CLP (common lymphoid progenitor) that gives rise to B cells and T cells (Kondo, Weissman and Akashi, 1997). The development of B cells starts in the bone marrow but the maturation process culminates in the spleen. B cell development occurs through several stages, each stage representing a change in the genome content of the antibody loci. In the V_H region there are three groups of genetic segments termed V (variable), D (diverse) and J (joining) that randomly recombine in a process known as VDJ recombination to produce a unique variable domain in the immunoglobulin of each individual B cell. Similar rearrangements occur in the V_L region, except that there are only two groups of genetic segments involved: V and J (Brack et al., 1978). Both VDJ and VJ recombination are dependent on RAGs (recombination activating genes), which collaborate in the insertion of DNA (deoxyribonucleic acid) double-strand breaks at consensus sequences to allow gene segment shuffling and re-joining (Schatz, Oettinger and Baltimore, 1989, Agrawal and Schatz, 1997). The random rearrangement of gene segments in the heavy and light chain loci ensures combinatorial diversity of the antigen receptor.

The different stages of B cell development are shown in Figure 1.3. In short, commitment to the B cell fate begins at the pre-pro-B cells stage. These cells express B220 but are still CD19 negative (Coffman, 1983). Eventually, development progresses to the pro-B cell stage, where the heavy chain is

rearranged. The V_H region is assembled by joining together a single copy from each of the V, D and J gene segments from the many found at the heavy chain locus (Brack et al., 1978). A correctly assembled V_H exon is co-transcribed with C_H gene segments to form a complete heavy chain. The heavy chain can pair up with a surrogate light chain and the Igα and Igβ proteins to form a pre-BCR complex. Expression of the pre-BCR is a hallmark of the pre-B cell stage and provides the first crucial checkpoint for B cell development. Cells expressing a non-functional pre-BCR will be eliminated. Signalling competent pre-BCRs will instead trigger cell division and inhibit any further rearrangement of the heavy chain locus on the homologous chromosome, a process known as allelic exclusion (Löffert et al., 1996). Pre-BCR signalling is also important for the initiation for the assembly of the light chain. The V_L exon is generated by joining together a single V and single J segment from the many ones found at the light chain loci. A correctly assembled V_L exon can be co-transcribed with a C_L exon to form a complete light chain, which can replace the surrogate one to form a functional BCR (Arakawa, Takeda and Takemori, 1996). Cμ is the first C_H to be used for the assembly of the heavy chain, thus the first BCR expressed by immature B cells is termed IgM. The requirement for the signalling competence of IgM provides the second checkpoint in B cell development. Tonic BCR signalling is required as proof of functionality and for allelic exclusion at the light chain locus. However, very low or strong intensity signalling in the B cells induces anergy, a state of long-lasting unresponsiveness, or clonal deletion, cell death by apoptosis. This process ensures that only functional and non-auto reactive B cells leave the bone marrow to the spleen (Nemazee and Buerki, 1989, Goodnow, 1992, Wardemann et al., 2003).

Once in the spleen, immature B cells express a second BCR termed IgD to complete maturation. Both IgM and IgD share the same variable region but different C_H. Finally, naïve mature B cells will recirculate through the lymph nodes, spleen and bone marrow in search of cognate antigen (Loder et al., 1999).

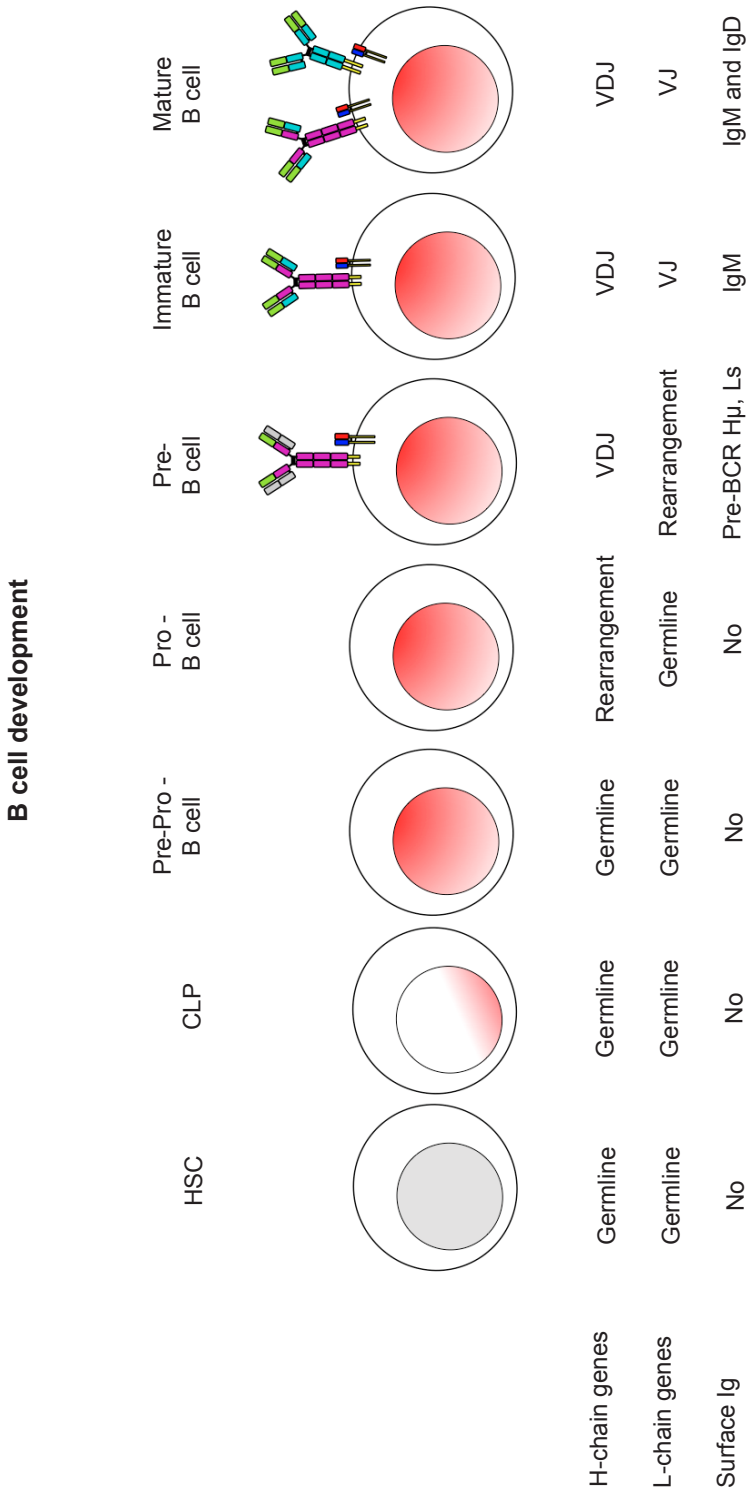

Figure 1.3 B cell development

Scheme displaying the different stages of B cell development in the bone marrow and the maturation process in the spleen. The rearrangement of the heavy and light chains and the expression of Ig in the membrane are detailed for each differentiation step.

1.3.2 B cells in secondary lymphoid organs

Mature B cells are mainly found in secondary lymphoid organs, where all the pathogens that have managed to cross the natural barriers of the body are drained. These organs include LNs (lymph nodes), spleen, Payer's patches and tonsils. Secondary lymphoid organs are essential for the capture of pathogens and to prevent their systemic spreading, a phenomenon that increases the likelihood of antigen encounter by lymphocytes. Secondary lymphoid organs possess a highly organised microarchitecture, which is essential for the compartmentalisation of numerous cellular interactions during an immune response (Scandella et al., 2008). Their importance in coordinating immune responses is evident from the severe impairment in lymphocyte activation in alymphoplastic and asplenic mice (Karrer, Althage and Odermatt, 1997). In my thesis I will focus on the regulation of the B cell response during infection in draining LNs, so I will describe their architecture here in more detail.

LNs are specialised rounded structures strategically distributed throughout the lymphatic system to enable antigenic sampling of lymphatic fluid. LNs are protected by an external collagen capsule covering the whole organ and immediately below the capsule, there is a lymphatic lumen termed the subcapsular sinus (SCS) where all the afferent lymphatics converge (Batista and Harwood, 2009). The ceiling and floor of the SCS are lined by LECs (lymphatic endothelial cells) (Ulvmar et al., 2014). Directly beneath the SCS there is a macrophage-rich layer of cells expressing high levels of the sialoadhesin molecule CD169, and which control the capture of incoming pathogens (Carrasco and Batista, 2007, Junt et al., 2007, Phan et al., 2007). This macrophage layer surrounds the B cell follicles or cortex, in which B-lymphocytes reside. These follicles are also rich in FDCs (follicular DCs), which are stromal cells involved in the presentation of unprocessed antigen and the production of the chemokine CXCL-13 (Heesters, Myers and Carroll, 2014). CXCL-13 controls the organisation of the follicles through interaction with the receptor CXCR-5 expressed by follicular B cells (Cyster et al., 2000). Between the different B cell follicles, we can find extensions of the lymphatic system known as the cortical sinus that allows the lymphatic fluid to pass between the follicles. These inter-follicular areas are populated by a network of spatially

prepositioned innate effector cells, such as NK cells, γδ T cells, NKT cells and innate-like $CD8^+$ T cells that can rapidly receive inflammatory signals from $CD169^+$ macrophages to initiate their activation (Kastenmüller et al., 2012) (Figure 1.4).

Adjacent to the B cell follicles we find the T cell zone or paracortex, where T cells are mainly located. The T cell area is also rich in antigen presenting cells (mainly DCs), HEVs (high-endothelial venules) and a conduit network surrounded by FRCs (fibroblastic reticular cells). The HEV network is composed of specialised capillaries that continuously supply the LN with lymphocytes and antigen presenting cells from the periphery (HE, 1985). The FRC network is a group of stromal cells that produce and surround collagen-rich reticular fibres. This fibrous network acts as a conduit system to transport low molecular mass molecules, such as cytokines and chemokines, from the SCS to the T cell zones and HEVs (Gretz, Anderson and Shaw, 1997). Moreover, they produce high levels of the chemokines CCL19 and CCL21, which attract peripheral dendritic cells and B cells to the T cell area of the LNs through interaction with the receptor CCR7 (Ohl et al., 2003). Importantly, the levels of CCR7 in peripheral DCs and B cells increase after the encounter antigen, a process that is necessary for them to relocate to the T cell zone (Förster, Davalos-Misslitz and Rot, 2008) (Figure 1.4).

Finally, the medulla is the innermost area of the LN and it is where the efferent lymphatic vessels originate. It contains both B cells and T cells organised in medullary cords, and is also rich in DC and macrophages. This area contains extra follicular plasma cells, which produce the first wave of antibodies after antigen encounter (Batista and Harwood, 2009) (Figure 1.4).

LNs constantly receive lymphatic fluid composed of blood plasma, chemokines, cytokines and antigens that have been collected from the body. Lymph enters the LN through the afferent lymphatic vessels and is subsequently filtered by the LN as it flows from the subcapsular, the cortical and the medullar sinuses towards the efferent lymphatic vessels. Lymphatic fluid is prevented from freely diffusing into the interior of the LN parenchyma by the sinus lining cells. The whole sinus system is interconnected and can be considered to be a unique

compartment, which directly links the afferent to the efferent vessels (HE, 1985, Lämmermann and Sixt, 2008) (Figure 1.4).

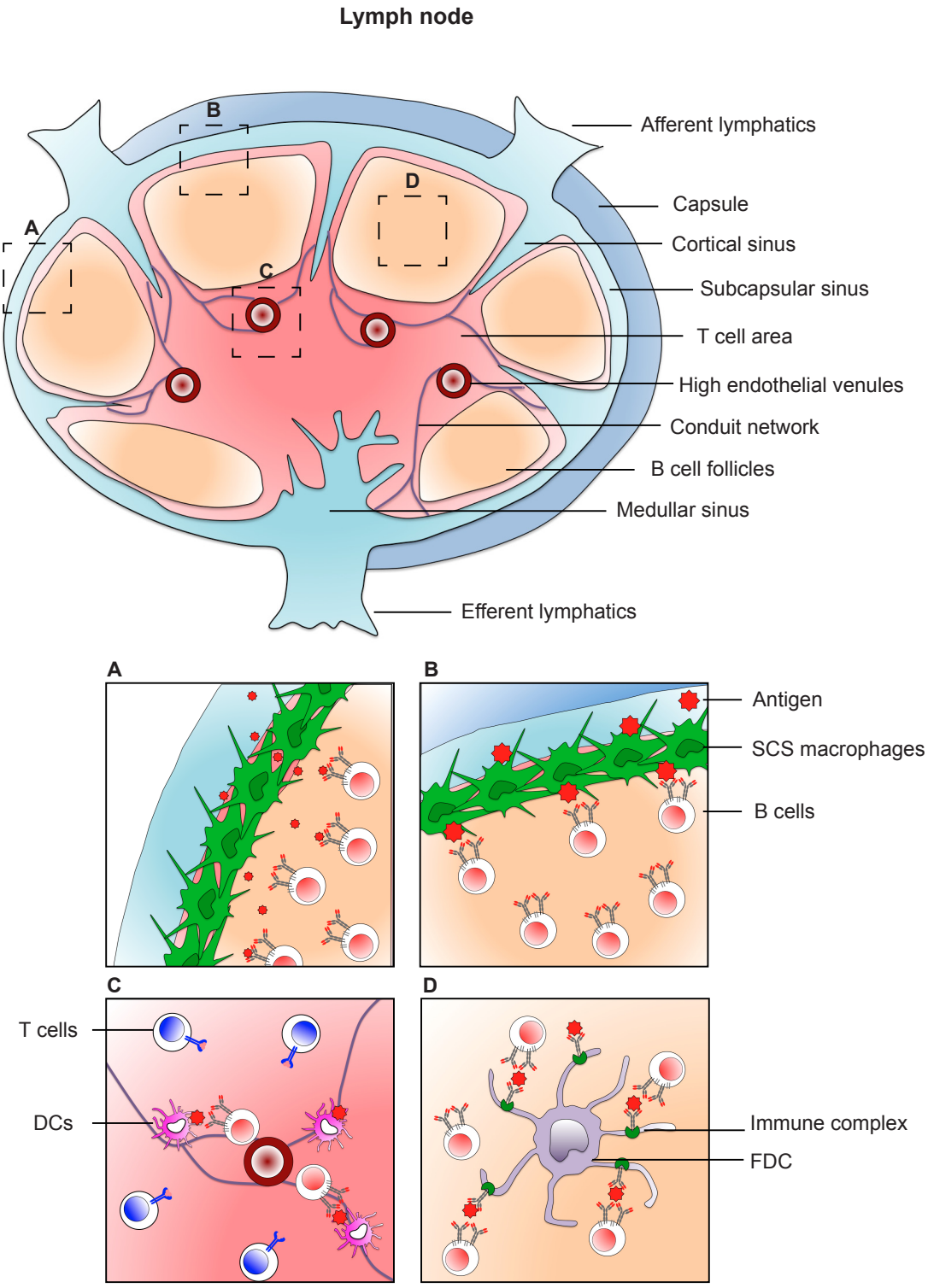

Figure 1.4 Schematics of a LN and mechanisms of B cell encounter of antigen

Cartoon representing the overall LN organisation. Lymphatic fluid enters the LNs through the afferent lymphatic vessels and sequentially passes through the SCS, the cortical sinus and the medullary sinus. It then leaves the LNs from the efferent lymphatics for eventual return to the general circulation. The cortical LN parenchyma is mainly divided into two different zones: the B cell area and the T cell area. (**A**) Soluble antigens with a molecular weight of less than 70 kDa can directly cross the SCS through pores where B cells can directly encounter them. (**B**) Follicular B cells recognise bigger antigens captured on the surface of SCS macrophages. (**C**) B cells entering through HEVs can recognise antigen retained on the surface of DCs. (**D**) B cells can also capture immune complexes presented on the surface of FDCs.

1.4 B cell encounter of antigen

During infection, B cells can rapidly detect pathogens and mount humoral responses to counteract them in secondary lymphoid organs. The mechanism by which B cells encounter antigens is dependent on their size. In the case of small soluble antigens, they can simply diffuse into the lymphatic tissue, where B cells can recognise them. However, in most cases, pathogens are bigger in size and presentation must be mediated by macrophages, DCs and FDCs (Batista and Harwood, 2009).

1.4.1 Encountering of soluble antigen

Once antigen has crossed the natural barriers of the body, it is rapidly transported to the draining LNs by the afferent lymphatic vessels. In fact, labelled antigen can be observed accumulating in the SCS of the LN within minutes of subcutaneous injection (Nossal et al., 1968). Antigens that are small enough (less than 70kDa) can enter the FRC system of conduits and reach the HEVs (Sixt et al., 2005). Recently, it has been shown that this size exclusion is regulated by the lymphatic endothelial protein PLVAP (plasmalemma vesicle-associated protein), which forms diaphragms in transendothelial channels (Rantakari et al., 2015). Follicular B cells can extend cellular protrusions into the FRC conduits and pick up cognate antigens travelling within it (Roozendaal et al., 2009). However, as most B cells are usually located in the follicles, lymph-borne antigens might gain access to follicular B cells in a manner that is independent of the conduit system, which is predominantly present in the T cell zone.

Electron microscopy studies have shown the presence of pores of approximately 0.1 to 1 μm diameter in the SCS (CLARK, 1962, Farr, Cho and De Bruyn, 1980). These pores potentially allow small soluble antigens arriving through the lymphatic vessels to directly cross the SCS into the follicles and gain access to B cells. Indeed, subcutaneous injection of labelled HEL (hen egg lysosome) showed a rapid diffusion of HEL to the LN follicles and acquisition of antigen by HEL-specific B cells (Pape et al., 2007). Importantly, this process is independent of cell-mediated transport of antigen and does not require B cell migration. Therefore, small antigens, such as low-molecular weight toxins, may gain access to the B cell follicles directly through diffusion from pores in the SCS. However, bigger antigens such as viruses and bacteria are excluded from this system. This selectivity is extremely important, as it prevents the entry of pathogens to the LN parenchyma and their systemic spreading to the rest of the body (Figure 1.4A).

1.4.2 Antigen presentation by SCS macrophages

Although direct diffusion of antigen through the SCS provides one possible mechanism for exposing B cells to small, soluble antigens, the access of larger particulate antigens to the B cell follicles, such as viruses or bacteria, is limited. Another mechanism might therefore exist to ensure B cell access to larger antigens in order to develop a humoral response. In 2007, three independent studies described that the population of macrophages sitting on the SCS floor and in direct contact with the afferent lymphatic fluid on the outer side and with the B cell follicles on the inner side (CLARK, 1962, Farr, Cho and De Bruyn, 1980, Fossum, 1980, Szakal, Holmes and Tew, 1983), are essential for presentation of larger antigens to B cells (Carrasco and Batista, 2007, Junt et al., 2007, Phan et al., 2007).

These studies show that soon after subcutaneous administration of antigen in the form of virus, bacteria or immune complexes (soluble antigens bound to antibodies), SCS macrophages are in control of retaining and accumulating these larger antigens coming through the lymphatic vessels. The mechanism by which these macrophages retain antigen is not clear, although it might be due to their high expression levels of CD169, a sialoadhesin molecule that binds the sialic acids present in a variety of pathogens. Moreover, SCS macrophages have limited

phagocytic activity, which favours the retention of unprocessed antigen on their surface. This low phagocytic activity is reflected in their lack or low-level expression of lysosomal enzymes, such as lysozyme, and phagocytosis-related receptors, such as mannose receptors (Phan et al., 2009). Importantly, depletion of these macrophages results in severely impaired antigen retention in the LNs (Junt et al., 2007).

The antigen retained on SCS macrophages is subsequently presented in its intact form to underlying follicular B cells. Antigen-specific B cells make stable cell-contact with these SCS macrophages and extract the antigen from their surface (Carrasco and Batista, 2007, Junt et al., 2007, Phan et al., 2007). After antigen acquisition, B cells internalise the antigen by the BCR before migrating to the B-T cell boundary, where they can receive specific T-cell help. Together, these studies provide the first clear demonstration of a role for SCS macrophages in the initiation of follicular B-cell responses (Figure 1.4B).

During the writing of this thesis, an article in eLife revealed that SIGN-R1^{+} (Specific Icam-3 grabbing nonintegrin-related 1) macrophages positioned in the interfollicular areas are able to capture the HIV-envelope glycoprotein gp-120 from the lymphatic fluid and present it to specific B cells. In contrast, non-glycosylated antigens were not captured by these macrophages, revealing a specialised LN antigen delivery system for pathogen- derived glycoproteins to B cells (Park et al., 2015). Whether, this new mechanism of antigen encounter contributes to the humoral response to glycoprotein-bearing pathogens remains to be elucidated.

1.4.3 Antigen presentation mediated by DCs

B cells enter the LNs through the HEVs present in the T cell area. Interestingly, this area is also occupied by DCs that have collected antigen from the periphery and have migrated to the LNs after antigenic challenge. As DCs are considered the most efficient cell type to present antigen to T cells (Itano et al., 2003, Dudziak et al., 2007), it is possible that these DCs would be also able to play a key role in antigen presentation to B cells.

In fact, it was shown by several groups that antigen-loaded DCs located

around HEVs can present intact antigen to B cells that are exiting the HEVs (Wykes et al., 1998, Colino, Shen and Snapper, 2002, Qi et al., 2006). Intravital microscopy studies showed that after administration of antigen-loaded DCs to mice, antigen-specific B cells exiting the HEVs show decreased motility and an increase residency time around DCs, where they can survey their antigenic contents (Qi et al., 2006). Furthermore, DCs are able to display unprocessed antigens on their surface due to the internalisation and recycling of antigen into non-degradative compartments, a process that is mediated by FcγRIIB and DC-SIGN (DC-specific Intercellular adhesion molecule-3-grabbing non-integrin) (Kwon et al., 2002, Bergtold et al., 2005). This phenomenon allows B cells to recognise antigens on the surface of DCs on their native conformation. The DC-mediated presentation of antigen to B cells in the paracortex provides a favourable environment for the following interaction between B cells and T cells to complete B cell activation (Figure 1.4C).

1.4.4 Antigen presentation mediated by FDCs

Historically, FDCs have been considered to be the cells that are mainly responsible for antigen presentation to B cells due to their localisation in the B cell follicles and their ability to retain unprocessed antigens on their surface (Tpw, Phipps and Mandel, 1980, Schwickert et al., 2007). FDCs mediate the retention of antigens in the form of immune complexes bound to proteins from the complement system. FDCs retain these immune complexes through the expression of Fc receptors that bind to the constant fragment of antibodies and complement receptors, which recognise the complement proteins bound to the antibodies (Heesters, Myers and Carroll, 2014). Despite the ability of FDCs to present unprocessed antigen, the importance of this pathway for the activation of naive B cells during the initiation of primary immune responses is not clear. This is due to the requirement of existing antibodies against specific pathogens to form these immune complexes. However, the pre-existence of natural antibodies produced by innate B cells might help with the rapid formation of immune complexes and the presentation of microbial antigens on the surface of FDCs (Heesters, Myers and Carroll, 2014). Immune complexes have a high-molecular weight; therefore they

cannot get access to the FDCs by simple diffusion through the SCS or by the conduit system. Instead, non-specific B cells can transport these immune complexes from the SCS to the FDCs through the binding to the complement proteins of the immune complexes (Phan et al., 2007) (Figure 1.4D).

All these diverse mechanisms of antigen-presentation to B cells provide an important flexibility in the initiation of the B cell response to pathogens during an infection. Moreover, and as I will show in chapter 3, the fact that antigen presentation to B cells is mainly cell-mediated and not simply by diffusion of antigen, implies an extensive regulation of this process.

1.5 B cell immunity

The main function of B cells is to produce pathogen-specific antibodies to counteract nascent infections. The first step in the B cell activation process consists of the recognition of antigens through the BCR on the surface of macrophages, DCs or FDCs as explained in the previous section. However, recognition of antigen is not enough to induce proliferation and differentiation of B cells into antibody-secreting cells. For this to happen, B cells need to receive a second activation signal from T cells. In the case of peptidic antigens, this help is provided by TfH (follicular helper) cells and in the case of lipidic antigens the help is provided by NKT cells.

1.5.1 Signal 1: Antigen recognition

Antigen recognition by B cells induces the activation of intracellular signalling cascades and endocytosis of the antigen, which will be then processed into antigen-derived molecules and presented on the surface of B cells. Signalling through the BCR is initiated by the crosslinking of BCR molecules by the antigen. This BCR aggregation induces the activation of the Src tyrosine kinase Lyn, which phosphorylates the Igα and Igβ chains of the BCR. This phosphorylation induces the recruitment of Syk kinase to the BCR, which then recruits PLC (phospholipase C) γ2 and the GEF (guanine nucleotide exchange factor) Vav to form the signalosome complex. The assembly of the signalosome is completed when PI3K

(phosphoinositide 3-kinase) is recruited to the BCR by the positive co-receptor CD19 and the B cell adaptor protein BCAP (Harwood and Batista, 2009, Castello et al., 2013). All these molecules trigger the most important signalling cascades involved in B cell activation. Vav activates the Rho GTPase Rac, which induces the activation of MAPK (mitogen-activated protein kinase) signalling. PI3K mediates the induction of the Akt survival pathway and PLCγ2 cleaves phospholipids from the membrane into IP3 (inositol triphosphate) and DAG (diacylglycerol). IP3 induces the release of Ca^{2+} from the ER (endoplasmic reticulum) and the activation of the NFAT (nuclear factor of activated T-cells) pathway. DAG induces PKC (Protein Kinase C) activation, which results in the induction of the NF-κB pathway (Harwood and Batista, 2009). The onset of the different signalling pathways leads to the activation of several transcription factors and the transcription of genes involved in survival, proliferation and differentiation of B cells (Figure 1.5).

Once the BCR is triggered, the BCR-antigen complex is internalised inside the cell and delivered to the endosomal compartments. These endosomes then fuse with lysosomes to form autolysosomes, where all the antigens are degraded into smaller molecules, a phenomenon known as antigen processing. This degradation is due to the progressive acidification of the vesicles and the consequent activation of catalytic enzymes that work under low pH conditions. Antigen-derived molecules are then loaded onto either MHCII molecules in the case of peptidic antigens, or onto CD1d molecules in the case of lipidic antigens, and presented on the B cell surface (Clark, Massenburg and Zhang, 2003). The antigen-derived peptides loaded on MHCII are then recognised by T cells, while antigen-derived lipids loaded on CD1d are recognised by iNKT cells. In the next section, I will focus on the classical B cell-TfH cell interaction during a B cell response and at the end I will discuss the recent discoveries regarding B cell-iNKT cell interactions.

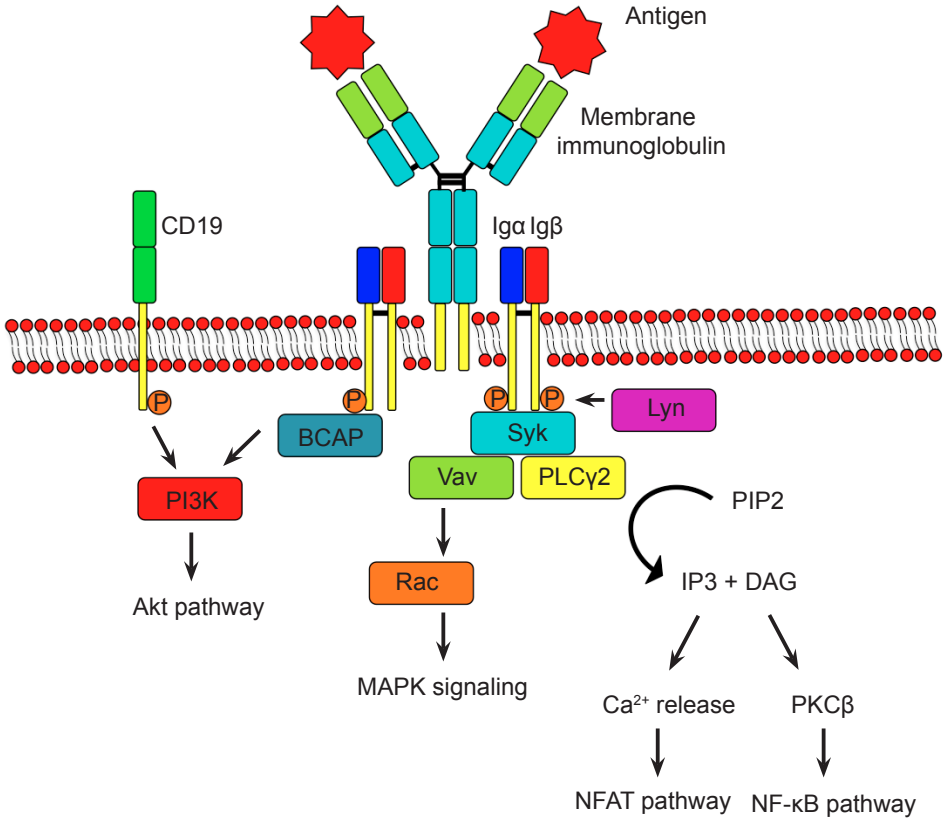

Figure 1.5 BCR signalling

Schematic depicting the early events in BCR signalling after antigen recognition. Antigen engagement leads to BCR crosslinking and phosphorylation of Igα and Igβ by the Src family kinase Lyn. This phosphorylation event initiates the formation of the signalosome, an assembly of intracellular signalling molecules, such as the kinase Syk, PLCγ2, PI3K and Vav. The signalosome allows the coordinated regulation of downstream cellular events, including signalling through secondary messengers such as calcium, the induction of gene expression and the internalisation of antigen for subsequent processing and presentation to T cells.

1.5.2 Signal 2: T cell help

As previously mentioned, after antigen recognition and internalisation through the BCR, B cells up regulate CCR7, which is the receptor for CCL19 and CCL21. These chemokines are present in high levels in the T cell zone, and induce the migration of activated B cells to the B-T cell border (Garside et al., 1998, Reif et al., 2002). There, they make contact with antigen-specific T cells that have been previously activated by migratory DCs. The B-T cell interaction is mediated by the T cell recognition of antigen-derived peptides in the context of MHCII in the surface of B cells (Amigorena et al., 1994). T cells then provide the second signal to B cells to

fully complete their activation. This interaction induces the expression of CD40 ligand (CD40-L) on the surface of T cells, which binds to CD40 expressed on the B cells and induces their proliferation (Lanzavecchia, 1985). Moreover, the level of MHCII on B cells increases after antigen recognition, allowing more, and better, presentation of antigenic peptides to the T cells. The expression of the adhesion molecules ICAM-1 (intercellular adhesion molecule 1) and LFA-1 (lymphocyte function-associated antigen 1) also increases on the B cell surface after activation. These proteins interact with their respective partners on the T cells, favouring a close contact between these two cell types to ensure an effective collaboration. Other proteins also increase on the surface of B cells after antigen recognition, such as the co-stimulatory molecules CD80 and CD86, and ICOS, which interacts with CD28 and ICOS-L respectively on the surface of the T cells. All these interactions between B cells and T cells favour the proliferation and differentiation of B cells into antibody-secreting cells. Importantly, the nature of this interaction is not only mediated by membrane receptors but also by soluble factors. For example, the secretion of cytokines by T cells, such as IL-4 and IL-21, is essential for B cell differentiation into effector cells (Ma et al., 2012) (Figure 1.6).

1.5.3 B cell fate

Following B-T cell interactions in the B-T cell border, T cells decrease the expression of CCR7 and increase the expression of CXCR5, the receptor for CXCL13. This phenomenon induces T cell migration from the T cell zone to the B cell follicles. On the other hand, after B-T interaction, B cells have two different fates. Some migrate to the medullary conduits where they differentiate into extra follicular plasma cells and produce the first wave of antibodies of the humoral response; mainly low-affinity IgM (MacLennan and Toellner, 2003). However, most of the B cells are attracted back into the follicles where they continue to proliferate and to form structures known as GCs (germinal centres) (Victora and Nussenzweig, 2012). These B cells now divide every 6 hours to become centroblasts, which will constitute the dark zone of the GCs. On the other hand, the light zone of these structures is mainly composed of FDCs, TfH cells and B cells. When centroblasts stop proliferating they abandon the dark zone of the GC and

move to the light zone where they become centrocytes (Victora and Nussenzweig, 2012). The differentiation of B cells in the GC allows for the production of antibodies that are more efficient in the control of pathogens during infection (Figure 1.6).

Several key processes take place in the GCs. The genes that codify the heavy and light chains of the antibodies undergo a series of important modifications that results in the production of antibodies with higher affinity for the antigen, a process defined as somatic hypermutation. Moreover, the constant regions of these antibodies are replaced by other isotypes, a process known as class switch recombination. Importantly, the GC also results in the development of adaptive immune memory (Victora and Nussenzweig, 2012).

Somatic hypermutation is the mechanism by which the genes that code for the variable regions of the light and heavy chains of the immunoglobulins undergo punctual mutations at a very high rate. As a consequence, after each cell division, daughter cells express different sequences in their variable regions to the original lymphocyte (Jacob et al., 1991). This process is initiated by the enzyme AID (activation induced cytidine deaminase), which is selectively expressed in B cells. This enzyme operates directly on the VDJ rearranged regions by removing an amine group from the cytidines and converting them into uracils. These uracils are then eliminated from the DNA and replaced by other bases by enzymes that make copy errors, giving rise to mutations (Muramatsu et al., 2000). As the mutations occur randomly, only those that increase the affinity of the BCR for the antigen will be selected in the GC, while all the others do not progress. After proliferation and mutation in the dark zone, B cells migrate to the light zone where the selection of B cells with high affinity immunoglobulins takes place. Centrocytes are programmed to die by apoptosis in a relatively short time unless they receive survival signals from specific TfH cells. Those B cells that have increased the affinity of their BCRs for the antigen will have more chance to extract antigen from FDCs and present it to TfH cells to receive surviving signals. Following selection, high-affinity B cells return to the dark zone, where they further proliferate and mutate their BCRs. Following several cycles of migration between dark and light zones, B cells are able to produce antibodies with much higher affinity that the ones initially produced

by extrafollicular plasma cells (Victora et al., 2010, Victora and Nussenzweig, 2012, Gitlin, Shulman and Nussenzweig, 2014, Gitlin et al., 2015).

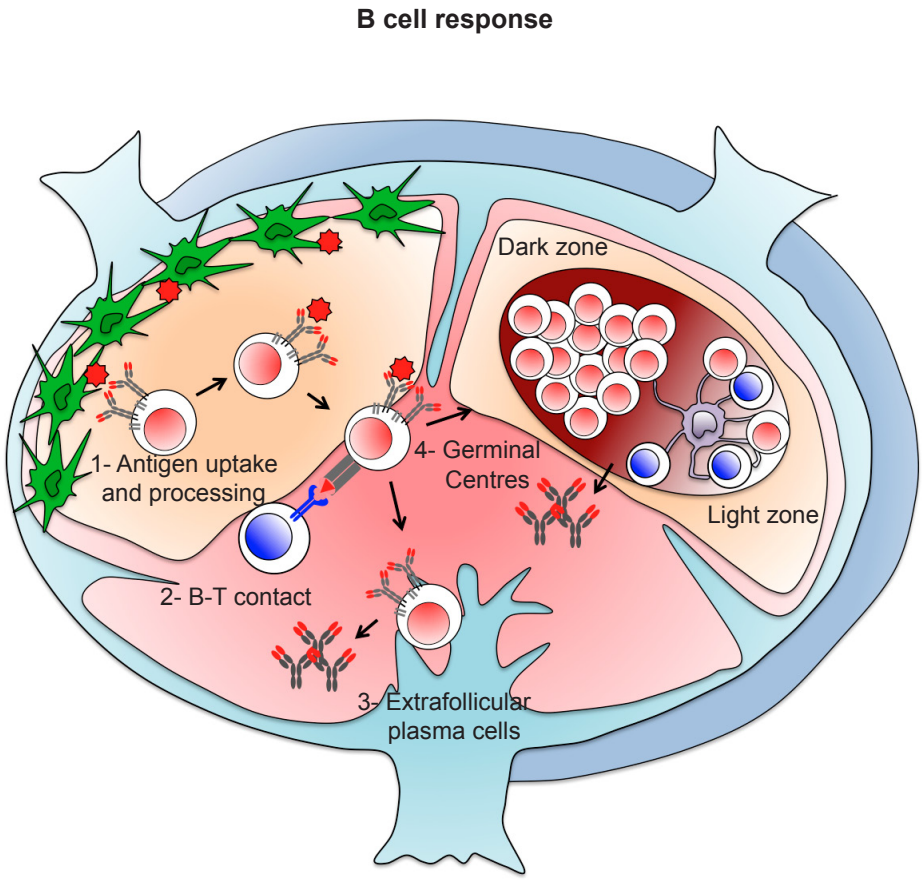

Figure 1.6 Representation of B cell response to pathogens

Schematic depiction of the main steps involved in B cell response following antigen challenge in the LN. After antigen recognition by B cells in the surface of SCS macrophages, DCs or FDCs, antigen is internalised, processed and presented in the surface of MHCII (1). B cells then migrate to the B-T cell border, where they receive T cell help (2). B cells can either directly differentiate into extrafollicular plasma cells to produce the first wave of low affinity antibodies (3) or enter into GCs (4). Once in the GCs, B cells undergo somatic hypermutation and class switch recombination, resulting in affinity maturation and production of high affinity antibodies.

In the GC there is a second important process that takes place: class switch recombination. During an immune challenge, the first wave of antibodies produced is always IgM. However, while the immune response progresses, antibodies with similar antigenic specificity but from different isotypes such as IgG, IgA and IgE are observed (Liu et al., 1996). This is the consequence of the removal of the μ and δ

C_H exons from the chromosome by a series of enzymes such as AID and endonucleases, and the association of the V_H portions with another C_H, such as γ, α or ε (Muramatsu et al., 2000). Class switch recombination is an essential part of the immune response and it has several advantages. For instance: a) IgG has a half-life in the serum of 21 days while that of IgM is only 5 days, b) the access of IgG to infected tissues is faster than IgM due to its lower molecular weight, c) IgG is the only immunoglobulin that crosses the placenta and confers immunity to the foetus and d) IgG but not IgM can stimulate different effector functions by binding to Fc receptors present on the immune cells (Vidarsson, Dekkers and Rispens, 2014).

As previously mentioned, the GC is the place where adaptive immune memory is generated. The B cells that survived the selection process differentiate into 2 types of cells: the ones expressing Blimp-1 (B lymphocyte-induced maturation protein-1) and XBP-1 (X-box binding protein 1) differentiate into long-lived plasma cells while the ones expressing Pax-5 (paired box 5) become memory B cells (Lin, Wong and Calame, 1997, Horcher, Souabni and Busslinger, 2001). Long-lived plasma cells migrate to the bone marrow due to the down regulation of CXCR5 and the up regulation of CXCR4, the receptor for CXCL12, which is highly expressed in the bone marrow. Long-lived plasma cells produce antibodies for prolonged times and maintain high levels of protective antibodies in the serum for several months or years (Nutt, Hodgkin and Tarlinton, 2015). On the other hand, memory B cells recirculate between the different lymphoid organs and they can also settle in these tissues. The expression of high affinity BCRs and high levels of MHCII by memory B cells favour their rapid response and protection against reinfection (Kurosaki, Kometani and Ise, 2015).

1.5.4 Antibody effector functions

The immune system has evolved in our vertebrate ancestors to produce highly specific antibodies to protect against infection. The survival advantage gained by producing these high-affinity antibodies must have been colossal, as their generation involves mechanisms of genetic recombination and somatic hypermutation. Therefore, why are antibodies so important in protecting us against

infection? One of their most important functions is to inhibit the infectious process by recognising and blocking the penetration of the cells by pathogens. Such antibodies are termed neutralising antibodies (Nutt, Hodgkin and Tarlinton, 2015). However, in most infectious processes, antibodies *per se* are unable to completely neutralise the pathogenic ability of the microorganism and to promote its clearance. Therefore, once they are bound to antigens and form immune complexes they can recruit additional effector mechanisms: the activation of the complement system and the induction of cellular responses by binding to the Fc receptors of innate immune cells (Vidarsson, Dekkers and Rispens, 2014). The activation of the complement system by immune complexes can induce inflammation, opsonisation of the pathogens, direct cytotoxic effect on the microorganisms, and potentiation of the B cell responses (Zipfel and Skerka, 2009). The binding of immune complexes to the Fc receptors of innate immune cells can also induce other effector functions:

a) Endocytosis of opsonised microorganisms and their elimination by phagocytic cells such as neutrophils and macrophages (Aderem and Underhill, 1999).

b) ADCC (antibody-dependent cell-mediated cytotoxicity), in which the microorganisms that are covered with specific antibodies are destroyed by innate immune cells such as NK cells, granulocytes and macrophages, that secrete granzymes, perforins and lysosomal enzymes (Delves and Roitt, 2000)

c) Cellular degranulation and increased production of cytokines, chemokines and inflammatory mediators by mastocytes, neutrophils, eosinophils and macrophages (Bryceson et al., 2005).

Antibodies therefore not only mediate the neutralisation of the pathogens to avoid the infectious process but also orchestrate a collection of innate effector mechanisms to mediate the clearance of invading pathogens.

1.5.5 Regulation of B cell immunity by NKT cells

As explained above, B cells need two different signals to become fully activated; the signal through the BCR that originates on recognition of antigen and the signal provided by T cells after antigen internalisation, processing and

presentation. In the case of peptidic antigens, the second signal is provided by TfH cells. For lipidic antigens however, it was not known until a few years ago who was giving this second signal. Two different studies revealed that NKT cells could provide this second signal to the B cells by recognising processed lipids in the context of CD1d through their restricted TCR (Barral et al., 2008, Leadbetter et al., 2008). By coupling peptidic antigens to glycosphingolipids, specific B cells internalise these antigens, process them and present the lipids in the context of CD1d. This CD1d-mediated presentation is essential to activate iNKT cells and induce the production of cytokines. Moreover, iNKT cells provide the help for B cells to proliferate and differentiate into extrafollicular plasma cells, which mediate the production of high titres of IgM and early class-switched antibodies (Barral et al., 2008, Leadbetter et al., 2008).

These groups further demonstrated in 2012 that iNKT cells engage in stable and prolonged cognate interactions with B cells *in vivo* after exogenous administration of lipids. These prolonged interactions induced the formation of early GCs. Furthermore, iNKT cells up regulate CXCR5 and PD-1 (programmed cell death 1) after interacting with B cells and then migrate to the B cell follicles, where they will later localise in GCs. As these characteristics are similar to those observed in TfH cells, the authors defined this population of NKT cells as NKTfH cells. The development of NKTfH cells requires high-level expression of Bcl-6 (B cell lymphoma 6 protein), signalling through the co-receptor CD28 and interaction with B cells. NKTfH cells secrete high levels of IL-21, which contributes to B cell mediated formation of GCs. However, unlike T cell-dependent GCs, those driven by NKTfH cells induce little affinity maturation and do not generate long lived plasma cells (Chang et al., 2012, King et al., 2012) (Figure 1.7).

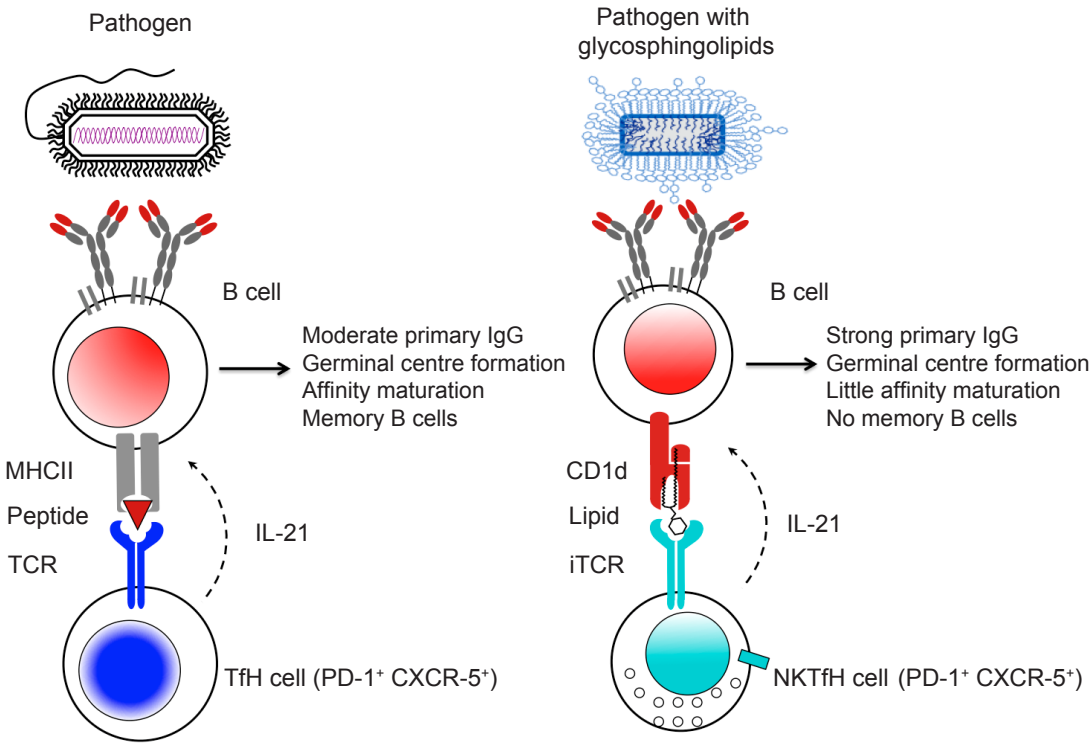

Figure 1.7 Differential outcomes of TfH and NKTfH cell help to B cells

B cell presentation of pathogen-derived peptides on MHCII to TfH cells is essential for the generation of high-affinity antibodies and memory responses. On the other side, presentation of pathogen-derived lipids on CD1d to NKTfH cells is necessary for a strong primary IgG response.

1.6 Thesis aim

The activation of B cells during an immune response and the production of pathogen-specific antibodies are highly regulated processes. Therefore, many factors can affect and shape B cell immunity. In the present thesis I will address three main different questions regarding B cell response to pathogens: How is B cell encounter of pathogens regulated during infection? Which processes are involved in the processing and presentation of antigen after pathogen encounter? How is the B cell response to pathogens modulated by different T cell populations?

In chapter 3, I will focus on the physiology of SCS macrophages during infection and how they regulate B cell encounter of antigen. SCS macrophages are important to capture pathogens entering through the lymphatic vessels and present them to B cells. To date, most studies have looked at the retention and

presentation of antigens at the initial stage of the immunisation process. However, infectious or inflammatory processes dramatically alter the architecture and function of the LNs. For instance, after local infection with LCMV (lymphocytic choriomeningitis virus) there is a global remodelling of the lymphoid tissue, involving an increase in the LN volume, in the B cell follicle size, and in the length of the HEV network (Kumar et al., 2010). Therefore, in chapter 3 I will look at the organisation of the SCS macrophage layer during infection/inflammation and whether an alteration in this population has an effect on the way B cells can respond to pathogens.

In chapter 4, I will briefly analyse the potential role of autophagy, an indispensable process for the recycling of cell components and for the fulfilment of cell energy demands, on the presentation of peptides and lipids by B cells. Moreover, I will analyse the signals that induce the formation of autophagosomes (the organelles involved in the autophagy process) and the signalling pathways involved.

Finally, in chapter 5 I will analyse the role of iNKT cells in modulating the B cell response during viral infection. iNKT cells have been shown to provide the necessary help to B cells in the presence of exogenous glycolipids (Barral et al., 2008, Chang et al., 2012). However, iNKT cell activation can occur even in the absence of pathogens containing these glycolipids, by a mechanism explained in chapter 5. In this case, the manner in which iNKT cells become activated *in vivo,* and their ability to regulate B cell responses, remain elusive. In chapter 5, by the use of several transgenic models, I will dissect the mechanisms involved in iNKT cell activation and the role of these mechanisms in promoting humoral responses during viral infection.

Chapter 2. Materials and methods

2.1 Materials

2.1.1 Media

Table 2.1 contains a complete list of all media that have been used in this study for the culture and maintenance of primary cells and cell lines and the growth of viruses and bacteria. RPMI, DMEM, Leibovitz, FCS (foetal calf serum), GlutaMax, HEPES (4-2-hydroxyethyl-1-piperazineethanesulfonic acid), penicillin/streptomycin and NEAA (non-essential amino acids) were purchased from Invitrogen, rmGM-CSF (recombinant mouse granulocyte macrophage colony-stimulating factor) was generated by Cancer Research UK, β-mercaptoethanol and BSA (bovine serum albumin) from Sigma, $NaHCO_3$ from Thermo, Na-Pyruvate from Lonza, DMSO (dimethyl sulfoxide) from Fisher Scientific, TPCK-treated trypsin from Worthington, Brain heart infusion broth from bioMerieux and Tryptic soy agar plates from BD.

Table 2.1 List of media and their composition

Medium	Components
RPMI medium	1x RPMI 1640 supplemented with 10 % FCS, 1x GlutaMAX, 10 mM HEPES, 10 U/ml penicillin/streptomycin, 50 µM β-mercaptoethanol
BM (bone marrow) - DCs medium	1x RPMI 1640 supplemented with 10 % FCS, 10 mM HEPES, 100 U/ml penicillin/streptomycin, 50 µM β-mercaptoethanol, 1mM Na-Pyruvate, 1x NEAA, 200 U/ml rmGM-CSF
Freezing medium	90 % FCS, 10 % DMSO
DMEM medium	1x DMEM supplemented with 10% FCS and 1x GlutaMAX
Infection medium	DMEM medium supplemented with 0.3% BSA + 1 µg/ml TPCK-treated Trypsin
Leibovitz medium (L-15)	1x Leibovitz L-15 supplemented with 10 mM HEPES, 100 U/ml penicillin/streptomycin and 0.075% $NaHCO_3$.

Brain heart infusion broth	1.75% Brain heart infusion, 1% digest of gelatine, 0.2% dextrose, 0.5%sodium chloride, 0.25% disodium phosphate
Tryptic soy agar plates	1.5% Bacto™ tryptone, 0.5% Bacto™ soytone, 0.5% sodium chloride, 1.5% agar and 5% sheep blood

2.1.2 Antibodies and tetramers

Table 2.2 provides a complete list of all antibodies and tetramers used in this thesis. It provides information about the reactivity, the clone, the conjugation, the manufacturer and the application.

Table 2.2 List of antibodies and their application

Reactivity	Clone	Conjugation	Manufacturer	Application
Isotype control	2A3	Non conjugated	BioXCell	Depletion
IL-2	JES6-1A12	Non conjugated	Biolegend	ELISA capture
	JES6-5H4	Biotin	Biolegend	ELISA detection
CD103	2E7	PE/APC	eBioscience	FC
CD138	281-2	PE	Biolegend	FC
CD19	1D3	PE-Cy7	eBioscience	FC
CD1d	1B1	PE	BD	FC
CD3	17A2	PE, APC-Cy7	Biolegend	FC
CD45.2	104	PerCP-Cy5.5	BD	FC
CD69	H1.2F3	PE-Cy7	BD	FC
CD8	53-6.7	PE	Biolegend	FC
CD95	15A7	FITC	eBioscience	FC
CXCR5	2G8	Biotin	BD	FC
DX5	DX5	FITC	eBioscience	FC
GL-7	GL7	A647	eBioscience	FC
Goat IgG	Polyclonal	A488, A647	Invitrogen	FC

IFN-γ	XMG1.2	PE-Cy7	eBioscience	FC
IgD	11-26C.2A	V450	BD	FC
IL-21	mhalx21	PE	eBioscience	FC
IL-4	11B11	PE	eBioscience	FC
Ly6G	1A8	PE, APC Non conjugated	BD BioXCell	FC Depletion
MHCII	M5/114.15.2	APC	eBioscience	FC
MyD88	Polyclonal	Non conjugated	R&D	FC
NK1.1	PK136	PE-Cy7 Non conjugated	eBioscience BioXCell	FC Depletion
PBS57-tetramer	N/A	APC	NIH tetramer facility	FC
PD-1	J43	FITC	eBioscience	FC
TCR β	H57-597	FITC	eBioscience	FC
α-Galcer-CD1d	L363	PE	eBioscience	FC
B220	RA3-6B2	PE, APC, PB APC-Cy7, NC650	BD eBioscience	IF FC
BCL-6	mGI191E	PE	eBioscience	IF
CD11b	M1/70	APC APC-Cy7, PB	Biolegend BD	IF FC
CD11c	HL3 N418	FITC PerCP-Cy5.5	BD Biolegend	IF FC
Langerin	929F3.01	A647	Dendritics	IF
Lyve-1	223322	Non conjugated	R&D	IF
Mac-3	M3/84	PE	BD	IF
Rat IgG	Polyclonal	A647	Invitrogen	IF
SIGN-R1	eBio22D1	A647	eBioscience	IF
Tubulin	Tub-1A2	Non conjugated	Sigma	IF

F4/80	BM8	PE, APC, PB	eBioscience	IF/FC
IL-7Rα	SB/199	PE	BD	IF/FC
CD169	Ser-4	A488, A555, A633	Hybridoma	IF/MF/FC
CD4	RM4-5	PE, eFluor450	eBioscience	IF/MF/FC
LC3B	Polyclonal	Non conjugated	Cell signalling	IF/WB (primary)
CD16/32	2.4G20	Non conjugated	BD	Neutralisation
E-cadherin	DECMA-1	Non conjugated	Millipore	Neutralisation
LFA-1	M17/4	Non conjugated	Abcam	Neutralisation
VLA-4	PS/2	Non conjugated	Abcam	Neutralisation
Mouse IgM	Polyclonal	Non conjugated	Jackson	Stimulation
		AF546	Invitrogen	IF/Stimulation
		Byotinilated	Southern Biotech	ELISA/ELISPOT
β-Actin	AC-15	Non conjugated	Sigma	WB (primary)
Mouse IgG	Polyclonal	HRP	Cell signalling	WB (secondary)
		A647	Invitrogen	IF
		Byotinilated	Southern Biotech	ELISA/ELISPOT
Rabbit IgG	Polyclonal	HRP	Pierce	WB (secondary)
		A488	Invitrogen	IF

IF (Immunofluorescence), FC (flow cytometry), MF (multiphoton), WB (Western blot).

2.1.3 Reagents

Table 2.3 provides a complete list of reagents used in the experiments described in this thesis.

Table 2.3 List of reagents and their application

Reagent	Manufacturer	Application
Chanazyne 2% Xylazine	Chanelle	Anaesthesia

IsoFlo® Isoflurane	Abbott	Anaesthesia
Narketan®-10 Ketamine	Vetoquinol	Anaesthesia
1,2-dioleoyl-*sn*-glycero-3-phsphocholine (DOPC)	Avanti Polar Lipids	Antigen preparation
EZ-Link-Sulfo-NHS-LC-LC-Biotin	Thermo	Antigen preparation
Hen egg lysozyme	Sigma	Antigen preparation
N-Cap PE-biotin	Avanti Polar Lipids	Antigen preparation
Ovalbumin	Sigma	Antigen preparation
Pierce™ Streptavidin	Thermofisher	Antigen preparation
Silica beads	Kisker GbR	Antigen preparation
Streptavidin polystyrene beads 0.093 µm	Bangs Laboratories	Antigen preparation
α-GalCer	Enzo life Sciences	Antigen preparation
Collagenase IV	Worthington	Cell Purification
DNAse I	Roche	Cell Purification
MACS B cell isolation kit	Miltenyi Biotec	Cell Purification
MACS $CD11c^+$ isolation kit	Miltenyi Biotec	Cell Purification
MACS $CD4^+$ T cell isolation kit	Miltenyi Biotec	Cell Purification
rm IL-2	R&D	ELISA
SIGMAFAST™ p-nitrophenyl phosphate tablets	Sigma	ELISA
Extravidin-Alkaline Phosphatase (AP)	Sigma	ELISA/ELISPOT
MultiScreen Filter Plates	Millipore	ELISPOT
SIGMAFAST™ BCIP®/NBT tablets	Sigma	ELISPOT

Cell stimulation cocktail plus protein transport inhibitor	eBioscience	FC
Celltrace violet	Invitrogen	FC
Cytometric Bead Array, Mouse Th1, Th2, TH17 cytokine kit	BD	FC
DAPI	Sigma	FC
Live/dead blue	Invitrogen	FC
Streptavidin A450	Invitrogen	FC
Cytofix/Cytoperm solution	BD	FC
Perm/Wash solution	BD	FC
Bovine Serum Albumin (BSA)	Sigma	IF
Fluoromount-G	Southern Biotech	IF
Goat serum	Sigma	IF
OCT mounting media	VWR	IF
SNARF	Invitrogen	IF
Triton X-100	Sigma	IF
CFSE	Invitrogen	IF/FC
NeutrAvidin yellow-green 0.2μm FluoSpheres	Invitrogen	IF/FC
3-methyladenine	Sigma	In vitro inhibition
Chloroquine diphosphate salt	Sigma	In vitro inhibition
Wortmannin	Sigma	In vitro inhibition
Diphtheria toxin	Sigma	In vivo inhibition
PBS/Clodronate liposomes	clodronateliposomes.org	In vivo inhibition
GM6001	Millipore	In vivo inhibition
Pertussis toxin	Sigma	In vivo inhibition
Kod Xtreme^{TM} Hot Start DNA Polymerase	Novagen	Long Range PCR

Gluture (topical tissue adhesive)	World Precision Instruments	MF
Platinum® SYBR® Green	Invitrogen	RT-PCR
QIAshredder (50)	Qiagen	RT-PCR
RNeasy Mini/Micro Kit	Qiagen	RT-PCR
SuperScript® III First-Strand Synthesis SuperMix	Invitrogen	RT-PCR
DIG-high prime DNA labelling and detection starter kit II	Roche	Southern blot
NEB buffer 1.1	New England Biolabs	Southern blot
Phusion® high fidelity DNA polymerase	New England Biolabs	Southern blot
Proteinase K	Sigma	Southern blot
Ribonuclease A from bovine pancreas	Sigma	Southern blot
SacI	New England Biolabs	Southern blot
Spermidine	Sigma	Southern blot
Ethidium bromide	Thermofisher	Southern blot/PCR
CpG (ODN 1826)	Sigma	Stimulation
Interferon-α	R&D	Stimulation
LPS from E. coli	Sigma	Stimulation
Prostaglandin E2	Sigma	Stimulation
rm IL-4	R&D	Stimulation
Tumour Necrosis Factor α	R&D	Stimulation
Agarose	Sigma	Virus preparation
Ultracentrifuge tubes	Beckman	Virus preparation
Complete protease inhibitors	Roche	WB
Dual-colour protein marker	Bio-Rad	WB

ECS solution	GE Healthcare	WB
Hyperfilm MP 24 × 30 cm	GE Healthcare	WB
Pre-cast 12% MiniPROTEAN TGX™ Gels 10 wells	Bio-Rad	WB
PVDF membranes	Bio-Rad	WB
ICG (Indocyanine green) dye	Sigma	Whole body imaging

2.1.4 Infectious agents

Table 2.4 provides a list of all infectious agents used in this thesis and their origin.

Table 2.4 List of infectious agents

Agent	Strain	Origin
Staphylococcus aureus	Subsp. Aureus Rosenbach	ATCC® BAA-1556™
Streptococcus agalactiae	Lancefield Group B, type Ib	ATCC® 12401™
Influenza A virus	Strain A/Puerto Rico/8/1934 H1N1	From Caetano Reis e Sousa
Vaccinia virus	Western Reserve	From Caetano Reis e Sousa

2.1.5 Buffers and solutions

Table 2.5 provides a comprehensive list of buffers and solutions used in the experiments described in this thesis.

Table 2.5 List of buffers and solutions

Buffer	Components
Crystal violet fixing solution	1x PBS, 0.05% crystal violet, 1% formaldehyde, and 1% methanol

DNA loading	0.25% bromophenol blue, 0.25% xylene lyanol FF and 30% glycerol
DNA lysis pH 8	100mM Tris-HCl, 5mM EDTA, 0.2% SDS and 200mM NaCl
FACS buffer	1x PBS, 1% FCS and 1% BSA
MACS buffer	1x PBS, 0.5% FCS and 2 mM EDTA
Maleic acid buffer pH 7.5	0.1M Maleic acid and 0.15M NaCl
$NaHCO_3$ 0.1M	0.1M $NaHCO_3$
Paraformaldehyde 4%	4% Paraformaldehyde
Phenol-chloroform-isoamyl alcohol	25:24:1 Phenol:chloroform:isoamyl alcohol saturated with 10 mM Tris pH 8,1
Pierce® Protein-free T20 (TBS) blocking buffer	From Thermo scientific
Red Blood Cell lysis	1 vol. Tris-HCl pH 7.6, 9 vol. NH_4Cl pH 7.2
SDS lysis	62.5 mM Tris pH 6.8, 2% SDS, 10% glycerol and 50mM DTT
Southern denaturation	1.5M NaCl and 0.5M NaOH
Southern detection pH 9.5	0.1M Tris-HCl and 0.1M NaCl
Southern neutralisation pH 7.4	1M Tris-HCl and 1.5M NaCl
Southern stringency wash 1	2x SSC and 0.1% SDS
Southern stringency wash 2	0.5x SSC and 0.1% SDS
Southern wash	Maleic acid buffer and 0.3% Tween 20
SSC	3M NaCl and 300mM Na citrate
Sucrose 30%	30% Sucrose
TBE pH 8.3	1% Tris, 0.5% Boric Acid and 0.01M EDTA
Tris Glycine SDS pH 8.6	25mM Tris, 192 mM glycine and 0.1% SDS

WB washing buffer	1x TBS and 0.1% Tween-20

2.1.6 Cell lines

The table 2.6 provides a comprehensive list of all cells lines used in this thesis.

Table 2.6 List of cell lines

Cell line	Species	Description	Source
DF-1	chicken	Immortalised cell line of chicken embryo fibroblasts	Courtesy of Dr Caetano Reis e Sousa
DN32.D3	mouse	$CD4^-CD8^-$ iNKT cell hybridoma	Courtesy of Dr Vincenzo Cerundolo
MDCK	dog	Kidney cells of a female adult Cocker Spaniel	Courtesy of Dr Caetano Reis e Sousa
Ser-4	rat	Hybridoma expressing the anti-CD169 antibody Ser-4	Courtesy of Dr Paul Crocker

2.1.7 Mice

Mice listed in table 2.7 were imported from the sources indicated. A reference for their first description is also given. Animals were used for experiments at an age of 8-24 weeks and were all in a C57Bl/6 background unless stated.

Table 2.7 List of mouse strains

Mouse strain	Description	Source
ASC	(Yamamoto et al., 2004)	Dr. G. Guarda
Batf3	(Hildner et al., 2008)	Dr. C. Reis e Sousa
BCAP	(Yamazaki et al., 2002)	Dr. T. Kurosaki
c-Cbl	(Murphy et al., 1998)	Dr. H. Gu
Caspase-1	(Kuida et al., 1995)	Dr. G. Guarda

CCR7	(Förster et al., 1999)	Dr A. Rot and Dr D. Withers
CD11c-Cre	(Caton, Smith-Raska and Reizis, 2007)	Dr. C. Reis e Sousa
CD11c-YFP	(Lindquist et al., 2004)	Dr. C. Reis e Sousa
CD169-DTR	(Miyake et al., 2007)	Riken Institute
CD19-Cre	(Rickert, Roes and Rajewsky, 1997)	Dr R. Rickert
$CD1d^{flox/flox}$ CD11c-Cre	Generated by me	Lymphocyte Interaction Lab
$CD1d^{flox/flox}$ CD19-Cre	Generated by me	Lymphocyte Interaction Lab
$CD1d^{flox/flox}$	Generated by me	Lymphocyte Interaction Lab
$CD1d^{flox/flox}$ Lyz2-Cre	Generated by me	Lymphocyte Interaction Lab
$CD1d^{flox/flox}$ Mb1-Cre	Generated by me	Lymphocyte Interaction Lab
CD1d1/2	(Mendiratta et al., 1997)	Dr A. Bendelac
CD45.1		Charles River
$Clec2^{flox/flox}$ CD11c-Cre	(Acton et al., 2014)	Dr C. Reis e Sousa
FLPo	(Wu et al., 2009)	Cancer Research UK
$IL\text{-}21^{-/GFP}$	(Lüthje et al., 2012)	Dr L. Corcoran
IL-2Rγ	(Shultz et al., 2005)	Dr D. Bonnet
Jα18	(Griewank et al., 2007)	Dr A. Bendelac
Langerin-DTR	(Kissenpfennig et al., 2005)	Dr C. Reis e Sousa
LC3-GFP	(Mizushima et al., 2004)	Dr S. Tooze
Lyz2-Cre	(Clausen et al., 1999)	Dr C. Reis e Sousa
Mb1-Cre	(Hobeika et al., 2006)	Dr M. Reth
MD4	(Goodnow et al., 1988)	Jackson Laboratory
MD4 TLR9	Crossed in the lab	Lymphocyte Interaction Lab
MyD88	(Adachi et al., 1998)	Dr C. Reis e Sousa

MyD88 $^{flox/flox}$	(Hou, Reizis and DeFranco, 2008)	Dr C. Reis e Sousa
MyD88$^{flox/flox}$ CD11c- Cre	Crossed in the lab	Lymphocyte Interaction Lab
MyD88$^{flox/flox}$ CD19-Cre	Crossed in the lab	Lymphocyte Interaction Lab
MyD88$^{flox/flox}$ Lyz2-Cre	Crossed in the lab	Lymphocyte Interaction Lab
MyD88/TRIF	Crossed in the lab	Dr C. Reis e Sousa
OT-II	(Barnden et al., 1998)	Charles Rivers
PLCγ2	(Takata, Homma and Kurosaki, 1995)	Dr T. Kurosaki
RAG2	(Shinkai et al., 1992)	Cancer Research UK
TLR7	(Lund et al., 2004)	Dr C. Reis e Sousa
TLR9	(Hemmi et al., 2000)	Dr S. Akira
TRIF	(Yamamoto et al., 2003)	Dr C. Reis e Sousa
ULK1	(Kundu et al., 2008)	Dr S. Tooze
ULK1/2	Crossed in the lab	Lymphocyte Interaction Lab
ULK2	(Cheong et al., 2011)	Dr S. Tooze
Wild-type		Charles River
μMT	(Kitamura et al., 1991)	Jackson Laboratory

2.2 Methods

2.2.1 Animal maintenance and generation

2.2.1.1 Animal breeding

Mice were bred and maintained at the animal facility of Cancer Research UK. All experiments were approved by the Animal Ethics Committee of Cancer Research UK and the United Kingdom Home Office.

2.2.1.2 Generation of transgenic animals

The generation of CD1d$^{flox/flox}$ animals is explained in detail in Chapter 5. For the generation of conditional mouse lines, CD1d$^{flox/flox}$ and MyD88$^{flox/flox}$ mice were crossed with animals expressing the Cre recombinase gene under the promoters of Mb1, CD19, CD11c and Lyz2. Genotyping of animals was performed by Transnetyx, Inc.

2.2.1.3 Bone marrow and foetal liver chimaeras

For the preparation of bone marrows, femurs and tibias of 8-12 weeks old wild-type and *Tlr9*$^{-/-}$ mice were harvested, cleaned of muscle and connective tissue and then cut at both ends under sterile conditions. The bone marrow was extracted by flushing through the bone ice-cold RPMI medium using a 1ml syringe and a 23G needle. For the preparation of foetal livers, livers were harvested from mouse embryos at day E14.5. Cell homogenates were generated by pressing the bone marrow or livers with the syringe plunge and passed through a 70µm nylon mesh cell strainer. Cells were washed in complete medium and either used immediately for transplant or frozen down in freezing medium until use. Mice of 4-6 weeks of age were kept on acidified water for one week prior and 3 weeks post irradiation treatment. 2 doses of 500 rad were given 4 hours apart to experimental animals. 24 hours later 2x10^6 bone marrow cells or one-third of a liver were injected i.v. in recipient animals in a total volume of 200µl of PBS. 8 weeks later, blood samples were collected and tested by flow cytometry for B and T cells reconstitution.

2.2.2 Cell Preparation, labelling and culture

2.2.2.1 Cell preparation

Single cells suspensions of lungs, LNs and spleens were obtained by pressing organs through a 70µm nylon mesh cell strainer with a plastic plunge in MACS buffer. When DC analysis was carried out, organs were previously incubated in serum-free RPMI medium supplemented with Collagenase IV (8 µg/ml) and DNAse I (20 µg/ml) for 30 minutes at 37^{o}C. For spleen and lungs, cell suspensions were further incubated with red blood cell lysis buffer for 5 minutes.

Purification of naive mouse B and T cells from spleen single cell suspensions was carried out by negative selection using a B- and a CD4+ T-cell purification kit respectively according to manufacturer's instructions and resulting in 95–98% B cell and 85-90% T cell enrichment. Purification of LN DCs was carried out by FACS (fluorescence-activated cell sorting) on a FACSAria (Becton Dickinson) using antibodies against MHCII (APC), CD11c (PerCP-Cy5.5), CD11b (Pacific blue) and CD103 (PE). Purification of LN iNKT cells was also performed by FACS using an antibody against TCRβ (FITC) and APC-conjugated CD1d-tetramer.

For the generation of BM-DCs, bone marrow cells were cultured at 37ºC in BM-DC medium, which was replaced with fresh medium every 48 hours. On day 5, adherent cells were harvested using PBS 2mM EDTA and DCs were enriched using a CD11c+ purification kit. DCs were incubated for 16 hours with 1µg/ml CpG or 10^{-6} M PGE2 + 1000 IU/mL IFN-α + 20ng/mL TNF-α.

2.2.2.2 Cell labelling

For labelling, single cells suspensions (10^7 cells/ml) were incubated for 10minutes at 37ºC in PBS supplemented with 1µM CFSE, 2µM SNARF or 5µM of Cell Trace violet (CTV) and then washed twice in complete medium.

2.2.2.3 Cell culturing

LN single cell suspensions and purified lymphocytes were normally cultured at 37ºC in RPMI medium unless differently specified. For cytokine production analysis, LN single cell suspensions were incubated 4 hours at 37ºC in RPMI medium supplemented with 1x Cell stimulation cocktail plus transport inhibitor. MDCK and DF-1 cells were cultured in DMEM medium at 37ºC.

2.2.3 Antigen preparation

2.2.3.1 HEL and OVA polybiotinylation

HEL and OVA were used at a concentration of 1mg/ml and mixed for 30 minutes at room temperature with 1 µg/ml of EZ Link Sulfo-NHS-biotin reagent. To remove excess free NHS-biotin, the mixture was dialysed against PBS at 4ºC.

2.2.3.2 Beads coating with biotinylated IgM, HEL and/or OVA

Neutravidin or streptavidin coated beads were washed in PBS 2% BSA to remove any trace of azide. For B-T cell coculture, mixtures of biotinylated IgM (1µg/µl beads) and increasing amount of biotinylated OVA (from 0.005 to 5 µg/µl beads) were prepared in a total volume of 100µl of PBS 2% BSA. For immunisation, a mixture of biotinylated HEL (0.75 µg/µl beads) and/or biotinylated OVA (0.25 µg/µl beads) was prepared in 100µl of PBS 2% BSA. Beads were resuspended in the different coating mixtures and incubated for 20 minutes at room temperature while shaking. Beads were then washed 3 times with PBS 2% BSA to remove any trace of unbound coating reagents.

2.2.3.3 α-GalCer-liposomes preparation

Liposomes were prepared as previously described (Barral et al., 2008). 5mg of DOPC, 100µg of N-Cap PE-biotin and 500µg of α-GalCer lipids were mixed and dried under argon and then under vacuum for 3hours. Lipids were resuspended in 10 ml of 25mM Tris, 150mM NaCl, pH 7.0 with vigorous mixing followed by 20-25 freeze-thaw cycles passing samples from liquid nitrogen to a 65ºC water bath in order to obtain a clear liposome solution. Liposomes were stored at 4ºC.

2.2.3.4 Beads coating with α-GalCer-liposomes and HEL or anti-IgM

For coating, 20 µl of silica microspheres were washed in PBS and incubated with 100µl of liposome preparation for 30 minutes at room temperature while shaking. Beads were then washed in FACS buffer, incubated with 20µg of streptavidin for 30 minutes, washed again and incubated 30 minutes more with either 20µg of biotinylated-HEL or biotinylated anti-IgM at room temperature. Silica beads were finally washed in FACS buffer and resuspended in 400µl of PBS.

2.2.4 Preparation of infectious pathogens

2.2.4.1 Bacterial culture

Group B streptococcus and *Staphylococcus aureus* were sourced from ATCC and were rehydrated in 1ml of brain-heart infusion broth and a few drops were used to inoculate a tryptic soy agar plate supplemented with 5% sheep blood which was cultured for 24 hours at 37ºC. Single colonies were picked and amplified

overnight in 5ml of brain-heart Infusion broth shaking at 37ºC and then diluted 1 in 20 in 100ml of brain-heart Infusion broth. 500µl samples were taken every 30 minutes to measure A_{600} or cultured at 37ºC over night on agar plates to estimate number of CFU (colony forming units)/ml. For experimental studies, cultures were stopped at 0.8-1.0 A_{600}, corresponding to about 10^9 CFU/ml. Bacteria were then pelleted, resuspended in PBS and injected in animals.

2.2.4.2 Preparation of viruses

MDCK cells were used for the amplification of PR8 influenza virus. Cells were grown in DMEM medium at 37ºC until confluence. Then, medium was replaced for infection medium and 1 PR8 viral particle/10 cells was added into the medium. Cells were incubated for 3-4 days at 37ºC until 100% of MDCK cells were dead. The medium containing the virus and dead cells was collected in a falcon and centrifuged at 4000 RPM for 5minutes to pellet dead cells. Supernatant was aliquoted and stored at -80ºC. For quantification of viral titer, MDCK cells were cultured in 6-well plates until 80% confluence. Cells were incubated with 200µl of different viral dilutions (10^{-3}, 10^{-4}, 10^{-5}, 10^{-6}, 10^{-7} and 10^{-8}) in DMEM alone for 1hour at 37ºC 5% CO2. Then, medium was replaced for L15 medium supplemented with 1% Agarose and 1 µg/ml TPCK Trypsin. After 3 days, the agarose was removed and 4ml of Crystal Violet fixing solution was added to each well for 15minutes at room temperature. Then, wells were washed with water and the number of plaques in the different dilutions was counted. The viral titer of the stock was calculated as: PFU (plaque forming units)/ml= Nº plaques x dilution factor. For concentration of viral particles, 15ml of medium containing virus was added on top of 22 ml of a 30% sucrose solution in ultracentrifuge tubes and spun at 25.000 RPM for 2hours at 4ºC in a SW32Ti rotor. The pellet was resuspended in PBS and frozen at -80ºC.

DF-1 cells were used for the preparation of VACV. Confluent cells were infected with 1 VACV particle/10 cells in DMEM medium. Cells were incubated for 3 days at 37ºC until 100% of DF-1 cells were dead. The infection medium was collected in a falcon and centrifuged at 4000 RPM for 5min to pellet the dead cells. Supernatant was discarded and dead cells were resuspended in 1 ml of PBS. After 3 cycles of freezing at -80ºC and thawing, tubes were centrifuged, pellet was discarded and

supernatants stored at -80ºC. Inactivation of VACV was carried out under 365 nm long-wave UV light for 10 minutes.

2.2.5 Infections and injections

2.2.5.1 Infections

Mice were anesthetised with isoflurane for footpad and ear infections or i.p. with Ketamine/Xylazine (100 mg/kg body) for intranasal infection. Anaesthetised mice were subcutaneously injected in the footpad with 10^4 PFU of vaccinia virus or 10^6 CFU of Group B *Streptococcus* in 20µl of PBS, ear inoculated with 10^7 CFU of *Staphylococcus aureus* in 5µl of PBS or intranasally inoculated with 10^2 PFU of influenza virus in 20µl of PBS.

2.2.5.2 Chemicals and antibodies administration

For inflammation induction, mice were injected in either hind footpads or ear pinna with PBS, 10µg of CpG or 50µg of LPS. For depletion of macrophages, mice were injected in the footpads or ear pinna with 5-20µl of empty or clodronate-loaded liposomes (ClodronateLiposome.com) or 50ng of diphtheria toxin 6 days before the experiment. For neutrophil depletion, mice received 500µg of anti-Ly6G i.p. or isotype control 24 hours before challenge and every day during the procedure. For NK cell depletion, mice received 500 µg of anti-NK1.1 i.p. or isotype control 24 hours before challenge and every day during the procedure. For the blockade of integrin or cadherin mediated adhesions, mice received in the footpad 50µg of anti-LFA-1 + 50µg of anti-VLA-4 or 50µg of anti-e-cadherin respectively. For chemokine signalling blockade, mice were injected with 500ng of pertussis toxin in the footpads. For metalloproteinase blockade, mice were injected i.p. with GM6001 (100mg/kg) every day over the period of the experiment. To analyse the role of the CLEC-2-podoplanin axis, 20µg of recombinant CLEC-2 Fc (kindly provided by Caetano Reis e Sousa) was injected in the footpads.

2.2.5.3 Antigen administration

For beads administration, Alexa488-conjugated avidin microspheres of 0.2µm diameter were loaded or not with biotinylated HEL and resuspended in 20µl of PBS for footpad injection. Approximately 1µl of the stock of fluorescent particles

(10^7 beads) were prepared per injection. For immunisations, 2.5µl of HEL-OVA beads or 1µl of HEL-α-GalCer beads were resuspended in 20µl of PBS and injected in the footpad of mice.

2.2.5.4 Adoptive transfer

5.10^6 B cells and/or 5.10^6 OT-II T cells were i.v. injected 24 hours before the initiation of indicated experiments. $3x10^6$ BMDCs in 20µl of PBS were injected in the hind footpads of anaesthetised animals.

2.2.6 B-T cell and B-NKT cell cocultures

2.2.6.1 B and T cell Proliferation Analysis

Purified splenic B cells from different mouse strains were labelled with CFSE while CD4+ T cells purified from the spleen of OT-II mice were labelled with Celltrace violet. B cells were cultured for 1hour at 37ºC at a density of $5x10^6$ cells/ml together with $2x10^{11}$ HEL-OVA-coated polystyrene beads/ml and then washed once in full media. B cells where then cultured together with OT-II CD4+ T cells both at a density of 10^6 cells/ml for 72 hours. Proliferation was measured by flow cytometry and IL-2 secretion by ELISA.

2.2.6.2 B - NKT cell coculture

Purified splenic B cells were cultured for 4 hours at 37ºC at a density of $5x10^6$ cell/ml together with $2x10^{11}$ anti-IgM-α-GalCer-coated silica beads/ml and then washed once in full media. B cells where then cultured together with DN32.D3 cells both at a density of 10^6 cells/ml for 24 hours. IL-2 levels were measured in the superanatants by ELISA.

2.2.7 Immunohistochemistry and confocal microscopy

2.2.7.1 Frozen sections

LNs were harvested from experimental animals and kept in PBS on ice before drying them on Wattman filter paper to remove any excess of water. Tissues were then placed at the centre of an OCT-filled mounting mould, which was then sunken for a few seconds in iso-pentane cooled over liquid nitrogen. Solidified OCT

was removed from the plastic mould and kept at -80ºC till sectioning. 10µm cryosections of LNs were cut at -20ºC using a Bright Cryostat OTF 5000 and placed on warm glass slides. Slides were stored at -80ºC until use. For immunofluorescence staining, tissue sections were thawed and dehydrated over silica beads for 30 minutes and then fixed for 10 minutes at room temperature with 4% paraformaldehyde. Slides were washed in PBS and, when intracellular staining was required, sections were permeabilised with PBS Triton 0.3% for 5 minutes. Then, slides were blocked with PBS containing 10% goat serum and 1% BSA for 30 minutes and further incubated for 1 hour at room temperature with appropriate antibodies diluted 1:100 in blocking buffer. Slides were then washed with PBS and glass coverslips were mounted onto tissue sections using Fluomount-G. Slides were kept in the dark at 4ºC till confocal microscopy imaging. Confocal microscopy images were acquired with an inverted Zeiss Axiovert LSM 780 microscope. Objectives used were 20x, 40x and 63x oil immersion objectives. Images were recorded with the same settings for control and treated LNs adjusted so that cells in treated LNs were clearly visible. Images were analysed using Imaris 6.3 × 64 software (Bitplane).

2.2.7.2 B cells on slides

$2x10^5$ purified naïve B cells were set in 8-well coverslips and incubated with 10µg/ml of labelled or unlabelled anti-IgM or 1µg/ml of CpG at 37ºC for indicated time points. Cells were fixed and permeabilised for 10 minutes on ice cold methanol, washed three times with PBS and stained for 1 hour with primary antibodies (1:100) at room temperature. Cells were washed three times and incubated for 1 hour more with secondary antibodies (1:100). Slides were finally washed again and glass coverslips were mounted onto them using Fluomount-G. Slides were kept in the dark at 4ºC till confocal microscopy imaging. Images were analysed using Imaris 6.3 × 64 software (Bitplane).

2.2.8 Multiphoton microscopy

Animals were injected in the hind footpads with 5µg of anti-CD169 A488 and/or CD4 eFluor450 and sacrificed after 10 minutes. Popliteal LNs were

immobilised on a glass-bottom 35mm culture dish by veterinary topical tissue adhesive. High resolution single xy plane images were acquired with an upright Olympus Fluoview FV1000 MPE2 Twin multi-photon microscope using a water-immersion 25 x 1.05 NA objective (Olympus XLPLNWMP) and a pulsed Ti:sapphire laser (Spectra Physics MaiTai HP DeepSee) tuned to 800nm. Collagen was detected as second harmonic generation signal through a bandpass filter 397-420nm, two-photon fluorescence of eFluor450 and Alexa488 were detected using 455-490nm and 500-540nm filters respectively. When simultaneous detection of eFluor450 and Alexa488 was performed, the amount of eFluor450 signal in the Alexa488 channel was determined with single labelled samples and removed from the Alexa488 channel using the channel arithmetic option in Imaris extensions. 3D imaging of explanted LNs was done using tiled z-stacks of 300µm depth, settings were chosen so that cells in treated samples were clearly visible while signal saturation in control samples was limited. For high resolution z-stacks, images of 1024 x 1024 pixels with 160nm pixel size and 0.7µm z-spacing were recorded while increasing laser power with depth, the display was adjusted using gamma = 1.7 to show cells with low and high intensities in a single image.

2.2.9 3View electron microscopy

SBF-SEM (serial block face-scanning electron microscopy) was carried out using a 3View2XP (Gatan, Abingdon) mounted on a Sigma VP field emission SEM (Zeiss, Cambridge), and images of the block face were recorded using a low voltage backscatter detector (Gatan, Abingdon). Sections were cut with a thickness of 100nm. Typical imaging conditions in variable pressure mode (10-30 pA), used to reduce charging when necessary: 20-25 nm pixels (xy), 2-3 kV, 3-5 us dwell time, 4096x4096 or 8192x8192 frame size. Typical imaging conditions in high vacuum mode: 21 nm pixels (xy), 1-1.3 kV, 4 us dwell time, 4096x4096 frame size.

2.2.10 Whole body imaging

Whole body imaging of lymphatic flow was carried out as previously described. 3 days after administration of CpG or PBS in the footpad, the lower half body fur of experimental mice was clipped. 24 hours later, 2µl of 1% indocyanine green dye was injected into the footpads of anaesthetised mice inside the IVIS Spectrum Whole Body Imaging System (Caliper Life Sciences). Image acquisition

and analysis was performed with Living Image 3 software (Caliper Life Sciences) using the following parameters: field of view 6.6, binning 8, and F-stop 2.70. Images were acquired every 4 seconds and sequences were mounted and annotated with ImageJ (NIH).

2.2.11 Flow cytometry

For flow cytometry staining of spleen and lung samples, one round of 5 minutes incubation in red blood cell lysis buffer was performed prior to staining. LN, spleen and lung single-cell suspensions were then incubated with anti-mouse CD16/32 (1:100) diluted in FACS buffer for 20 minutes on ice to block nonspecific antibody binding. Cells were washed in FACS buffer and stained for 20 minutes on ice with the appropriate combination of antibodies, tetramers or live/dead reagents diluted in FACS buffer. When using biotinylated antibodies, cells suspensions were washed following antibody labelling and incubated for 20 minutes on ice with fluorescently labelled streptavidin. Cells were washed and resuspended in FACS buffer. For intracellular staining, surface-stained cells were fixed and permeabilised with Cytofix/Cytoperm for 30 minutes on ice and washed twice with Perm/Wash buffer. Then, cells were incubated for 30 minutes with intracellular antibodies (1:100) in Perm/Wash buffer and for further 30 minutes with labelled secondary antibodies (1:100) when required. Finally, cells were resuspended in 400µl of FACS buffer and data were collected on a Fortessa cytometer (BD Biosciences) and analysed with FlowJo (TreeStar).

For the cytokine bead array measurements, the mouse Th1, Th2, Th17 CBA kit was used, which measures IL-2, IL-4, IL-6, IFN-γ, TNF-α, IL-17A and IL-10. Assay was performed according to manufacturer's instructions. All standards and samples were measured in duplicate. Data were acquired on a BD™ FACS Calibur flow cytometer.

2.2.12 RT-PCR

Lung single cell suspensions or sorted DCs or iNKT cells from mediastinal LNs were lysed and mRNA was extracted using RNeasy mini or micro Kit. Between

10^4 and 10^5 cells were used in each condition. mRNA was reversely transcribed into cDNA using random hexamers from the SuperScript III first-strand system. cDNA was amplified using custom primer sets (Sigma) and SYBR green PCR master mix on a 7500 real-time PCR system (Applied Biosystems). Table 2.8 provides a list of all DNA primers that were used in this thesis for mRNA quantification. The relative mRNA abundance of target genes was determined by means of the ΔC_T method:

$$relative\ X\ mRNA\ levels = 2^{(C_{T,X}-C_{T,R})_{control}-(C_{T,X}-C_{T,R})_{test}}$$

$C_{T,X}$= Threshold cycle for the gene of interest

$C_{T,R}$= Threshold cycle for the endogenous reference gene (*cph*)

Table 2.8 List of primers used for RT-PCR analysis

Name of target	Orientation	Sequence
A3GALT2	forward	5'-GGAACCATTTCGAGCCCTTGT-3'
A3GALT2	reverse	5'-GCGGCCACGGGAGATAATAG-3'
CPH	forward	5'-ATGGTCAACCCCACCGTG-3'
CPH	reverse	5'-TTCTTGCTGTCTTTGGAACTTTGTC-3'
HEXB	forward	5'-GACTGGAAGGTTGGTCCAAAGAC-3'
HEXB	reverse	5'-TACAACAGCCGCGGGAACATC-3'
IFN-γ	forward	5'-ACTGGCAAAAGGATGGTGAC-3'
IFN-γ	reverse	5'-TGAGCTCATTGAGAATGCTTGG-3'
IL-21	forward	5'-TCAGCTCCACAAGATGTAAAGGG -3'
IL-21	reverse	5'-GGGCCACGAGGTCAATGAT-3'
IL12p40	forward	5'-GGAAGCACGGCAGCAGAATA-3'
IL12p40	reverse	5'-AACTTGAGGGAGAAGTAGGAATGG-3'
NP1	forward	5'-CTCGTCGCTTATGACAAAGAAG-3'
NP1	reverse	5'-AGATCATCATGTGAGTCAGAC-3'

2.2.13 Western blotting

For western blot analysis, 10^6 primary B cells were stimulated for the indicated times and concentrations with anti-IgM, IL-4, CpG and LPS at 37ºC. When indicated, 100µM chloroquine was added to the medium 15 minutes before the end of incubation. After incubation, cells were pelleted and lysed with SDS lysis buffer and boiled for 5 minutes at 100ºC. Samples and ladders were loaded on pre-cast 4-20% Mini-PROTEAN® TGX™ gels and ran for 35 minutes at a constant voltage of 200V. Proteins were transferred on PVDF membranes for 7minutes (25V, 2.5A) using the TransBlot® Turbo™ transfer system (170-4155, Bio-Rad). Membranes were blocked with 5% BSA for 1 hour at room temperature and incubated over night at 4ºC with primary antibodies diluted in western blot washing buffer. Membranes were washed three times and incubated 1 hour at room temperature with HRP-conjugated secondary antibodies diluted in western blot washing buffer. Membranes were incubated with ECL solution for 1 minute at room temperature. Chemiluminescence was detected with Hyperfilm and developed in a JP-33 (Jpi) film developer. For quantifications, developed chemiluminescence films were scanned using a CanoScan 8800F (Canon) at a resolution of 300 dpi. Total fluorescence of bands was measured in ImageJ (NIH) by drawing a box-shaped ROI around the specific band and using the background-subtracted total fluorescence as a measure for band intensity. This was done for the band of interest and - using the same ROI – for the band of the loading control of the specific lane. Intensities of bands of interest were normalised to intensities of corresponding loading controls. All lanes were then further normalised relative to unstimulated samples.

2.2.14 ELISA

ELISAs (enzyme-linked immunosorbent assays) were used to quantify the production of cytokines and antigen-specific antibodies. To measure IL-2 production, 96-well plates were coated over night at 4ºC with anti-mouse IL-2 (1:125, clone JES6-1A1) in 0.1 M $NaHCO_3$. Plates were washed with PBS 0.01% Tween and then blocked for 1 hour at room temperature with PBS 2.5% FCS. Plates were then incubated for 4 hours at room temperature with co-culture

supernatants or serial dilutions of recombinant mouse IL-2 as standard. Plates were washed with PBS 0.01% Tween and probed for 1hour at room temperature using a biotinylated antibody against mouse IL-2 (1:500, clone JES6-5H4) diluted in PBS 2.5% FCS. Plates were then washed with PBS 0.01% Tween, incubated for 30 minutes at room temperature with streptavidin-AP (1:5000) in PBS 2.5% FCS and then finally washed again in PBS 0.01% Tween. To measure PR8-specific antibodies, plates were coated with 1µg/ml of PR8 virus in PBS over night at 4ºC, blocked with Pierce protein-free solution for 2 hours at room temperature and then incubated for further 2 hours with serial dilutions of blood serum collected at 9 days post-influenza infection. Plates were probed for 1 hour using biotinylated antibodies against mouse IgM or IgG (1:1000) diluted in Pierce buffer. All ELISA plates were developed using p-NitrophenylPhosphate. 405nm absorbance was detected using a SPECTRAmax190 plate reader (Molecular Device).

2.2.15 ELISPOT

ELISPOT (enzyme-linked immunosorbent spot) multiscreen filtration plates were activated with absolute ethanol, washed with PBS and coated overnight at 4ºC with 1µg/ml of HEL or VACV diluted in PBS. Plates were subsequently blocked for 1 hour with complete medium and incubated for 24 hours at 37ºC with serial dilutions of LN single cell suspensions. Plates were washed with PBS 0.01% Tween and incubated for 1 hour with 1µg/ml of biotinylated anti-IgM or anti-IgG diluted in PBS 1% BSA. Then, plates were washed and incubated for 1 hour with 1µg/ml streptavidin-alkaline phosphatase. Finally plates were washed and developed with SigmaFast BCIP/NBT. Enzymatic reactions were stopped by dH_2O wash and dots counted manually.

2.2.16 Southern blot

2.2.16.1 DNA extraction

Embryonic stem cells were digested in 500µl of DNA lysis buffer complemented with 30µl of Proteinase K (10mg/ml stock) overnight at 56°C with constant agitation. 500µl phenol-choloroform-isoamylalcohol were added each tube

under a chemical hood. After vigorous shaking, samples were spun for 5 minutes at maximum speed in a tabletop centrifuge. The upper layer was transferred to a new tube, mixed with 500µl of chloroform, shaken, and spun again. The upper phase was again collected, transferred into a new tube and the DNA was precipitated using isopropanol. After centrifugation, the supernatant was carefully removed and the DNA pellet was washed once with 70% ethanol. Finally, DNA was resuspended in dH_2O and the DNA concentration was measured with a Nanodrop.

2.2.16.2 DNA digestion

20-30µg of DNA were digested with the restriction enzyme SacI. The digestion mix was prepared as described in Table 2.9. Digestions were allowed to proceed overnight at 37°C. The next day, 10 units of SacI were added to the reaction in 5µl of the same buffer for 5 more hours at 37°C.

Table 2.9 Digestion mix for Southern blotting

Reagent	Final amount	Volume (µl)
DNA	20-30µg	10
SacI	60 units	3
NEB1 10x digestion buffer	1x	4
BSA 100x	200µg/ml	0.4
Spermidine 100mM	1mM	0.5
RNase A 50x	400µg/ml	0.8
dH_2O	to 40µl	21.3

2.2.16.3 Electrophoresis and capillary transfer

A 0.8% w/v agarose gel was prepared in TBE buffer and Ethidium Bromide was incorporated in the gel at 0.5µg/ml. Digested samples were diluted with 6x DNA loading buffer, loaded onto the gel and ran for up to 16 hours under a constant voltage of 20V. After migration, a picture of the gel was taken under a UV illuminator. This allowed to control for the efficiency of the digestion and to keep a record of the position of the different bands of the ladder. Gels were then submitted

to two sequential 30 minutes rounds of incubation in Southern denaturation buffer with gentle agitation. Efficient denaturation resulted in a change in the colour of the DNA loading dye to dark blue/green. Subsequently, gels were transferred into Southern neutralisation buffer and incubated 45 minutes at room temperature with gentle agitation, after which the buffer was replaced and neutralisation continued for further 15 minutes. A capillary transfer was then set up on an inverted gel tray in a pyrex container, which was covered with two sheets of Whatman 3MM filter paper wetted in 10x SSC. The gel was placed upside down on top of the Whatman paper and two individual nylon membranes cut to the size of the gels were placed directly on top of the gel. The container was filled with 10x SSC and all the edges were covered with parafilm to prevent evaporation. Subsequently, a thick pile of paper towels (15-20cm) was added on top and pressure was applied by putting an item of about 500g on top of the stack. After overnight incubation, the set up was dismantled and the gel was imaged under a UV lamp to check the transfer efficiency.

2.2.16.4 Probe preparation

To generate the Southern probes, regions of interest were amplified by PCR from genomic DNA using the Phusion high fidelity DNA polymerase system. The primers used were the following and the PCR mix was prepared as shown in Table 2.10.

Forward primer: 5'CTCCAGGCACCCTTTAGCTGCTA3'
Reverse primer: 5'TGTTTTCTTGAATACCATTCAAGCA3'

Table 2.10 PCR mix for probe generation

Reagent	Volume (µl)
Template DNA	1
Phusion^{TM} buffer 5X	4
10 mM dNTPs	0.4
Forward primer 10µM	1
Reverse primer 10µM	1

Phusion^{TM} DNA polymerase	0.2
dH_2O	12.4

The PCR program used for the amplification of the probe was the one shown in Table 2.11:

Table 2.11 PCR program for probe generation

Cycle Step	Temperature (^{o}C)	Time	Cycles
Initial denaturation	98	30seconds	1
Denaturation	98	10seconds	
Annealing	64	30seconds	35
Elongation	72	30seconds	
Final extension	72	10minutes	1

Amplification of the correct PCR products was checked by electrophoresis in agarose gel. PCR product were used to produce the labelled probe using the DIG High Prime DNA labelling and detection Starter Kit II following manufacturer's instructions. Successful labelling was checked by electrophoresis, as correctly labelled probes migrate less than their unlabelled counterparts in agarose gels. Labelled probes were kept at -20°C until use. Before use, probes were denatured at 70°C for 30 minutes and diluted in DIG Easy Hyb solution at the required concentration.

2.2.16.5 Hybridisation

Membranes were rinsed in 6x SSC for 5 minutes. Then, the DNA was cross-linked to the membranes by exposing the DNA-side of the membranes to UV source for 2 minutes at full power. Membranes were then hybridised using the DIG detection Starter Kit following manufacturer's instructions. Briefly, membranes were pre-hybridised for 1hour at 42°C in pre-heated DIG Easy Hyb solution in a roller bottle of a hybridisation oven. The pre-hybridisation solution was poored off, replaced with the probe and membranes were hybridised overnight at 42°C.

2.2.16.6 Detection

Membranes were washed 2 times for 5 minutes in Southern stringency wash 1 at 25°C in a hybridisation oven. Then, they were washed two times for 15 minutes in southern stringency wash 2 at 68°C, and subsequently for 15 minutes in southern wash buffer at room temperature. After these various incubations, membranes were blocked for 30 minutes in 100ml of southern blocking buffer (from the DIG detection Starter Kit). The solution was then replaced with 20ml of southern blocking buffer complemented with 2µl of anti-DIG antibody for 30 minutes. Membranes were washed twice for 15 minutes in southern wash buffer, and equilibrated for 5 minutes in southern detection buffer. Membranes were developed with CSPD ready-to-use solution following manufacturer's instructions. Chemiluminescence was detected with Hyperflim, which was developed using a JP-33 (Jpi) film developer. Developed films were scanned using a CanoScan 8800F (Canon) at a resolution of 600 dpi.

2.2.17 Long-range PCR

To screen embryonic stem cell clones, long-range PCR from genomic DNA was performed using the KOD Xtreme^{TM} hot start DNA polymerase system. The primers used were the following and the PCR mix was prepared as shown in Table 2.12.

Forward Primer: 5'GTTCTCTAGTGAGAGAGATGCCCATA3'

Reverse Primer: 5'CTACCCGTGATATTGCTGAAGAG3'

Table 2.12 PCR mix for long-range PCR

Reagent	Final amount	Volume (µl)
Xtreme Buffer 2x	1x	5
dNTPs (2mM each)	0.4µM	2
PCR grade water		0.2
Forward Primer 10 µM	0.3µM	0.3
Reverse Primer 10 µM	0.3µM	0.3

Template DNA (10 ng/µl)	2ng/µl	2
KOD Xtreme™ Hot Start DNA polymerase (1U/µl)	0.02U/µl	0.2
Total reaction volume		10

The PCR program used for the amplification was the one shown in Table 2.13. Amplification was checked by electrophoresis on agarose gel.

Table 2.13 Amplification program used for long-range PCR

Cycle Step	Temperature (°C)	Time	Cycles
Initial denaturation	94	2minutes	1
Denaturation	98	10seconds	
Annealing	60	30seconds	40
Elongation	68	8minutes	
Final extension	68	10minutes	1

2.2.18 Statistics

All statistical analyses were performed using Prism (GraphPad Software), two-tailed t-test, and p values <0.05 were considered significant

Chapter 3. Inflammation-induced disruption of the SCS macrophage layer shuts down B cell responses to secondary infection

3.1 Introduction

The highly organised architecture of the LN is critical for mounting effective immune responses against pathogens. One particular facet of this organisation is the layer of $CD169^+$ macrophages at the SCS floor. These macrophages are strategically positioned at the lymph-tissue interface to capture pathogens as they enter the LN. This capture not only prevents systemic dissemination of pathogens but also mediates the activation of innate and innate-like cells and the presentation of antigen to lymphocytes to initiate the humoral and cell-mediated immune response.

3.1.1 SCS macrophages prevent systemic spreading of pathogens

Several studies have shown that SCS macrophages are critical to prevent systemic dissemination of viruses and bacteria, such as VSV (vesicular stomatitis virus), VACV (vaccinia virus) and *Pseudomonas Aeruginosa* (Junt et al., 2007, Kastenmüller et al., 2012). In these studies, local depletion of SCS macrophages with clodronate liposomes, results in spreading of virus and bacteria to the blood, spleen and further LNs following local infection. Moreover, LN SCS macrophages function as crucial gatekeepers to the central nervous system by limiting its invasion following peripheral infection with neurotropic virus. This phenomenon is due to the ability of SCS macrophages to produce type I IFN following VSV infection, what limits intranodal nerves viral invasion. Therefore, local depletion of SCS macrophages results in paralysis and morbidity of mice due to invasion of VSV to the central nervous system (Iannacone et al., 2010).

The ability of SCS macrophages to limit pathogen dissemination is dependent on B cell-expressed lymphotoxin a1b2, which maintains a protective SCS macrophage phenotype in the LNs. SCS macrophages from mice lacking lymphotoxin a1b2 selectively in B cells display an aberrant phenotype: they

express high levels of SIGN-R1 and F4/80 and low levels of CD169, as medullar macrophages do. In the absence of lymphotoxin a1b2, SCS macrophages fail to limit pathogen replication and produce type I IFN, allowing fatal invasion of pathogens to central organs (Phan et al., 2009, Moseman et al., 2012).

3.1.2 SCS macrophages mediate activation of innate and innate-like cells

Recent studies have demonstrated an active cooperation between SCS macrophages and lymphoid subsets closely localised in the inter-follicular areas. Upon arrival of microbes in the afferent lymph, the inflammasome complex is activated on SCS macrophages, what induces the cleavage and release of active IL-1 and IL-18. IL-18, together with other cytokines such as IL-12 and type I IFN, induces the activation of NK cells, NKT cells, γδ T cells and memory $CD8^+$ T cells, which start producing high-levels of IFNγ within the first 2 to 4 hours of infection (Kastenmüller et al., 2012).

The IFNγ produced by these cells acts back on the SCS macrophages to enhance their capacity for intracellular resistance to microbe replication, potentially through up-regulation of iNOS (inducible nitric oxide synthase) (Kastenmüller et al., 2012). Additionally, the IFNγ production by these lymphoid populations induces the expression of CXCL9 by SCS macrophages. CXCL9 triggers the recruitment of LN-resident NK cells and memory CD8+ T cells to the SCS area through interaction with CXCR3. Once there, NK cells and memory CD8+ T cells commit into long-lasting interactions with SCS macrophages (Chtanova et al., 2009, Coombes et al., 2012, Garcia et al., 2012, Sung et al., 2012, Kastenmüller et al., 2013).

Furthermore, the IL-1 produced by SCS macrophages following pathogen recognition and inflammasome activation, mediates the recruitment of neutrophils from the periphery to the LNs. Once the neutrophils have reached the LN, they localise close to the SCS and they form highly dynamic clusters called neutrophil swarms. These neutrophil swarms result in localised loss of SCS macrophages and help to fight against extracellular pathogens (Chtanova et al., 2008, Kastenmüller et al., 2012).

The fact that the effector lymphoid cells are concentrated in close proximity to the SCS macrophages or re-localise close to them following infection, enhances the efficiency of the innate immune response and reduces the time needed for this response to develop in order to control lymph-born pathogens.

3.1.3 SCS macrophages present antigen to lymphocytes

SCS macrophages not only limit the systemic spreading of pathogens and activate innate and innate-like cells through the secretion of cytokines and chemokines but also mediate the presentation of antigen to cells from the adaptive immunity. Particulate antigens arriving through the lymphatic vessels to the SCS of the LN are captured by SCS macrophages. These macrophages are positioned such that their cell bodies are in the sinus lumen but their cellular processes extend into the adjacent B cell follicles. This location allows them to capture antigens from the SCS lumen with their cell bodies and trans-display these materials on processes extending into the follicles. In this way, B cells from underlying follicles can survey macrophage-bound antigens and cognate B cells can commit into long-last interactions with them to extract antigen for internalisation and following presentation to T cells (Carrasco and Batista, 2007, Junt et al., 2007, Phan et al., 2007). Furthermore, non-specific B cells can extract immune complexes from SCS macrophages by binding to the complement proteins associated with them and transport the immune complexes from the SCS to the FDCs to drive affinity maturation (Phan et al., 2007, 2009).

SCS macrophages not only present intact antigens to B cells but they can also behave as true antigen presenting cells by up-taking, processing and presenting pathogen-derived lipids to NKT cells in the context of CD1d. NKT usually reside in the inter-follicular areas of the LNs in close contact to SCS macrophages even before infection (Kastenmüller et al., 2012). Following antigen administration, NKT cells establish long-lasting interactions with SCS macrophages in a CD1d-dependent manner. This interaction is required for NKT cell activation, cytokine production and population expansion (Barral et al., 2010).

Interestingly, the antigen presentation ability of SCS macrophages is not restricted to pathogens but they can also phagocytose dead tumour cells transported via the lymphatics and subsequently crosspresent tumour antigens to CD8+ T cells. In fact, while subcutaneous immunisation with irradiated tumour cells protects mice from syngeneic tumour, the activation of tumour-specific CD8+ T cell and subsequent antitumor immunity are severely impaired in mice where $CD169^{+}$ macrophages were depleted (Asano et al., 2011).

The strategic position of SCS macrophages at the interface between the lymphatic fluid entrance and the LN immune cells makes them central in the initiation of the immune response. They not only avoid the systemic spreading of infectious pathogens but they also mediate the early activation of innate and adaptive immune cells.

3.2 Infection and inflammation disrupt SCS macrophage organisation in draining LNs

The microanatomy of the LNs defines the ability of the organism to respond to pathogens. At the same time, the global architecture of these organs is extremely adaptable to environmental changes. For instance, during infection or inflammation, draining LNs undergo a dramatic remodelling of their structure. These morphological changes include an increase in LN size and B cell follicle volume, an expansion of the HEV network and lymphatic vasculature and a substantial reorganisation of antigen presenting cells, lymphoid subsets and FRC network. These changes are in part caused by changes in chemokine levels, temporary shutdown of lymphocyte egress, recruitment of new lymphocytes and activated DCs and clonal expansion of antigen-specific lymphocytes (Odermatt et al., 1991, Heikenwalder et al., 2004, Mueller et al., 2007, Junt, Scandella and Ludewig, 2008, Scandella et al., 2008, Kumar et al., 2010, Acton et al., 2014, Astarita et al., 2015). However, the effect that infection has on the organisation of the SCS macrophage layer is not well defined. I therefore decided to study the

effect that inflammation or bacterial and viral infections have on the spatiotemporal organisation of this central population of cells.

3.2.1 Bacterial and viral infection interrupt the integrity of the LN barrier

To address this question, I proceeded to visualise the distribution of SCS macrophages in draining LNs after localised infection with a variety of pathogens. Initially, I chose a *Staphylococcus aureus* infection model, as *S. aureus* is the most common etiological organism of skin and soft tissue infection and is often involved in respiratory diseases and food poisoning (David and Daum, 2010). I infected C57BL/6 mice in the ear skin with 10^6 CFU of *S. aureus*, and one week after, superficial cervical LNs were harvested from infected and non-infected mice. Frozen LN sections were stained with anti-B220 to stain the B cell follicles and with anti-CD169 to stain SCS macrophages, then examined by confocal microscopy. In the steady state, LNs were relatively small, B cell follicles were structurally defined and a continuous layer of $CD169^+$ macrophages was observed surrounding the entire LN. In contrast, after bacterial infection the overall dimensions of the LNs increased around four-fold with a considerable enlargement of the B cell follicles (Figure 3.1A). Even though B cell follicles were dramatically enlarged, their defined structure was conserved. Surprisingly, these changes in LN and B cell follicle size were accompanied by an unprecedented disruption of the $CD169^+$ macrophage layer in the SCS area. This disruption resulted in the loss of macrophage layer continuity and integrity and a retraction of these macrophages to inner follicular areas of the LN (Figure 3.1A).

In order to quantify the extent of the macrophage layer disruption and the distance of macrophages to the LN border after infection, we developed, together with Andreas Bruckbauer, the disruption score and the distance score. For this, confocal images of LN sections were analysed in Imaris (Bitplane) using the build in tools for spot detection and surfaces as well as Matlab in combination with Imaris extensions. To measure the disruption score, $CD169^+$ cells were detected as surfaces using a low threshold value (14 for 8 bit files, smoothing 5µm, background subtraction 5µm) and the number of individual surface objects within a 50µm zone on the edge of the follicle was counted along the SCS interface. In LNs from non-

infected mice, macrophages form a continuous line at these low threshold settings and this resulted in a low number of surface objects. In contrast, disrupted macrophage layer in LNs from infected mice show a larger number of individual objects at the same threshold settings. The disruption score is the number of surface objects identified this way. To measure the distance of the macrophages to the follicle border, the position of the cells was detected using spot detection with background subtraction (15µm estimated diameter) and surfaces representing the follicles were created manually. The follicle edge was then detected as a 2D object using an in-lab developed Matlab script. The shortest distance of each cell to the edge was calculated. In brief, an increase of these two parameters, as observed after *S. aureus* infection, reflects an increase in the disruption of the macrophage layer and a retraction of these cells from the SCS, respectively.

The next question was whether macrophage layer disruption was a general feature associated with bacterial infections. For this, I chose another bacterial infection model. GBS (group B *Streptococcus*) was selected in this case as it represents a severe infectious disease in newborn babies (Iroh Tam, Delair and Obaro, 2015). Mice were infected with 10^6 CFU of GBS in the footpad, and 4 days later popliteal LNs were harvested and frozen. Cryosections were stained with anti-B220 and anti-CD169 and then examined by confocal microscopy. Similar changes in the LN architecture were observed in popliteal lymph nodes of infected mice, including increased LN and B cell follicle size and a disruption of the SCS macrophage layer (Figure 3.1B). This result demonstrates that the loss of macrophage layer integrity in draining LNs is a common feature associated with bacterial infections.

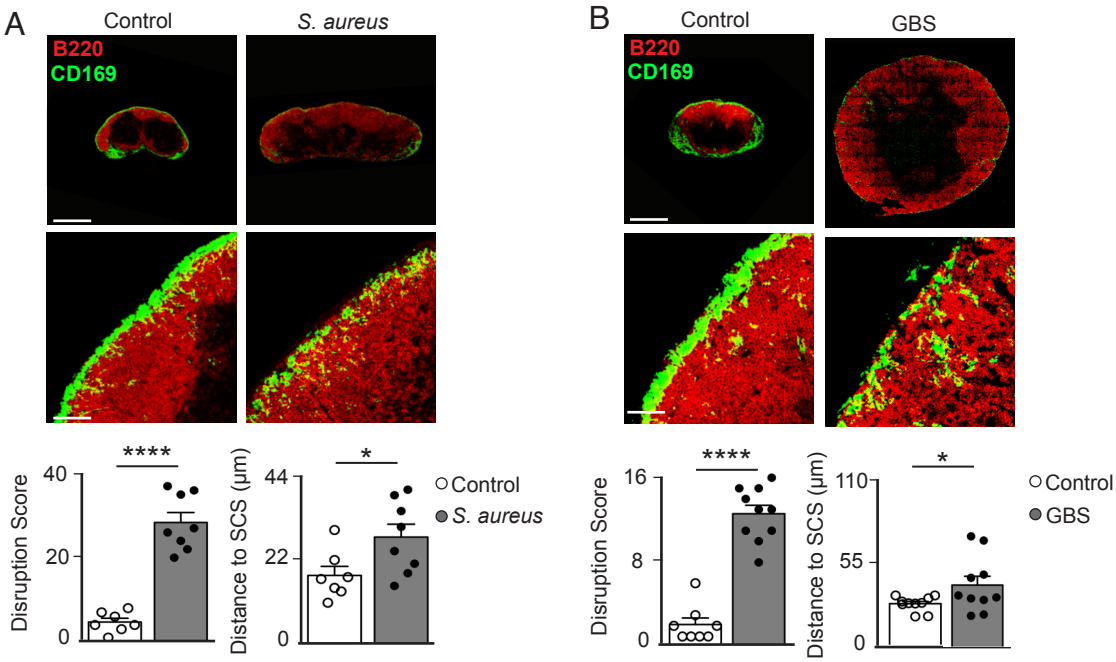

Figure 3.1 Bacterial infection disrupts SCS macrophage barrier in draining LNs

(**A**) Cervical or (**B**) popliteal LN cryosections stained for CD169 (green) and B220 (red) derived from mice administered with either PBS (control), (A) 10^6 CFU of *S. aureus* in the ear 7 days previously or (B) 10^6 CFU of GBS in the footpad 4 days previously. Scale bars, 300µm (top); 60µm (bottom). Bar charts show the quantification of SCS macrophage disruption and distance of macrophages to LN border in each condition for an individual experiment. Each dot represents the analysis of a distinct follicle. Mean ± s.e.m. Data are representative of at least three independent experiments with three mice per condition. Student t test, *p<0.05, ****p<0.0001.

Next, I analysed whether the disruption of the SCS macrophage layer was a process specifically related to bacterial infection or whether viral infection would also induce a similar phenomenon. Influenza A virus was chosen as a viral infection model due to its importance in the clinical setting. Influenza A virus is the main causative agent of influenza, commonly known as the “flu”, and complications with this disease can induce viral pneumonia, secondary bacterial pneumonia, sinus infections and worsening of previous health problems such as asthma or heart failure (Chowell et al., 2009, Perez-Padilla et al., 2009). Influenza constitutes a major threat to children, the elderly, and immunocompromised patients and causes 500.000 deaths per year worldwide (Waffarn and Baumgarth, 2011). Due to the high mutation rate of the virus, the influenza vaccine usually confers protection for no more than a few years and is therefore one of the most studied viruses in the

world, together with HIV (Impagliazzo et al., 2015). I then went on to infect mice intranasally with 200 PFU of influenza (strain A/Puerto Rico/8/1934 H1N1). Seven days later, mediastinal LNs were harvested, frozen, and cryosections stained with anti-B220 and anti-CD169. Confocal microscopy analysis showed a significant increase in B cell follicle size after infection together with a complete disruption of the SCS macrophage layer (Figure 3.2A) as observed during bacterial infection.

To assess whether macrophage disruption was a general process associated with viral infections, I chose VACV (vaccinia virus) as an alternative infection model. The study of VACV biology has been important for the development of vaccines against smallpox, as immune responses generated from VACV infection protects a person against lethal smallpox infection (Walsh and Dolin, 2011). I therefore went on to infect mice with 10^4 PFU of VACV in the footpad, and after 4 days popliteal LNs were harvested and stained with anti-B220 and anti-CD169 as before. Interestingly, VACV infection induced an increase of the B cell follicles and a similar disruption of the SCS macrophage layer in the draining popliteal LNs (Figure 3.2B). Taken together, the data above show that the disruption of the $CD169^+$ macrophage layer emerges as a common feature associated with bacterial or viral infections.

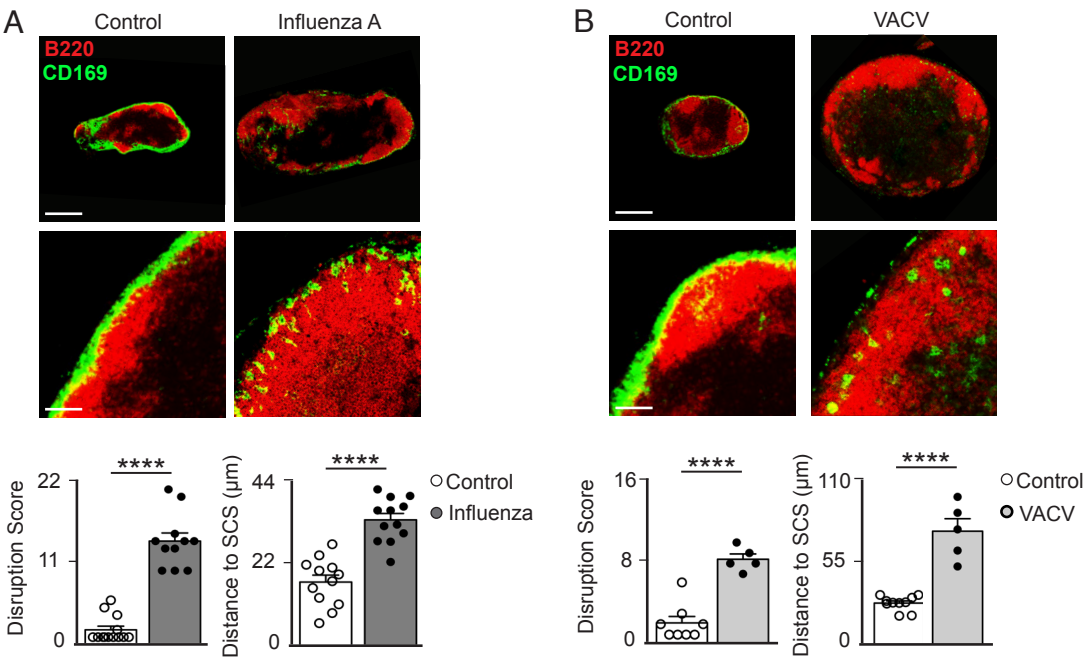

Figure 3.2 Viral infection disrupts SCS macrophage barrier in draining LNs

(A) Mediastinal or **(B)** popliteal LN cryosections stained for CD169 (green) and B220 (red) derived from mice administered with either PBS (control), (A) 10^2 PFU of influenza virus intranasal 7 days previously or (B) 10^4 PFU of VACV in the footpad 4 days previously. Scale bars, 300µm (top); 60µm (bottom). Bar charts show the quantification of SCS macrophage disruption and distance of macrophages to LN border in each condition for an individual experiment. Each dot represents the analysis of a distinct follicle. Mean ± s.e.m. Data are representative of at least three independent experiments with three mice per condition. Student t test, ****p<0.0001.

The next question was whether macrophage disruption in the draining LNs was specific to the process of infection or whether merely the arrival of antigen could induce a similar process. To address this question, I injected 10^6 inert beads or 10^4 UV-inactivated PFU of VACV into the footpad of mice. After 4 days, popliteal LNs were harvested, cryosections were stained with anti-B220 and anti-CD169 and then analysed by confocal microscopy. Neither enlargement of the B cell follicles nor disruption of the macrophage layer was observed in either case. This result indicates that infection, or a process associated with it, is necessary for the induction of the macrophage layer disruption (Figure 3.3).

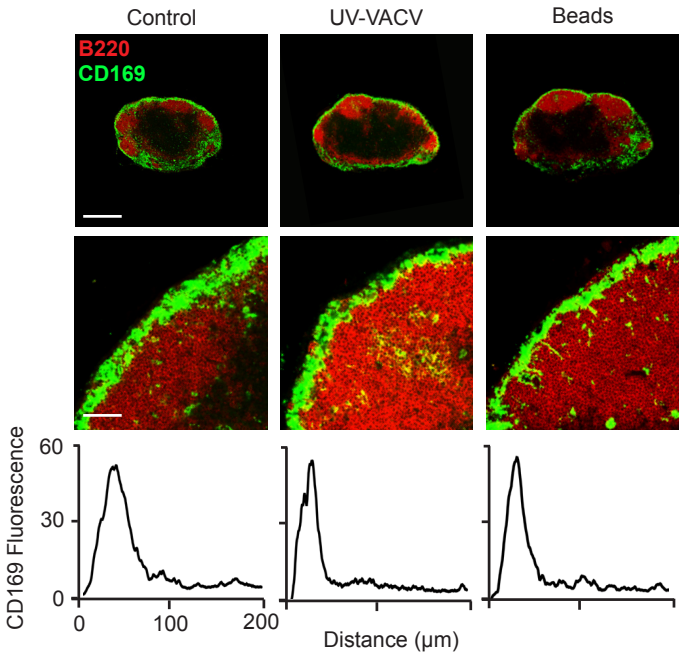

Figure 3.3 Inert antigens do not disrupt SCS macrophage barrier

Popliteal LN cryosections stained for CD169 (green) and B220 (red) derived from mice that were injected with PBS, 10^4 PFU of UV-inactivated VACV or 0.2 µm inert beads in the footpad 4 days previously. Histograms represent CD169 fluorescence measured from the outer edge of the LN to the follicles. Data are representative of two independent experiments with two mice per condition.

Due to the complexity in the calculation of the disruption and distance scores, for some supportive experiments the disruption of the macrophage layer was analysed in a simpler way: CD169 fluorescence was measured from the outer edge of the LN to the follicles and mean fluorescence was represented in histograms. In the case of LNs from non-immunised mice, there is a peak of CD169 fluorescence in the histograms that corresponds to the continuous macrophage layer. In contrast, after infection/inflammation this clear peak of CD169 in the histogram is lost due to the loss of integrity of the macrophage layer.

3.2.2 Inflammation induces temporary disruption of the macrophage layer

To investigate whether the disruption of the SCS macrophage layer can occur as a direct consequence of the inflammation associated with the infection process, I went on to induce inflammation in the absence of infecting pathogens. For this, I used the TLR9 agonist CpG and the TLR4 agonist LPS. Unmethylated

CpG sequences in DNA molecules are relatively common in bacterial genomes or viral DNA in comparison to their rare abundance in vertebrate genomes (less than 1%). LPS is a large molecule consisting of a lipid and a polysaccharide and is commonly found in the outer membrane of Gram-negative bacteria. Recognition of CpG-rich motives in DNA by TLR9 and LPS on the cell surface by TLR4 elicits intracellular signalling, finally leading to pro-inflammatory response (Poltorak et al., 1998, Hemmi et al., 2000). Mice were injected in the footpad with PBS (control), 10µg of CpG or 50µg of LPS. Four days later, popliteal LNs were harvested and analysed. The overall dimensions of draining LNs were increased more than three times after CpG or LPS administration, presumably in part due to the expansion of $B220^+$, $CD3^+$ and $B220^-CD3^-$ cell populations as revealed by flow cytometry (Figure 3.4A). Cryosections from frozen LNs were stained with anti-B220 and anti-CD169. Confocal analysis revealed that TLR-mediated inflammation triggers a similar disruption of SCS macrophages as seen following bacterial and viral infection (Figure 3.4B). Furthermore, in these cases the retraction of $CD169^+$ macrophages to the inner follicular areas of the LN was more evident than during infection. This results in a substantial increase in the disruption and distance scores compared to LNs from non-immunised animals. All together, these results demonstrate that the inflammation process *per se* is sufficient to induce disruption of the SCS macrophage layer in draining LNs.

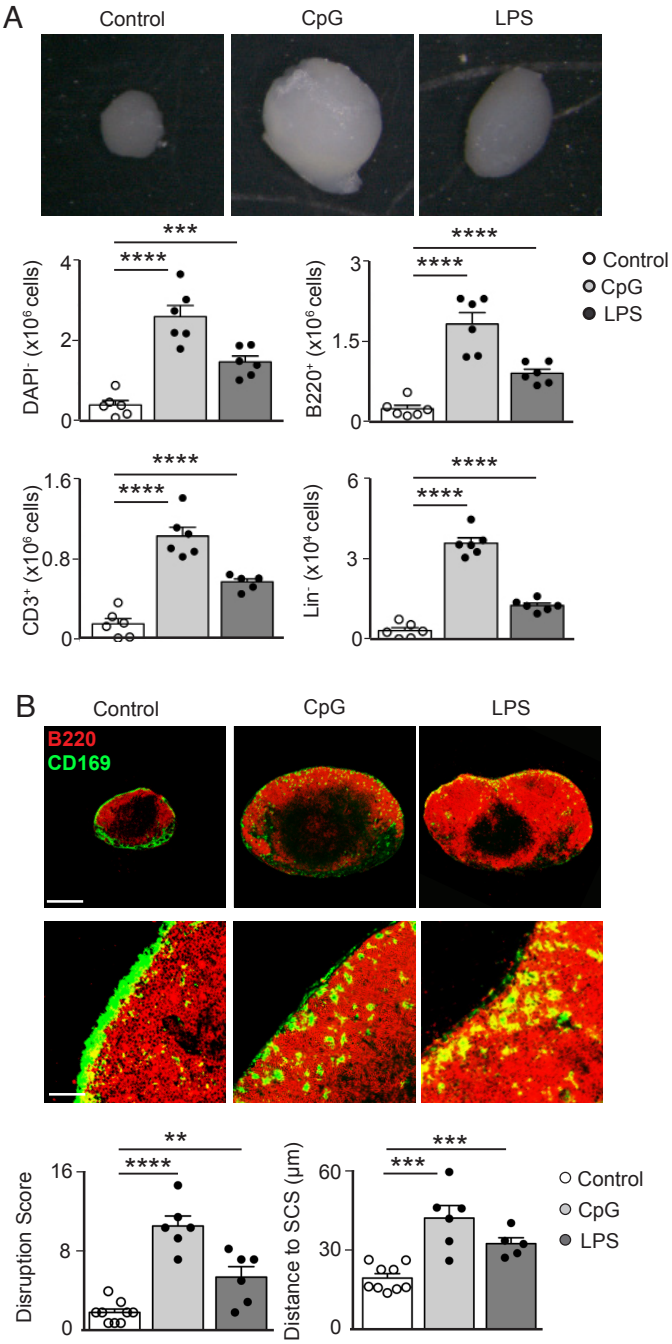

Figure 3.4 CpG and LPS induce SCS macrophage disruption in draining LNs

(**A**) Representative popliteal LNs harvested 4 days after footpad injection of PBS, 10µg of CpG or 50µg of LPS. Bar charts show flow cytometry quantification of $DAPI^-$, $B220^+$, $CD3^+$ and $B220^-CD3^-$ (Lin^-) cells from two independent experiments. Each dot represents a single mouse. (**B**) Popliteal LN cryosections stained for CD169 (green) and B220 (red) derived from mice treated as in (A). Scale bars, 300µm (top); 60µm (bottom). Bar charts show the quantification of SCS macrophage disruption and distance of macrophages to LN border in each condition for an individual experiment. Each dot represents the analysis of a distinct follicle. Data are representative of at least three independent experiments with

three mice per condition. Mean ± s.e.m. Student t test, **p<0.01, ***p<0.001, ****p<0.0001.

These findings are particularly intriguing, as SCS macrophages are a relatively static population in the LN; indeed complete recovery of these cells after depletion with clodronate liposomes can take up to 5 months (Delemarre et al., 1990). I visualised the rate at which the layer of SCS macrophages recovers after inflammation. Mice were injected with CpG in the footpad and popliteal LNs were harvested from 7 to 28 days later. Cryosections of the different time points were stained with anti-B220 and anti-CD169 and analysed using confocal microscopy. Interestingly, while considerable scattering of these macrophages was noted even up to three weeks after CpG administration, the compact uniform layer of CD169$^+$ macrophages at the SCS was re-established by day 28 (Figure 3.5). Thus, the disruption of the SCS macrophages layer after inflammation is a temporary process.

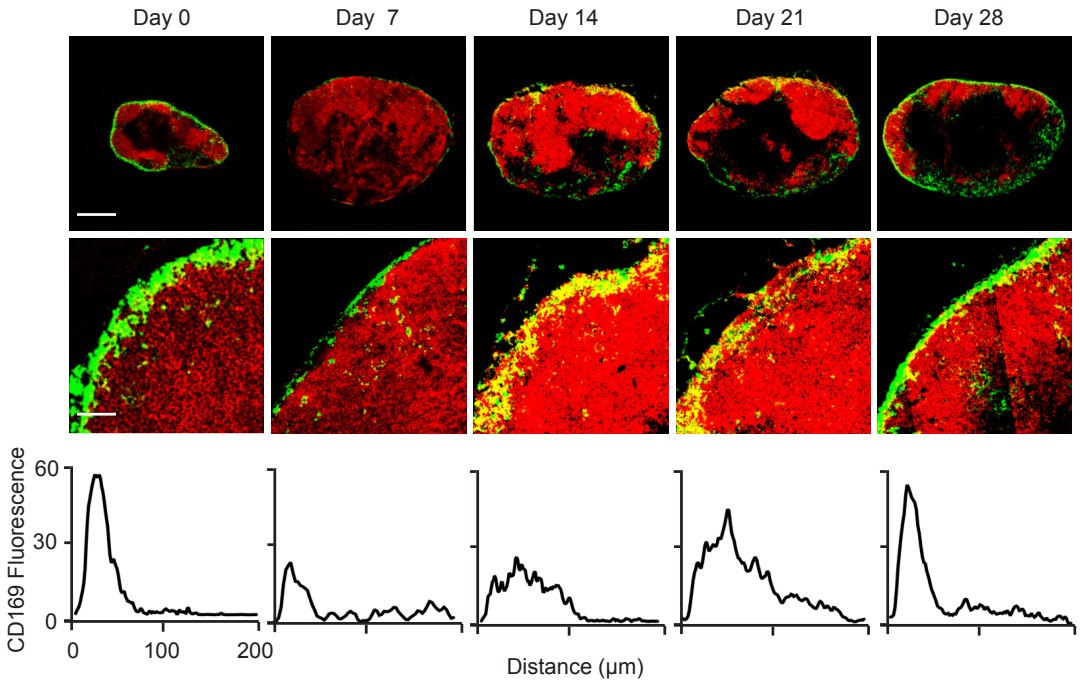

Figure 3.5 Disruption of the macrophage barrier is a temporary process

Confocal microscopy analysis of popliteal LN cryosections stained for CD169 (green) and B220 (red) after 1 to 4 weeks of footpad injection with CpG. Histograms represent CD169 fluorescence measured from the outer edge of the

LN to the follicles. Data are representative of two independent experiments with three mice per condition. Scale bars: 300µm (top); 60µm (bottom).

3.2.3 3D analysis of the LN macrophage layer during inflammation

To further characterise the loss of integrity in the SCS macrophage layer after inflammation, I employed two independent high-resolution technologies: 3D multiphoton microscopy and 3D electron tomography. These approaches allow 3D analysis of whole LNs instead of single section analysis.

Firstly, I used 3D multiphoton imaging of explanted popliteal LNs from mice that were injected with PBS (control) or CpG in the footpad on day 0, injected in the footpad with labelled anti-CD169 on day 4 and sacrificed after 10 minutes of antibody injection. The surrounding capsule of the LN (cyan) was detected by the second harmonic signal generated by the collagen fibers present in this structure and SCS macrophages were detected by CD169 labelling. In the steady state, macrophages with their characteristic cytoplasmic projections were found all around the LN surface with a uniform organisation (Figure 3.6). Interestingly, in LNs from CpG-treated mice, macrophages were found more distant from each other and their characteristic projections were no longer visible (Figure 3.6). A side view of the LNs from control mice showed a uniform layer of $CD169^+$ macrophages immediately below the collagen capsule. In contrast, this uniform layer of macrophages was lost in LNs from CpG-treated mice and macrophages were found to be more retracted from the collagen capsule, supporting the previous data obtained by confocal microscopy of cryosections (Figure 3.6).

The 3D projection obtained with this technology allowed us to quantify, with Andreas Bruckbauer, the density and number of $CD169^+$ macrophages in the LNs. Cell numbers were quantified by detecting $CD169^+$ cells using the spot detection tool in Imaris. The surface area of the LN spherical cap was measured using the second harmonic signal and the surface tool in Imaris, dividing by two to account for the outer and inner side of the 3D surface object. The macrophage density was calculated by dividing the cell number by the measured surface area. The total number of cells was estimated by assuming a spherical geometry of the lymph

node, estimating the surface of the sphere *A,* from the measured height *h,* and radius at the base *a* of the measured spherical cap, using $A = \pi(a^2 + h^2)$ and multiplying this area by the surface density calculated before. By employing this method, a number of $3x10^4$ $CD169^+$ macrophages was calculated to be in LNs from control mice with a mean density of $5x10^{-3}/\mu m^2$. Importantly, a significant decrease in both, number and density of $CD169^+$ macrophages was observed in LNs from CpG-injected mice (Figure 3.6).

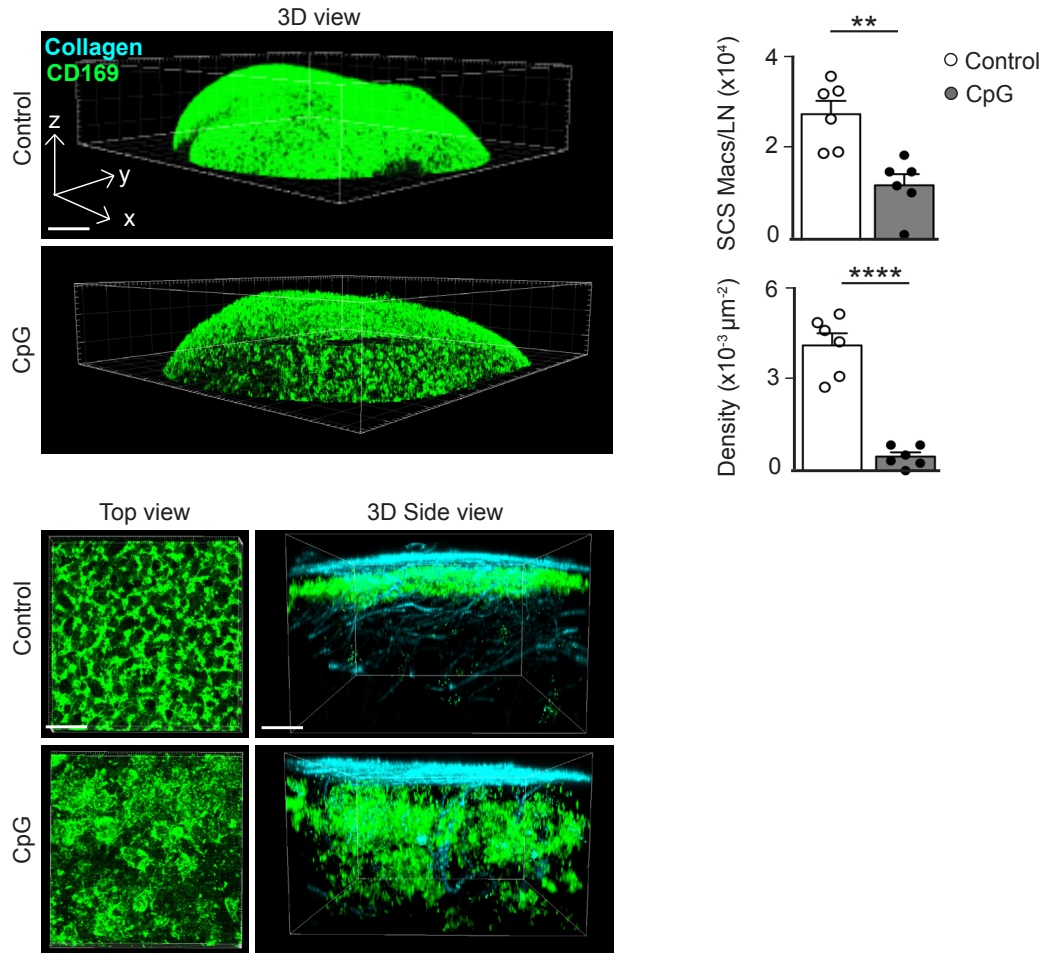

Figure 3.6 3D multiphoton analysis of SCS macrophage disruption

3D multiphoton microscopy of explanted popliteal LNs from animals injected in the footpad with either PBS or CpG (4 days) and anti-CD169 antibody (green) 10 minutes before dissection. Second harmonic signal generated by collagen fibrils is shown (cyan). Scale bars, 500µm (top); 40µm (bottoms). Bar charts show the number and density of $CD169^+$ macrophages in the SCS in each condition from three independent experiments. Each dot represents an individual LN. Mean± s.e.m. Student t test, **p<0.01, ****p<0.0001.

Secondly, together with the electron microscopy facility of CRUK and Angelo Castello, we used 3D electron tomography of explanted LNs. This technology allows the visualisation of the LN 3D structure and cellular and sub-cellular organisation without the need of antibody staining. 3D electron tomography scanning 100nm sections over a total distance of 100µm was performed on popliteal LNs harvested from mice after 4 days of PBS or CpG injection in the footpad. Macrophages have a very particular morphology and are easily identified due to their large size and abundant intracellular organelles (Sutton and Weiss, 1966). In the steady state, macrophages were positioned longitudinally on the inner wall of the SCS, with the cell body frequently projecting into the SCS lumen and the nucleus located within the parenchyma (Figure 3.7). In contrast, four days after CpG treatment, macrophages were located deeper in the follicles with cell bodies retracted from the SCS (Figure 3.7). In addition, there was an expansion of the SCS lumen after inflammation and a large influx of dendritic cells, easily detectable due to their convoluted cytoplasm and the presence of dendrites (Inaba, 1992). The combination of electron microscopy and 3-view analysis allowed me to quantify the macrophages' distance to the LN SCS, which is significantly increased during inflammatory conditions (Figure 3.7).

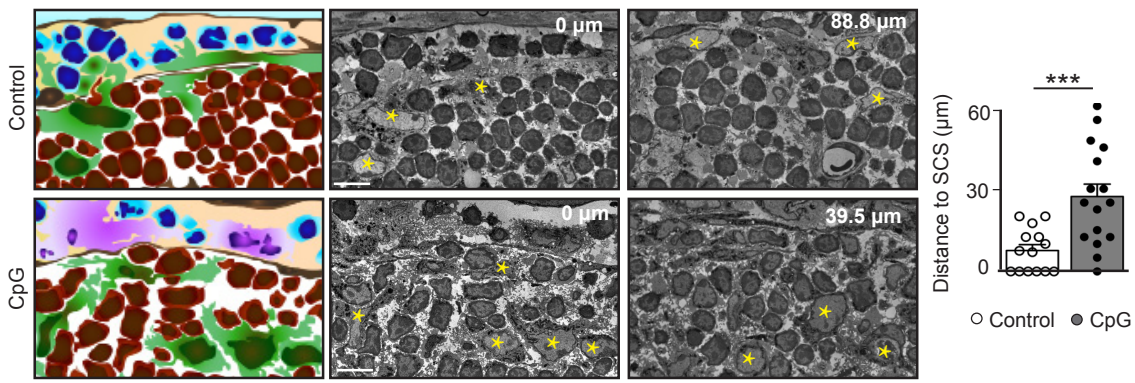

Figure 3.7 3D electron tomography analysis of SCS macrophage disruption

Representative Z sections (right panels) and schematics (left panels) of 3View electron microscopy analysis of popliteal LNs after 4 days of PBS or CpG administration. Yellow stars indicate macrophages. Scale bar, 5µm. Bar chart represents the distance of macrophages to LN SCS in an individual experiment. Each dot indicates a single macrophage. Mean ± s.e.m. Data are representative of two independent experiments with two mice per condition. Student t test, ***p<0.001.

Therefore, the characteristic disruption of macrophages at the SCS is not simply a result of cell loss as observed by 3D multiphoton microscopy but is due, at least in part, to the retraction of these cells towards inner follicular areas during inflammation.

3.2.4 Characterisation of the CD169$^+$ population following inflammation

CD169 is not only expressed by SCS macrophages but also by medullar macrophages and some DCs (Batista and Harwood, 2009, Asano et al., 2011). In order to confirm that the CD169$^+$ cells in which I focussed my study were coming from the SCS and not from somewhere else, I performed several *in situ* stainings of popliteal LNs cryosections from mice that were previously injected with PBS or CpG. CD169$^+$ cells expressed high levels of the macrophage markers Mac-3 and CD11b (Figure 3.8), suggesting that these cells are, in fact, macrophages. Moreover, if the disruption and retraction scores were calculated using CD11b or Mac-3 fluorescence instead of CD169, a similar increase in these parameters was observed following CpG-mediated inflammation (Figure 3.8).

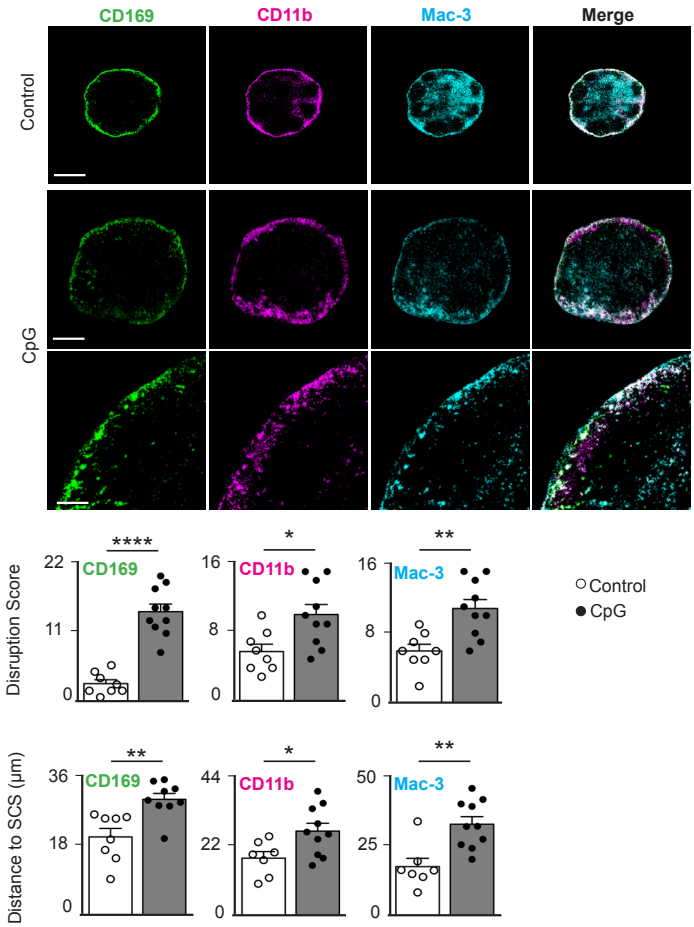

Figure 3.8 Disrupted SCS macrophages express CD11b and Mac-3

Popliteal LN cryosections from mice injected 4 days previously with PBS (control) or CpG in the footpad were stained for CD169 (green), CD11b (magenta) and Mac-3 (cyan). Scale bars, 300µm (top and middle); 60µm (bottom). Bar charts show the quantification of SCS macrophage disruption and distance of macrophages to LN border in each condition from three independent experiments with two mice per condition. Mean ± s.e.m. Each dot represents the analysis of a distinct follicle. Student t test, *p<0.05, **p<0.01, ****p<0.0001.

It was recently reported that perivascular macrophages and SCS macrophages express high levels of CD4, which was normally used as a specific marker to identify T cells (Gray et al., 2012, Abtin et al., 2014). I therefore checked the expression of CD4 by these CD169^{+} macrophages in steady state conditions and following CpG administration using confocal and 3D multiphoton microscopy. In addition to CD4^{+} staining in the paracortex, CD169^{+} cells in the SCS also expressed CD4 (Figure 3.9A-B), in agreement with these reports. Remarkably, under inflammatory conditions, CD169^{+} cells also express high levels of CD4 (Figure 3.9A-B).

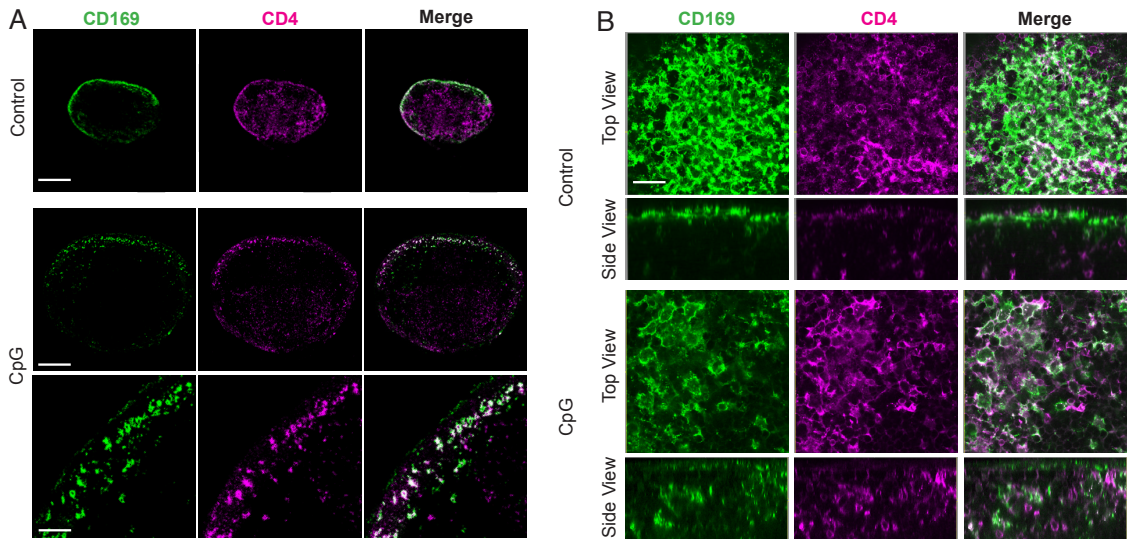

Figure 3.9 Disrupted SCS macrophages express CD4

(**A**) Popliteal LN cryosections from mice injected 4 days previously with PBS (control) or CpG in the footpad were stained for CD169 (green) and CD4 (magenta). Scale bars, 300μm (top and middle); 60μm (bottom). (**B**) Multiphoton microscopy of explanted popliteal LNs from animals injected in the footpad with either PBS or CpG (4 days) and anti-CD169 antibody (green) and anti-CD4 (magenta) 10 minutes before dissection. Top and side views of the LNs are shown. Scale bar, 40μm. Data are representative of two independent experiments with two mice per condition.

To add further evidence that these CD169$^+$ macrophages are coming from the SCS and not from the medulla, I stained cryosections with CD169, F4/80 and SIGN-R1. In the steady state, both SCS and medullary macrophages express CD169 while only medullary macrophages express F4/80 and SIGN-R1 (Figure 3.10A) (Moseman et al., 2012). The disrupted CD169$^+$ macrophage population observed in the SCS following inflammation was also negative for F4/80 or SIGN-R1 (Figure 3.10A). This result strongly suggests that the disrupted macrophage population corresponds to SCS macrophages and not CD169$^+$ macrophages migrating from the medulla during inflammatory conditions.

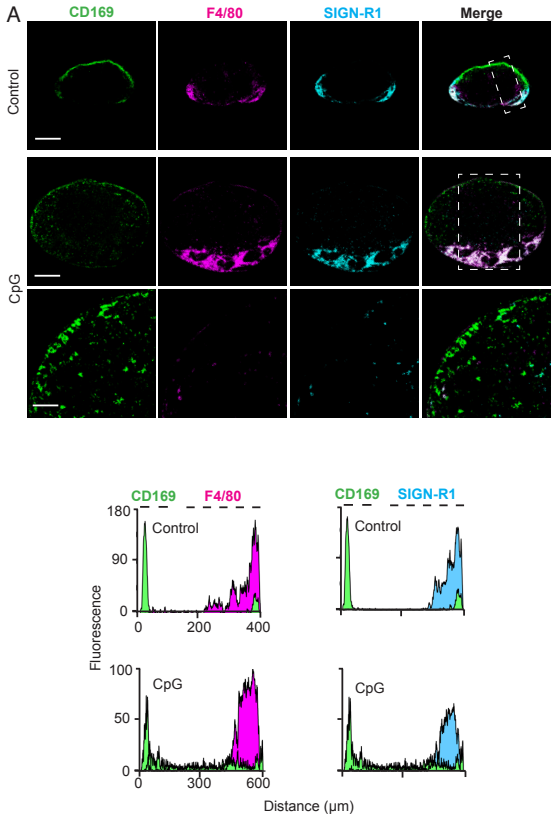

Figure 3.10 Disrupted CD169$^+$ macrophages are not medullar cells

Popliteal LN cryosections from mice injected 4 days previously with PBS (control) or CpG in the footpad were stained for CD169 (green), F4/80 (magenta) and SIGN-R1 (cyan). Scale bars, 300µm (top and middle); 60µm (bottom). Histograms represent the different markers' fluorescence measured from the outer edge to the LN interior on the dashed squares. Data are representative of two independent experiments with two mice per condition.

It was previously reported that when LN architecture is perturbed during tissue preparation, ILCs present in the LN could acquire membrane blebs from CD169$^+$ macrophages (Gray et al., 2012). To investigate whether these CD169$^+$ cells observed in the SCS following inflammation were, actually, macrophages and not ILCs that had acquired CD169$^+$ blebs, I performed an *in situ* staining of ILCs. Cryosections were prepared from popliteal LNs of mice previously injected with PBS or CpG and stained with anti-CD169 and anti-IL-7Rα. IL-7Rα is normally expressed by T cells, but ILCs express very high levels of this receptor, allowing their identification by immunohistochemistry (Gray et al., 2012). While IL-7Rα$^+$ cells were observed in close association with disrupted CD169$^+$ macrophages following inflammation, the markers did not co-localise with each other (Figure 3.11). This

result indicates that the disrupted CD169^{+} macrophages found in the SCS are not ILCs that had acquired CD169^{+} membrane blebs following inflammation. In conclusion, the cells on which I had focused my studies were SCS macrophages as they expressed high levels of CD169, CD11b, Mac-3 and CD4 but undetectable levels of F4/80, SIGN-R1 and IL-7Rα.

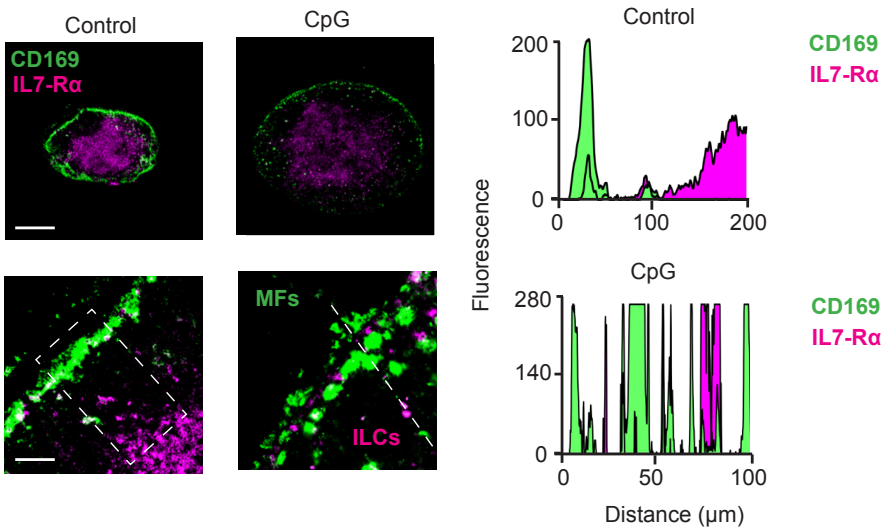

Figure 3.11 Disrupted CD169^{+} macrophages are not ILCs

Popliteal LN cryosections from mice injected 4 days previously with PBS (control) or CpG in the footpad were stained for CD169 (green) and IL-7Rα (magenta). Scale bars, 300μm (top); 20μm (bottom). Histograms represent the different markers' fluorescence measured from the outer edge to the LN interior on the dashed square and lines. Data are representative of two independent experiments with two mice per condition.

All together, the combination of different imaging techniques with various inflammation and infection models demonstrate that during an infectious or inflammation process there is a temporary loss of integrity of the SCS macrophage layer in the draining LNs. This disruption is the result of both, cell loss and retraction of these cells from the SCS to inner follicular areas.

3.3 DC arrival at draining LN during inflammation is necessary for SCS macrophage disruption

To dissect the mechanism by which inflammation triggers the alteration of SCS macrophage organisation I used a series of transgenic mouse strains, blocking antibodies, and depleting agents to target different components of the immune system.

3.3.1 Maintenance of the SCS macrophage layer in the steady state

Firstly, I investigated whether the localisation of $CD169^+$ macrophages in the SCS during the steady state was dependent on adhesion molecules or chemokines, as it is the case for other immune cells. For example, the retention of B cells in the marginal zone of the spleen is dependent on the integrins LFA-1/VLA-4 and their interaction with the ligands ICAM-1 and VCAM-1 (vascular cell adhesion protein 1), respectively (Lu and Cyster, 2002). The use of blocking antibodies against LFA-1 and VLA-4 (very late antigen 4) causes a release of B cells from the marginal zone. During LPS-mediated inflammation, B cells move away from the marginal zone due to down regulation of integrin-mediated adhesion (Lu and Cyster, 2002). Moreover, the retention of B cells in the marginal zone is also tightly regulated by the levels of sphingosine 1-phosphate (S1P) and the chemokine CXCL-13. While CXCL-13 attracts marginal zone B cells to migrate to the follicles, S1P retains B cells in the marginal zone (Cinamon et al., 2008). Another example of the regulated immune cell localisation by adhesion molecules is the retention of dendritic cells in the skin and epithelia through E-cadherin homotypic interactions with epithelial cells. When DCs detect the presence of pathogens, they down regulate E-cadherin levels so they can detach from the skin and epithelial cells, and migrate to draining LNs (Hammad and Lambrecht, 2008).

In order to address the requirement of adhesion molecules by $CD169^+$ macrophages to reside in the SCS under steady state conditions, I attempted to block these adhesion molecules using a combination of blocking antibodies. Mice were injected in the footpad with either i) PBS, ii) 50µg anti-LFA-1 + 50µg anti-VLA-

4 or iii) 50µg anti-E-Cadherin (DECMA-1). After 1, 2 or 4 days, popliteal LNs were harvested and cryosections stained with anti-B220 and anti-CD169. Confocal analysis revealed that the macrophage layer was intact following the blockade of integrin-mediated adhesion with anti-LFA-1 and anti-VLA-4 (Figure 3.12A). This is in line with previous observations, where, despite the striking effect that integrin-blocking antibodies have on marginal zone B cells, they do not affect marginal zone macrophages in the spleen (Lu and Cyster, 2002). In contrast, treatment with DECMA-1 induced partial scattering of $CD169^+$ macrophages, but they do not retract to the B cell follicles (Figure 3.12B). Therefore, $CD169^+$ macrophage localisation on the SCS under steady state conditions is independent of integrin-mediated adhesion, but might require E-cadherin interaction between themselves and other cell types in the SCS, such as sinus lining cells. Whether E-cadherin levels on $CD169^+$ macrophages are down regulated during inflammatory conditions is an interesting question that could be addressed in the future.

I then wondered whether the retention of $CD169^+$ macrophages in the LN SCS was dependent on chemokine signalling. To test this, I injected PBS (control) or *Pertussis* toxin in the footpad of mice. *Pertussis* toxin is an inhibitor of G protein-coupled chemokine receptors that blocks intracellular chemokine signalling (Cyster and Goodnow, 1995). After 4 days, popliteal LNs were harvested and cryosections stained with anti-B220 and anti-CD169. Surprisingly, a single injection of *Pertussis* toxin induced a complete disruption of $CD169^+$ macrophages in the SCS of the LNs (Figure 3.12C). This observation indicates that the retention of $CD169^+$ macrophages in the SCS of the LNs on steady state is dependent on chemokine signalling. Whether changes in chemokine levels during inflammation or infection induces the loss of the macrophage barrier integrity needs further investigation.

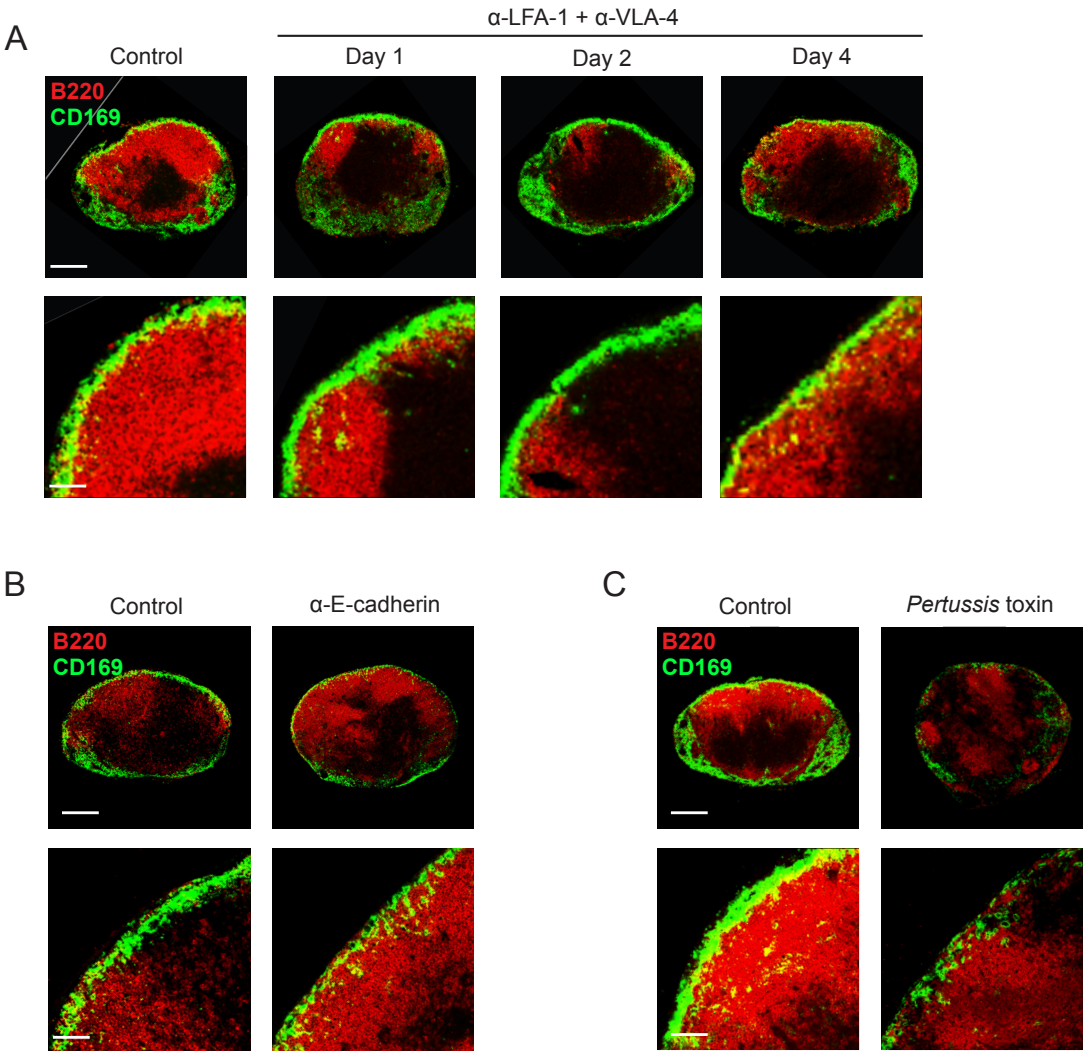

Figure 3.12 E-cadherins and chemokines maintain macrophage layer integrity

Popliteal LN cryosections stained for CD169 (green) and B220 (red) derived from mice administered in the footpad with either PBS (control) or (**A**) 50µg anti-LFA-1 + 50µg anti-VLA-4 for 1, 2 or 4 days, (**B**) 50µg of anti-E-Cadherin for 4 days or (**C**) 500ng of *Pertussis* toxin for 4 days. Scale bars, 300µm (top); 60µm (bottom). Data are representative of two independent experiments with three mice per condition.

3.3.2 Role of pyroptosis on macrophage layer disruption

I then moved on to investigate the mechanism responsible for the disruption of the macrophage layer in draining LNs during inflammatory conditions. It has recently been reported that during *Pseudomonas aeruginosa* infection, SCS macrophages produce high levels of IL-1β and IL-18 to activate innate effector cells, such as $CD8^+$ T cells, NK cells, NKT cells and γδ T cells (Kastenmüller et al.,

2012). IL-1β and IL-18 are initially synthetised as inactive forms pro-IL-1β and pro-IL-18, which are then cleaved to their active forms during inflammation (DINARELLO, 1998). This cleavage is mediated by Caspase-1, the main catalytic component of the inflammasome complex and by the adaptor protein ASC (van de Veerdonk et al., 2011). Usually, the activation of the inflammasome complex and the release of IL-1β and IL-18 during inflammation induces pyroptosis of the cells, which is a programmed cell death initiated during antimicrobial responses (Miao et al., 2010). I therefore wondered whether CpG-mediated inflammation would induce inflammasome-mediated activity on the macrophages that would lead to pyroptosis of these cells and depletion of them from the SCS.

In order to test the impact of pyroptosis on the disruption of SCS macrophages during inflammation, I injected CpG in the footpad of wild type, Caspase1-deficient and ASC-deficient mice. After 4 days of CpG injection in the footpad, popliteal LNs were harvested, frozen, and cryosections stained with anti-B220 and anti-CD169. Confocal analysis of LNs from Caspase-1 and ASC-deficient mice shows that the SCS macrophage layer was disrupted at a similar level as that observed in LNs from wild type mice (Figure 3.13). This demonstrates that pyroptosis, a death-related inflammatory response, might not be involved in disruption of SCS macrophage layer following inflammation.

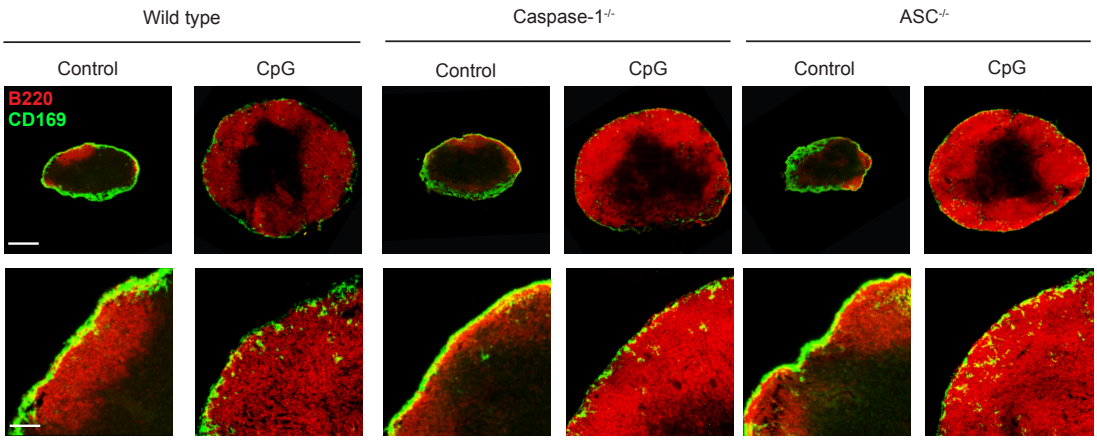

Figure 3.13 Macrophage layer disruption is not dependent on pyroptosis

Popliteal LN cryosections stained for CD169 (green) and B220 (red) derived from wild type, Caspase-1$^{-/-}$ or ASC$^{-/-}$ mice administered in the footpad with either PBS (control) or 10µg of CpG 4 days previously. Scale bars, 300µm (top); 60µm

(bottom). Data are representative of two independent experiments with four mice per condition.

3.3.3 Role of different immune cells on macrophage layer disruption

As intrinsic macrophage pyroptosis is not involved in the loss of layer integrity during inflammation, I next asked whether other immune cells would extrinsically induce this phenomenon. To start delineating this hypothesis, I took advantage of the CpG-mediated inflammation model and a series of mouse strains that are unable to respond to CpG (TLR9-deficient mice) or are impaired in TLR signalling due to lack of signalling adaptors (MyD88-deficient, TRIF-deficient and MyD88/TRIF-doubly deficient mice). Wild type mice and mice from these four strains were injected in the footpad with PBS or CpG and popliteal LNs were harvested after 4 days of injection. The overall dimensions of draining LNs were analysed and then LN cryosections were stained with anti-B220 and anti-CD169 to assess the organisation of SCS macrophages following inflammation. Mice deficient in either TLR9 or doubly deficient in MyD88/TRIF did not exhibit an increase in LN size and did not display SCS macrophage disruption as observed in wild type mice (Figure 3.14). This result indicates that CpG needs to signal through TLR9 and the adaptor proteins MyD88 and/or TRIF to induce inflammation. However, the TRIF adaptor is dispensable for the effect of CpG, as popliteal LNs were expanded and SCS macrophage layer was disrupted in TRIF-deficient mice (Figure 3.14). In contrast, the MyD88 adaptor is essential for this process, as MyD88-deficient mice do not exhibit LN expansion or SCS macrophage disruption during CpG-induced inflammation (later, Figure 3.17). These results are concordant with the notion that responses to CpG are mediated by TLR9 signalling via MyD88 (Hemmi et al., 2003).

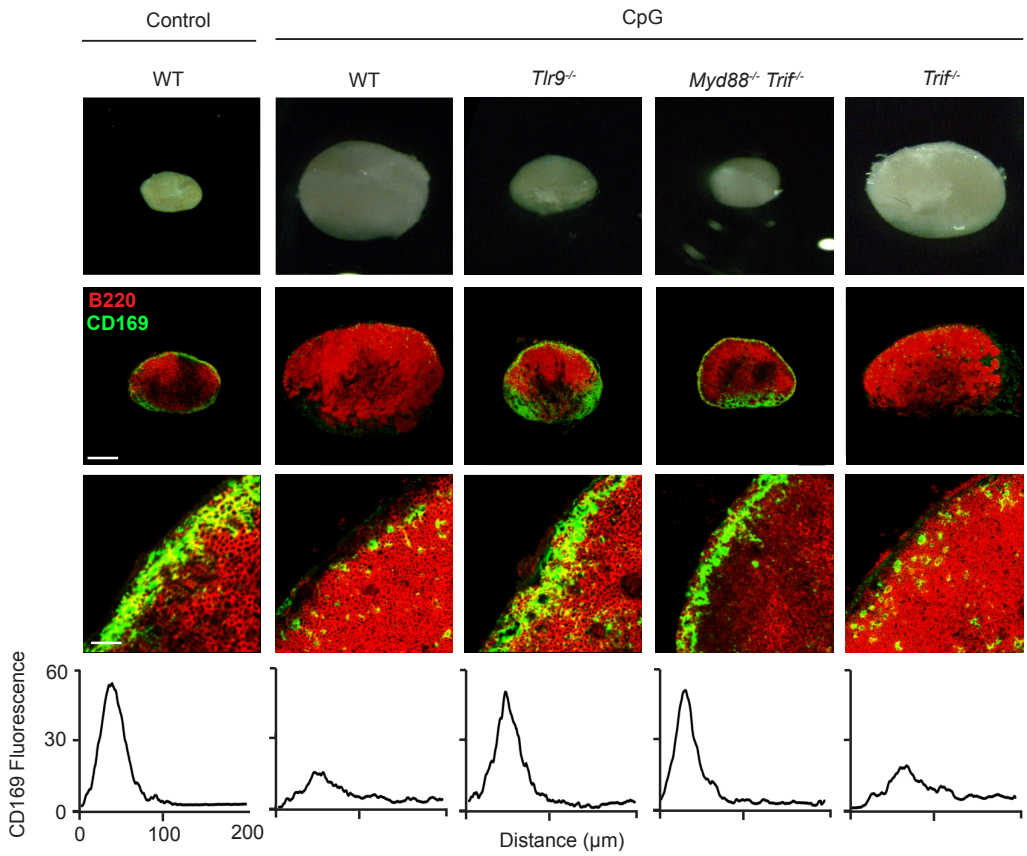

Figure 3.14 Role of TLR9 and MyD88/TRIF adaptors on macrophage disruption

Representative popliteal LNs from wild type, Tlr9$^{-/-}$, Myd88$^{-/-}$Trif$^{-/-}$ and Trif$^{-/-}$ mice collected 4 days after footpad administration of PBS or CpG (upper panels). Confocal microscopy images of respective popliteal LN cryosections stained with mAbs to CD169 (green) and B220 (red) are shown on lower panels. Scale bars, 300μm (top); 60μm (bottom). Histograms represent CD169 fluorescence measured from the outer edge of the LN to the follicles. Data are representative of two independent experiments with three mice per condition.

I next investigated which MyD88-expressing immune cell population is required for the disruption of SCS macrophages during inflammation. Animals selectively lacking MyD88 in individual cell types were generated by crossing mice carrying the MyD88$^{flox/flox}$ allele with others expressing Cre recombinase under the CD19, CD11c or Lyz2 promoters for deletion of MyD88 in B cells, DCs or macrophages/neutrophils respectively. I assessed the deletion efficacy of the MyD88-floxed allele by flow cytometry analysis of MyD88 protein levels in the different LN cell populations. For this, LN single cell suspensions were stained with anti-B220 and anti-MHCII to identify B cells, anti-CD11c and anti-MHCII to identify resident (CD11c^{hi} MHCII^{int}) and migratory (CD11c^{int} MHCII^{hi}) DCs or anti-Ly6G and

anti-CD11b to identify neutrophils. To identify LN macrophages, I stained single cells suspensions with anti-B220, anti-CD3, anti NK1.1 and anti-IL-7Rα in order to gate out B cells, T cells, NK cells and ILCs and avoid contamination on the macrophage gate (Gray et al., 2012). $CD169^+$ macrophages were recognised as $CD169^+$ $CD11c^{low}$ and further separated into SCS ($F4/80^-$) and medullar ($F4/80^+$) macrophages (Figure 3.15).

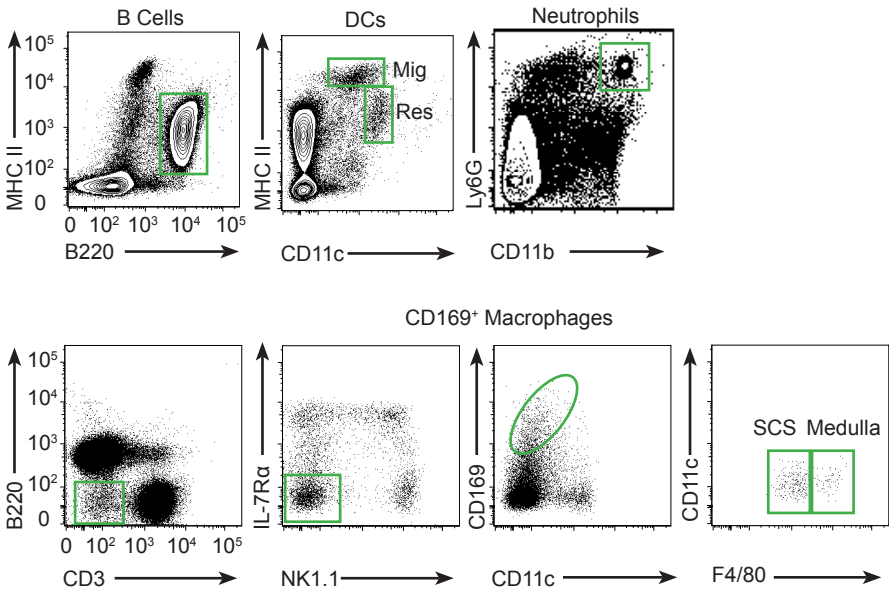

Figure 3.15 Gating strategy for the identification of LN cell populations

Flow cytometry plots of LN single cell suspensions showing the gating strategy for B cells ($MHCII^{int}$ $B220^+$), migratory DCs ($MHCII^{hi}$ $CD11c^{int}$), resident DCs ($MHCII^{int}$ $CD11c^{hi}$), neutrophils ($Ly6G^+$ $CD11b^+$), SCS macrophages ($CD169^+$ $CD11c^{low}$, $B220^-$, $CD3^-$, $IL\text{-}7R\alpha^-$, $NK1.1^-$, $F4/80^-$) and medullary macrophages ($CD169^+$ $CD11c^{low}$, $B220^-$, $CD3^-$, $IL\text{-}7R\alpha^-$, $NK1.1^-$, $F4/80^+$). Data are representative of three different experiments.

After surface staining, LN cell suspensions were fixed, permeabilised and intracellularly stained for MyD88. As the staining for MyD88 is quite dim, in all cases MyD88-deficient LN cells were used to set up the background levels of the antibody (grey curve) (Figure 3.16).

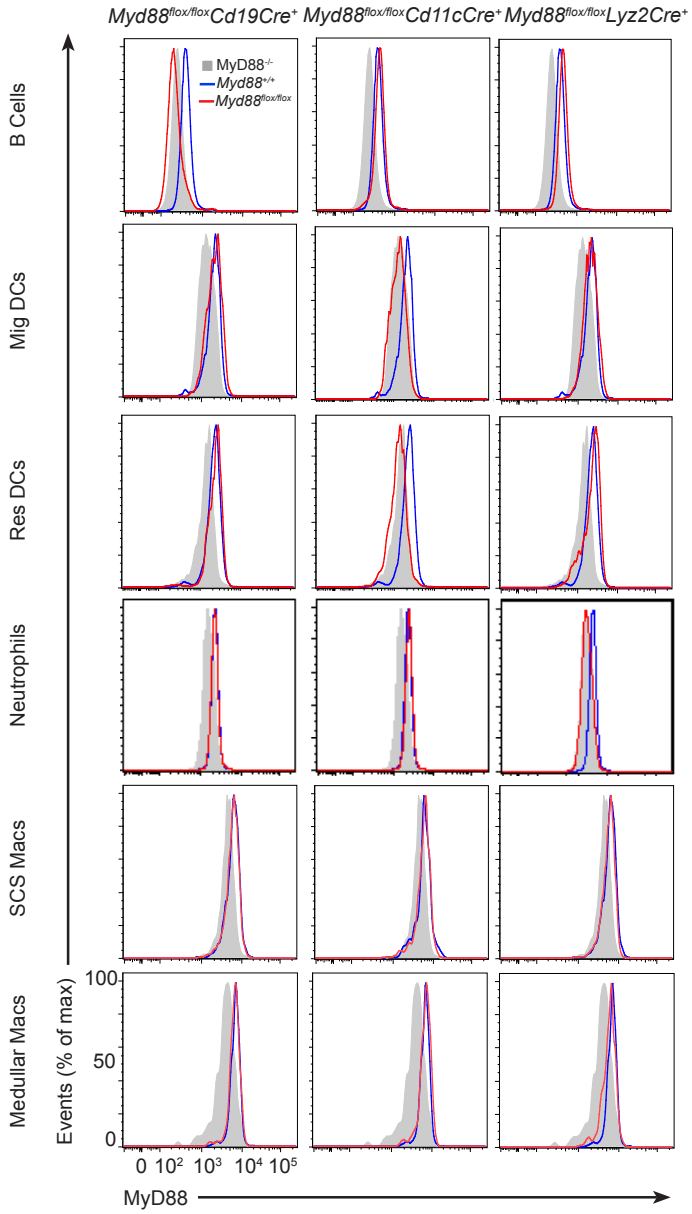

Figure 3.16 MyD88 deletion in different immune cell populations

Histograms display the levels of MyD88 in MyD88$^{+/+}$ (blue line), Myd88$^{-/-}$ (grey solid) and Myd88$^{flox/flox}$ (red line) mice in the populations gated in Figure 3.15. Data are representative of three independent experiments with three mice per condition.

Complete ablation of MyD88 was observed in B cells in MyD88$^{flox/flox}$ CD19-Cre^{+} mice, while the levels of MyD88 in B cells remained unaltered in the other transgenic models (Figure 3.16). Moreover, complete ablation of MyD88 was observed in both migratory and resident DCs in MyD88$^{flox/flox}$ CD11c-Cre^{+} mice (Figure 3.16). Importantly in the latter animals, I observed no deletion in other LN cell populations, indicating that MyD88 deletion was specific for DCs, at least in

these organs (Figure 3.16). Surprisingly, in MyD88$^{flox/flox}$ Lyz2-Cre^{+} mice, although I observed full deletion of MyD88 in neutrophils, the levels of MyD88 in SCS and medullar macrophages were not altered (Figure 3.16), potentially due to low expression of lysozyme by these cell populations (Phan et al., 2009). I therefore restricted the analysis to the potential role of MyD88 in B cells, neutrophils and DCs in the disruption of SCS macrophages during inflammation.

Then I moved on to inject these different transgenic animals with CpG in the footpad and popliteal LNs were harvested after 4 days. The overall dimensions of draining LNs were assessed and cryosections were immunostained with anti-B220 and anti-CD169 for confocal microscopy analysis. In agreement with my previous data, LNs from wild type animals were enlarged and the macrophage layer was disrupted following inflammation (Figure 3.17). However, these processes were abrogated in MyD88-deficient animals (Figure 3.17).

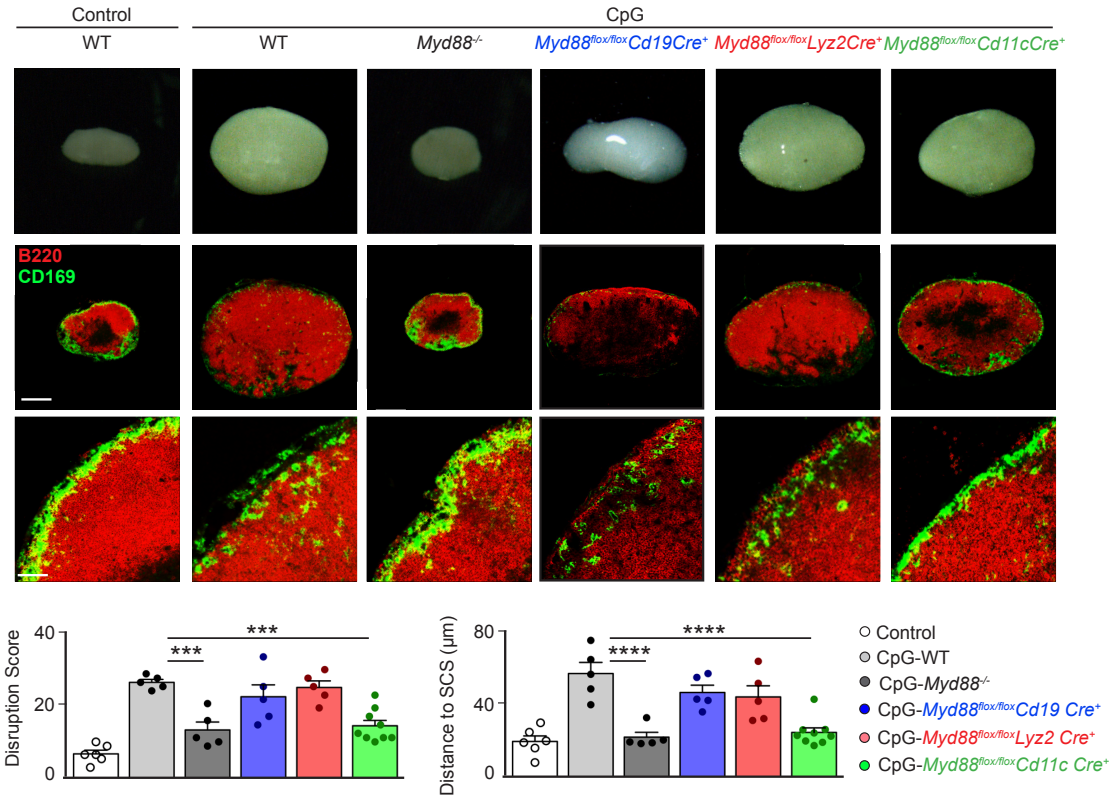

Figure 3.17 MyD88 expression on DCs is necessary for macrophage disruption

Representative popliteal LNs from WT, *Myd88*$^{-/-}$, *Myd88*$^{flox/flox}$ *Cd19Cre*$^{+}$, *Myd88*$^{flox/flox}$ *Lyz2Cre*$^{+}$ and *Myd88*$^{flox/flox}$ *Cd11cCre*$^{+}$ mice collected 4 days after footpad administration of PBS or CpG (upper panels). Confocal microscopy images

of popliteal LNs cryosections stained with mAbs to CD169 (green) and B220 (red) (middle and lower panels). Scale bars, 300μm (middle); 60μm (bottom). Bar charts represent quantification of SCS macrophage disruption and distance of macrophages to LN border in each condition for an individual experiment. Each dot represents a distinct follicle. Mean ± s.e.m. Data are representative of three independent experiments with three mice per condition. Student t test, ***p<0.001, ***p<0.0001.

Interestingly, LN enlargement and disruption of the SCS layer were also observed in MyD88$^{flox/flox}$ CD19-Cre^{+} mice (Figure 3.17). This result demonstrates that MyD88-mediated signalling in B cells is not essential for the alteration of SCS macrophages following inflammation. I then wondered whether B cells could be playing an indirect role in the disruption of SCS macrophages regardless of direct recognition of CpG by them. To this end, I used Rag2-deficient mice, which lack mature lymphocytes owing to an inability to initiate V(D)J rearrangement (Shinkai et al., 1992). Wild type and Rag2$^{-/-}$ mice were injected with PBS or CpG in the footpad and after 4 days popliteal LNs were harvested. Cryosections were stained with anti-B220, anti-CD169 and anti-Lyve1. Lyve-1 was used to easily differentiate the medullar region from the SCS, as the popliteal LNs in these animals are relatively small. F4/80 and SIGN-R1 could not be used in this case as SCS macrophages aberrantly express these markers in B cell deficient animals (Moseman et al., 2012). Interestingly, I observed a similar disruption of the SCS macrophage layer in popliteal LNs of Rag2$^{-/-}$ mice compared to wild type animals after 4 days of CpG injection (Figure 3.18). This result demonstrates that SCS macrophage disruption does not require the presence of B cells or T cells (Figure 3.18).

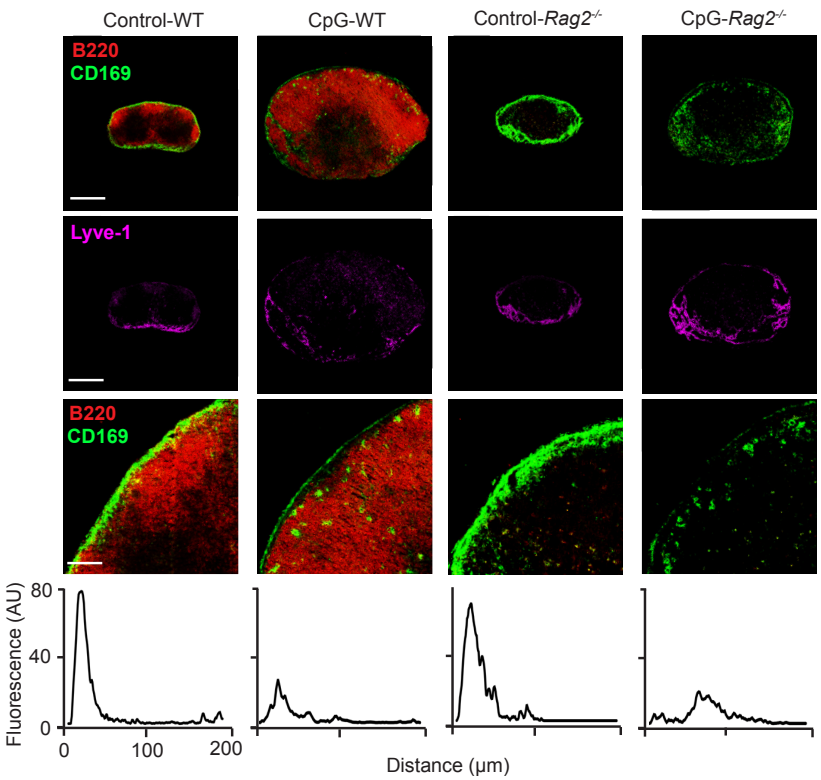

Figure 3.18 Macrophage disruption does not require B and T cells

Confocal microscopy images of popliteal LNs cryosections stained with mAbs to CD169 (green), Lyve-1 (magenta) and B220 (red) from WT and $Rag2^{-/-}$ mice collected 4 days after footpad administration of PBS or CpG. Scale bars, 300µm (top); 60µm (bottom). Histograms represent CD169 fluorescence measured from the outer edge of the LN to the follicles. Data are representative of two independent experiments with two mice per condition.

I detected LN enlargement and SCS macrophage disruption after CpG administration in $MyD88^{flox/flox}$ $Lyz2\text{-}Cre^{+}$ mice, indicating that signalling via the adaptor MyD88 in neutrophils is not essential for SCS macrophage disruption (Figure 3.17). However, while MyD88 in neutrophils themselves is not necessary for the effect, this does not rule out a MyD88 independent role of neutrophils in this process. I therefore decided to analyse macrophage disruption following inflammation in mice in which neutrophils were absent from the periphery. For neutrophil depletion, mice were injected with the commercial anti-Ly6G depleting antibody (Kastenmüller et al., 2012). As neutrophil turnover is relatively fast, I performed daily i.p. injections of this antibody in order to guarantee a complete ablation of this population during the time frame of the study. Effective neutrophil depletion in popliteal LNs was confirmed by flow cytometry (Figure 3.19A). Even

complete ablation of neutrophils from the periphery did not prevent the disruption of the macrophage layer following CpG administration (Figure 3.19B). Altogether, these experiments demonstrate that neutrophils are dispensable for the disruption of the SCS macrophage layer during CpG-mediated inflammation.

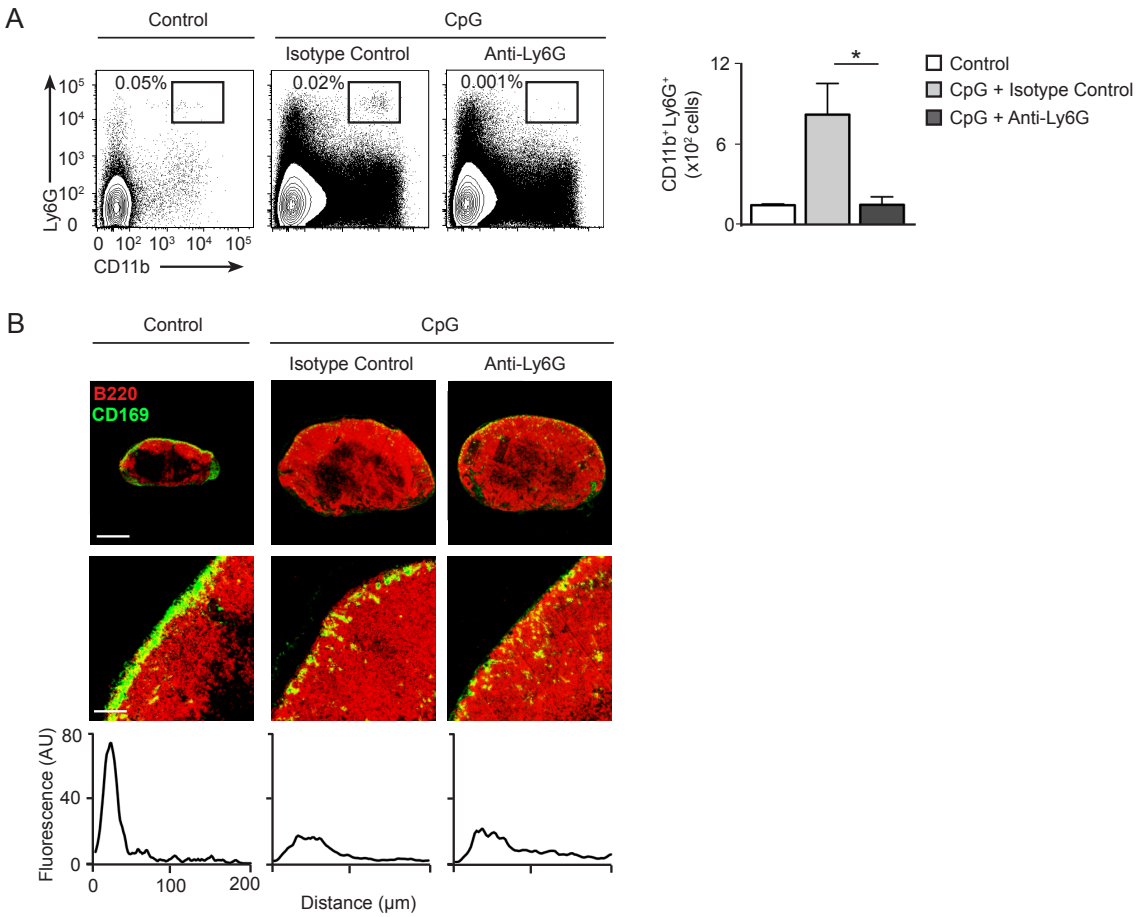

Figure 3.19 Neutrophils do not mediate SCS macrophage disruption

(**A**) Flow cytometry analysis of popliteal LN cell suspensions following 4 days of PBS (control) or CpG injection in the footpad. Mice were also injected i.p. with either anti-Ly6G depleting antibody or isotype control once a day over the period of the experiment. Neutrophils are gated as $CD11b^+$ $Ly6G^+$ cells. Bar chart depicts the numbers of neutrophils in popliteal LNs in each condition for a single experiment. Mean± s.e.m. Student t test, *p<0.05. (**B**) Confocal microscopy images of popliteal LN cryosections treated as in (A) and stained with mAbs to CD169 (green) and B220 (red). Scale bars, 300µm (top); 60µm (bottom). Histograms represent CD169 fluorescence measured from the outer edge of the LN to the follicles. All data are representative of two independent experiments with three mice per condition.

During infection with vaccinia virus or *Toxoplasma gondii*, there is a collective migration and subsequent accumulation of NK cells in the SCS of the lymph nodes, where they interact with the capsule's collagens fibres and with $CD169^{+}$ macrophages (Coombes et al., 2012, Garcia et al., 2012). Therefore, I wondered whether NK cells contributed to the destruction of the SCS macrophage layer following inflammation. To this end, I used two different approaches in order to eliminate NK cells from the system: the use of transgenic $Rag2^{-/-}$ IL-2R$\gamma^{-/-}$ mice, which do not have lymphocytes and NK cells, and the injection of an anti-NK1.1 depleting antibody. For the first approach, I injected PBS (control) or CpG in the footpad of wild type and $Rag2^{-/-}$ IL-2R$\gamma^{-/-}$ and tried harvesting the popliteal LNs after 4 days. However, I could not find the popliteal LNs in $Rag2^{-/-}$ IL-2R$\gamma^{-/-}$ mice. This is in line with previous studies reporting that these mice, besides being severely immunocompromised, have aberrant spleen morphology, markedly diminished LN cellularity and lack of some lymphoid structures (Shultz et al., 2012). Therefore, I moved on to the second approach, where I injected anti-NK1.1 or isotype control antibodies i.p. every other day during the time frame of the study. These animals were also administered with PBS or CpG in the footpad, and popliteal LNs were harvested after 4 days. NK cell depletion was assessed in popliteal LNs by flow cytometry using a dual staining of NK cells with anti-DX5 and anti-NK1.1. An almost complete ablation of NK cells was observed following antibody treatment (Figure 3.20A). However, NK cell depletion did not prevent SCS macrophage disruption after CpG injection, indicating that NK cells are also dispensable for SCS macrophages disruption following inflammation (Figure 3.20B).

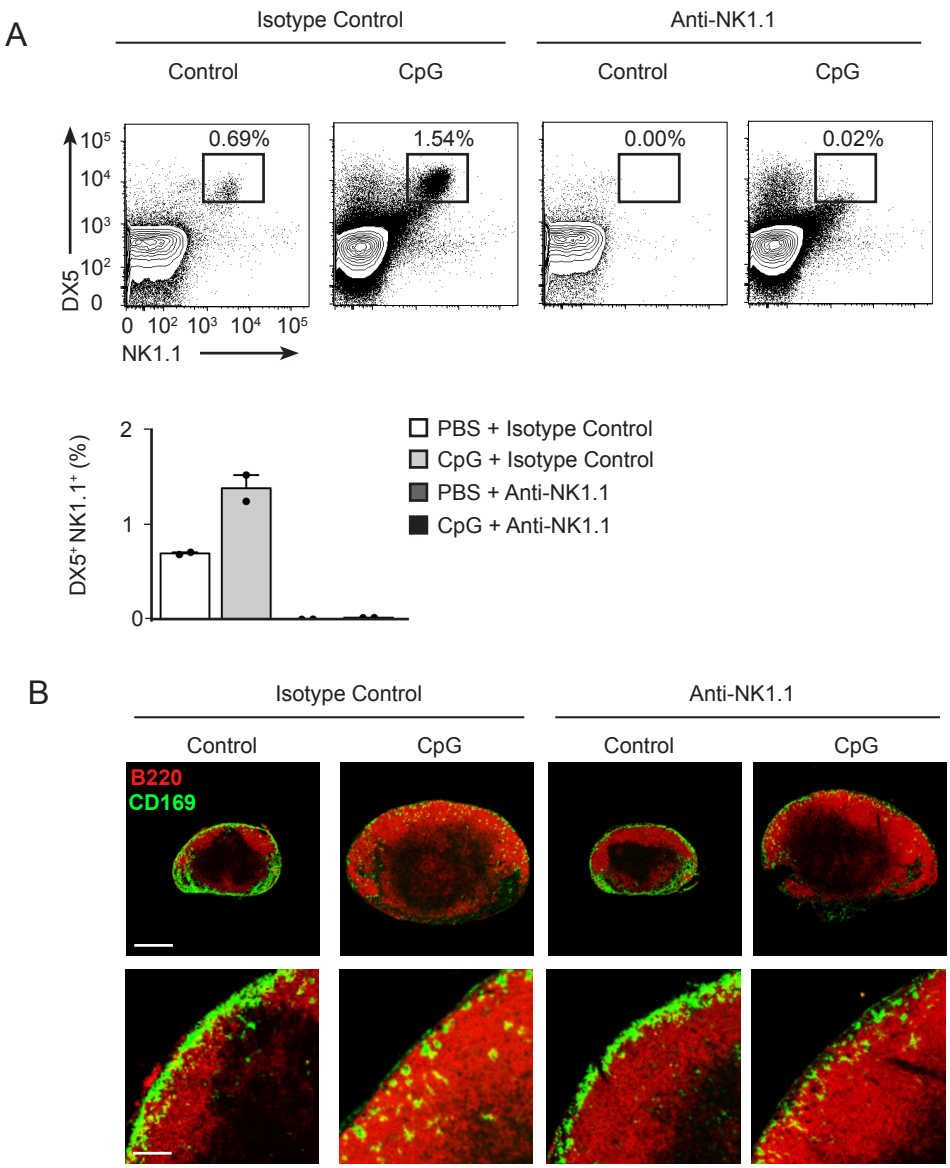

Figure 3.20 NK cell depletion does not interfere with macrophage disruption

(**A**) Flow cytometry analysis of popliteal LN cell suspensions following 4 days of PBS (control) or CpG injection in the footpad. Mice were also injected i.p. with either anti-NK1.1 depleting antibody or isotype control every other day over the period of the experiment. NK cells are gated as $DX5^+$ $NK1.1^+$ cells. Bar chart depicts the numbers of NK cells in popliteal LNs in each condition for a single experiment. Mean± s.e.m. (**B**) Confocal microscopy images of popliteal LN cryosections treated as in (A) and stained with mAbs to CD169 (green) and B220 (red). Scale bars, 300μm (top); 60μm (bottom). All data are representative of two independent experiments with three mice per condition.

In the final step of this experimental thread, I moved on to analyse the role of DCs on the disruption of SCS macrophages. To this end, I injected CpG in the footpad of wild type and MyD88$^{flox/flox}$ CD11c-Cre^{+} animals and harvested popliteal LNs after 4 days. Flow cytometry analysis revealed a marked reduction in the number of migratory DCs (MHCII^{hi} CD11c^{int}) in the draining LNs of MyD88$^{flox/flox}$ CD11c-Cre^{+} animals compared to their wild type counterparts (Figure 3.21). This would most probably be due to the inability of peripheral DCs to directly detect the presence of CpG and migrate to the draining LNs in these transgenic mice. But, most surprisingly, the draining LNs from MyD88$^{flox/flox}$ CD11c-Cre^{+} mice displayed a near-intact layer of SCS macrophages while still showing substantially enlargement (Figure 3.17). This phenomenon results in a marked and significant reduction in both disruption and distance scores in MyD88$^{flox/flox}$ CD11c-Cre^{+} mice compared to wild type animals (Figure 3.17). These observations are particularly striking as they demonstrate that the disruption of SCS macrophages during inflammation is not simply due to the associated enlargement of draining LNs but that it also requires MyD88-signalling in the DC population.

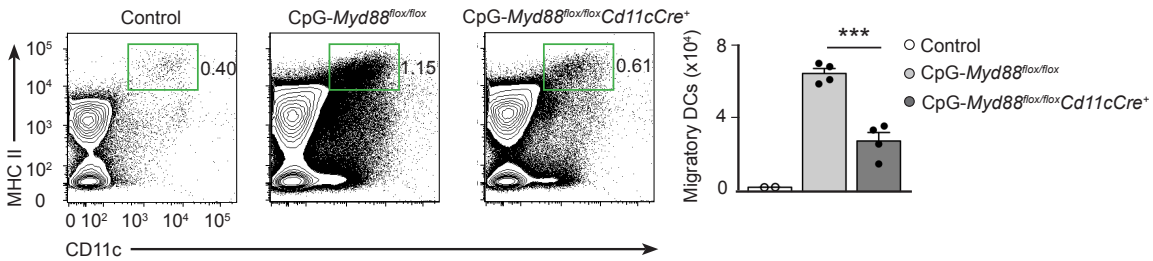

Figure 3.21 DC migration is reduced in MyD88$^{flox/flox}$CD11c-Cre^{+} mice

Flow cytometry analysis of popliteal LN cell suspensions 4 days after PBS (control) or CpG injection in the footpad of wild type or *Myd88$^{flox/flox}$ Cd11cCre^{+}* mice. Migratory DCs are gated as CD11c^{int} MHCII^{hi} cells. Bar charts show the numbers of migratory DCs in each condition for an individual experiment. Each dot represents a different mouse. Mean± s.e.m. Student t test, ***p<0.001. Data are representative of two independent experiments with three mice per condition.

3.3.4 DC migration regulates SCS macrophages disruption

In order to provide additional evidence for the role of DCs on the disruption of SCS macrophages I used independent systems to target DCs. However, most mouse models that are used to deplete DCs also induce depletion of macrophages. For example, after injection with DT in CD11c-DTR mice, not only DCs, but also SCS macrophages, plasmablasts, activated T cells, NK cells and Ly-6C^{low} monocytes are depleted (van Blijswijk, Schraml and Reis e Sousa, 2013). Another example includes the MAFIA (Macrophages Fas-Induced Apoptosis) mice, where DCs as well as macrophages are depleted after administration of the reagent AP20187 (Burnett et al., 2004). Due to these technical limitations for depleting all the subsets of DCs without affecting SCS macrophages, I thought of using Batf3$^{-/-}$ mice, a mouse model were CD8^{+} DCs are absent, while all the other DCs subsets and SCS macrophages remain intact (Hildner et al., 2008). I therefore injected PBS or CpG in wild type and Batf3$^{-/-}$ mice and popliteal LNs were harvested after 4 days. While scattering of macrophages was still evident in Batf3$^{-/-}$ mice following CpG administration, the disruption of the layer was not as dramatic as observed in wild type animals (Figure 3.22). This result indicates that CD8^{+} DCs might play a role in SCS macrophage disruption and at the same time suggests that other DC subtypes, such as plasmocytoid, CD11b^{+} and Langerin^{+} DCs might be collectively inducing this disruption process.

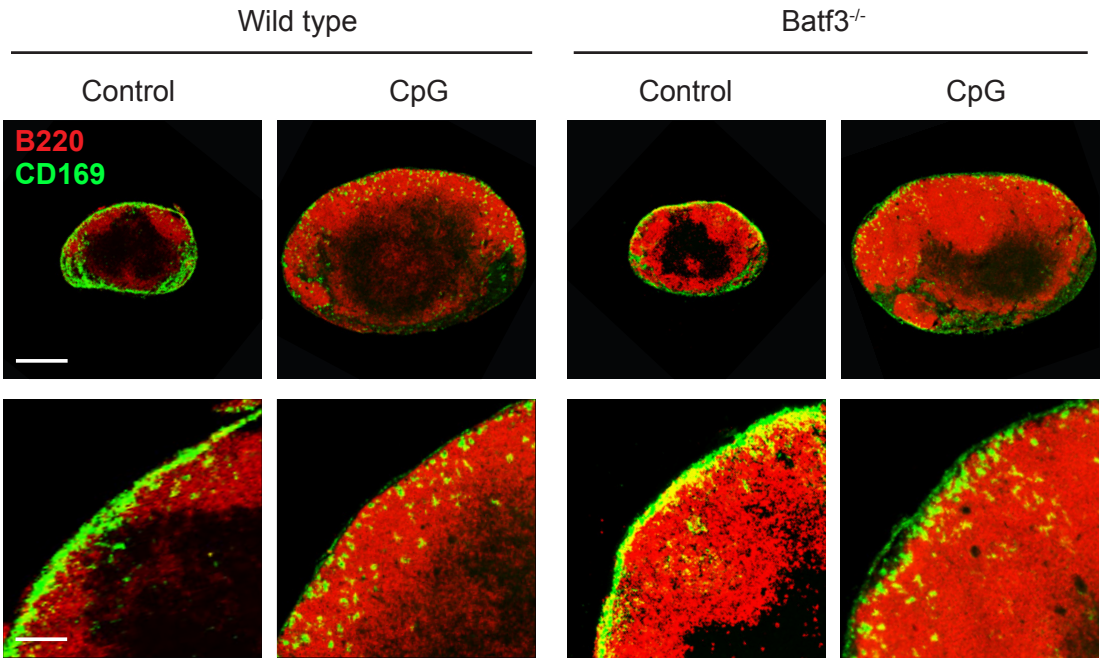

Figure 3.22 Macrophage disruption is partially reduced in Batf3$^{-/-}$ mice

Confocal microscopy images of popliteal LNs cryosections stained with mAbs to CD169 (green) and B220 (red) from WT and Batf3$^{-/-}$ mice collected 4 days after footpad administration of PBS or CpG. Scale bars, 300μm (top); 60μm (bottom). Data are representative of two independent experiments with three mice per condition.

Given the importance of DCs in this process, I went on to visualise the distribution of these cells during CpG-induced inflammation. To this end, I injected PBS or CpG in the footpad of mice, and popliteal LNs were harvested after 4 days. Frozen sections were stained with anti-CD169 to label SCS macrophages and with anti-Langerin or anti-CD11c to stain DCs followed by confocal microscopy. In the steady state, DCs are located mainly in the paracortex and medulla (Figure 3.23A-B), far from the SCS. In contrast, a clear accumulation of Langerin^{+} and CD11c^{+} DCs were observed interspersed between the SCS macrophages after inflammation (Figure 3.23A-B). The levels of CD11c, Langerin and CD169 fluorescence were measured across the LN sections and plotted together in histograms. While the mean fluorescence peaks of CD11c and Langerin are far from the CD169 peak in steady state conditions, during inflammation clear peaks for both CD11c and Langerin are observed before that of CD169 (Figure 3.23A-B).

These results indicate that during inflammation there is a clear accumulation of migratory DCs in the SCS.

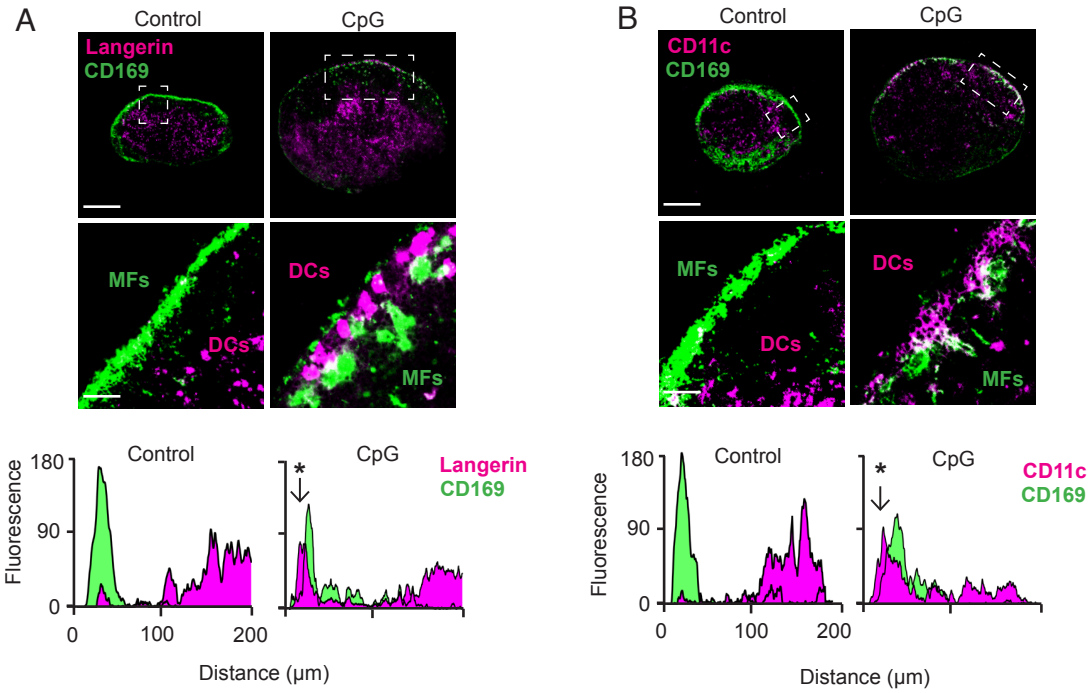

Figure 3.23 DCs accumulate in the SCS following inflammation

(**A** and **B**) Confocal microscopy images of popliteal LN sections stained with mAbs to CD169 (green) and (A) langerin (magenta) or (B) CD11c (magenta) derived from mice that were injected with PBS or CpG 4 days previously. Scale bars, 300μm (top); 60μm (bottom). Histograms represent CD169, langerin and CD11c fluorescence measured from the outer edge of the LN to the inner areas. Stars indicate DCs at the SCS. Data are representative of three independent experiments with two mice per condition.

I further confirmed the recruitment of DCs to the SCS by 3D multiphoton imaging and 3D electron tomography. In the first case, I injected PBS or CpG in the footpad of CD11c-YFP mice and 4 days later anti-CD169 was injected into the footpad of mice to label SCS macrophages in vivo. After 10 minutes, LNs were harvested and imaged by multiphoton microscopy. During steady state, a clear layer of macrophages (green) is observed below the collagen capsule (cyan) with no clear YFP^+ cells (magenta) in this area. In contrast, after inflammation I observed an accumulation of YFP^+ cells in the SCS, located inbetween the disrupted layer of macrophages (Figure 3.24A). Moreover, DCs with their characteristic convoluted cytoplasm and extended processes were found in the SCS of LNs from CpG-treated mice at high-resolution in electron microscopy

images examined with 3View (Figure 3.24B). In contrast, control animals did not exhibit any accumulation of DCs in the SCS region of the draining LN (Figure 3.24B).

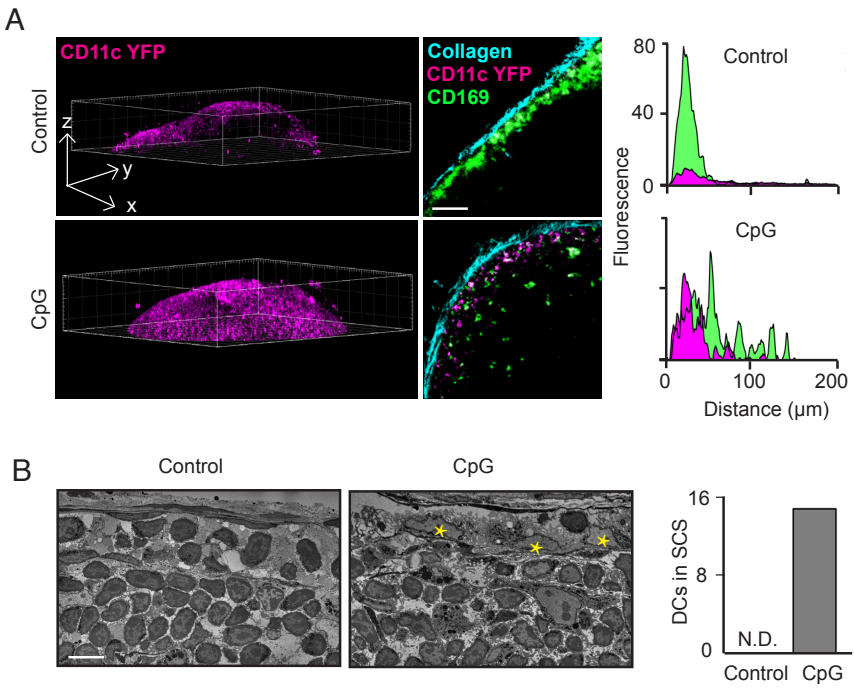

Figure 3.24 3D analysis of DC accumulation in the SCS after inflammation

(**A**) 3D multiphoton microscopy of explanted popliteal LNs from *Cd11c*-YFP animals injected in the footpad with either PBS or CpG (4 days) and anti-CD169 antibody (green) 10 minutes before dissection. YFP signal is shown in magenta and second harmonic signal in cyan. Scale bar, 60μm. Histograms represent CD169 and YFP fluorescence measured from the outer edge of the LN to the inner areas. (**B**) Representative Z sections of 3View electron microscopy analysis of popliteal LN SCS after 4 days of PBS or CpG injection. Yellow stars indicate DCs located at the SCS. Scale bar, 5μm. All data are representative of two independent experiments with two mice per condition.

In summary, after inflammation there is a substantial accumulation of migratory DCs in the SCS. Furthermore, direct sensing of CpG by DCs is absolutely necessary in inducing SCS macrophage layer disruption. These facts led me to investigate whether the arrival of migratory DCs from the periphery to the SCS could be potentially involved in altering the SCS macrophage distribution after inflammation. DC migration to the draining LNs is controlled by the main LN-homing chemokine receptor CCR7 (Ohl et al., 2004). I therefore went on to analyse the macrophage disruption process in mice lacking CCR7. For this, I injected PBS

or CpG into either wild type or CCR7$^{-/-}$ mice and after 4 days, LNs were harvested and analysed by flow cytometry and confocal microscopy. A complete blockade in DC migration was observed in CCR7$^{-/-}$ deficient animals by flow cytometry (Figure 3.25A). Moreover, the characteristic disruption of the SCS macrophage layer observed in wild type mice was abrogated in CCR7-deficient animals (Figure 3.25B). This resulted in a significant decrease in both disruption and distance scores compared to wild type animals. These observations are consistent with the notion that DC arrival to the draining LNs is indeed necessary for the alteration of SCS macrophage organisation during inflammation.

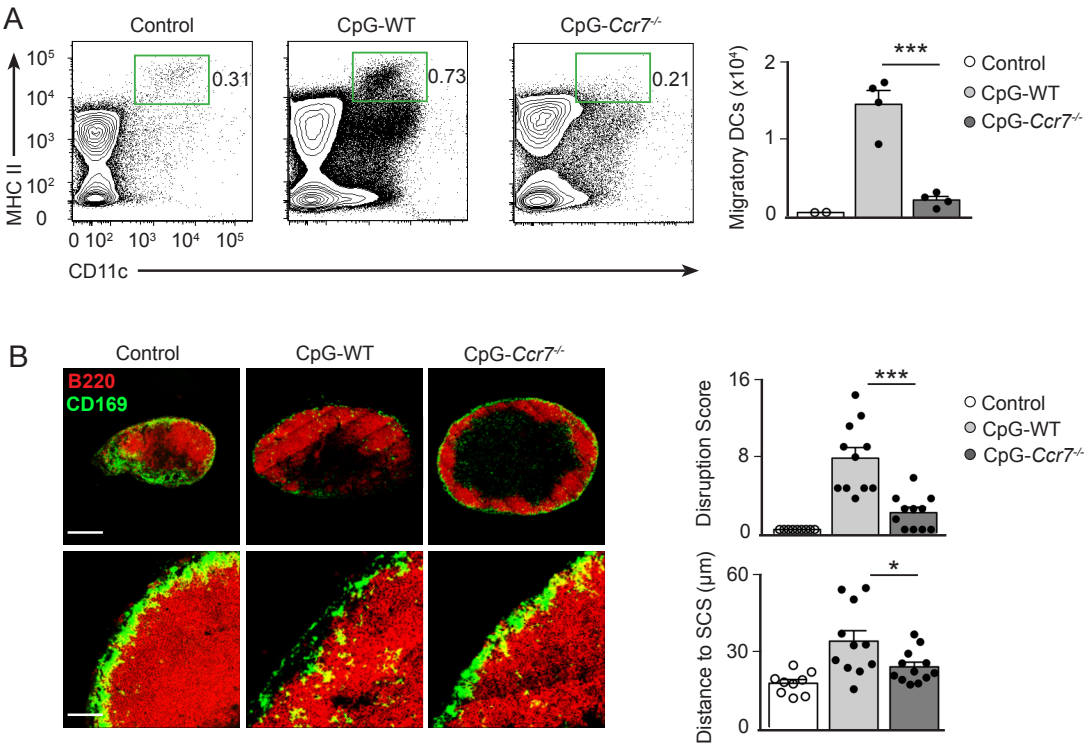

Figure 3.25 DC migration is necessary for SCS macrophage disruption

(**A**) Flow cytometry analysis of popliteal LN cell suspensions 4 days after PBS (control) or CpG injection in the footpad of wild type or *Ccr7*$^{-/-}$ mice. Migratory DCs are gated as CD11c^{int} MHCII^{hi} cells. Bar charts show the numbers of migratory DCs in each condition for an individual experiment. Each dot represents a different mouse. Mean± s.e.m. (**B**) Confocal images of popliteal LNs cryosections stained with mAbs to CD169 (green) and B220 (red) from wild-type and *Ccr7*$^{-/-}$ mice treated as in (A). Scale bars, 300 µm (top); 60 µm (bottom). Bar charts represent quantification of SCS macrophage disruption and distance of macrophages to LN border in each condition for an individual experiment. Each dot represents a distinct follicle. Mean ± s.e.m. Student t test, *p<0.05, ***p<0.001. Data are representative of three independent experiments with three mice per condition.

It is important to highlight that DCs are not the only cell population that express CCR7; B cells and T cells also express this chemokine receptor. However, these lymphocytes are not required for SCS macrophage disruption as this process occurs normally in Rag2 deficient animals, which lack both B and T cells (Figure 3.18). I therefore propose that the lack of disruption of the SCS macrophage layer in $CCR7^{-/-}$ mice following CpG administration might be due to the inability of DCs to migrate to the LNs. I sought to obtain $CCR7^{flox/flox}$ CD11c-Cre^{+} mice in order to specifically delete CCR7 in the DC compartment, but unfortunately this strain has still not been generated.

To formally test whether the arrival of DCs per se is sufficient in disrupting the layer of macrophages, I decided to transfer activated DCs to wild type animals and analyse the integrity of the macrophage layer. For this, CD45.2 BM-DCs were generated by treatment of bone marrow precursors with GM-CSF and then treated with PBS (control) or CpG for 16 hours. BM-DCs were then labelled with CFSE and adoptively transferred into the footpad of CD45.1 recipient mice. After four days, popliteal LNs were harvested and subjected to flow cytometry and immunohistochemistry. While a population of $CD45.2^{+}$ $CFSE^{+}$ cells was observed in popliteal LNs from mice receiving CpG-treated BM-DCs, almost no $CD45.2^{+}$ $CFSE^{+}$ cells were observed in LNs from mice receiving PBS-treated BMDCs (Figure 3.26A). This result indicates that activation of DCs is required in order to migrate to draining LNs. Interestingly, immunohistochemistry analysis showed a dramatic disruption of the SCS macrophage layer in the draining LNs of animals receiving CpG-treated BM-DCs but not control DCs (Figure 3.26B). CpG-treated BM-DCs were interspersed with SCS macrophages and located in the paracortex having gained entry into the LN interior (Figure 3.26B). On the other hand, the disruption of the SCS macrophage layer and the entry of DCs into the paracortex were severely reduced in mice receiving CpG-treated BM-DCs taken from a TLR9-deficient donor (Figure 3.26A-B). This observation indicates that the disruption of SCS macrophages is not due to residual CpG remaining on the surface of BM-DCs but rather to the migratory effect that CpG induces on DCs.

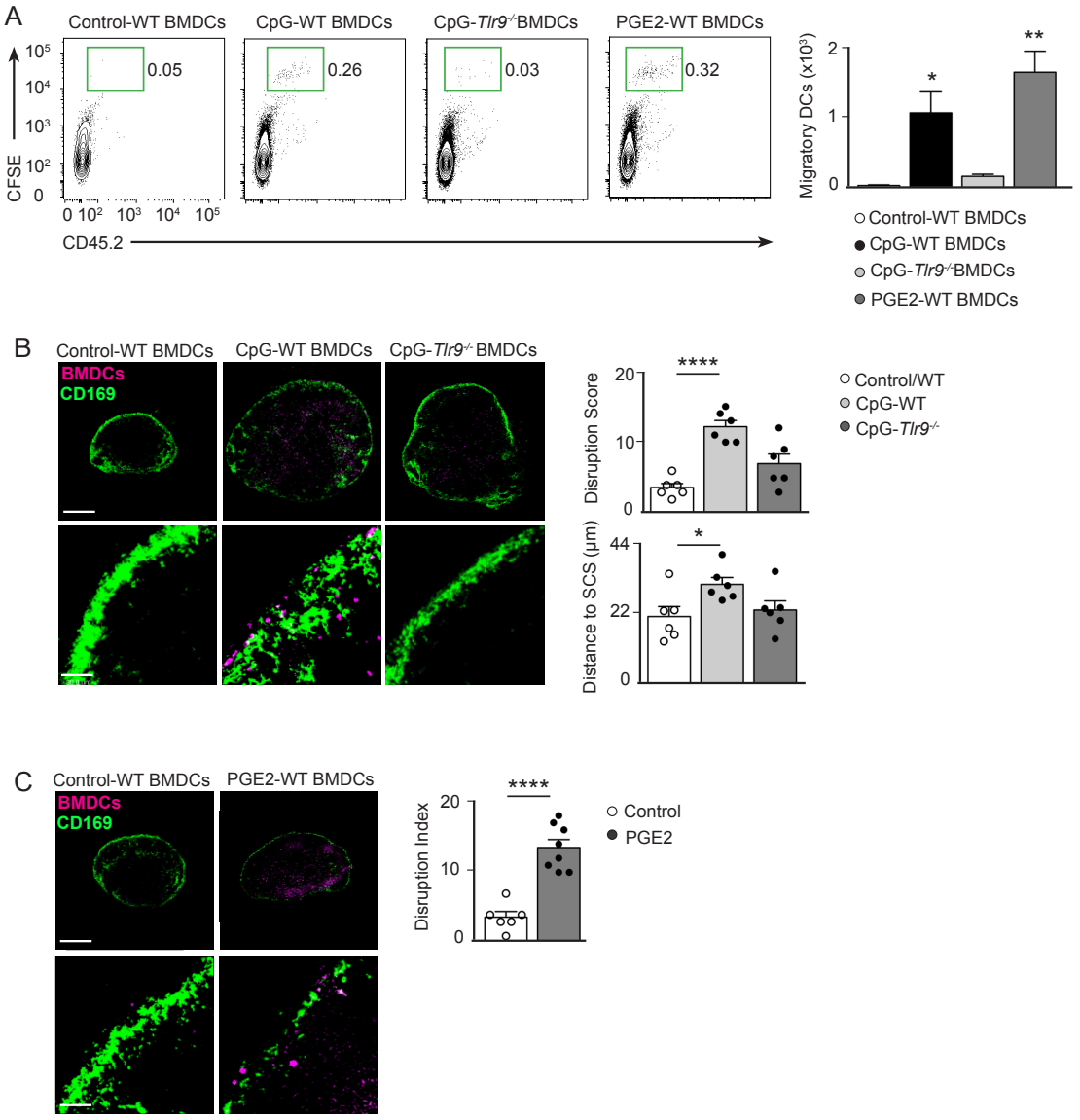

Figure 3.26 DC migration is sufficient to induce SCS macrophage disruption

(**A**) Flow cytometry analysis of popliteal LN after 4 days of footpad injection with 3.10^6 CFSE-labelled CD45.2 control BM-DCs, CpG-treated wild type BM-DCs, CpG-treated *Tlr9*$^{-/-}$ BM-DCs or PGE2-treated wild type BM-DCs in CD45.1 recipient mice. Bar charts show the numbers of BM-DCs in popliteal LNs in each condition for a single experiment. Mean ± s.e.m. (**B** and **C**). Confocal images of popliteal LN cryosections 4 days after footpad injection with 3.10^6 CFSE-labelled (magenta) control BM-DCs, (B) CpG-treated WT BM-DCs, CpG-treated *Tlr9*$^{-/-}$ BM-DCs or (C) PGE2-treated BM-DCs. Sections were stained with mAb to CD169 (green). Bar charts represent quantification of SCS macrophage disruption and distance of macrophages to LN border in each condition for an individual experiment. Each dot represents a distinct follicle. Mean ± s.e.m. Student t test, *p<0.05, **p<0.01, ****p<0.0001. All data are representative of at least two independent experiments with three mice per condition.

In order to establish that DC migration and not any other feature of DCs requiring MyD88 signalling is what disrupts SCS macrophages, I decided to induce DC migration independently of TLR signalling. To this end, I adoptively transferred $CD45.2^{+}CFSE^{+}$ BM-DCs previously treated with PGE2 (prostaglandin E2) in combination with TNF-α and IFN-α. Under these conditions BM-DCs were reported to migrate to draining LNs (Yen, Khayrullina and Ganea, 2008). After 4 days, a clear population of $CD45.2^{+}CFSE^{+}$ cells was detected in popliteal LNs by flow cytometry (Figure 3.26A), indicating that prostaglandin E2 treatment does induce DC migration. Importantly, the arrival of prostaglandin-treated DCs to the LNs also induces SCS macrophage disruption (Figure 3.26C), supporting the idea that DC migration and not any other feature of DCs requiring MyD88 signalling induces SCS macrophage disruption.

Together, these results demonstrate that the CCR7-mediated arrival of mature DCs during inflammation is necessary and sufficient to trigger the disruption of SCS macrophages in the LNs.

3.3.5 DC-mediated regulation of LN macrophage disruption

How does the arrival of mature DCs to the LN induce the disruption of SCS macrophages? When DCs sense the presence of pathogens in the periphery they start a process of maturation that involves the up regulation of MHCII and CCR7, the down regulation of E-cadherins and the increased production of MMPs (matrix metalloproteases), especially MMP-9 (Hammad and Lambrecht, 2008). MMPs participate in tissue remodelling by degrading all kinds of proteins, helping DCs to detach from the skin and epithelia and to migrate to the draining LNs (Yen, Khayrullina and Ganea, 2008). I therefore wondered whether the secretion of MMPs by DCs would also induce a remodelling of the SCS extracellular matrix that would lead to a disruption of the macrophage layer during inflammation. To address this question, mice were injected i.p. with PBS (control) or the MMP general inhibitor GM6001 (Mirastschijski et al., 2004) every day during the course of the study. These animals were then injected in the footpad with CpG and four days later, popliteal LNs were collected. Cryosections were stained with anti-B220

and anti-CD169 and analysed by confocal microscopy. I observed an expansion of the B cell follicles in both groups of animals. Moreover, MMP inhibition did not prevent the disruption of the macrophage layer, suggesting that the disruption process is independent of extracellular matrix remodelling by MMPs (Figure 3.27).

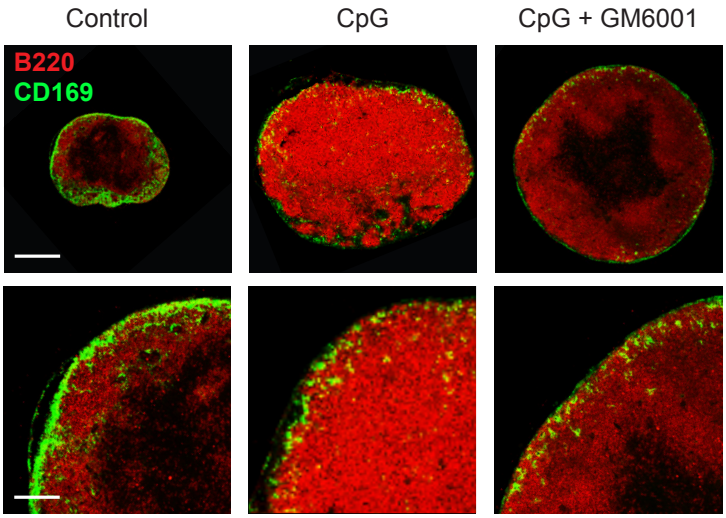

Figure 3.27 MMP activity is not involved in macrophage disruption

Confocal microscopy of popliteal LN cryosections stained for CD169 (green) and B220 (red) from mice that were previously injected with PBS (control) or CpG in the footpad. Mice were also injected i.p. with PBS or GM6001 every day over the period of the experiment. Scale bars, 300µm (top); 60µm (bottom). Data are representative of two independent experiments with two mice per condition.

Recently, several groups have shown that migratory DCs initiate the expansion of LNs during an inflammatory response. Migratory DCs express high levels of the C-type lectin CLEC-2, which interacts with the podoplanin expressed on the FRC network. This interaction between DCs and FRCs induces the relaxation of the FRC network and the consequent expansion of draining LNs. In fact, administration of CLEC-2 protein to immunised mice augments LN expansion, whereas selective ablation of CLEC-2 on DCs results in significantly smaller LNs (Acton et al., 2014, Astarita et al., 2015).

I therefore wondered whether relaxation of the FRC network induced by the interaction between migratory DCs and FRCs would induce the scattering and disruption of the macrophage layer. To analyse this, I followed two different approaches. Firstly, I injected PBS or recombinant CLEC-2 protein in the footpad of mice and after 4 days popliteal LNs were harvested. Cryosections were stained

with anti-B220 and anti-CD169 and analysed by confocal microscopy. The macrophage layer remained intact after CLEC-2 injection, demonstrating that CLEC-2 by itself does not induce SCS macrophage scattering (Figure 3.28A). Secondly, I wondered whether specific deletion of CLEC-2 on DCs would interfere with the reorganisation process of the macrophage layer following inflammation. To this end, I injected PBS or CpG in the footpad of wild type and CLEC-2$^{flox/flox}$ CD11c-Cre^{+} mice, which do not express CLEC-2 in the DC compartment. After 4 days popliteal LNs were harvested and cryosections stained with anti-B220 and anti-CD169. While an intact layer of macrophages was observed in non-immunised mice, a similar level of disruption was observed in wild type and CLEC-2$^{flox/flox}$ CD11c-Cre^{+} mice (Figure 3.28B). All together, these results indicate that the CLEC-2-mediated relaxation of the FRC network in the LNs is not involved in the disruption process of the macrophage layer.

The exact mechanism by which migratory DCs induce the disruption of the macrophage layer remains to be elucidated. However, as the retention of CD169^{+} macrophages on the SCS requires chemokine signalling, it is tempting to speculate that migratory DCs would induce some changes on the steady state levels of chemokines after inflammation. These changes might result in the migration of macrophages towards the LN follicles and the subsequent alteration in the organisation of the SCS macrophage barrier.

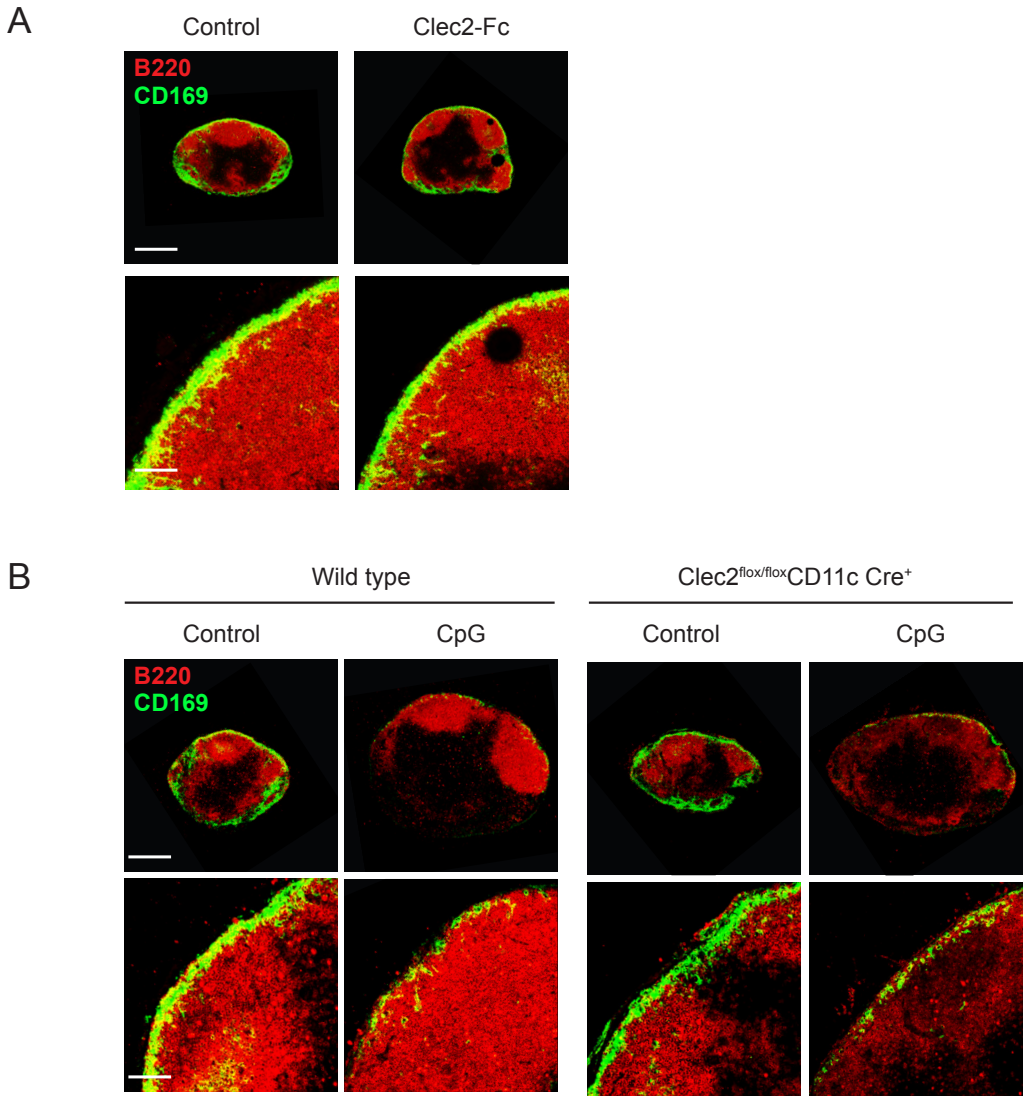

Figure 3.28 Clec-2 expression by DCs is dispensable for macrophage disruption

(**A**) Confocal images of popliteal LN cryosections 4 days after footpad injection of PBS or Clec2-Fc. Sections were stained with mAb to B220 (red) and CD169 (green). (**B**) Confocal images of popliteal LN cryosections stained as in (A) from wild-type and *Clec2*$^{flox/flox}$*CD11c-Cre*$^{+}$ mice following 4 days of footpad injection with PBS or CpG. Scale bars, 300 μm (top); 60 μm (bottom). Data are representative of two independent experiments with two mice per condition.

3.4 Inflammation impedes acquisition of subsequent antigen by SCS macrophages and cognate B cells

The strategic position of SCS macrophages at the lymph-tissue interface allows them to capture pathogens entering the LN and to present them to underlying B cells (Carrasco and Batista, 2007, Junt et al., 2007, Phan et al., 2007). Therefore, the observed disruption to the integrity of the SCS macrophage layer during infection or inflammation raises the important question of the functional implications of this phenomenon for retention and presentation of antigen arriving in a subsequent wave.

3.4.1 Macrophage layer disruption impedes retention of subsequently arriving antigen

In order to investigate the consequences of either inflammation or viral and bacterial infection on the retention of a second incoming antigen to the LNs, mice were initially injected in the footpad with PBS (control), CpG, 10^4 PFU of VACV or 10^6 CFU of GBS. Four days later, mice were challenged in the footpad with 10^8 highly fluorescent microspheres as a surrogate antigen. These 0.2 μm microspheres, which are similar in size to a virus, allow visualisation and quantification of antigen retention by immunofluorescence (Carrasco and Batista, 2007). Six hours after antigen challenge, popliteal LNs were harvested; cryosections were stained with anti-CD169 and anti-B220 and examined by confocal microscopy to reveal the distribution of the microspheres. Bead fluorescence in the LN compartments was quantifed using Image J (RBS). In line with previous reports, a considerable deposition of microspheres was observed at the SCS in draining LNs of control mice (Carrasco and Batista, 2007) (Figure 3.29A–C). Moreover, a substantial number of beads also gained access to the underlying follicles (Figure 3.29A-C). In contrast, this accumulation of antigen in the SCS and in the follicles was dramatically diminished in the LNs of mice that had previously received CpG, VACV or GBS (Figure 3.29A–C).

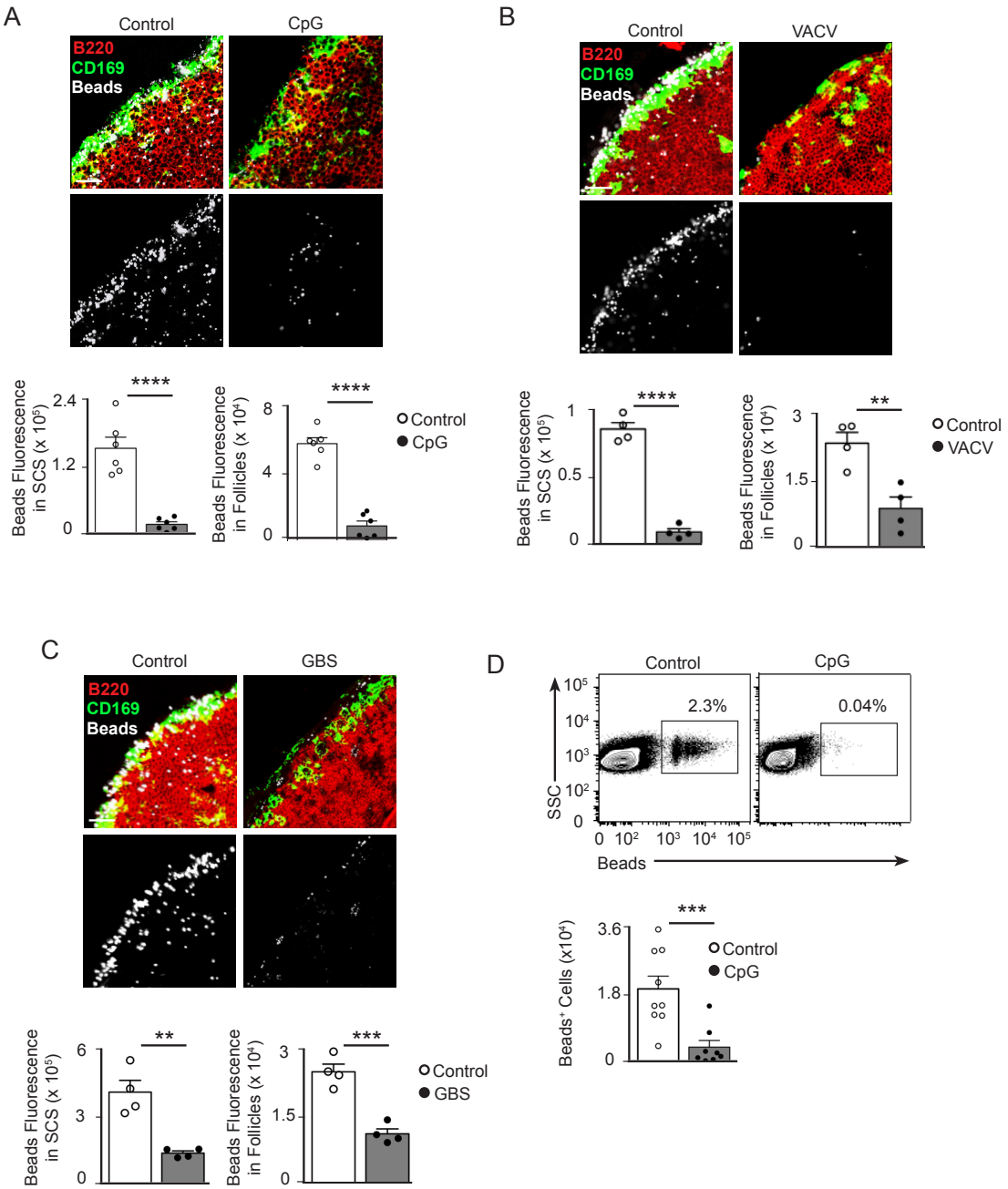

Figure 3.29 Inflammation and infection hinder retention of subsequent antigen

(**A**-**C**) Confocal microscopy images of popliteal LNs from mice injected in the footpad with PBS (control) or (A) 10μg of CpG, (B) 10^4 PFU of VACV or (C) 10^6 CFU of GBS and 4 days later injected again with $8x10^8$ polystyrene fluorescent microspheres (0.2 μm, white). Sections were labelled with antibodies to B220 (red) and CD169 (green). Scale bar, 60μm. Bar charts represent antigen fluorescence quantification in the SCS and follicles for a single experiment. Data are representative of three experiments. (**D**) Flow cytometry analysis of popliteal LNs from animals treated as in (A). Representative dot plots depict bead acquisition by $B220^-CD3^-$ cells. Quantification of bead-positive cells from three independent

experiments is shown in the bar chart. In all panels, each dot represents a single LN. Mean ± s.e.m. Student t test, **p<0.01, ***p<0.001, ****p<0.0001.

Taking an independent approach, I also analysed the extent of antigen retention in draining LNs by flow cytometry. Mice were injected in the footpad with PBS or CpG and 4 days later, challenged with 10^8 fluorescent beads. After 6 hours, popliteal LNs were harvested and single cell suspensions were stained with anti-B220, anti-CD3 and DAPI in order to exclude dead cells and lymphocytes from the analysis. The percentage of cells that were positive for beads was quantified in control and CpG-treated mice. While around $2x10^4$ cells had acquired fluorescent beads in LNs from control animals, this acquisition was severely impaired in LNs from mice receiving CpG (Figure 3.29D). Together, these results suggest that primary inflammation or infection severely impedes the capture of antigen coming on a subsequent wave to the LNs.

3.4.2 Lymphatic flow is not altered during CpG-mediated inflammation

I wondered whether this impairment in the capture of a second antigen was due to the loss of the integrity of the macrophage barrier or to a disruption of the lymphatic flow to the LN after inflammation. To test this, I looked at the drainage of a soluble dye in vivo with the assistance of Sophie Lutter and Angelo Castello. The chosen dye was ICG (indocyanine green), which binds tightly to soluble proteins and remains confined to the vascular system. The infrared absorbance and emission spectrum of ICG allows for deep tissue imaging with minimal signal scattering (Alander et al., 2012). Animals were injected with PBS or CpG in the left footpad, injected again with ICG 4 days after and imaged every 4 seconds using the IVIS Spectrum Whole Body Imaging System. The ICG signal progressively moved along the hind limb from the site of injection, with most of the fluorescence clearly restricted to the vascular compartment. After 60 seconds, fluorescence intensity peaked in the draining popliteal LNs (Figure 3.30). The progressive movement and accumulation of the soluble dye ICG in the draining LNs were similar in both mice receiving PBS or CpG four days before (Figure 3.30). Taken together these results suggest that the failure to capture a subsequent incoming antigen following primary inflammation is not due to a disruption in the lymphatic

flow. Instead inflammation is most likely to affect the antigen retention capacity of the LN by inducing the disruption of the macrophage barrier.

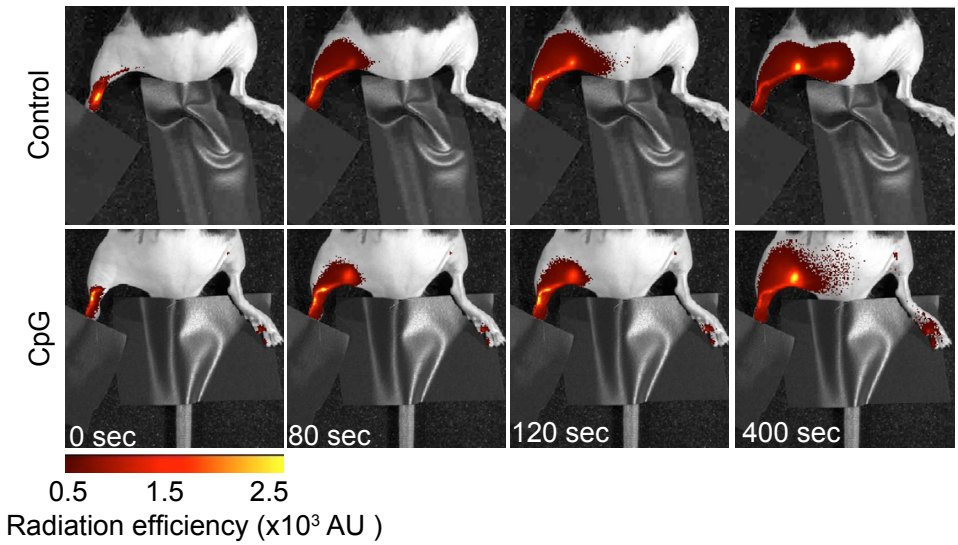

Figure 3.30 Lymphatic flow is not affected by CpG administration

Time-lapse whole body imaging of lymphatic flow in mice that were injected in the footpad with either PBS or CpG and injected again 4 days later with ICG dye. False-colour scale bar shows signal radiant efficiency. Data are representative of two independent experiments with two mice per condition.

3.4.3 Antigen retention capacity is subsequently recovered

As shown in Figure 3.5, the macrophage layer is recovered at the SCS after around four weeks after the induction of inflammation. I therefore wondered if the recovery of the macrophage layer would restore the antigen retention capacity of the LN. To analyse this, mice were injected with PBS or CpG in the footpad and after 28 days, mice were re-challenged with 10^8 fluorescent 0.2 μm microspheres. Six hours after bead administration, popliteal LNs were harvested and cryosections stained with anti-CD169 and anti-B220. As observed in Figure 3.29, an extensive accumulation of fluorescent beads was detected in the SCS of draining LNs from control mice (Figure 3.31). Importantly, a similar extent of bead deposition was observed in the SCS of LNs harvested from mice that were injected with CpG four weeks previously (Figure 3.31). This demonstrates that the ability to retain antigen is restored around four weeks after the initiation of inflammation, a timeframe in line with the recovery of the SCS macrophage layer.

Collectively, these results show that the temporary disruption of the SCS macrophage layer during inflammation or infection has an important functional impact on the capacity of the LN to retain antigen arriving in a subsequent wave.

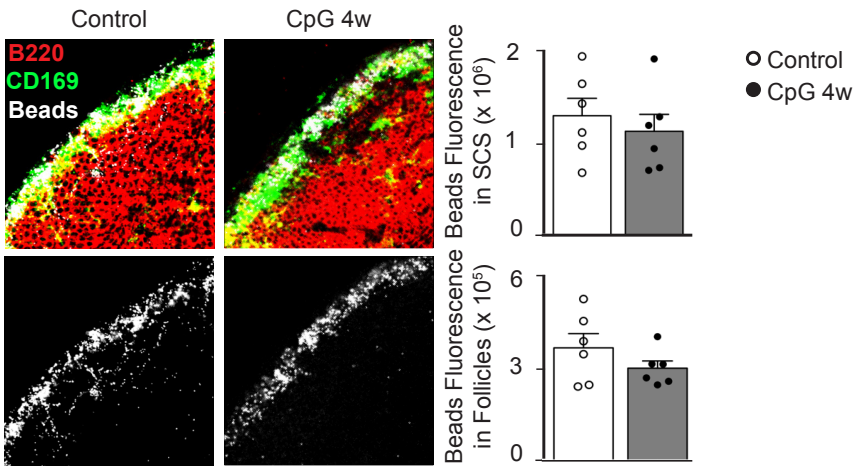

Figure 3.31 Antigen retention is restored after macrophage layer recovery

Confocal microscopy images of LN cryosections from mice treated with PBS or CpG and injected again 4 weeks later with 8.10^8 fluorescent microspheres (0.2 µm, white). Sections were labelled with antibodies to B220 (red) and CD169 (green). Scale bar, 60µm. Bar charts represent antigen fluorescence quantification in SCS and follicles for a single experiment. Data are representative of two independent experiments with three mice per condition.

3.4.4 Macrophage layer disruption impedes acquisition of subsequent arriving antigen by cognate B cells

As antigen retained by SCS macrophages can be presented to follicular B cells, I examined the impact of inflammation on the ability of cognate B cells to acquire antigen arriving to the node in a subsequent wave. To this end, I generated $TLR9^{-/-}$ $MD4^{+}$ transgenic mice in order to obtain B cells that express a transgenic BCR with high affinity for HEL (hen egg lysozyme) and are unable to directly sense the presence of CpG. By using $TLR9^{-/-}$ B cells I could exclude any possible secondary effect on B cells of the CpG used to induce inflammation. Primary B cells from $TLR9^{-/-}$ $MD4^{+}$ mice were isolated and labelled with SNARF, in order to track them during the experiment. $5x10^6$ labelled $TLR9^{-/-}$ $MD4^{+}$ primary B cells were

adoptively transferred into wild type recipient animals. The following day, these mice were injected in the footpad with either PBS (control) or CpG and four days later, they were challenged with either uncoated or HEL-coated fluorescent microspheres. After six hours popliteal LNs were harvested, cryosections stained with anti-B220 (blue) and analysed by confocal microscopy to quantify the extent of BCR-mediated antigen acquisition by adoptively transferred B cells in vivo. At this time, in LNs from control mice, around 50% of antigen specific MD4 B cells (red) had acquired between 1 and 5 HEL-coated microspheres (green) (Figure 3.32A). This uptake was dependent on the BCR as it was not seen upon administration of uncoated microspheres (Figure 3.32A). In contrast, after treatment with CpG, I observed that only 3% of MD4 B cells acquire HEL-coated microspheres and never more than one antigen particle per cell (Figure 3.32A).

I also analysed the extent of B cell acquisition of cognate antigen following inflammation by flow cytometry. A similar adoptive transfer and immunisation protocol was followed. Briefly, CD45.2 TLR9$^{-/-}$ MD4^{+} B cells were transferred into CD45.1 recipient animals. This was useful in order to gate on CD45.2^{+} cells when analysing antigen retention by MD4 B cells. Then, mice were injected with PBS or CpG and challenged with HEL-coated fluorescent beads as before. Popliteal LNs were harvested after six hours, single cell suspensions were stained with anti-CD45.1, anti-CD45.2, anti-B220 and DAPI and analysed by flow cytometry. CD45.1^{+} DAPI^{+} cells were gated out to exclude dead cells and cells from the host (Figure 3.32B). The percentage of CD45.2^{+} B220^{+} cells that were also positive for beads was then analysed. While around 15% of cognate B cells had acquired HEL-coated beads in LNs from control mice, I observed a dramatic reduction in the amount of antigen acquisition by MD4 B cells in mice previously treated with CpG (Figure 3.32B). Thus, in line with the reduction of antigen retention by SCS macrophages, the acquisition of cognate antigen by B cells is reduced in draining LNs after inflammation.

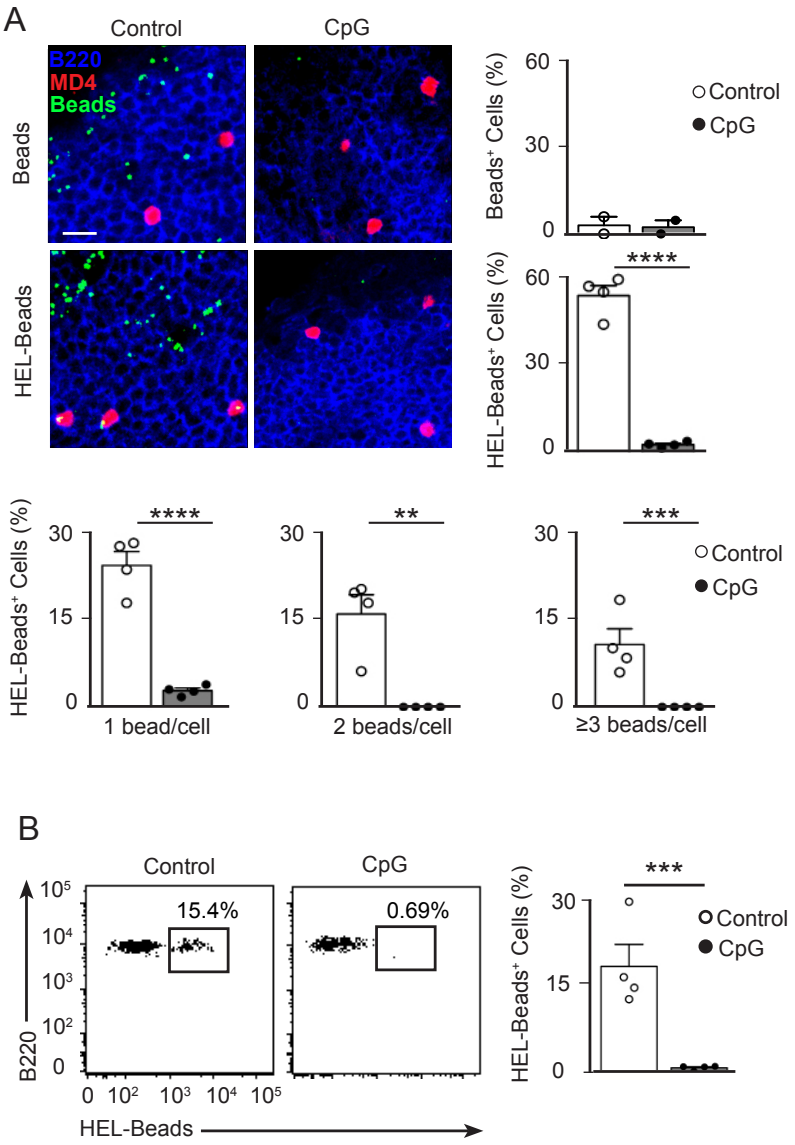

Figure 3.32 Inflammation hampers acquisition of subsequent antigen by B cells

(**A**) Confocal microscopy images of LN from mice that were adoptively transferred with 5x10^6 SNARF-labelled MD4$^+$ *Tlr9*$^{-/-}$ B cells (red) on day 0, footpad administrated with PBS or CpG on day 1, injected again with 8x10^8 avidin fluorescent particles (green) coated or not with HEL on day 5 and sacrificed after 6 hours. Sections were stained with B220 antibody (blue). Scale bar, 20μm. Bar charts represent the proportion of MD4 B cells loaded with different amount of particles for an individual experiment. (**B**) Flow cytometry analysis of popliteal LNs from CD45.1 animals that were treated as (A). Gating is on B220$^+$ cells that have acquired HEL-beads. Quantification of beads-positive cells from a single experiment is shown in the bar chart. In all panels, each dot represents a single mouse. Mean ± s.e.m. All date are representative of at least three experiments. Student t test, **p<0.01, ***p<0.001, ****p<0.0001.

3.4.5 B cell response to 2nd incoming antigen is impaired after inflammation

I then wondered whether this observed reduction in antigen acquisition during inflammation has an effect on the capacity of B cells to respond to subsequent antigenic challenge in vivo. When B cells capture antigen through the BCR, they receive the first activation signal. However to complete the activation and start producing antigen-specific antibodies, they need the help from T cells (Batista and Harwood, 2009). To analyse the formation of antibody secreting cells in response to antigen during normal or inflammatory conditions, I decided to use two different approaches in which B cells receive help from different T cell subsets.

In the first approach, I used the MD4-OTII / HEL-OVA system. In this case, MD4 B cells capture HEL-OVA beads due to the high-affinity of their BCR for HEL. They then present OVA peptides in the context of MHCII and receive help from OT II $CD4^+$ T cells, which express a transgenic TCR specific for OVA (Goodnow et al., 1988, Barnden et al., 1998). This process maximizes the production of HEL-specific antibodies by MD4 B cells. To this end, I adoptively transferred $5x10^6$ $TLR9^{-/-}$ MD4 B cells and $5x10^6$ OT-II T cells into recipient wild type mice. These mice were then treated with either PBS (control) or CpG in the footpad, and six days later were challenged with 2.5µl of HEL-OVA coated microspheres in each footpad. After a further seven days, draining LNs were harvested and ELISPOTs were used to quantify the number of ASCs (antibody secreting cells). The LNs of control mice contained HEL-specific ASCs to the order of 10^3 (Figure 3.33A). In contrast, when local inflammation was induced with CpG before particulate antigen administration, the number of ASCs in the draining LNs was dramatically reduced (Figure 3.33A).

For the second strategy, I used the MD4-NKT / HEL-αGalCer system. αGalCer is a glycolipid antigen that is presented by B cells in the context of CD1d. This allows the recruitment of endogenous NKT cells to complete B cell activation (Barral et al., 2008). Initially, $5x10^6$ $TLR9^{-/-}$ MD4 B cells were adoptively transferred into wild type recipient mice. These mice were then treated with either PBS (control) or CpG in the footpad, and six days later received microspheres coated with both HEL and α-GalCer. After seven further days, popliteal LNs were

harvested and the number of ASCs was examined by ELISPOT. This analysis revealed that the number of HEL-specific ASCs formed in LNs from control mice was in the order of 10^2 (Figure 3.33B). However, in mice that had been previously treated with CpG, the formation of HEL-specific ASCs was significantly reduced (Figure 3.33B). In summary, these two approaches demonstrate that inflammatory signals do indeed have a direct effect on the extent to which B cells can acquire and respond to further antigenic challenge in vivo.

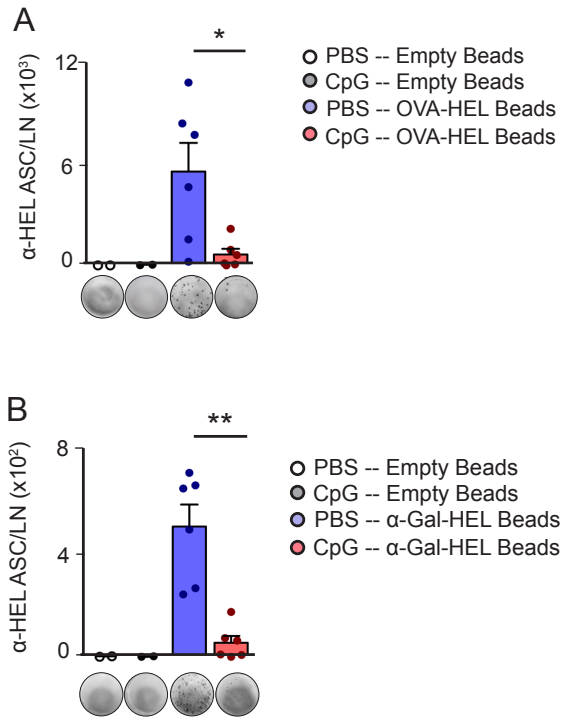

Figure 3.33 Inflammation blocks B cell response to subsequent incoming antigen

(**A** and **B**) ELISPOT analysis of HEL-specific ASCs (day 14) in popliteal LNs of animals that were adoptively transferred with (A) 5 x 10^6 MD4 *Tlr9*$^{-/-}$ B cells and 5 x 10^6 OT-II T cells or (B) 2 x 10^6 MD4 *Tlr9*$^{-/-}$ B cells, footpad injected with PBS or CpG on day 1 and injected again with (A) OVA-HEL beads or (B) αGalCer-HEL beads on day 7. Bar charts represent the number of HEL-specific ASCs in each condition for an individual experiment. Data are representative of three independent experiments. Each dot in bar charts represents a single mouse. Mean± s.e.m. Student t test, *p<0.05, **p<0.01.

All together these experiments demonstrate that the disruption of SCS layer by inflammatory signals have a direct effect on the extent to which B cells can acquire a subsequent incoming antigen as well as on their overall capacity to respond to further antigenic challenge in vivo.

3.5 Inflammation and primary infection shut down B cell responses to subsequent pathogens

During a local infection or inflammation, there is a temporary disruption of the SCS macrophage barrier in the draining LNs. This process temporarily impairs the retention of a subsequent incoming antigen to draining LNs, resulting in less acquisition of antigen by B cells. I therefore next investigated the potential effect that this local and temporary disruption might have on the B cell responses to secondary pathogens.

3.5.1 Inflammation dampens B cell response to subsequent viral infection

Firstly, I analysed the effect of local inflammation on the B cell response to a subsequent viral infection. To this end, wild type mice were injected with PBS (control) or CpG in the footpad and seven days later locally infected with 10^4 PFU of VACV. After seven further days, popliteal LNs were harvested and the antiviral B cell response analysed. B cell differentiation into GCs was analysed by flow cytometry and immunohistochemistry. For flow cytometry, single cells suspensions were stained with anti-B220 and the GC markers: anti-GL7 and anti-CD95. Following VACV infection, LNs from PBS-treated mice exhibited a dramatic expansion of the $GL7^+Fas^+$ B cell population (Figure 3.34A). In contrast, this expansion was substantially impaired in popliteal LNs from CpG-treated mice (Figure 3.34A). I further analysed GC formation by the staining of cryosections with anti-B220 (red) and the GC marker Bcl6 (cyan) (Calado et al., 2012). Following 9 days of VACV infection, the formation of $Bcl6^+$ structures, corresponding to GCs, was observed in the B cell follicles of control mice (Figure 3.34B). However, the formation of GC structures was substantially impaired in the LNs from CpG-treated mice (Figure 3.34B).

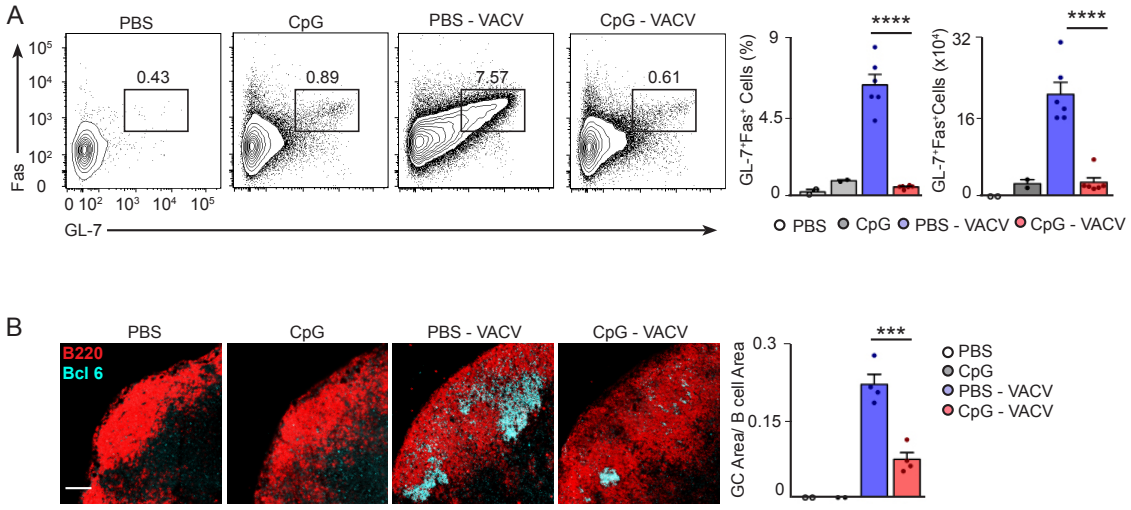

Figure 3.34 Inflammation shuts down GC response to subsequent viral infection

(**A**) Flow cytometry analysis of GC formation (day 14) in popliteal LNs from mice that were administered with PBS or CpG in the footpad and 7 days later infected with 10^4 PFU of VACV. Representative contour plots display the percentage of $B220^+$ cells that are $GL\text{-}7^+Fas^+$. Bar charts display the quantification of $GL\text{-}7^+Fas^+$ B cells in the different conditions for a single experiment. (**B**) Confocal microscopy analysis of popliteal LNs from mice treated as in (A). Sections were stained with mAbs to B220 (red) and Bcl-6 (cyan). Scale bar, 60µm. Quantification of the GC area for an individual experiment is depicted on the right bar chart. Experiments were performed at least three times and each dot represents a different mouse. Mean ± s.e.m. Student t test, ***p<0.001 and ****p<0.0001.

I went on to analyse the B cell differentiation into PCs (plasma cells) by flow cytometry and ELISPOT. For flow cytometry, single cell suspensions were stained with anti-B220, the PC marker CD138 and anti-IgD. PCs express high levels of CD138, intermediate levels of B220 and low or undetectable levels of IgD in the surface (Shi et al., 2015). After VACV infection, LNs from control mice display an expansion of the $CD138^+IgD^-$ PC population (Figure 3.35A). In contrast, PC differentiation was severely decreased in popliteal LNs from CpG-treated mice (Figure 3.35A). I also analysed the formation of VACV-specific ASCs by ELISPOT. After 7 days of VACV infection, VACV-specific ASCs were detected in the order of 10^3 in control mice (Figure 3.35B). In contrast, the formation of VACV-specific ASCs, both IgM and IgG secreting cells, was completely impaired in LNs from CpG-treated mice (Figure 3.35B). Collectively, these results show that local

inflammation impairs the B cell response to subsequent viral infections in the draining LNs.

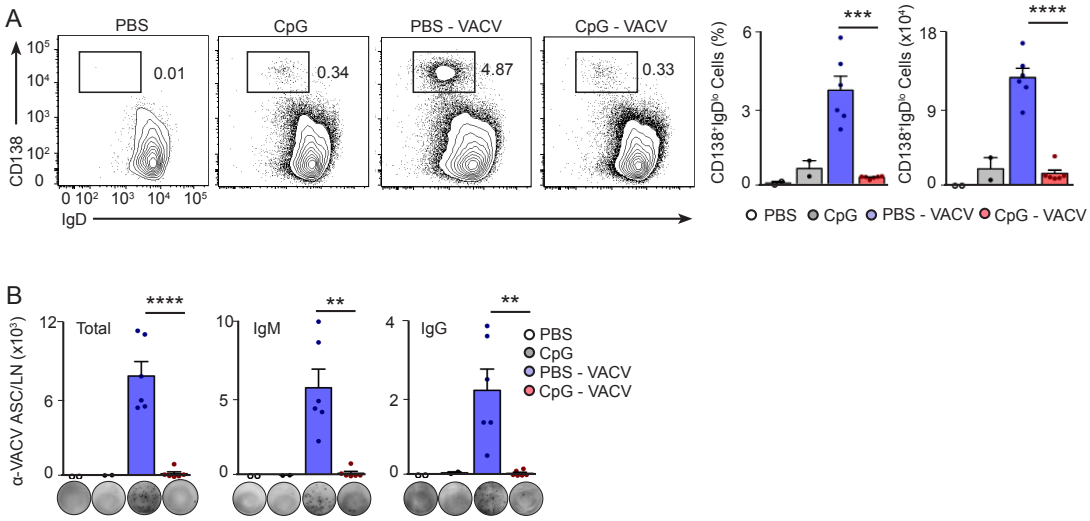

Figure 3.35 Inflammation blocks PC formation to subsequent viral infection

(**A**) Flow cytometry analysis of PC formation (day 14) in popliteal LNs from mice that were administered with PBS or CpG in the footpad and infected 7 days later with 10^4 PFU of VACV. Representative contour plots show the percentage of $B220^+$ cells that are also $CD138^+IgD^{low}$. The quantification of $CD138^+IgD^{low}$ B cells for a single experiment is shown on the right bar charts. (**B**) ELISPOT analysis of total, IgM and IgG VACV-specific ASCs in popliteal LNs from mice that were treated as in (A). Bar charts represent the number of VACV-specific ASCs for an individual experiment. Experiments were performed at least three times and each dot represents a different mouse. Mean ± s.e.m. Student t test, **p<0.01, ***p<0.001 and ****p<0.0001.

3.5.2 Antiviral B cell response is subsequently recovered

As shown in Figure 3.5, the disruption of the SCS macrophage layer after inflammation is temporary and the layer is recovered around 4 weeks later. The recovery of the structural integrity of this barrier also restores the antigen retention capacity of the LN (Figure 3.31). Therefore I wondered whether the recovery of the macrophage layer and its antigen retention capacity after inflammation would restore the B cell response to following incoming virus to the LN. To analyse this, mice were injected in the footpad with PBS or CpG and after 4 weeks they were locally infected with 10^4 PFU of VACV. LNs were harvested 7 days later and GC response was analysed by flow cytometry and PC differentiation by flow cytometry and ELISPOT. Importantly, the formation of $GL7^+Fas^+$ GCs, $CD138^+IgD^-$ PCs and

VACV-specific ASCs, were similar in both groups of mice (Figure 3.36A–C). The restoration of B cell responses towards the second wave of infection was consistent with the timeframe of recovery of the structural integrity of the SCS macrophage layer and its capacity to retain antigen four weeks after inflammation.

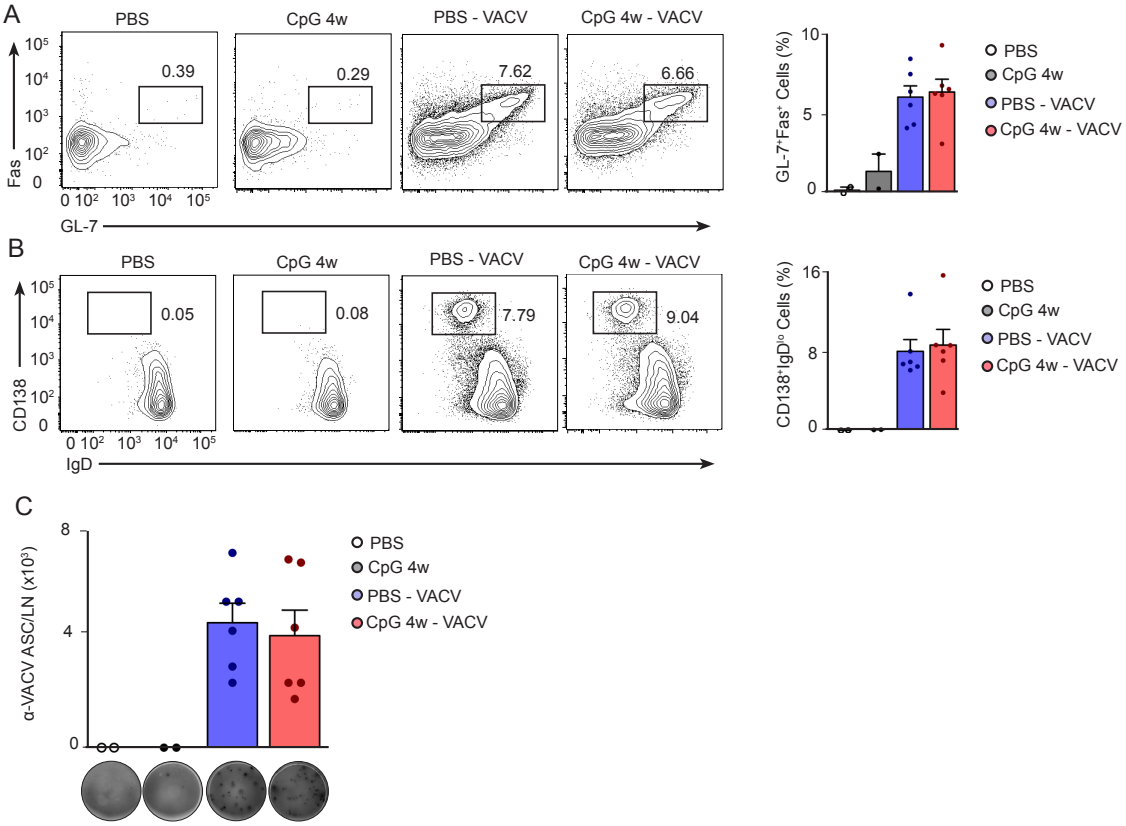

Figure 3.36 Humoral response is restored following macrophage layer recovery

(**A** and **B**) Flow cytometry analysis of GC and PC formation in mice injected with PBS or CpG and infected 4 weeks later with 10^4 PFU of VACV. Popliteal LNs were harvested 7 days after infection. Representative contour plots display the percentage of $B220^+$ cells that are (A) $Fas^+GL\text{-}7^+$ or (B) $CD138^+IgD^{low}$. The quantification of GCs and PCs in the different conditions for a single experiment is shown in the bar charts on the right. (**C**) ELISPOT analysis of total VACV-specific ASCs in popliteal LNs from mice that were treated as in (A and B). All data are representative of two independent experiments. Each dot represents a different animal. Mean ± s.e.m.

3.5.3 Chemical and genetic ablation of SCS macrophages hamper B cell immunity

To formally establish that impaired responses to VACV result from SCS macrophage disruption after CpG treatment, I employed two alternative ways of depleting SCS macrophages in the LN. In the first, SCS macrophages were depleted by the use of clodronate liposomes. Macrophages are highly phagocytic cells that digest microorganisms and non-self particles. When macrophages phagocytose these liposomes, the clodronate inside the liposome vesicles is released and accumulates inside the cell. Once this soluble clodronate reaches a certain intracellular concentration, it induces apoptosis of the macrophages (van Rooijen, Sanders and van den Berg, 1996). I injected PBS-containing liposomes (control) or clodronate-containing liposomes in the footpad of mice. After 6 days, popliteal LNs were harvested and cryosections stained with anti-B220 and anti-CD169 to assess the depletion efficacy. An almost complete depletion of SCS macrophages was observed in mice receiving clodronate-liposomes, but not in those receiving PBS-containing liposomes (Figure 3.37A). Importantly, medullar macrophages were also targeted by this technique. As this approach was consistently working, I went on to infect mice with 10^4 PFU of VACV in the footpad, six days after initial injection of PBS- or clodronate-containing liposomes. Popliteal LNs were harvested one week after viral infection and B cell response was assessed by flow cytometry and ELISPOT. While a considerable expansion of the GCs, PCs and VACV-specific ASCs was observed in mice receiving PBS-liposomes, this process was significantly reduced in mice receiving clodronate-containing liposomes (Figure 3.37B-D). The results suggest that the structural integrity of the macrophage barrier is essential for the development of the B cell response against an incoming virus to the LN. However, the local use of clodronate-containing liposomes, not only depletes SCS macrophages, but also the other phagocytic cells present in the draining LNs such as medullary macrophages, and to a lesser extent, DCs.

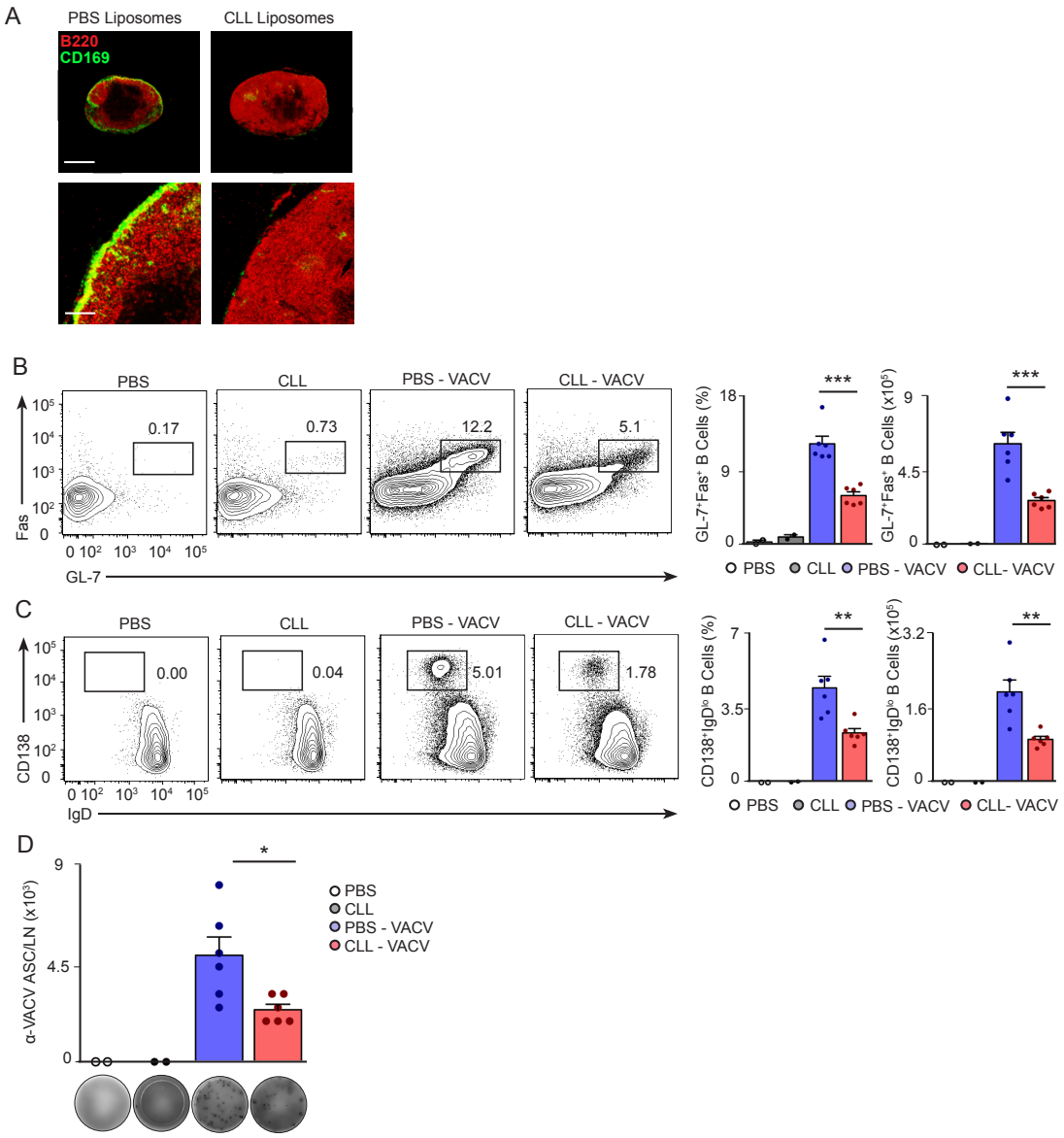

Figure 3.37 Clodronate treatment reduces antiviral B cell response

(**A**) Confocal microscopy analysis of popliteal LNs 6 days after footpad injection of PBS- (control) or clodronate-containing (CLL) liposomes in wild type mice. Sections were stained with mAbs to B220 (red), and CD169 (green). Scale bars, 300µm (top); 60µm (bottom). (**B** and **C**) Flow cytometry analysis of (B) GC and (C) PC formation in wild type mice that were injected with PBS or CLL liposomes and 6 days later infected with 10^4 PFU of VACV. Popliteal LNs were harvested after 7 days of infection and analysed by flow cytometry. Representative contour plots display the percentage of $B220^+$ cells that are (B) $GL\text{-}7^+Fas^+$ or (C) $CD138^+IgD^{lo}$. Quantifications of GCs and PCs in the different conditions for a single experiment are shown in the right bar charts. (**D**) ELISPOT analysis of total VACV-specific ASCs in popliteal LNs from mice that were treated as in (B and C). Data are representative of two independent experiments. Each dot represents a different animal. Mean ± s.e.m. Student t test *p<0.05, **p<0.01 and ***p<0.001.

I therefore considered using a more specific way of targeting SCS macrophages. To this end, I imported a mouse strain from the Riken Institute in Japan that expresses the human DTR (difteria toxin receptor) under the CD169 promoter (Miyake et al., 2007). When DT is administered to these mice, it induces cell death in CD169-expressing cells by inhibiting the protein synthesis process. I injected PBS or DT in the footpad of $CD169^{DTR/+}$ mice. After 6 days, popliteal LNs were harvested and cryosections stained with anti-B220 and anti-CD169 to assess the efficiency of this procedure. A near-complete depletion of SCS macrophages was observed in $CD169^{DTR/+}$ mice following DT but not PBS administration (Figure 3.38A). Importantly, in this case, medullar macrophages were not as reduced as in the case of clodronate-containing liposome injection. This could be due to the lower level expression of CD169 compared to their SCS counterparts. Moreover, DCs would not be affected in this procedure, as the great majority of them do not express CD169. With this technique I was mostly targeting SCS macrophages, so I proceeded to infect $CD169^{DTR/+}$ mice with 10^4 PFU of VACV in the footpad, six days after initial administration of PBS or DT. As before, popliteal LNs were harvested one week after viral infection and the development of GCs and PCs was quantified using flow cytometry. The formation of both GCs and PCs was dramatically reduced in the $CD169^{DTR/+}$ mice that received DT prior to infection with VACV compared to the ones that received PBS (Figure 3.38B-C). Together, these two approaches indicate that the presence of $CD169^{+}$ macrophages in the LN SCS is important for the initiation of the B cell response during a viral infection.

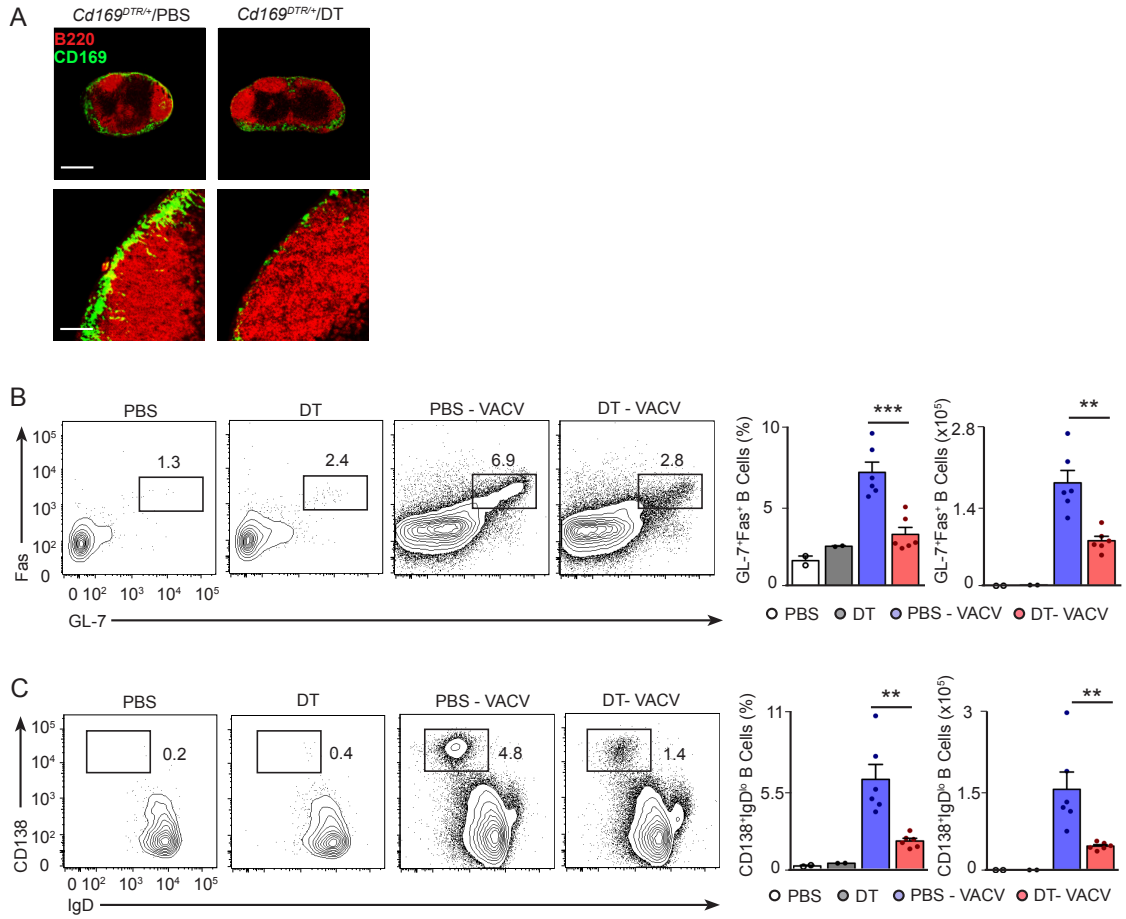

Figure 3.38 CD169-DTR mice have reduced antiviral B cell response

(**A**) Confocal microscopy analysis of popliteal LNs 6 days after footpad injection of PBS or DT in *Cd169-DTR*$^{+}$ mice. Sections were stained with mAbs to B220 (red), and CD169 (green). Scale bars, 300µm (top); 60µm (bottom). (**B** and **C**) Flow cytometry analysis of (B) GC and (C) PC formation in *Cd169*$^{DTR/+}$ mice that were injected with PBS or DT and 6 days later were infected with 10^4 PFU of VACV. Popliteal LNs were harvested after 7 days of infection and analysed by flow cytometry. Representative contour plots display the percentage of B220^{+} cells that are (B) GL-7^{+}Fas^{+} or (C) CD138^{+}IgD^{lo}. Quantifications of GCs and PCs in the different conditions for a single experiment are shown in the right-hand bar charts. All data are representative of three independent experiments. Each dot represents a different animal. Mean ± s.e.m. Student t test **p<0.01 and ***p<0.001.

3.5.4 Inflammation dampens B cell-mediated immunity to subsequent bacterial infection

I then wondered whether this disruption of the SCS macrophage barrier during inflammation or its inducible depletion would also interfere with the B cell response during localised bacterial infections. To analyse this, I injected PBS, CpG

or clodronate-containing liposomes in the ear dermis. After seven days, cervical draining LNs were harvested and cryosections stained with anti-B220 and anti-CD169 to assess the integrity of the macrophage barrier. After CpG treatment, cervical LNs were greatly expanded, with a substantial enlargement of the B cell follicles (Figure 3.39A). Importantly, the macrophage barrier was severely disrupted as observed in popliteal LNs following footpad injection of CpG (Figure 3.39A). In the case of clodronate treatment, cervical LNs were also somewhat expanded and a complete depletion of SCS and medullar macrophages was observed (Figure 3.39A). I therefore moved to inject mice with PBS, CpG or clodronate in the ear dermis and after seven days locally infected them with 10^7 CFU of *Staphylococcus aureus*. Seven days after infection, cervical LNs were harvested and the B cell response was analysed by flow cytometry. A dramatic expansion of GCs and PCs was observed after *S. aureus* infection compared to non-infected mice (Figure 3.39B-C). In contrast, a significant reduction in GC and PC formation was observed when mice received CpG or clodronate in the ear before infection with *S. aureus* (Figure 3.39B-C). Therefore, it does indeed appear that the local disruption of the SCS macrophage layer triggered by inflammation dramatically affects the ability of B cells to mount responses to viral or bacterial antigen arriving in a secondary wave.

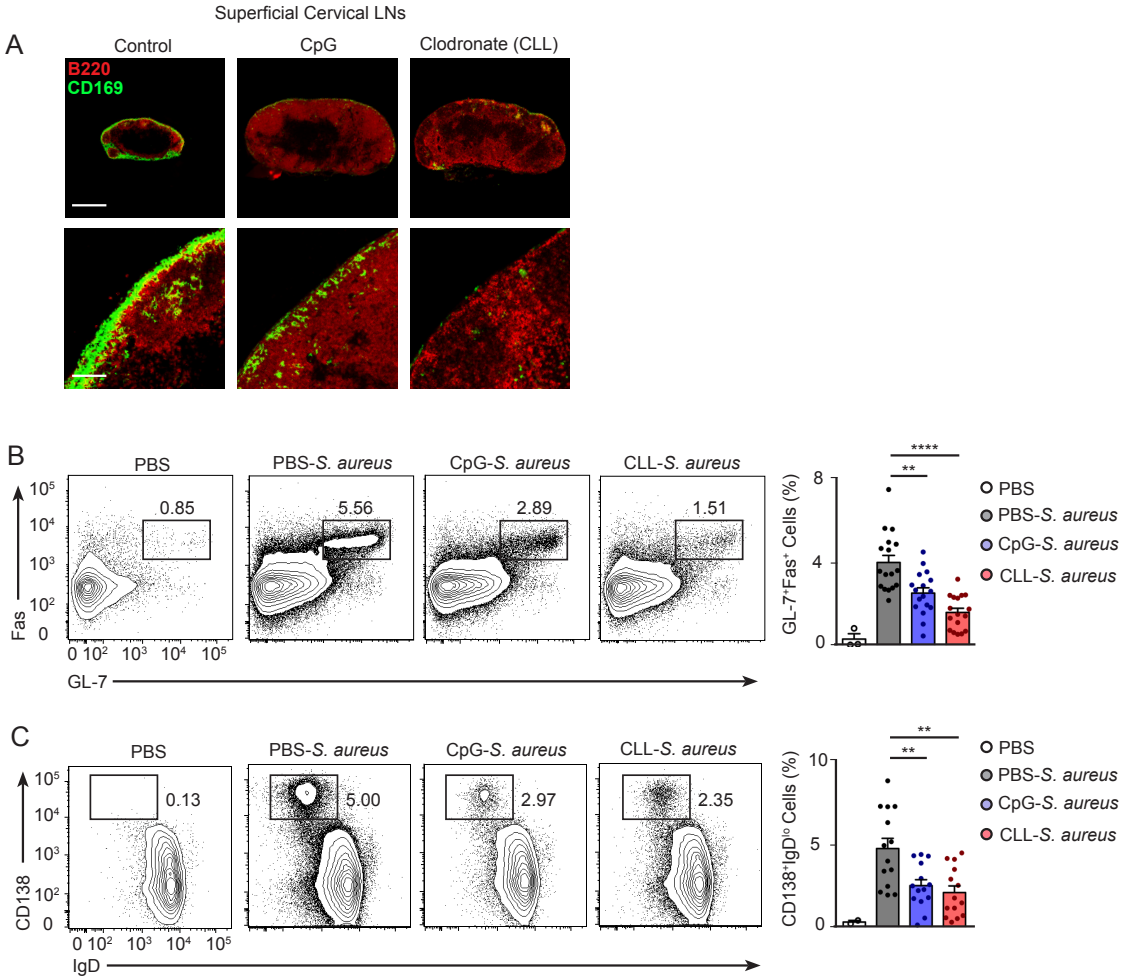

Figure 3.39 SCS macrophage disruption reduces B cell response to *S. aureus*

(**A**) Confocal microscopy analysis of superficial cervical LNs 7 days after ear administration of PBS, CpG or CLL-liposomes. Sections were stained with mAbs to B220 (red), and CD169 (green). Scale bars, 300µm (top); 60 µm (bottom). (**B** and **C**) Flow cytometry analysis of GC and PC formation in mice administered with PBS, CpG or CLL liposomes and infected 7 days later with 10^7 CFU of *S. aureus*. Superficial cervical LNs were harvested 7 days after infection. Representative contour plots display the percentage of $B220^+$ cells that are (B) $Fas^+GL\text{-}7^+$ or (C) $CD138^+IgD^{low}$. The quantification of GCs and PCs in the different conditions from three independent experiments is shown on the right-hand bar charts. Each dot represents a different animal. Mean ± s.e.m. Student t test **p<0.01 and ****p<0.0001.

3.5.5 Primary infection impairs B cell response to secondary pathogens

Finally, I wondered whether SCS macrophage disruption during a primary infection hampers the ability of B cells to respond to a secondary pathogen. To address this, I set up a bacteria-virus double infection model. I first injected mice

with PBS (control) or 10^6 CFU of Group B *Streptococcus* in the footpad. After 7 days, when a complete disruption of the macrophage layer was observed (Figure 3.1B), mice were infected with 10^4 PFU of VACV. After a further 7 days, popliteal LNs were harvested and the formation of VACV-specific ASCs was measured by ELISPOT. The development of VACV-specific ASCs, both IgM and IgG-secreting cells, was significantly reduced in mice previously infected with GBS (Figure 3.40). This result is consistent with the idea that the loss of integrity of the SCS macrophage layer during primary local infections severely affects the capacity of B cells to respond to secondary pathogens.

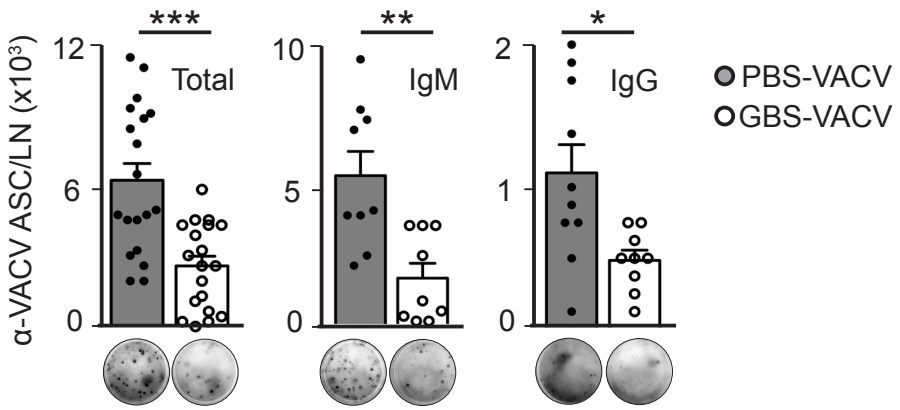

Figure 3.40 Primary infection shuts down B cell response to secondary pathogen

ELISPOT analysis of total, IgM and IgG VACV-specific ASCs (day 14) from mice that were footpad-administered with PBS or 10^6 CFU of GBS and then infected with 10^4 PFU of VACV on day 7. Bar charts represent the number of VACV-specific ASCs from three independent experiments. Each dot represents a different mouse. Mean ± s.e.m. Student t test, *p<0.05, **p<0.01, ***p<0.001.

3.6 Discussion

In recent years, SCS macrophages have been placed at the heart of anti-pathogen responses due to their key role in antigen trapping and immune response initiation (Carrasco and Batista, 2007, Junt et al., 2007, Phan et al., 2007, Chtanova et al., 2008, 2009, Gonzalez et al., 2010, Coombes et al., 2012, Garcia et al., 2012, Kastenmüller et al., 2012). In this chapter, I have shown that after local infection or inflammation, draining LNs undergo a dramatic architectural reorganisation. This phenomenon not only involves an increase in the B cell follicles' size but also a severe disruption of the SCS macrophage layer. Analysis of this process by a set of different imaging techniques revealed that this structural rearrangement of the macrophage layer is a result of both cell loss and the retraction of these cells from the SCS to inner follicular areas. This disruption process is initiated by the arrival of peripheral DCs into draining LNs after local inflammation and, importantly, it is a localised and temporary event, being restricted to draining LNs and lasting for a defined period of time. I found that the temporary loss of macrophage layer integrity has a severe impact on the ability of these LNs to retain and capture antigen from a subsequent wave of infection. This impairment has deep consequences in the ability of follicular B cells to acquire cognate antigen and to mount an appropriate immune response during subsequent secondary infections (Figure 3.41) (Gaya et al., 2015).

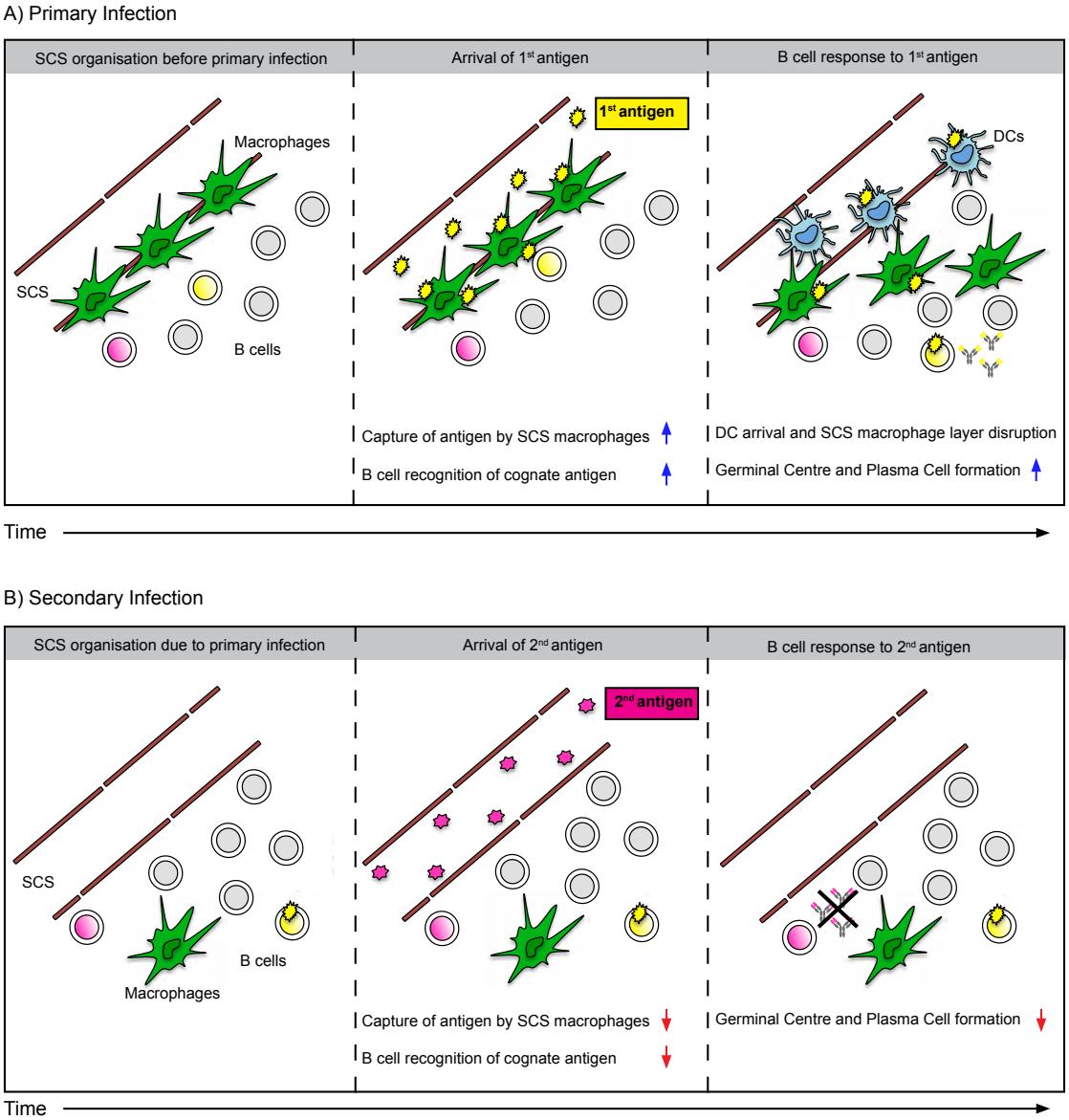

Figure 3.41 SCS macrophages: guardians of the B cell response

Model proposed for (**A**) the effect of a primary infection or inflammation on the organisation of CD169$^+$ macrophages at the SCS and (**B**) the consequences of this process on the B cell response to secondary pathogens.

Early electron microscopy and more recent dynamic imaging studies have shown that during steady state conditions, CD169$^+$ macrophages are a sessile population that lay longitudinally on the SCS floor, with their cell bodies projected into the SCS lumen and their nucleus located within the LN parenchyma (Farr, Cho and De Bruyn, 1980, Fossum, 1980, Szakal, Holmes and Tew, 1983, Carrasco and

Batista, 2007, Junt et al., 2007, Phan et al., 2007). The exact mechanisms dictating the placing and orientation of these cells however, is still poorly understood. Some reports have suggested that lymph-borne signals play an important role based on the observation that cessation of afferent lymphatic flow causes the inward movement and eventual disappearance of these cells (Mebius et al., 1990, 1991). In addition, B cell-derived lymphotoxin-a1b2 signalling is required for the establishment and differentiation of this macrophage population, as mice lacking lymphotoxin-a1b2 on B cells have reduced number of SCS macrophages, and those remaining have an immature phenotype (Phan et al., 2009, Moseman et al., 2012). In this chapter, I have shown that the blockage of E-cadherin- but not integrin-mediated adhesions, results in the partial scattering of the SCS macrophages. Therefore, even though the maintenance of the SCS macrophage layer in steady state conditions is not dependent on integrin-mediated adhesions, it might involve E-cadherin-mediated interactions. Furthermore, I found that chemokine signalling is essential for the retention of $CD169^+$ macrophages at the LN SCS in the steady state, as blockage of intracellular chemokine signalling with *Pertussis* toxin induces an almost complete disruption of this macrophage layer in the SCS. This effect could be due to direct inhibition of chemokine signalling in SCS macrophages or an indirect effect caused by the interruption of chemokine signalling in other LN cells. For example, the lack of specific chemokine receptors in LECs can hinder the migration of DCs from the SCS to the LN parenchyma, even though intrinsic signalling in DCs remains unaltered. This is due to the ability of some cells to regulate chemokine gradients in the different LN compartments (Ulvmar et al., 2014). In my case, as CXCR5 signalling in B cells induces lymphotoxin-a1b2 upregulation (Cyster et al., 2000), it could then be that pertussis toxin might inhibit the production of lymphotoxin-a1b2 by B cells, compromising in this way, the integrity of the macrophage layer. In the future, it would be important to define the mechanism by which chemokine signalling is involved in the maintenance of $CD169^+$ macrophages at the SCS.

SCS macrophages are stably positioned in their location during steady state conditions. However, whether these macrophages change their distribution and organisation during the course of an immune response was not clear. A previous work by Ellen Robey's group showed that neutrophil migration to the LN

after *Toxoplasma gondii* infection induces the clearance of SCS macrophages in the sites of neutrophil cluster formation (Chtanova et al., 2008). Although it is not clear what induces this cell loss, the authors suggest that it might be mediated by the secretion of matrix metalloproteinases by neutrophils arriving at the SCS. Here, I established that local infection with virus or bacteria, and the inflammation process associated with that infection, induces a general disruption of the SCS macrophage layer. This phenomenon is quite different from the one described above. Firstly, the loss of macrophage layer integrity covers the whole of the SCS and not just small, delimited areas. Moreover, this process is not only due to cell loss, as observed during parasite infection, but also because of a massive retraction of these macrophages to inner follicular areas. The differences may come from the nature of the pathogens used in the studies and by the effector immune responses elicited in each case.

The local loss of the macrophage integrity after inflammation is a temporary process, as the layer is restored within three to four weeks of inflammation induction. The recovery could be due to the return of macrophages to their initial position after transiently moving inwards into the B cell follicles. An alternative is that macrophages remaining in the SCS undergo local proliferation to re-cover the whole area of the SCS, as observed with pleural macrophages following parasite infection (Jenkins et al., 2011). Thirdly, this recovery could be due to the recruitment of *de novo* peripheral macrophages to the SCS. In fact, a previous study showed that incoming macrophages could completely repopulate the popliteal LN within two to five months of their clodronate-mediated depletion (Delemarre et al., 1990). The faster recovery observed in my study could be due to inflammation triggering the initial disruption of the SCS macrophage layer and at the same time speeding up the recruitment of new macrophages to restore the original cell layer. Furthermore, clodronate-liposomes could also be depleting macrophage progenitors and therefore delaying the recovery of the macrophage layer.

This loss of integrity of the SCS macrophage layer during inflammation could be occurring for several reasons: expansion of the LN SCS without expansion of local macrophages, inflammation-induced death of macrophages,

intrinsic signalling in these cells that induces migration and/or other immune cells extrinsically mediating this disruption. The first explanation implies that this phenomenon would be merely a passive process caused by the increase in LN dimensions. 3View electron microscopy showed that following inflammation, SCS lining cells stretch out to accommodate the increase in size. It might be that the macrophages, anchored to these SCS lining cells, are simply pulled apart in the expansion process. Although this could explain the lateral scattering of the cells, it fails to explain the inward movement of macrophages to the follicles. Furthermore, although MyD88$^{flox/flox}$ CD11c-Cre^{+} and CCR7$^{-/-}$ mice displayed enlarged LNs after inflammation, the SCS macrophage layer remained almost intact, suggesting that this disruption process is not just due to an increase in LN dimensions. The second hypothesis, which suggests that macrophage layer disruption is the result of inflammation-induced cell death, arose from a recent report showing that *Pseudomonas aeruginosa* infection induces IL-1β and IL-18 production by SCS macrophages. The synthesis of these cytokines is mainly dependent on inflammasome activation, which usually concludes with pyroptosis of the cells (Kastenmüller et al., 2012). However, the disruption of SCS macrophages is not a result of inflammasome-mediated pyroptosis, as genetic interference with the assembly of the inflammasome complex did not prevent the disruption of the macrophage layer. The third possibility implies that direct detection of inflammation by macrophages induces the migration of these cells from the SCS to the inner parenchyma. Although this could be a potential scenario to explain the disruption of the macrophage layer, I was not able to experimentally address it. This is due to the genetic targeting of components of the TLR-signalling pathway in these macrophages proving to be ineffective. I attempted to abrogate MyD88 expression on SCS macrophages by developing MyD88$^{flox/flox}$ Lyz2-Cre^{+}, however, MyD88 levels remain unchanged in these macrophages, probably due to their low expression of lysozyme (Phan et al., 2009). The generation of CD169-Cre mice would be valuable to enable genetic targeting of this macrophage population.

To address the fourth hypothesis, I genetically and biologically targeted various immune cells. Even though B cells are required for SCS macrophage development and differentiation (Phan et al., 2009, Moseman et al., 2012), the prevention of B cell recognition of inflammatory signals or their absence does not

prevent SCS macrophage disruption. T cells are also not involved in this disruption as lymphocyte-deficient mice display a normal disruption of the macrophage layer after inflammation. NK cells and neutrophils are recruited to the LN SCS after infection: NK cells are known to mediate the lysis of infected cells and neutrophils have been shown to induce the localised clearance of SCS macrophages during parasite infection (Chtanova et al., 2008, Coombes et al., 2012, Garcia et al., 2012, Kastenmüller et al., 2012). However, biological depletion of NK cells or neutrophils did not prevent the disruption of the macrophage layer after the induction of inflammation. Therefore, even though the huge influx of neutrophils into the LN SCS after parasite infection mediates the localised destruction of SCS macrophages, this process seems not to be a general feature of inflammation. I found that the arrival of migratory DCs to the LN SCS during inflammation is involved in the disruption of the macrophage layer. In fact, inhibition of DC sensing of inflammatory molecules, or blockage of their migration to the LNs, results in a dramatic decrease of the macrophage layer disruption. Furthermore, local administration of mature BM-DCs induces similar structural rearrangements of the macrophage layer to those observed during inflammation. Importantly, these observations parallel the findings made by Förster and colleagues, who found that intralymphatic injection of mature BM-DCs induces profound changes in the SCS floor, with $CD169^+$ macrophages elongated and aligned in parallel to immigrating DCs (Braun et al., 2011). The mechanism by which incoming DCs induce the disruption of the macrophage layer is not known. It could be possible that in order to gain access to the lymphoid tissue, DCs pass through the SCS inner wall fenestrations, pushing away the $CD169^+$ macrophages that normally occlude these fenestrations (CLARK, 1962). However, if this event were simply a consequence of macrophage disturbance by incoming DCs as they traverse the SCS floor, then the disruption would be greater in the inter-follicular areas, where there is active transmigration of DCs (Schumann et al., 2010, Gerner et al., 2012). In contrast, the macrophage layer is equitably disrupted along the whole length of the SCS, suggesting that rather than displacing macrophages, incoming DCs might signal them to migrate as well (Hickman, 2015). As the retention of $CD169^+$ macrophages on the SCS requires E-cadherin interactions and chemokine signalling, it might be possible that incoming DCs produce soluble factors that mediate the loosening of

E-cadherin interactions, such as IL-1 or TNF-α (Jakob and Udey, 1998), or which induce changes in the steady state levels of chemokines in the SCS.

The loss of integrity of the macrophage layer during a primary immune response renders draining LNs temporarily blind to pathogens entering on a secondary wave. This phenomenon might not only affect the initiation of the B cell response to subsequent pathogens but also interfere with other processes that require a functional layer of macrophages. For example, Cyster and colleagues showed that the relay of immune complexes from SCS macrophages to non-cognate B cells and then to FDCs plays a key role in the antibody affinity maturation process (Phan et al., 2009). It is conceivable then, that the transport of immune complexes from SCS macrophages to FDCs is also impaired during this period. Furthermore, several studies showed that SCS macrophages are essential to prevent systemic dissemination of pathogens (Iannacone et al., 2010, Kastenmüller et al., 2012). This temporary disruption might, therefore, result in the spreading of pathogens to other lymphoid organs, such as spleen and further LNs following local infection. It is feasible that these organs might take control of the secondary infection while local LNs focus the response on primary pathogens.

The temporary inability of local LNs to respond to subsequent challenges provides a potential explanation for the increased susceptibly of the organism to contract secondary bacterial infections, such as *Streptococcus pneumoniae*, during influenza pandemics and epidemics (Brundage and Shanks, 2008). Furthermore, the initial fragmentation of the SCS macrophage layer following primary infection might explain the suboptimal immune response induced by vaccines when children are unwell at the time of vaccination (Zepp, 2010). My findings are in line with previous observations which show that failure of host defences to counteract secondary infections results from the loss of lymphoid tissue integrity (Odermatt et al., 1991, Scandella et al., 2008). For example, systemic infection with LCMV and MCMV (mouse cytomegalovirus) induce downregulation of CCL19 and CCL21, leading to a temporary destruction of splenic T cell areas (Benedict et al., 2006, Mueller, Hosiawa-Meagher and Konieczny, 2007, Scandella et al., 2008). This process, which might be triggered by the cytokine storms accompanying acute infections (Heikenwalder et al., 2004, Mueller, Hosiawa-Meagher and Konieczny,

2007), induces a transient loss of immunocompetence against secondary infections (Odermatt et al., 1991, Scandella et al., 2008). Studies performed by Medzhitov and colleagues offer an alternative view, where the increased susceptibility to secondary infections would be due to compromised innate host defence or impaired ability to tolerate further tissue damage after primary infection (Jamieson et al., 2010, 2013).

The fact that the disruption of the macrophage layer temporarily reduces B cell responses to proximal secondary challenges raises the important question of the potential benefit of such phenomenon. At this stage, I can only speculate as to the answer, although it might help to focus the immune system on primary pathogens by favouring the development of the immune response. For instance, it is possible that the movement of macrophages away from the SCS may favour the entry of afferent lymph-derived immune cells directly through the SCS floor. Cells entering in this way may be better placed to encounter trapped cognate antigen and thus respond to it. In fact, morphological changes on the SCS floor allow lymph-derived T cells to entry the LN through the SCS floor (Braun et al., 2011). Alternatively, the retraction of macrophages from the SCS to the follicular interior might maximise the presentation of antigen to B cells or facilitate antigen relay to FDCs. These two scenarios, concomitantly with the processes of LN shutdown and lymphocyte clonal expansion, would enhance immune responses to primary infecting pathogens. In this way, SCS macrophages might function as a valve that detects inflammation within draining LNs, triggering the temporary suspension of humoral responses to secondary infections to prioritise the effective control of contemporaneous lymph-borne infecting pathogens.

In the future it would be important to analyse the integrity of the macrophage layer in the case of chronic inflammation. This process is commonly observed during persistent infection with tuberculosis or HIV or during autoimmune diseases such as rheumatoid arthritis, lupus or multiple sclerosis (Marshak-Rothstein and Rifkin, 2007, Sasindran and Torrelles, 2011, Deeks, Tracy and Douek, 2013). As inflammation per se can trigger SCS macrophage disruption and shut down antibody responses, this phenomenon may minimise autoimmune responses that develop after lymph drainage of self-antigens (Marshak-Rothstein and Rifkin,

2007). It will be also important to analyse this process in the context of cancer development, as cancer cells frequently use lymphatic vessels and lymph nodes to spread to other parts of the body (Stacker et al., 2014). Furthermore, it would be interesting to analyse the integrity of the macrophage layer in mesenteric LNs, which display a constant arrival of antigens from the intestine and spontaneous formation of GCs (Koni et al., 1997).

I believe that the results presented here might have implications on the rational design of vaccination programs. For example, if children are vaccinated against pathogen A in one arm, then any vaccination against pathogen B, if performed shortly after the previous vaccination, should be applied on the other arm (and therefore different draining LNs) to induce a good immune response.

Chapter 4. BCR and TLR signalling in B cells induce ULK-independent autophagosome formation through the PLCγ2 pathway

4.1 Introduction

4.1.1 B cells and autophagy

B cells are an essential part of the adaptive immunity as they provide specific protection from a variety of potential pathogens. B cells are activated after the recognition of specific antigens by the BCR, which induces intracellular signalling and the internalisation of antigen-loaded BCRs. Following internalisation, antigens are processed into small peptides or lipids followed by loading onto MHC II or CD1d molecules respectively, for presentation at the cell surface. The peptides are recognised by specific $CD4^+$ T cells, and the lipids by NKT cells, both of which then stimulate B cell proliferation and differentiation into antibody-secreting cells (Batista and Harwood, 2009).

Autophagy is an intracellular degradation system that delivers cytoplasmic constituents to the lysosome and is indispensable for the recycling of cell components and for the fulfillment of cell energy demands (Mizushima, 2007). In the present, it is believed to play an important role in the antigen-processing pathway. Different studies have established that tumor, viral and cytosolic self-antigens can enter the MHC II compartments through autophagy for B cell presentation (Paludan et al., 2005, Schmid, Pypaert and Münz, 2007, Ireland and Unanue, 2011). However, the signals that induce this process in B cells and its contribution in the presentation of extracellular pathogens have not yet been investigated.

4.1.2 Autophagosome formation

Autophagy is a highly regulated pathway that can be differentially activated by energy deprivation, ER stress and immune signals, such as viral and bacterial

infection. This process results in the formation of double-membrane organelles called autophagosomes, which engulf macromolecular complexes and organelles for recycling, and pathogens for clearance. Autophagosomes then fuse with lysosomes and mature into autolysosomes, in which all the intravesicular components are degraded (Figure 4.1). In this way, the autophagy response contributes to survival under low-nutrient conditions and also provides protection against pathogens (Levine, Mizushima and Virgin, 2011).

The autophagosome formation involves the interaction between many different protein complexes. Upon autophagy induction, mTOR (mammalian target of rapamycin) complex is inactivated, inducing the translocation of the ULK1 (unc51-like autophagy activating kinase 1) complex to the ER. This process mediates the activation of the ER-specific class III PI3K complex, which catalyses the production of PtdIns3P (phosphatidylinositol-3-phosphate) and recruits effector proteins such as DFCP1 (double FYVE-containing protein 1) and WIPI (WD-repeat protein interacting with phosphoinoside). DFCP1 and WIPI generate ER-associated isolation membranes, also known as omegasomes. The final step of the autophagosome formation involves the elongation and closure of these isolation membranes. This process is mediated by two ubiquitin-like complexes: the Atg12–Atg5-Atg16L1 complex and the LC3 (microtubule-associated protein light chain 3)-phosphatidylethanolamine-conjugate complex (Mizushima, 2007).

The potential interrelation between the components of the different complexes, the mechanisms by which the different stimuli induce the formation of these double-membrane organelles and the origin of the isolation membranes are still very controversial subjects. In the latter case, while it was commonly accepted the isolation membrane was derived from the ER, it has been recently reported that the plasma, nuclear, and even mitochondrial membranes can contribute to the initiation of this process (Tooze and Yoshimori, 2010) .

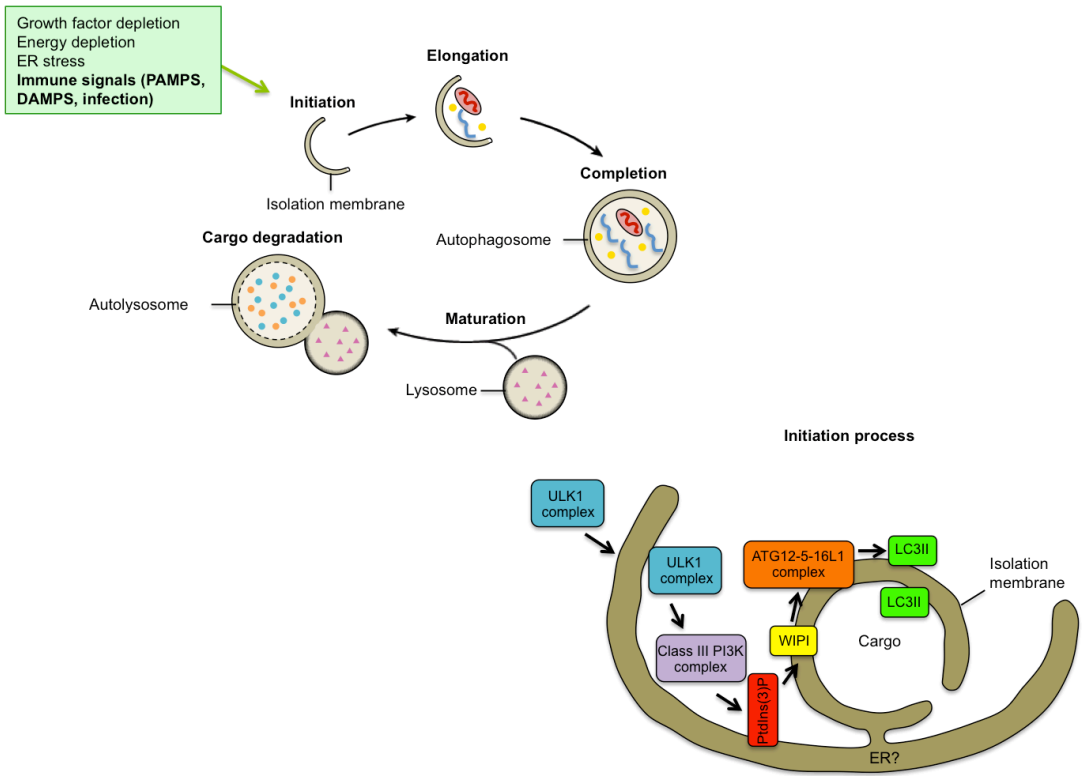

Figure 4.1 Schematic overview of autophagy and its regulation

The top left schematic shows a simplified model of the different steps involved in the autophagosome “life cycle”: membrane initiation, elongation and completion. The major membrane source is thought to be the ER, although several other membrane sources, such as mitochondria and the plasma or nuclear membrane, may contribute. The bottom right schematic shows a simplified model of the current understanding of the molecular events involved in membrane initiation. After induction of autophagy, the ULK1 complex translocates to the ER and activates the ER-localised autophagy-specific class III PI(3)K complex. The PtdIns(3)P formed on the ER membrane recruits WIPIs effector proteins. WIPIs and the Atg12–Atg5–Atg16L1 complex are present on the outer membrane, and LC3–PE is present on both the outer and inner membrane of the isolation membrane.

4.1.3 MHC II compartments receive antigens from autophagosomes

Extracellular antigens are commonly internalised by antigen presenting cells and degraded in lysosomes. Subsequently, antigen-derived peptides, products of lysosomal proteolysis, are loaded on MHCII molecules and presented to $CD4^+$ T cells. Although the main source of MHCII ligands comes from exogenous antigens, it has been shown that several intracellular peptides can gain access to MHCII

compartments through the binding of autophagosomes to these vesicles. This is the case for cytosolic viral peptides and also for citrullinated self-proteins, usually produced during autoimmune diseases (Paludan et al., 2005, Ireland and Unanue, 2011). Thus, autophagy would not only strengthen immune responses to viral infections but also play an important role in the regulation of autoimmunity. Furthermore, coupling of extracellular antigens to LC3, targets antigens to autophagosomes, what leads to a substantial increase in MHCII presentation of extracellular antigens and $CD4^+$ T cell proliferation (Schmid, Pypaert and Münz, 2007). However, whether uncoupled extracellular antigens are delivered to autophagosomes or whether autophagy plays a role in their presentation on MHCII is not established.

4.1.4 Autophagy in B cell responses

Autophagy has recently been shown to be an important regulator of B cell responses. Following antigenic challenge, differentiating plasma cells, long-lived plasma cells and memory B cells display high levels of autophagy, with increased expression of genes that regulate autophagy initiation and autophagosome maturation (Pengo et al., 2013, Chen et al., 2014). Interestingly, B cell-specific ablation of autophagy proteins such as Atg5 or Atg7, results in reduced numbers of long-lived bone marrow plasma cells and memory B cells. This phenomenon results in defective primary or secondary antibody responses after infection with pneumococcus or influenza virus respectively (Pengo et al., 2013, Chen et al., 2014). Autophagy is, therefore, an essential process for the survival of long-lived plasma cells and antigen-specific memory B cells and the maintenance of protective antibody responses required to combat infections. The specific signals that induce autophagosome formation in B cells, and the role of autophagy in the presentation of exogenous pathogens are far from being defined.

4.2 BCR and TLR signalling control autophagosome formation through the PLCγ2 pathway

4.2.1 LC3II accumulation as an indicator of autophagy flux

In order to investigate which signals induce autophagosome formation in B cells, I decided to follow the formation of autophagosomes after B cell stimulation with different stimuli. For this, I measured the accumulation of LC3, which is a specific marker for these double-membrane vesicles (Mizushima, Yoshimori and Levine, 2010). During autophagy, a cytosolic form of LC3 (LC3-I) is conjugated to phosphatidylethanolamine to form LC3-II conjugates; LC3-II is then recruited to autophagosomal membranes (Levine, Mizushima and Virgin, 2011). The detection of LC3 conversion (LC3-I to LC3-II) by western blot is one of the most widely used approaches to measure autophagosome formation, as the amount of LC3-II is directly correlated with the number of autophagosomes. Because of the degradation of cytosolic components and LC3-II during the formation of autophagolysosomes, the interpretation of LC3 levels by Western blot is somewhat problematic (Mizushima and Yoshimori, 2007). In order to measure the formation of autophagosomes independently of their degradation, lysosome inhibitors should be added to the system to prevent LC3-II degradation. The most common inhibitor used in this case is chloroquine, which inhibits the acidification of the lysosomes, leading to an inhibition in the lysosomal enzymes that require a low pH to work (Mizushima and Yoshimori, 2007).

4.2.2 BCR signalling induces autophagosome formation

Firstly, I wondered whether signalling through the BCR, the most important receptor on B cells, would induce formation of autophagosomes. To address this question, primary B cells were purified from the spleen of C57BL/6 mice and stimulated through the BCR with different concentrations of anti-IgM (0, 10 or 20μg/ml) for 1 to 16 hours. In all the cases, PBS or chloroquine was added to the medium 30 minutes before the end of the time point. Cells were collected, lysed and the protein cell lysates were subject to electrophoresis. The samples were then transferred to PVDF membranes, which were incubated with primary antibodies

against LC3IIB and actin (used as loading control). After incubation with the corresponding secondary antibodies, membranes were developed using an ECL kit. The levels of LC3-II were increased after chloroquine addition even in the absence of stimulation (anti-IgM 0μg/ml, no chloroquine vs. chloroquine) (Figure 4.2A). This reflects the basal rate of autophagosome formation in naïve B cells. Interestingly, BCR stimulation induces accumulation of LC3II levels since the first two hours of stimulation and these levels remained increasing after 3 hours of BCR crosslinking to overnight stimulation (anti-IgM 0μg/ml vs 10 or 20μg/ml) (Figure 4.2A). These results indicate that stimulation of B cells through the BCR leads to the formation of autophagosomes.

Stimulation of B cells through the BCR in the absence of survival cytokines or co-stimulation molecules usually leads to apoptosis of these cells. In order to inhibit the apoptotic process, B cells were stimulated for 5 hours with anti-IgM (0, 10 or 20μg/ml) in the presence of IL-4, which protects primary B cells from entering into the apoptosis program (Wurster et al., 2002). Chloroquine was added to the system 30 minutes before the end point in order to induce autophagosome accumulation. Cells were collected, lysed and the protein lysates were subject to electrophoresis and Western blot as indicated before. IL-4 alone does not induce a significant accumulation of LC3-II (Figure 4.2B). In contrast, a massive increase in the levels of LC3-II was observed after BCR crosslinking in the presence of IL-4 (Figure 4.2B). This result indicates that autophagosome formation in B cells after signalling induced through the BCR is not just a consequence of programed cell death.

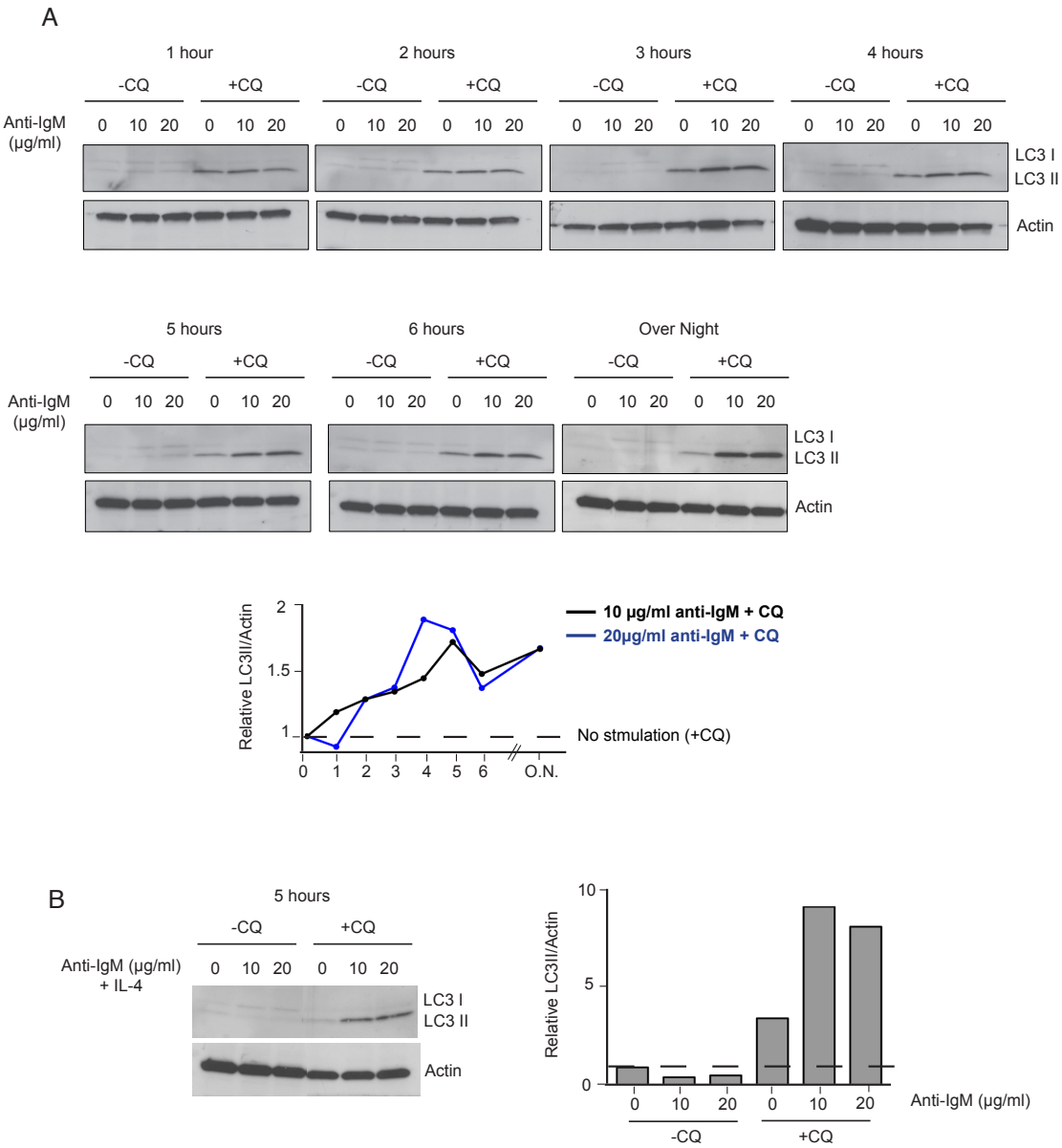

Figure 4.2 BCR crosslinking induces autophagosome formation

(A) Western blot analysis of cellular lysates derived from wild type B cells using anti-LC3IIB and anti-actin antibodies. B cells were stimulated with 0, 10 or 20µg/ml of anti-IgM for 1 to 16 hours and PBS or chloroquine were added to the culture 30 minutes before lysing. Signal intensities were quantified with ImageJ and LC3-II/actin signal ratios were normalised to non-stimulated samples (0 µg/ml anti-IgM plus chloroquine). Relative LC3-II/actin levels after different times of stimulation were plotted in the chart. (B) Western blot analysis of cellular lysates derived from wild type B cells using anti-LC3IIB and anti-actin antibodies. B cells were stimulated with 0, 10 or 20µg/ml of anti-IgM in the presence of IL-4 (5ng/ml) for 5 hours and PBS or chloroquine were added to the culture 30 minutes before lysing. LC3-II/actin signals ratios were normalised to non-stimulated samples (0 µg/ml anti-IgM minus Chloroquine). Relative LC3-II/actin levels following BCR stimulation were plotted in the bar chart. All data are representative of three independent experiments.

4.2.3 TLR signalling induces autophagosome formation

B cells not only recognise and respond to pathogens through the surface BCRs, they also express a series of TLRs that allow them to recognise a variety of pathogen-associated molecular patterns (Pasare and Medzhitov, 2005). In particular, B cells express high levels of TLR9, which is located on intracellular endosomes and recognises CpG motifs and TLR4, which is located on the B cell surface and recognises LPS. The triggering of TLRs on B cells initiates an intracellular MyD88/TRIF-mediated signalling that results in proliferation, cytokine secretion and antibody production (Browne, 2012). Therefore, I wondered whether the stimulation of B cells through TLR9 or TLR4 would also induce the formation of autophagosomes as observed following BCR crosslinking.

For this, I stimulated primary B cells for 3 or 5 hours with increasing concentrations of CpG (0, 0.5, 1 and 5μg/ml) or LPS (0, 0.1 and 1μg/ml). Chloroquine was added to the culture 30 minutes before harvesting the cells and protein cell lysates were subject to electrophoresis and Western blot to detect the levels of LC3II. CpG stimulation led to an increase in the levels of LC3II after 3 and 5 hours of stimulation in a dose dependent manner (Figure 4.3A). Importantly, the accumulation of LC3II after CpG stimulation required signalling through TLR9, as the levels of LC3II remained similar to basal levels when primary B cells from TLR9-deficient mice were stimulated with CpG (Figure 4.3A). Moreover, stimulation of B cells with LPS also induced up regulation of LC3II levels, although this up regulation was not as strong as observed with CpG (Figure 4.3B). All together, signalling via BCRs as well as TLRs induces autophagosome formation in B cells.

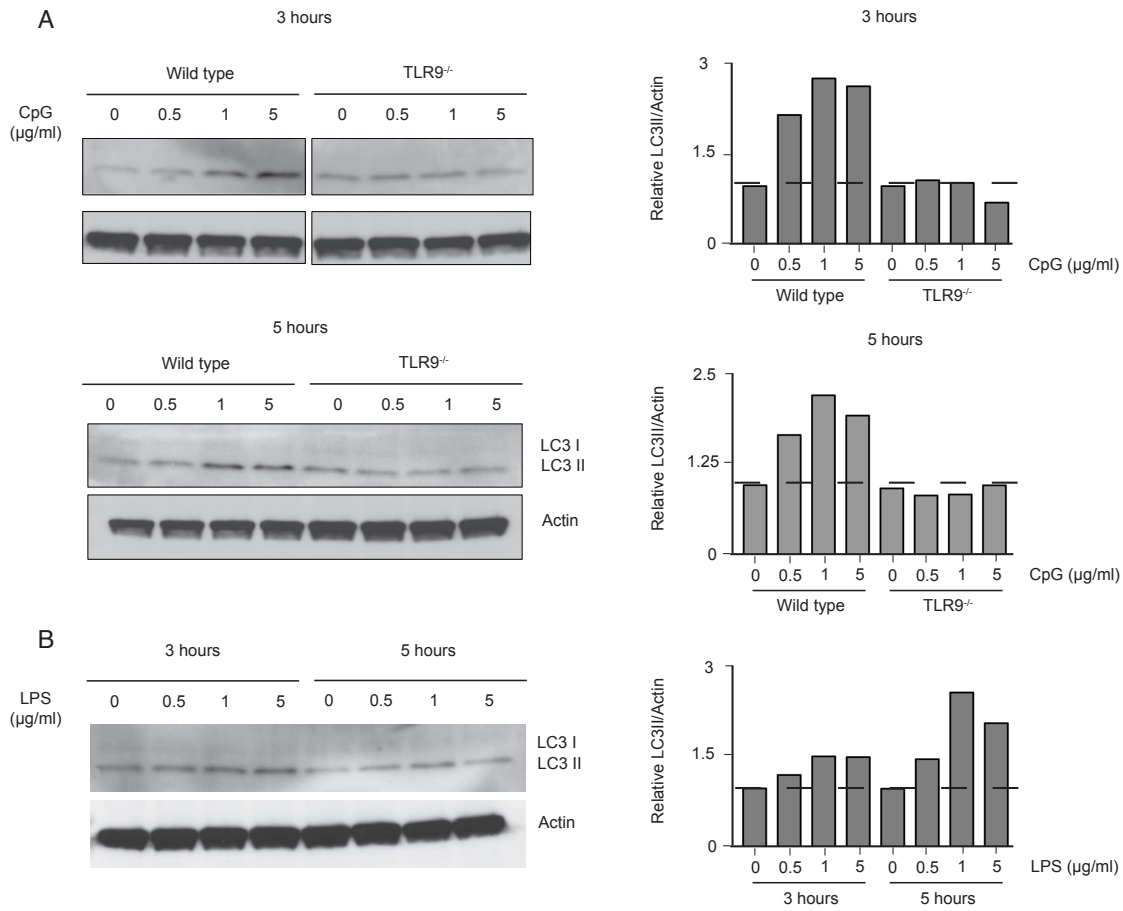

Figure 4.3 TLR4 and TLR9 signalling induces autophagosome formation

Western blot analysis of cellular lysates derived from wild type or *Tlr9*$^{-/-}$ B cells using anti-LC3IIB and anti-actin antibodies. B cells were stimulated with 0, 0.5, 1 and 5µg/ml of (A) CpG or (B) LPS for 3 or 5 hours and chloroquine was added to the culture 30 minutes before lysing. Signal intensities were quantified and LC3-II/actin signals ratios were normalised to non-stimulated samples. Relative LC3-II/actin levels are plotted in the bar charts. All data are representative of two independent experiments.

4.2.4 BCR and TLR signalling induces accumulation of LC3^{+} vesicles

The previous results showed that stimulation of B cells through the BCR or TLRs induces accumulation of LC3II levels. To visualise the formation of these double-membrane organelles by confocal microscopy, primary B cells were stimulated *in vitro* with PBS (control), 10µg/ml of anti-IgM or 1µg/ml of CpG. After 3 hours, B cells were washed with PBS, fixed and permeabilised with methanol and stained for LC3. Confocal analysis revealed a substantial accumulation of LC3-containing vesicles after both BCR crosslinking and TLR9 stimulation (Figure 4.4A).

To quantify the number of LC3 foci per cell in the different conditions I used the spot detection tool in Imaris. Following stimulation with anti-IgM and CpG, an average of ten LC3 foci per B cell were observed (Figure 4.4B). On the other hand, most of non-stimulated B cells contained between zero to two $LC3^+$ vesicles (Figure 4.4B). All together, the analysis of LC3II accumulation by Western blot and the quantification of LC3 foci by confocal microscopy show that stimulation of B cells through the BCR and TLR9 induce the formation of autophagosome vesicles.

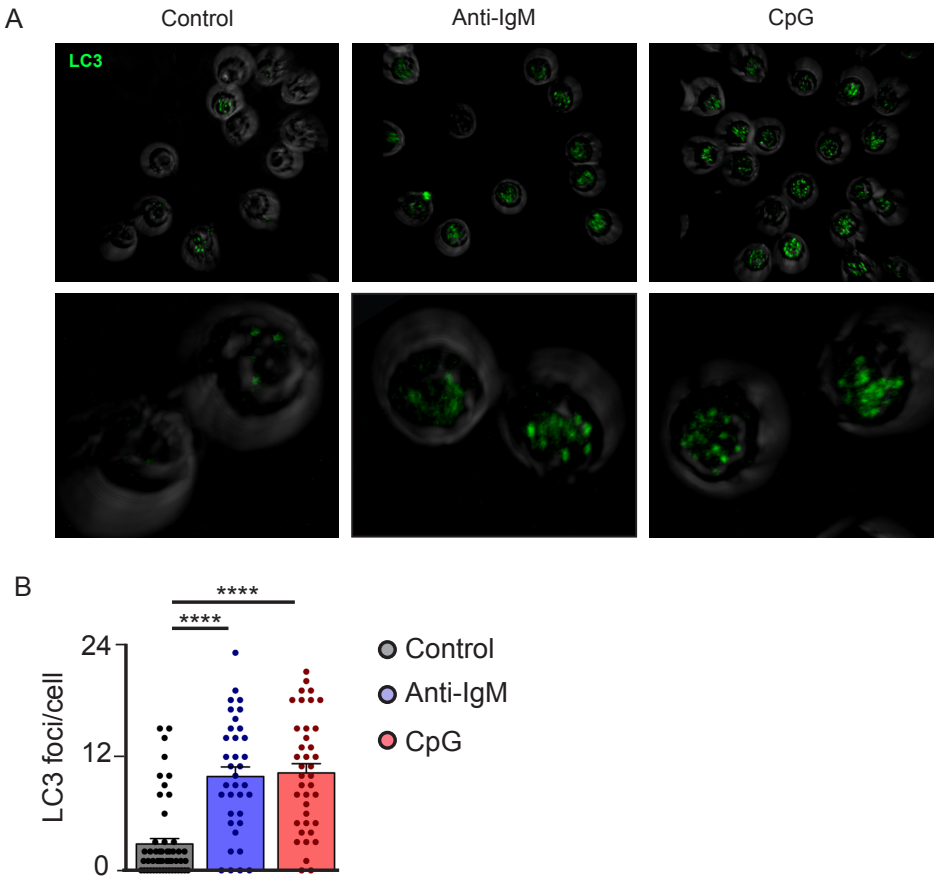

Figure 4.4 BCR and TLR9 signalling induces accumulation of $LC3^+$ vesicles

(A) Confocal images of primary B cells that were stimulated for three hours with PBS (control), 10 µg/ml of anti-IgM or 1 µg/ml of CpG, fixed, permeabilised and stained with anti-LC3 (green). (B) Quantification of LC3 foci per cell in B cells that were treated as in (A). Quantification was performed using the spot detection tool in Imaris. Data are representative of two independent experiments. Student t test, **** $p<0.0001$.

4.2.5 PLCγ2 is a central regulator of BCR and TLR-induced autophagy

I moved on to analyse which molecules involved in BCR signalling are required for the formation of these autophagosomes. Crosslinking of the BCR after antigen recognition leads to a multitude of downstream signalling events. In short, BCR crosslinking leads to the early phosphorylation of the BCR complex and the recruitment of intracellular signalling molecules such as the kinase Syk, PLCγ2 and PI3K. Syk activates the E3 ubiquitin ligase c-Cbl, which is involved in BCR internalisation. PLCγ2 catalyses the production of the secondary messengers DAG and IP3 to ensure signal propagation. Finally, PI3K recruitment to the BCR by the protein adaptors BCAP and CD19 ensures the survival of B cells following activation (Harwood and Batista, 2009, Castello et al., 2013).

To analyse the role of these different molecules in autophagosome formation after BCR crosslinking, primary B cells were isolated from wild type, c-Cbl$^{-/-}$, BCAP$^{-/-}$, CD19$^{-/-}$ and PLCγ2$^{-/-}$ mice. B cells were stimulated for 5 hours with increasing concentrations of anti-IgM (0, 10 or 20μg/ml) and chloroquine was added to the medium 30 minutes before the end time point. Protein cell lysates were subject to electrophoresis and Western blot to detect the levels of LC3II. I observed an increase in the intensity of LC3II after BCR stimulation in both wild type and c-Cbl deficient B cells (Figure 4.5A). This indicates that c-Cbl is not required for the formation of these organelles following BCR stimulation. Surprisingly, the increase in the levels of LC3II after BCR crosslinking was also observed in CD19- and BCAP-deficient B cells (Figure 4.5B), indicating that PI3K recruitment to the BCR by these two adaptors is not necessary for the autophagosome formation. In contrast, the induction of LC3II up-regulation following BCR crosslinking was abrogated in PLCγ2-deficient B cells (Figure 4.5C), indicating that the PLCγ2 pathway is essential for the formation of these double membrane vesicles after BCR signalling.

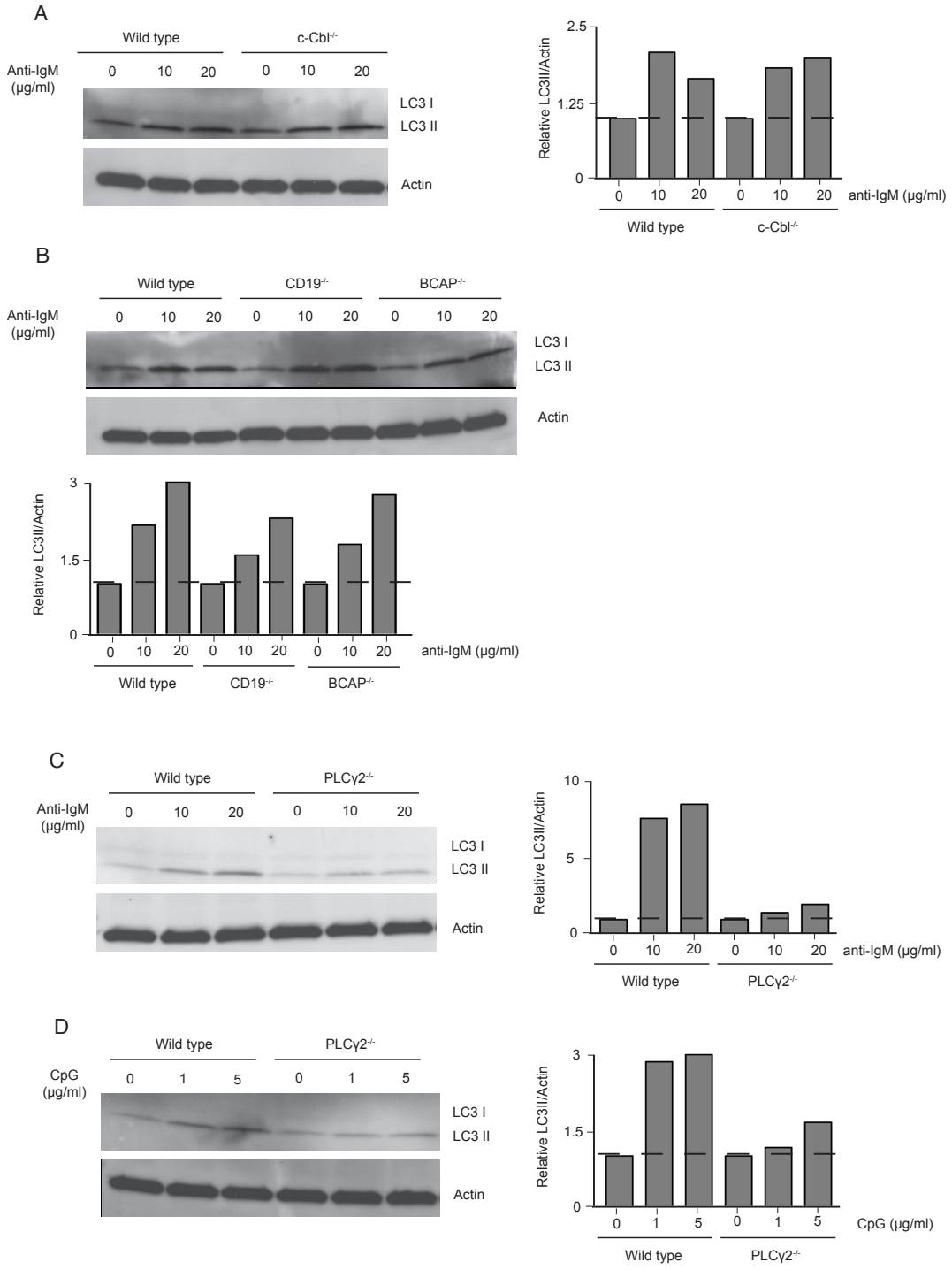

Figure 4.5 PLCγ2 regulates BCR- and TLR-induced autophagosome formation

Western blot analysis of cell lysates derived from wild type or (A) *c-Cbl*$^{-/-}$ (B) *CD19*$^{-/-}$ or *BCAP*$^{-/-}$ and (C and D) PLCγ2$^{-/-}$ B cells using anti-LC3IIB and anti-actin antibodies. B cells were stimulated with (A to C) 0, 10 and 20µg/ml of anti-IgM or (D) 0,1 or 5µg/ml of CpG for 5 hours. Chloroquine was added to the culture 30 minutes before lysing. Signal intensities were quantified and LC3-II/actin signal ratios were normalised to non-stimulated samples. Relative LC3-II/actin levels are

plotted in the bar charts. All data are representative of two independent experiments.

I wondered whether PLCγ2 is also involved in the formation of autophagosomes following TLR stimulation. For this, primary B cells were isolated from wild type and PLCγ2$^{-/-}$ mice and stimulated for 5 hours with increasing concentrations of CpG (0, 1 or 5μg/ml). Chloroquine was added to the medium 30 minutes before harvesting the cells, and cell lysates were subject to electrophoresis and Western blot to detect the levels of LC3II. As expected, the levels of LC3II were increased in wild type B cells after CpG stimulation (Figure 4.5D). In contrast, the up regulation of LC3II after TLR stimulation was dramatically decreased in PLCγ2-deficient B cells (Figure 4.5D).

Together these results suggest that PLCγ2 could act as a central hub for the induction of autophagosome formation following recognition of pathogens by B cells, through the BCR or TLRs. The lipase activity of PLCγ2 cleaves PIP2 (phosphatidylinositol 4,5-bisphosphate) into IP3 and DAG, which then function as secondary messengers. IP3 binds to IP3 receptors in the ER to induce the release of Ca^{2+} while DAG activates PKC, which phosphorylates other cytosolic proteins. Therefore, through Ca^{2+} and PKC, PLCγ2 could be controlling the formation of autophagosomes following antigen challenge. To directly assess the role of these two distinct pathways in the autophagy process, it would be important to analyse the formation of autophagosomes following BCR and TLR stimulation in PKC-deficient or IP3 receptor deficient B cells.

4.3 BCR- and TLR-induced autophagy is ULK1/2-independent

4.3.1 BCR accumulates in autophagosomes after internalisation

When BCR recognises antigen, the BCR-antigen complex is internalised inside the cell onto specific cellular compartments. These compartments are rapidly polarised towards the MTOC (microtubule organising centre) and are where antigen is loaded onto MHCII molecules for presentation to T cells (Thaunat et al., 2012, Burbage et al., 2015). As autophagosome formation is induced following BCR crosslinking, I wondered whether these structures were localising near the

internalised antigen. To visualise the formation and localisation of autophagosomes, primary B cells were isolated from GFP-LC3 mice. Then, they were incubated with 10μg/ml of labelled anti-IgM for 0, 15 or 60 minutes at 37^{o}C. The use of labelled anti-IgM not only allows the stimulation of B cells through the BCR but also serves as a labelled antigen that can be easily tracked after internalisation. At each time point, B cells were washed with PBS, and fixed and permeabilised with methanol. Cells were then stained with anti-α-tubulin, to stain the microtubules and the MTOC, and with anti-GFP to increase the signal of LC3.

Confocal analysis revealed that in the steady state, BCR is detected on the surface of B cells and LC3 was seen diffuse in the cytoplasm (Figure 4.6A). After 15 minutes of activation, BCR is no longer observed on the B cell surface and it is found in rounded intracellular vesicles. Moreover, LC3 is less diffuse than in steady state and starts accumulating on small vesicles. Interestingly, most of these LC3^{+} vesicles were co-localising with the antigen-loaded ones, suggesting that antigen could be delivered to LC3^{+} vesicles following internalisation (Figure 4.6B). After 1 hour of stimulation, individual vesicles of antigen could not longer been observed. Instead, antigen is accumulated on big compartments polarised towards the MTOC, easily identified due to its bright staining with α-tubulin. Surprisingly, LC3 is also detected as a large cluster polarised towards the MTOC co-localising with the antigen (Figure 4.6C). These results suggest that following BCR internalisation, antigen is delivered to autophagosome compartments where it might be loaded onto MHCII molecules for antigen presentation.

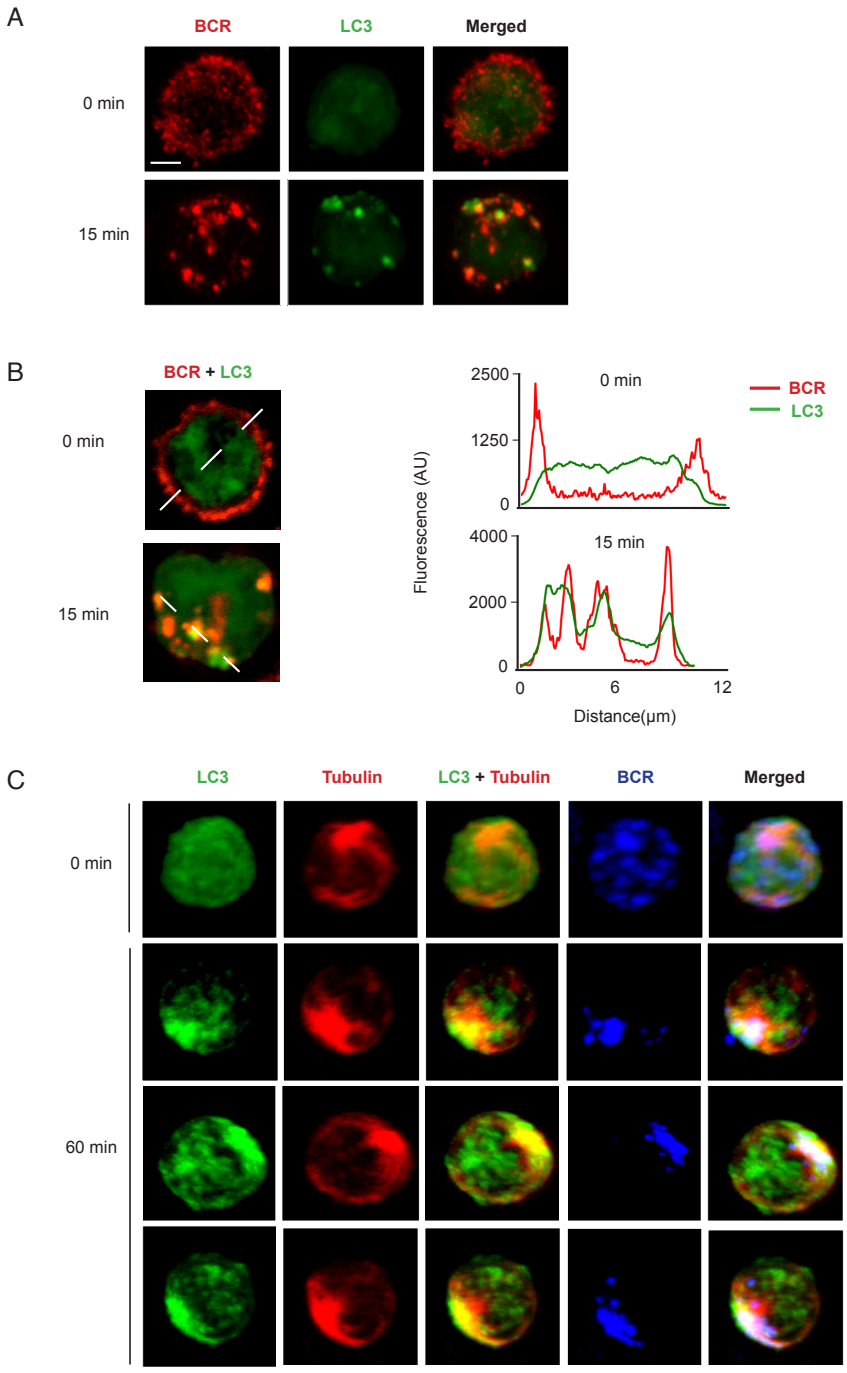

Figure 4.6 BCR localises in autophagosomes after internalisation

(A) Confocal 3D projections of primary B cells from GFP-LC3 mice that were stimulated with 10μg/ml of anti-IgM AF546 for 0 or 15 minutes, fixed, permeabilised and stained with anti-GFP (green). (B) Confocal single plane images of B cell treated as in (A). Histograms represent GFP and AF546 fluorescence measured across the dashed lines. (C) Confocal 3D projections of primary B cells from GFP-LC3 mice that were stimulated with 10μg/ml of anti-IgM AF546 for 0 or 60 minutes,

fixed, permeabilised and stained with anti-GFP (green) and anti-tubulin (blue). Data are representative of two independent experiments.

4.3.2 PI3K inhibitors block antigen presentation by B cells

As the BCR localises in autophagosome compartments following internalisation, I wondered whether autophagosome formation was necessary for the presentation of extracellular antigens by B cells. Autophagosome formation is a complex and tightly regulated process that requires the interaction of several different proteins. As detailed in the introduction, this process is initiated when the ULK1 complex translocates to the ER and activates the ER-specific class III PI3K that catalyse the production of PtdIns3P. PtdIns3P generate ER-associated isolation membranes which then mature into autophagosomes (Levine, Mizushima and Virgin, 2011)

As a first approach to block the formation of autophagosomes, I used two well-known autophagy inhibitors: wortmannin and 3-methyladenine. Both drugs are inhibitors of type III PI3K, which is required for the initial assembly of these double-membrane organelles. However, wortmannin might also inhibit type I and type II PI3K (Ireland and Unanue, 2011). To test whether these drugs inhibit BCR-induced formation of autophagosomes, primary B cells were stimulated with 10µg/ml of labelled anti-IgM in the absence or presence of 10nM Wortmannin or 1mM 3-methyladenine. After 15 minutes, cells were washed, fixed, permeabilised and stained for LC3. Following BCR crosslinking, both BCR^+ and $LC3^+$ vesicles were formed in control samples. In contrast, while antigen-containing vesicles could be observed in the presence of PI3K inhibitors, the formation of $LC3^+$ vesicles was abrogated (Figure 4.7). As PI3K inhibitors inhibit BCR-induced formation of autophagosomes without affecting the internalisation of antigen, I went on to analyse the antigen presentation capacity of B cells in the presence or absence of these inhibitors.

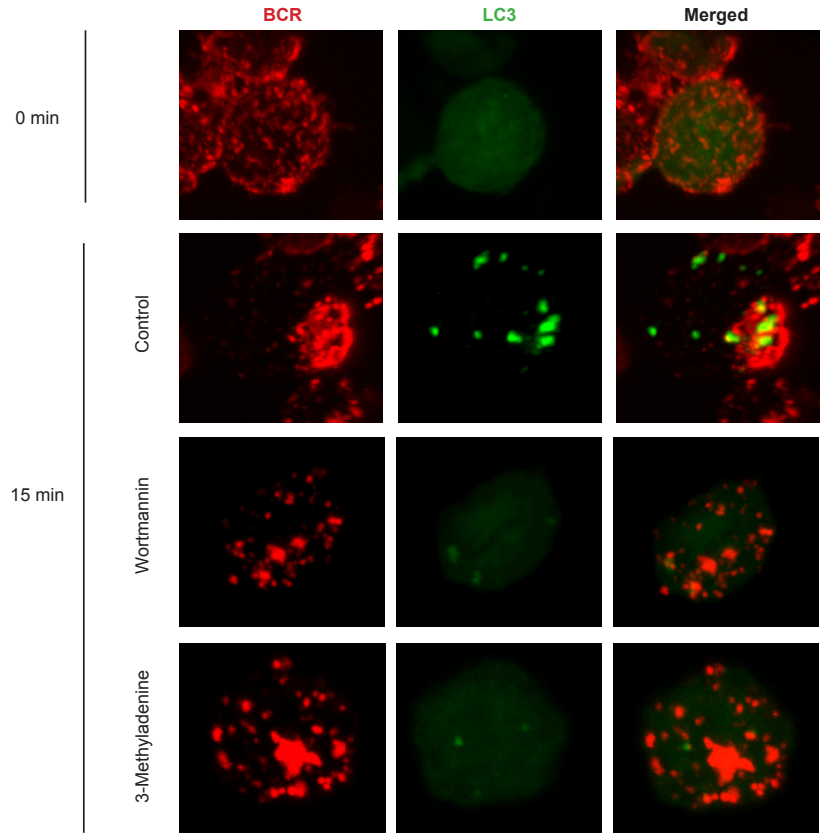

Figure 4.7 Wortmannin and 3-methyladenine inhibit autophagosome formation

(A) Confocal 3D projections of primary B cells that were stimulated with 10µg/ml of anti-IgM AF546 for 0 or 15 minutes in the presence of PBS (control), 10nM Wortmannin or mM 3-methyladenine. Cells were fixed, permeabilised and stained for LC3. Data are representative of two independent experiments.

To measure antigen presentation I performed the well-established technique of B-T cell co-culture. For this, I isolated primary B cells and labelled them with CFSE. B cells were then cultured with beads coated with anti-IgM and OVA in the absence or presence of 10nM Wortmannin or 1mM 3-methyladenine. In a normal situation, B cells internalise these beads, process the OVA and load OVA peptides on MHCII for presentation. Beads and inhibitors were washed from the culture after 1 hour and B cells were co-cultured with OT II $CD4^+$ T cells previously labelled with CellTrace™ Violet. As OT II T cells have a TCR specific for OVA, they recognise OVA peptides presented by B cells and proliferate and secrete IL-2. As the extent of T cell division is proportional to the amount of antigen presented by B cells, the measurement of T cell division by CellTrace™ Violet dilution and IL-2 secretion are

indicative of how much antigen is being presented by the B cells. B cell division can also be followed by measuring dilution of CFSE by flow cytometry.

After 3 days of co-culture, B cell and T cell division were measured by flow cytometry and IL-2 secretion by ELISA. In the absence of inhibitors, B cells and T cells undergo several rounds of cell division after 3 days of co-culture, as judged by the dilution of CFSE and CellTrace™ Violet respectively (Figure 4.8A–B). Moreover, T cells actively secrete IL-2, as observed by ELISA (Figure 4.8C). In contrast, the proliferation of B cells and T cells, as well as the secretion of IL-2, were abrogated in the presence of Wortmannin or 3-methyladenine (Figure 4.8A–C). This experiment indicates that type III PI3K and probably autophagosome formation might be necessary for antigen presentation.

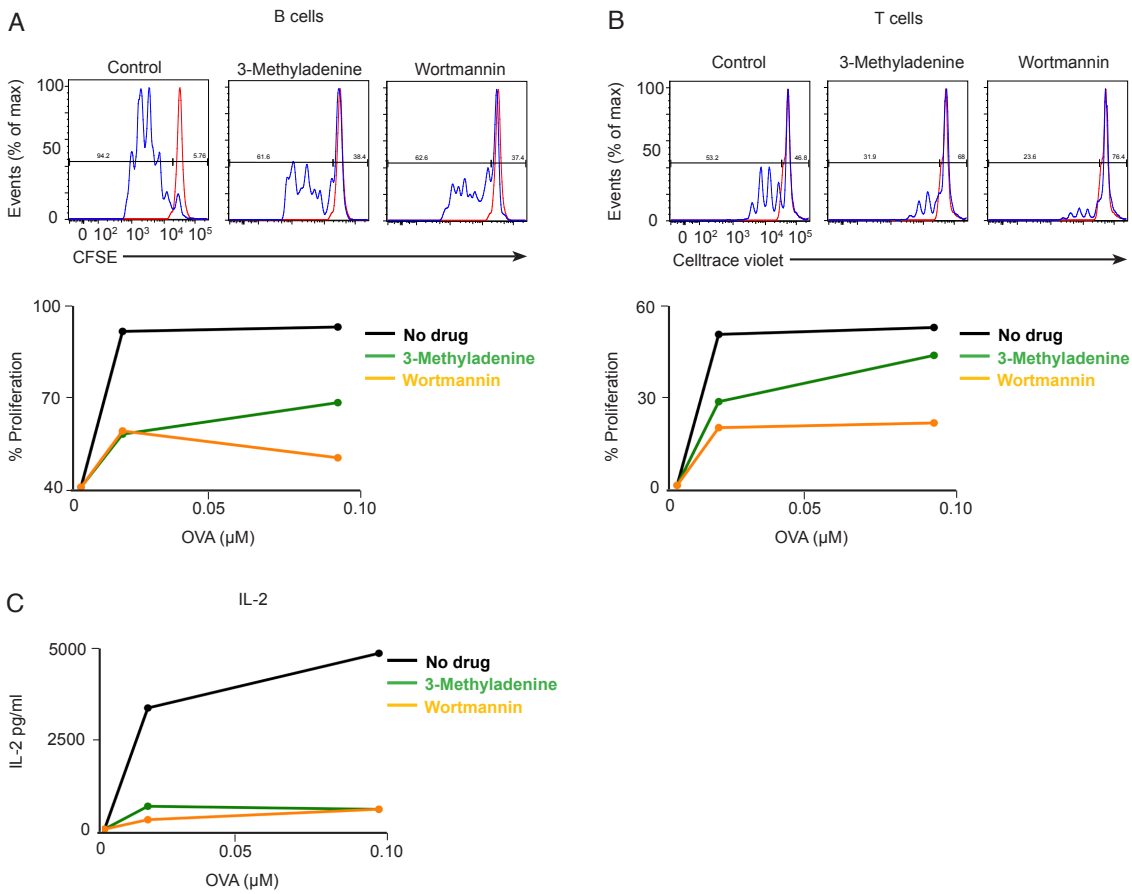

Figure 4.8 PI3K inhibitors interfere with B cell antigen presentation

Flow cytometry analysis of (A) CFSE and (B) celltrace violate dilution from CFSE-labelled primary B cells stimulated with anti-IgM and OVA-coated beads in the presence of PBS, 10 nM Wortmannin or 1mM 3-methyladenine and co-cultured

with CellTrace™ Violet labelled-OT-II T cells for 72 hours. The percentage of divided B cells and T cells are depicted in the graphs. Red curve: no stimulated cells, blue curve: stimulated cells. (C) IL-2 levels measured in co-culture supernatants from (A and B) by ELISA after 72 hours. Data are representative of two independent experiments.

4.3.3 ULK1/2 are dispensable for B cell antigen presentation

3-methyladenine can have off targets effects (Ito et al., 2007, Hou et al., 2012) and wortmannin inhibits all three types of PI3K and not only the type III autophagy-specific one (Vanhaesebroeck et al., 2001). I therefore moved on to genetically target diverse components of the autophagosome complex machinery to directly assess the role of autophagy on the antigen presentation process. As mentioned previously, autophagosome formation is initiated by the recruitment of the ULK complex (ULK1 and ULK2) to the ER (Lee and Tournier, 2011). I therefore analysed the antigen presentation capacity of primary B cells derived from wild type; ULK1-deficient and ULK2-deficient mice using the B-T cell co-culture technique explained above. Increasing concentrations of OVA were used to coat the beads (from 0.001 to 1μM) in order to titrate the T cell response. After 3 days of co-culture, B cell proliferation, T cell proliferation and IL-2 secretion were analysed.

The rate of B cell and T cell proliferation and IL-2 secretion directly increases with the amount of OVA used to coat the beads (Figure 4.9A–C). However, no significant differences were observed in these parameters between wild type B cells and ULK1-deficient or ULK2-deficient B cells (Figure 4.9A–C). This result indicates that ULK1 and ULK2 are not required for B cell antigen presentation to $CD4^+$ T cells. However, these proteins share 78% homology within their protein kinase domains and have redundant functions to mediate autophagy under nutrient-deprivation (Lee and Tournier, 2011). I therefore thought to analyse antigen-presentation on primary B cells from ULK1/ULK2 double-deficient mice.

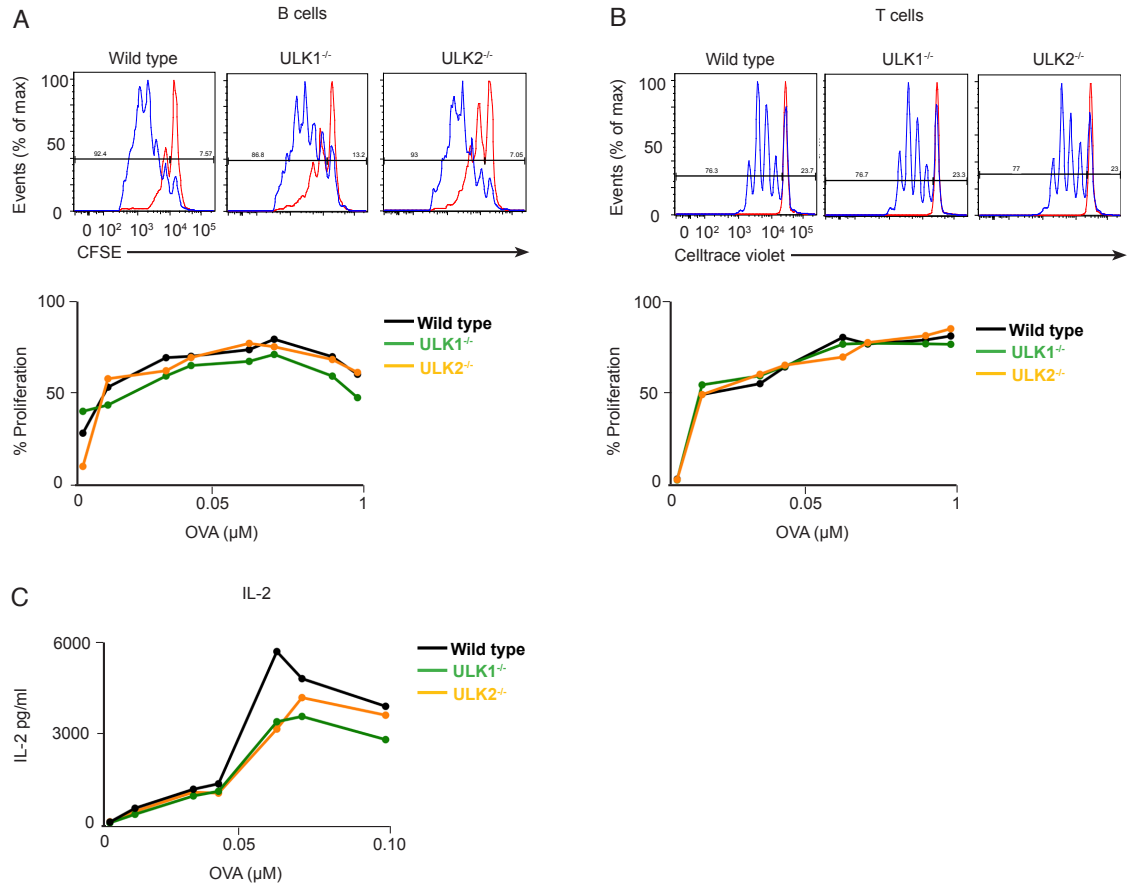

Figure 4.9 ULK1 and ULK2 are dispensable for B cell antigen presentation

Flow cytometry analysis of (A) CFSE and (B) celltrace violate dilution from wild type, *ULK1*$^{-/-}$ and *ULK2*$^{-/-}$ B cells stimulated with beads coated with anti-IgM and increasing amount of OVA and co-cultured with OT-II CD4^{+} T cells for 72 hours. The percentage of divided B cells and T cells are depicted in the graphs. Red curve: no stimulated cells, blue curve: stimulated cells. (C) IL-2 levels measured in co-culture supernatants from (A and B) by ELISA after 72 hours. Data are representative of two independent experiments.

ULK1/2-deficient mice die within one week after birth due to feeding-related problems (Cheong et al., 2011). As at this time the B cell compartment is still not fully developed, I thought to generate chimeras from fetal liver hematopoietic stem cells of ULK1/2 deficient embryos. For this, embryos were collected at day E14.5, genotyped using their tails, and liver cells from either wild type or ULK1/2-deficient embryos were injected into sub-lethally irradiated Rag2$^{-/-}$ mice. Eight weeks post-transplant, primary B cells were isolated from wild type and ULK1/2$^{-/-}$ chimeras and the antigen presentation capacity of these cells was analysed using the B-T cell co-culture technique. After 3 days of co-culture, B cell proliferation, T cell proliferation

and IL-2 secretion were analysed as before. Surprisingly, the rate of B cell and T cell proliferation and IL-2 secretion were similar independently of whether B cells originated from wild type or ULK1/2$^{-/-}$ chimeras (Figure 4.10A–C). These results indicate that ULK proteins are not involved in the presentation of antigen by B cells to CD4^{+} T cells.

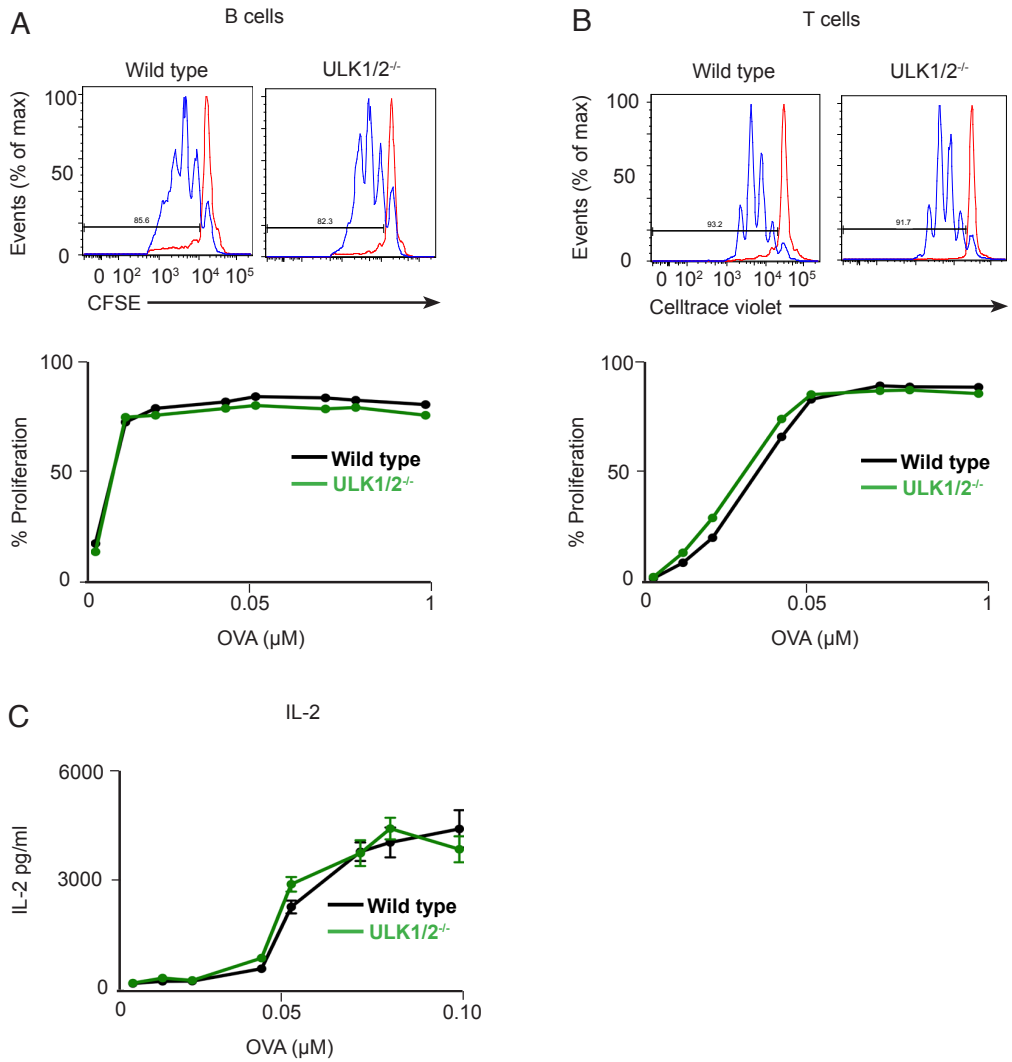

Figure 4.10 ULK complex is dispensable for B cell antigen presentation

Flow cytometry analysis of (A) CFSE and (B) celltrace violate dilution from wild type and *ULK1/2*$^{-/-}$ B cells stimulated with beads coated with anti-IgM and increasing amounts of OVA and co-cultured with OT-II CD4^{+} T cells for 72 hours. The percentage of divided B cells and T cells are depicted in the graphs. Red curve: no stimulated cells, blue curve: stimulated cells. (C) IL-2 levels measured in co-culture supernatants from (A and B) by ELISA after 72 hours. Data are representative of two independent experiments.

B cells not only present antigen-derived peptides to CD4+ T cells, but they can also present lipid antigens to NKT cells in the context of CD1d (Barral et al., 2008). I therefore wondered whether ULK proteins would be involved in the B cell presentation of lipids to NKT cells. To test this hypothesis, I performed a B cell-NKT cell co-culture. For this technique, I isolated primary B cells from wild type and ULK1/2$^{-/-}$ chimeras and stimulated them with beads coated with anti-IgM and increasing concentrations of α-GalCer-containing liposomes. In normal conditions, B cells internalise these beads and load α-GalCer on CD1d for presentation (Barral et al., 2008). After 1 hour, beads were washed from the culture and B cells were co-cultured with an NKT cell hybridoma (DN32.D3) that produces IL-2 after α-GalCer recognition on CD1d (Bendelac et al., 1995). The extent of IL-2 production by the NKT cell hybridoma is proportional to the amount of α-GalCer presented by B cells. After 24 hours of co-culture, supernatants were collected and IL-2 measured by ELISA. As observed in Figure 4.11A, IL-2 production increases with the amount of α-GalCer used to coat the beads. However, the production of IL-2 was similar independently of NKT cells being cultured with wild type or ULK1/2 deficient B cells. This result indicates that ULK proteins are not necessary for B cell presentation of lipids to NKT cells.

I went on to measure the amount of α-GalCer loaded on CD1d in the surface of B cells by using a labelled antibody that recognises α-GalCer-CD1d complex. To test this, primary B cells from wild type and ULK1/2$^{-/-}$ chimeras were cultured with beads coated with anti-IgM and increasing concentrations of α-GalCer-containing liposomes. After overnight culture, B cells were washed and stained with labelled anti-α-GalCer-CD1d complex. Flow cytometry analysis showed that the levels of α-GalCer loaded on CD1d are proportional to the amount of α-GalCer used to coat the beads (Figure 4.11B). However, α-GalCer presentation was similar in wild type and ULK1/2 deficient B cells (Figure 4.11B). This result, together with the B cell-NKT cell co-culture, demonstrates that ULK proteins are not necessary for the presentation of lipids in the context of CD1d to NKT cells.

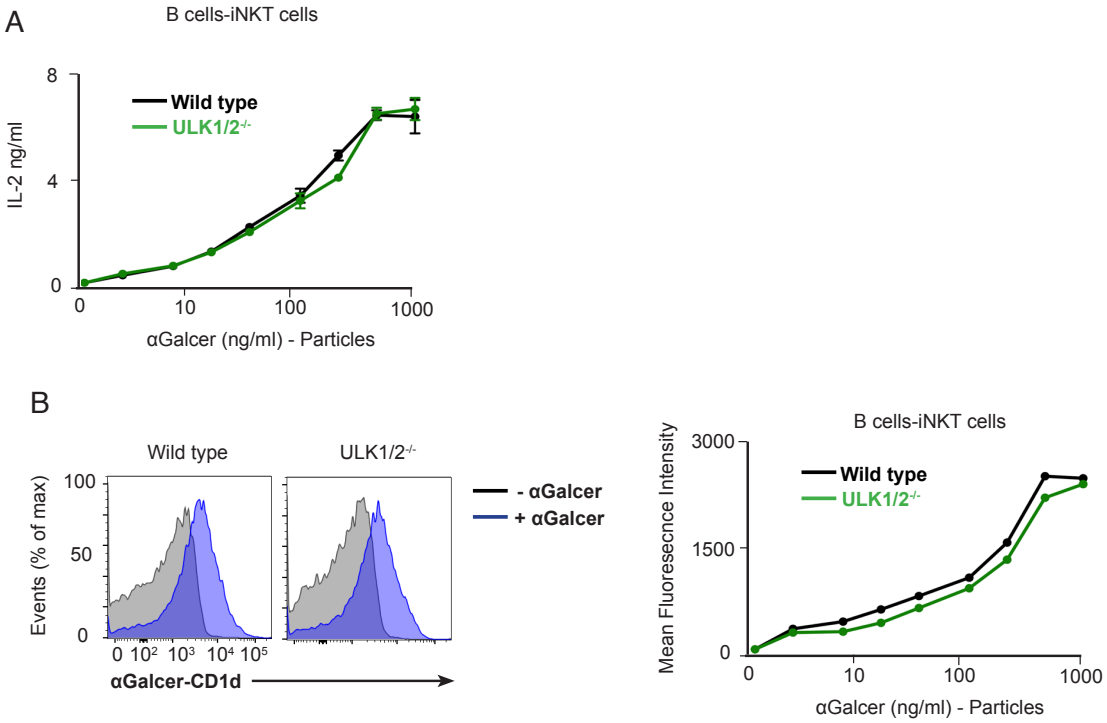

Figure 4.1 The ULK complex is dispensable for B cell lipid presentation of CD1d

(A) IL-2 levels measured by ELISA in supernatants from wild type and *ULK1/2*$^{-/-}$ B cells stimulated with beads coated with anti-IgM and increasing amounts of α-GalCer and co-cultured with DN32.D3 hybridoma cells for 24 hours. (B) Flow cytometry analysis of the amount of α-GalCer loaded on CD1d from wild type and *ULK1/2*$^{-/-}$ B cells stimulated with beads coated with anti-IgM and increasing amounts of α-GalCer for 24 hours. The mean fluorescence intensity of α-GalCer-CD1d for each concentration of α-GalCer used is depicted in the graph. Data are representative of three independent experiments.

4.3.4 ULK1/2 are dispensable for BCR and TLR-induced autophagy

While the treatment of B cells with PI3K inhibitors reduces the ability of B cells to present antigen to T cells, the deletion of ULK proteins does not affect the antigen presentation capacity of B cells. I wondered whether the formation of autophagosomes following BCR and TLR stimulation was blocked in the absence of ULK proteins. To analyse this, primary B cells from wild type and ULK1/2$^{-/-}$ chimeras were stimulated for 5 hours with increasing concentrations of anti-IgM (0, 10 and 20μg/ml) or CpG (0, 1 and 5μg/ml). Chloroquine was added to the culture 30 minutes before harvesting the cells and protein cell lysates were subject to electrophoresis and western blot to detect the levels of LC3II. Surprisingly, BCR

and TLR stimulation induced up regulation of LC3II in both wild type and ULK1/2-deficient B cells (Figure 4.12A–B). In fact, the levels of LC3II were higher in ULK1/2-deficient compared to wild type B cells, not only after stimulation but also in steady state conditions (0μg/ml of stimulus).

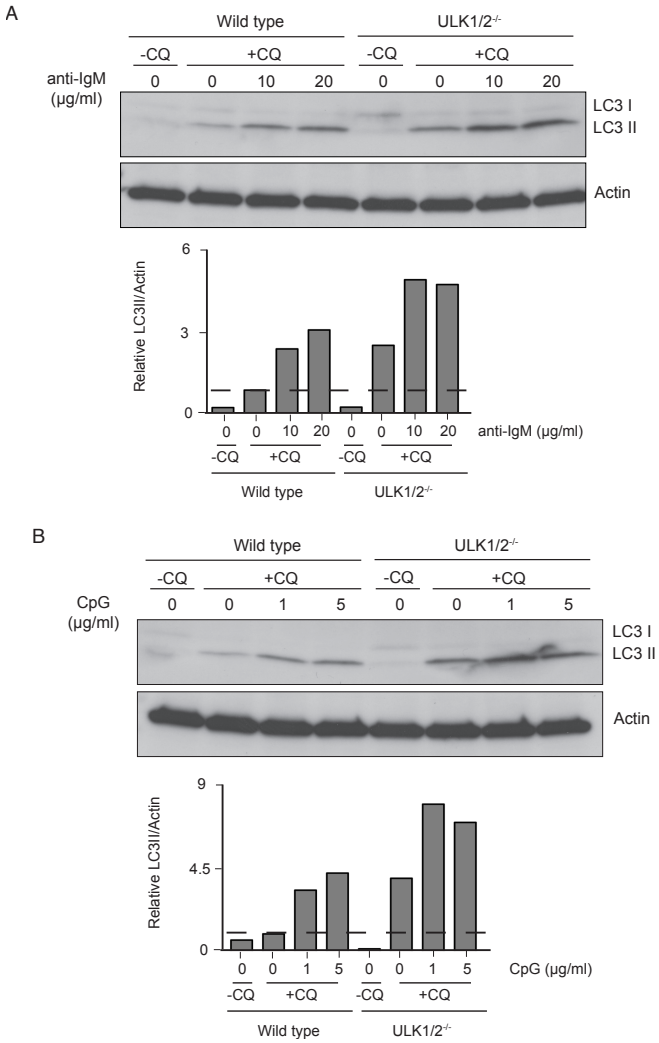

Figure 4.12 BCR- and TLR-induced autophagy are independent of the ULK complex

Western blot analysis of cellular lysates derived from wild type or ULK1/2-/- B cells using anti-LC3IIB and anti-actin antibodies. B cells were stimulated with (A) 0, 10 and 20μg/ml of anti-IgM or (B) 0, 1 or 5μg/ml of CpG for 5 hours. PBS or chloroquine was added to the culture 15 minutes before lysing. Signal intensities were quantified and LC3-II/Actin signals ratios were normalised to wild type non-stimulated samples. Relative LC3-II/actin levels are plotted in the bar charts. Data are representative of two independent experiments.

These results are striking as they demonstrate that ULK proteins, despite being essential for the induction of autophagy under nutrient-deprived conditions (Lee and Tournier, 2011), are dispensable for the formation of autophagosomes after B cell stimulation. Therefore, BCR and TLR-dependent formation of autophagosomes in B cells involves an ULK-independent pathway, different from the conserved one triggered during starvation.

In summary, BCR and TLR signalling induces autophagosome formation in B cells through a non-conserved pathway where the ULK complex is dispensable. In contrast, PLCγ2 could act as a central regulator for the induction of autophagosome formation following recognition of pathogens by B cells. Importantly, antigens colocalise with autophagosomes following internalisation. However, as autophagy is not blocked in ULK1/2-deficient B cells, I cannot conclude whether autophagosome formation is important for the presentation of exogenous antigens by B cells. In the future, it would be important to analyse the requirement of other conserved components of the autophagy machinery, such as Atg5, Atg7 or Atg16L in the formation of autophagosomes following B cell stimulation. In that case, it would be interesting to assess their role on the presentation of exogenous antigens by B cells.

4.4 Discussion

Autophagy is the cellular process of degradation of the cell's own cytoplasm and organelles to generate energy and build new proteins and membranes (Mizushima, 2007). In this chapter I have shown that signalling through the BCR or through TLRs induces autophagy in B cells. This process is strictly dependent on the PLCγ2 pathway and does not require the presence of the conserved proteins ULK1 and ULK2. Furthermore, antigen localises in close contact with autophagosome vesicles after internalisation, suggesting a potential role for this process in antigen presentation.

Although B cells are small in size (10μm) and most of their cytoplasmic volume is occupied by the nucleus, they express high levels of the autophagy proteins Atg5, Atg7 and LC3 (McLeod, Jia and He, 2012). Autophagy might

therefore play an important role in the tightly-controlled organisation of organelles and the metabolic environment taking place in such a limited space. In this chapter I showed that even though B cells do not seem to display high levels of autophagy in the steady state, this process is increased after antigen recognition. BCR crosslinking results in up regulation of the autophagy flux, as already described for B cell lines and splenic B cells (Watanabe et al., 2008, Ireland and Unanue, 2011). Importantly, BCR signalling induces autophagy even in the presence of the co-stimulatory molecule IL-4, which serves as a survival factor, suggesting that autophagy induction is not just the result of apoptosis. This observation differs somewhat from those made by Watanabe and collaborators, who suggest that BCR signalling in the presence of co-stimulatory molecules does not induce autophagy (Watanabe et al., 2008). The differences may come from the fact that in their study, they use transformed B cell lines instead of primary B cells. Furthermore, the recognition of PAMPS such as LPS and CpG through TLRs induces autophagosome formation to a similar extent as observed after BCR crosslinking. As activated B cells need to pass through several rounds of proliferation to expand, high levels of autophagy might support B cell energy demands to successfully complete this process.

The autophagy pathway followed after BCR and TLR engagement seems to be quite unique compared to the conserved mechanisms present in many other systems (Levine, Mizushima and Virgin, 2011, McLeod, Jia and He, 2012). In B cells, this process is strictly dependent on PLCγ2 pathway and is independent of ULK1 and ULK2 factors. PLCγ2 is a central protein in the propagation of signals after B cell recognition of antigens. PLCγ2 catalyses the degradation of membrane-bound PIP2 into DAG and IP3. While DAG activates the PKC pathway, IP3 binds to IP3 receptors in the ER and induces the release of intracellular Ca^{2+} (Weber et al., 2008). Although a potential role of PKC in autophagy initiation remains undefined, the rise of free cytosolic Ca^{2+} has been shown to be a potent inducer of autophagy (Høyer-Hansen et al., 2007). Therefore, through PKC or most probably Ca^{2+}-signalling, PLCγ2 acts as a central hub for autophagy induction in B cells. It would be important, in the future, to define the importance of these two branches of PLCγ2-mediated signalling on the induction of the autophagy program.

ULK1 and ULK2 are conserved proteins involved in autophagosome formation in response to stress and nutrient starvation (Cheong et al., 2011, Lee and Tournier, 2011). Under such conditions, mTOR activity is inhibited, which results in ULK1/2 phosphorylation and activation of class III PI3K complex (Kim et al., 2011). Class III PI3K complex generates PtdIns3P, which induces the generation of phagophores that later mature into autophagosomes (Mizushima, 2007). Even though ULK-deficiency renders cells unable to form autophagosomes under nutrient starvation (Cheong et al., 2011, Lee and Tournier, 2011, Russell et al., 2013), it does not interfere with the induction of autophagy in B cells after BCR or TLR stimulation. In fact, autophagosome formation is enhanced in the absence of ULK proteins. These results indicate that B cells undergo a non-conserved type of autophagy that occurs after the recognition of pathogens that does not require ULK proteins. In line with this idea, recent reports showed that autophagy induction in T cells after TCR engagement is independent of mTOR complex and class III PI3K (Jia and He, 2011, O'Brien et al., 2011). However, proteins that are involved in the later steps of the autophagosome formation, such as Atg5 or Atg7, are essential for autophagy induction in lymphocytes (McLeod, Jia and He, 2012, Pengo et al., 2013, Chen et al., 2014).

BCR recognition of antigen induces mTOR activation though PI3K (Limon and Fruman, 2012). Triggering of mTOR might block the initial steps involved in the generation of isolation membranes from the ER (ULK1/2, type III PI3K, WIPIs) and at the same time, induce a non-conserved version of autophagy where isolation membranes are directly provided by BCR-containing endosomes. In fact, this seems to be the case, as BCR co-localises with LC3 in the same compartments shortly after BCR crosslinking. Therefore, the use of BCR-containing endosomes as isolation membranes would allow B cells to bypass the early conserved steps of autophagosome formation. As lymphocytes have a very limited cytoplasmic space, and they require a lot of energy for their massive proliferation, this short version of the autophagy machinery would allow them to rapidly generate autophagosomes and fulfil their energy demands. In the future, it will be interesting to analyse the role of different initiation, nucleation and elongation factors in the induction of B cell autophagy and assess whether BCR-containing endosomes can function as isolation membranes to form autophagosomes.

Regardless of the signalling pathways involved in autophagosome formation in B cells, it is important to understand the role of this process in B cell physiology. It has been shown that autophagy is necessary for the survival of long-lived plasma and memory B cells (Pengo et al., 2013, Chen et al., 2014). However, its importance in the early steps of B cell function is not clear. Antigen internalised through the BCR localises on autophagosome vesicles polarised towards the MTOC. This suggests that autophagosomes may serve as compartments for antigen processing and loading on MHC II molecules before presentation on the membrane. Interestingly, MHC II has been shown to co-localise with antigen in autophagosomes after B cell activation (Ireland and Unanue, 2011). I attempted to analyse the role of autophagosomes not only in MHC II but also in CD1d-dependent antigen presentation through the use of ULK1/2 deficient B cells. However, as B cell autophagy is independent of these proteins, I was not able to address this question. It is interesting to analyse in the future, the antigen presentation capacity of B cells deficient in elongation factors, such as Atg5 or Atg7.

As an alternative to roles in antigen presentation, autophagosomes might play part in connecting the BCR to other co-stimulatory receptors, such as TLR9, for antigens containing nucleic acids. TLR9 is an intracellular TLR, localised in endosome vesicles in the steady state. As B cells are poorly phagocytic, the only way TLR9 can make contact with nucleic acid containing antigens is through translocation to BCR-containing vesicles (Chaturvedi, Dorward and Pierce, 2008, Eckl-Dorna and Batista, 2009). In fact, after BCR engagement, TLR9 translocates to autophagosome-like structures together with the BCR, what amplifies B cell responses to nucleic-acid containing antigens (Chaturvedi, Dorward and Pierce, 2008, Eckl-Dorna and Batista, 2009). Furthermore, this mechanism also has implications on the development of autoimmune responses, as BCR synergistic interaction with TLR9 or TLR7 has been shown to enhance the production of DNA- and RNA-specific autoantibodies (Marshak-Rothstein, 2006). A recent study showed that in a mouse model for SLE (systemic lupus erythematosus) where the RNA ligand for TLR7 is overexpressed, inhibition of B cell autophagy completely abrogates the production of autoantibodies through a blockage of TLR7 encounter with RNA ligands. Therefore, a tight regulation of the autophagy process is required

not only to fulfil energy demands or enhance antigen presentation, but also to prevent the development of autoimmune responses.

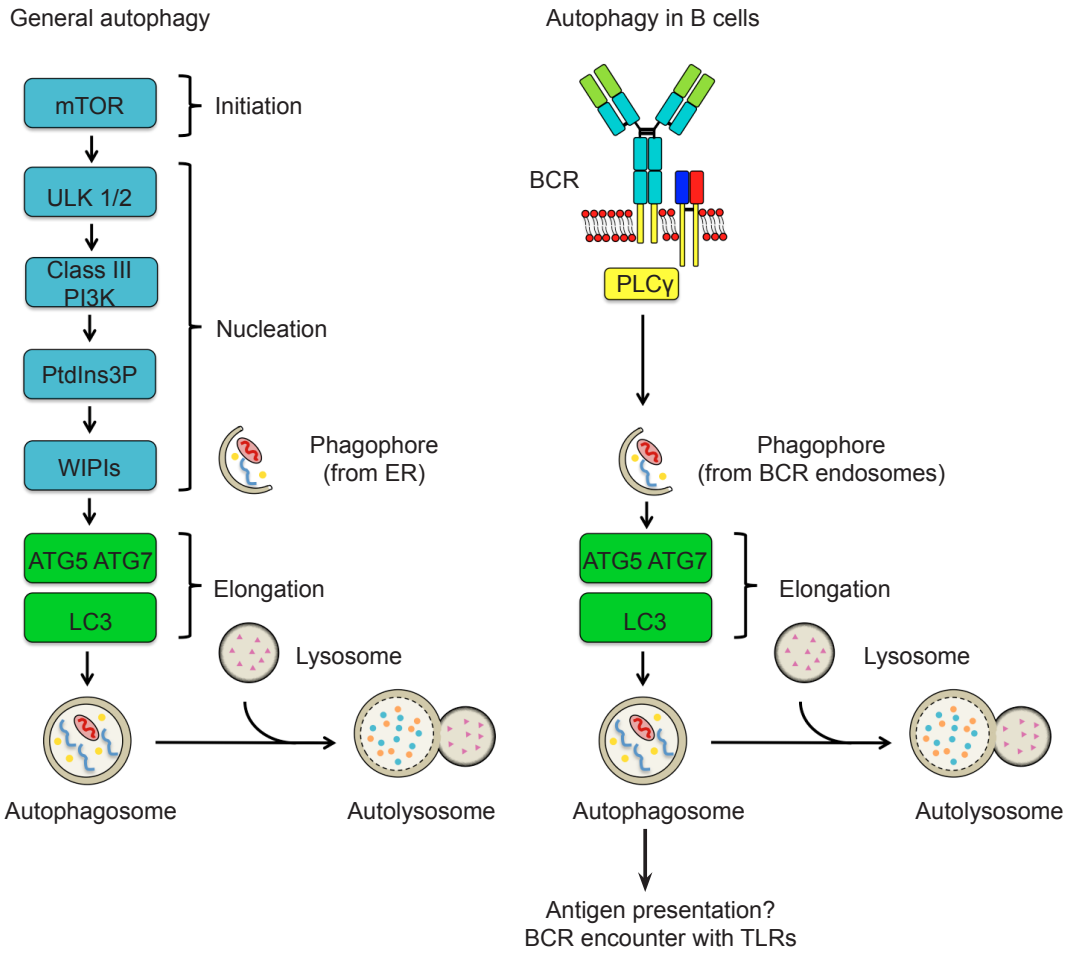

Figure 4.13 Suggested model for autophagy in B cells

The general mechanism of autophagosome formation is evolutionarily conserved and involves the stages of initiation, nucleation, elongation and closure, and degradation. In B cells, a non-conserved route of autophagy may bypass the initiation and nucleation steps through the provision of BCR-containing endosomes as a source of phagophores. This pathway is dependent on PLCγ2 and may participate in antigen presentation and BCR encounter with intracellular TLRs

Chapter 5. iNKT cell activation by CD103$^+$ DCs regulates germinal centre response to viral infection

5.1 Introduction

NKT cells are a distinct subset of T lymphocytes that express an invariant CD1d-restricted TCR and NK cell lineage receptors (Bendelac, Savage and Teyton, 2007). NKT cells play a key role in the host defense against pathogens due to their ability to recognise special glycolipids present on the surface of a variety of microbes such as *Borrelia* sp., the causative agent of Lyme disease (Kinjo et al., 2006), *Sphingomonas* sp., usually a hospital-acquired organism (Kinjo et al., 2005), and *Streptococcus pneumoniae*, the major cause of pneumonia (Kinjo et al., 2011). The recognition of exogenous glycolipids induces NKT cells to secrete a broad range of cytokines and provide cognate help to B cells, promoting both humoral and cell-mediated immunity (Brennan, Brigl and Brenner, 2013).

Remarkably, the importance of NKT cells in the immune response against pathogens is not restricted to glycolipid-bearing organisms. In fact, NKT cells have the unique ability to recognise atypical lysosomal glycolipids produced by particular immune cells during an inflammatory process. This allows NKT cells to support the immune response against a broader spectrum of microorganisms even in the absence of pathogen-derived glycolipids, as in the case of viral infections (Mattner et al., 2005). The understanding of NKT cell biology during infection is an exciting and emergent field of research that has been relatively limited due to the lack of tools to address questions *in vivo*. For instance, the role that different antigen presenting cells play on the activation of NKT cells during infection and the potential role of these innate T lymphocytes in the modulation of antibody responses remain largely unexplored.

5.1.1 NKT cell development and distribution

There are two main subsets of NKT cells: type I NKT cells, also known as iNKT (invariant NKT) cells, which express a highly restricted TCR repertoire (Vα14-

Jα18 combined with Vβ7, Vβ8 or Vβ2 chains) and type II NKT cells or non-iNKT cells which express a more diverse TCR repertoire (Benlagha et al., 2000). While both subsets are CD1d-restricted, iNKT cells are known to recognise glycolipid antigens while the ligands for non-iNKT cells are still not well defined. Some studies have demonstrated that sulphatides and sulphonates in the context of CD1d could stimulate non-iNKT cells, although only a subset (Blomqvist et al., 2009). Non-iNKT cells are much less abundant than iNKT cells and their biology has not been studied in detail due to the lack of specific markers and agonistic antigens. For the rest of my thesis I will focus on the biology of iNKT cells.

Both iNKT cells and conventional MHC-restricted T cells develop in the thymus from a common $CD4^-$ $CD8^-$ precursor (Pear, Tu and Stein, 2004). In this stage, double negative thymocytes rearrange the variable region of the TCRβ chain though VDJ recombination, a similar process to that described for B cells in Chapter 1. Those thymocytes that have successfully rearranged the TCRβ chain become $CD4^+$ $CD8^+$ thymocytes. These double positive progenitors undergo stochastic rearrangement of their TCRα chain and those expressing the specific Vα14-Jα18 rearrangement will give rise to the iNKT cell lineage. These cells will be positively selected following recognition of self-glycolipid antigens in complex with CD1d on the surface of other double positive thymocytes (Das, Sant'Angelo and Nichols, 2010). The nature of these self-antigens is quite controversial, although plasmalogen lysophosphatidyl-ethanolamine, a glycolipid present mainly in the peroxisomes, was recently identified as a candidate for positive selection in the thymus (Facciotti et al., 2012). The Vα14-Jα18 TCRα chain of iNKT cells associates with a restricted set of Vβ segments (Vβ7, Vβ8 and Vβ2), as only those TCR combinations are able to recognise lipids in the context of CD1d and generate a relatively strong TCR signal (Wei et al., 2006). This signal leads to expression of Egr1 and Egr2 (early growth response proteins) (Seiler et al., 2012), which direct the expression of the transcription factor PLZF (promyelocytic leukaemia zinc finger protein), the master regulator for iNKT cells (Kovalovsky et al., 2008, Savage et al., 2008). It is important to mention that a recently described subset of iNKT cells residing in the adipose tissue does not require PLZF but the E4BP4 master transcription factor instead (Lynch et al., 2015). In addition to signals through the TCR, positive signals are provided to iNKT cells during positive selection through

SLAM (signalling lymphocytic activation molecule) proteins (Griewank et al., 2007) (Figure 5.1).

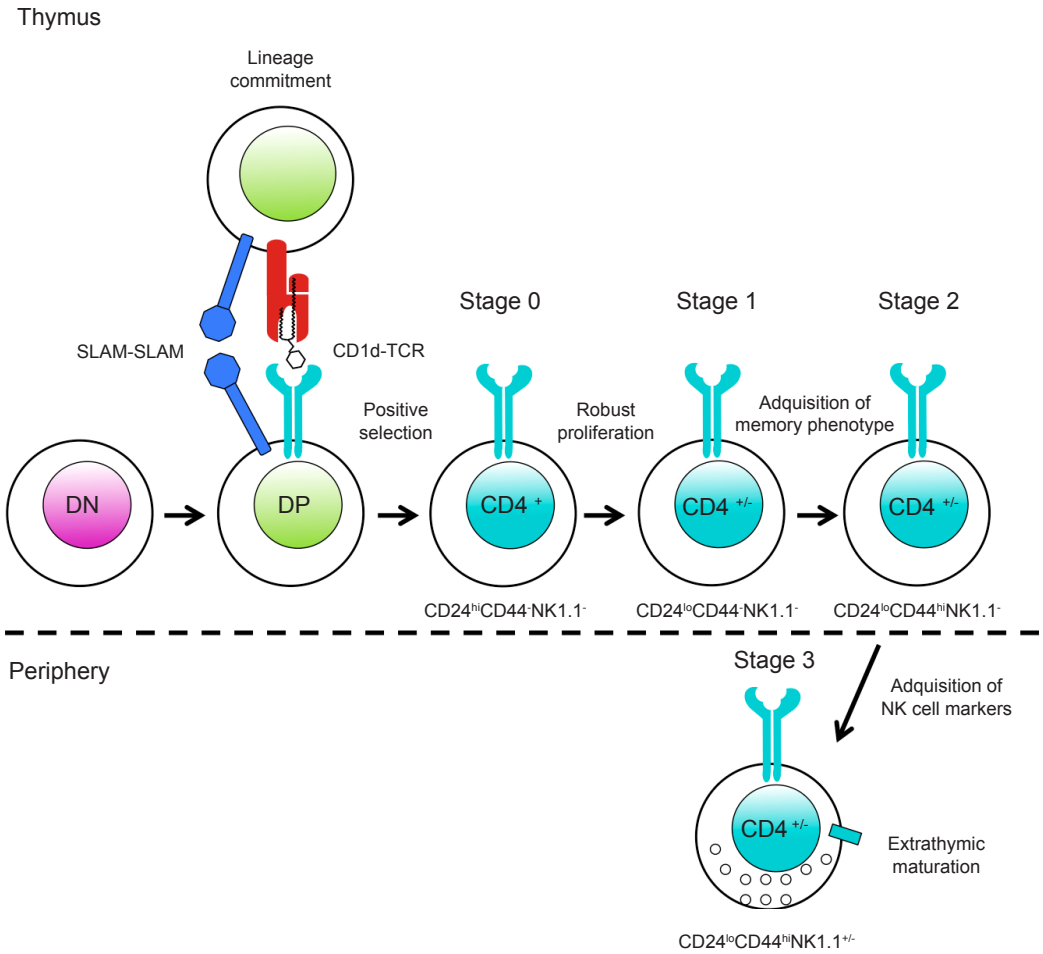

Figure 5.1 Stages of iNKT cell development

iNKT cell development occurs in the thymus from a pool of $CD4^{-}CD8^{-}$ double negative cells that differentiate into $CD4^{+}CD8^{+}$ double positive (DP) common precursors. Those thymocytes expressing an invariant TCR able to recognise glycolipids in the context of CD1d are selected and committed to the NKT cell lineage. After positive selection, immature iNKT cells undergo expansion and acquire a memory phenotype. They exit from the thymus while they are still immature and complete the maturation process in the periphery, where they might acquire NK cell lineage markers.

Following positive selection, iNKT cells are believed to undergo negative selection to eliminate highly autoreactive cells. However, the existence of this process remains quite controversial and requires further study. Then, iNKT cells progress through different stages of maturation defined by the differential

expression of CD24, CD44 and NK1.1. The most immature iNKT cells are defined as $CD24^{hi}CD44^{lo}NK1.1^{-}$ (Stage 0), followed by $CD24^{lo}CD44^{lo}NK1.1^{-}$ (Stage 1), $CD24^{lo}CD44^{hi}NK1.1^{-}$ (Stage 2), and finally $CD24^{lo}CD44^{hi}NK1.1^{+}$ (Stage 3). The transition of iNKT cells from stage 0 to stage 1 is marked by a robust proliferation and the loss of CD4 marker in a subset of iNKT cells. As cells progress to Stage 2, they up regulate CD44 and acquire an activated phenotype. These cells leave the thymus during stage 2 and finish the maturation process in the periphery, where they can acquire NK cell-specific markers (Stage 3) or remain NK1.1 negative (Figure 5.1) (Das, Sant'Angelo and Nichols, 2010).

iNKT cells have a particular distribution in the organism. They represent 0.5% of total T cells in the blood and peripheral LNs and 2.5% of T cells in the spleen and mesenteric LNs (Bendelac, Savage and Teyton, 2007). iNKT cell localisation is highly strategic, as they are found in the inter-follicular areas of the LNs and the red pulp and marginal zone of the spleen, in close contact with the sites of pathogen arrival (Barral et al., 2012, Kastenmüller et al., 2012). Interestingly, iNKT cells can represent up to 30% of total T cells in the liver. The preferential location might be in part explained by their high expression of CXCR6 that matches the expression of CXCL16 in the liver sinusoids. iNKT cells usually patrol liver sinusoids and they arrest to exert effector functions following activation by lipid antigens, specific cytokines or even by adrenergic signals produced during a stroke (Geissmann et al., 2005, Lee et al., 2010, Wong et al., 2011). In humans, iNKT cells are not highly enriched in the liver but they represent up to 10% of total T cells in the omentum, which is a double fold of the peritoneum connecting the stomach and other abdominal organs (Lynch et al., 2009). Furthermore, iNKT cells also reside in the lungs, skin, gastrointestinal tract and adipose tissue. Lung-resident iNKT cells are located inside the vasculature and extravasate to the lung parenchyma after activation to support the inflammatory response (Scanlon et al., 2011). In contrast, iNKT cells in the skin, intestine and adipose tissue seem to attenuate inflammation through the production of IL-10 (McKee, Mattarollo and Leggatt, 2014, Olszak et al., 2014, Lynch et al., 2015).

5.1.2 iNKT cell activation

How are iNKT cells, with such limited TCR diversity, able to respond to different infectious pathogens? During the last decade, two mechanisms of iNKT cell activation have been delineated: direct, where iNKT cells directly recognise microbial glycolipid antigens through their TCR and indirect, where TCR recognition of pathogens is dispensable (Brennan, Brigl and Brenner, 2013).

In the first mechanism, antigen-presenting cells, such as dendritic cells, macrophages or B cells, present processed lipids derived from the cell wall of specific bacteria in the context of CD1d molecules. These lipids include α-glycosphingolipids found in the cell wall of *Sphingomonas* sp., α-glycosylated diacylglycerols present in the cell wall of *Borrelia* sp. and *Streptococcus pneumoniae* and α-galactosylceramide (α-GalCer) isolated from marine sponge-resident bacteria (Kawano et al., 1997, Kinjo et al., 2005, 2006, 2011). The α refers to the orientation of the glycosidic linkage between the carbohydrate head group and the lipid backbone. The α-linkage provides a potential foreign structural motif for antigenicity, as mammals do not usually attach carbohydrates to lipids in the α-orientation (Kain et al., 2015). iNKT cells recognise these exogenous glycolipids presented in the context of CD1d by antigen-presenting cells and become activated (Figure 5.2A). The crystal structure of CD1d with α-GalCer revealed that CD1d has a hydrophobic antigen-binding cleft with two main pockets: the A', where the acyl chain of α-GalCer is buried, and the F', where the phytosphingosine chain is buried. In contrast, the α-galactosyl head group protrudes from the cleft, so it is directly available to make contact with the iNKT cell TCR (Koch et al., 2005) (Figure 5.3).

In the second mechanism of iNKT cell activation, recognition of pathogen-derived lipids is not required. In this case, the presentation of endogenous lipids and/or the production of cytokines by the antigen-presenting cells are sufficient to induce iNKT cell activation (Brigl et al., 2003, Paget et al., 2007). Antigen-presenting cells can recognise a full range of pathogens through their TLRs; for example, they can recognise LPS from *Salmonella* sp. and *Escherichia coli* through TLR4 and microbial nucleic acids through TLR7 and TLR9. TLR signalling through MyD88 on the antigen presenting cells is sufficient to induce iNKT cell activation

This is due to the ability of antigen-presenting cells to produce IL-12 and present endogenous lipids in the context of CD1d after TLR signalling (Brigl et al., 2003, Mattner et al., 2005). (Figure 5.2B).

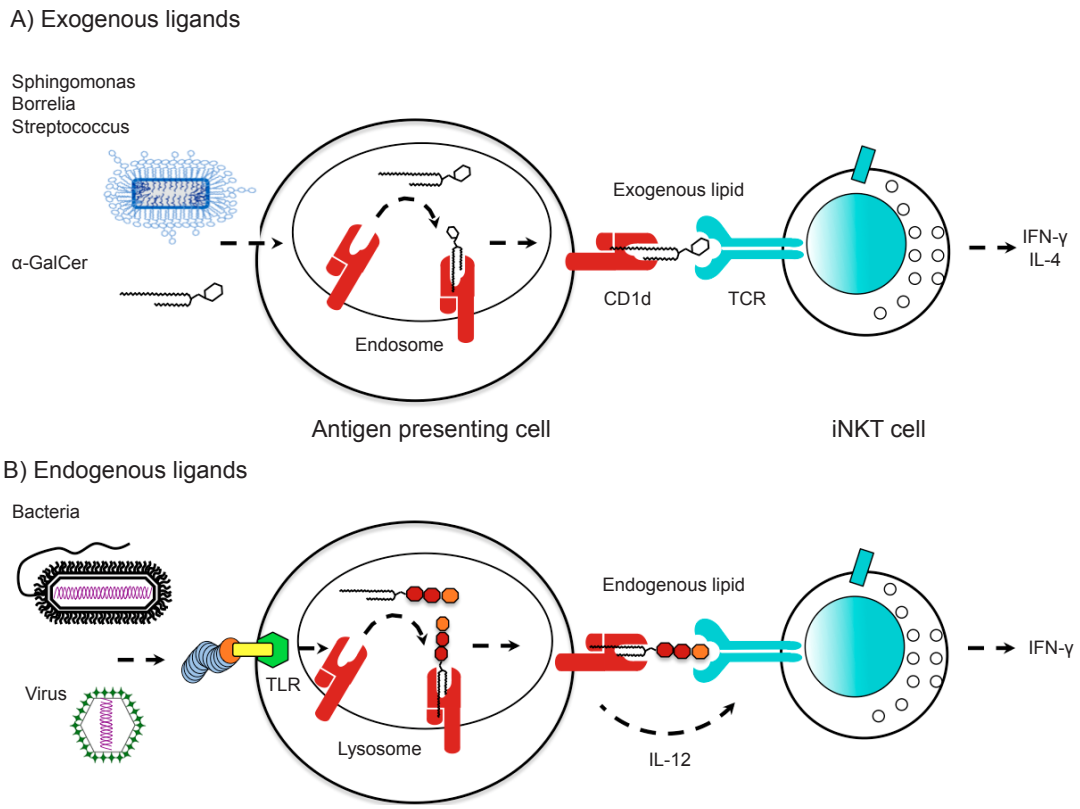

Figure 5.2 Mechanisms of iNKT cell activation

(**A**) Direct iNKT cell activation can occur via uptake of glycolipid-containing pathogens by antigen presenting cells and presentation of these exogenous lipids on CD1d to iNKT cells. (**B**) Indirect iNKT cell activation is triggered by recognition of pathogens through TLRs by antigen presenting cells, what induces IL-12 secretion and presentation of endogenous lipids on CD1d to iNKT cells.

The nature of these endogenous molecules is quite controversial. Initially, the lysosomal glycolipid iGb3 (isogloboside 3) was suggested as a potential endogenous lipid mediating iNKT cell development and activation (Zhou et al., 2004). However, recent studies showed that mice deficient in iGb3 synthase display normal iNKT cell development and activation (Porubsky et al., 2007, Christiansen et al., 2008). Later, two studies analysed the lipidome of thymic and

antigen presenting cells by HPLC (high-pressure liquid chromatography) and MS (mass spectrometry) and found that β-anomers of glycosylceramides found in these cells are potent activators of iNKT cells (Brennan et al., 2011, Facciotti et al., 2012). However, the significance of these β-glycosylceramides as self-antigens has been called into question by a study in 2014 that claims that the commercial β-glycosylceramides used in those studies were contaminated with low amounts of α-anomers (Kain et al., 2014). Surprisingly, this recent study revealed that immune cells are able to produce small quantities of α-glycosylceramides, such as α-GluCer and α-GalCer, and those are the major source of endogenous ligands for iNKT cells (Kain et al., 2014). The intracellular levels of α-GluCer and α-GalCer in immune cells are extremely low due to their constant degradation by the lysosomal enzyme α-galactosidase (GLA). In fact, GLA-deficiency induces increased amounts of self-ligands on the surface of thymocytes and antigen presenting cells, and hyper activation of iNKT cells. Interestingly, TLR stimulation on the antigen-presenting cells inhibits the activity of this enzyme, leading to an increase in the accumulation and presentation of α-glycosylceramides on CD1d and induced activation of iNKT cells (Darmoise et al., 2010) (Figure 5.3).

As mentioned, indirect activation of iNKT cells by antigen-presenting cells involves the presentation of endogenous lipids on CD1d molecules and the production of IL-12. However, some subsets of iNKT cells can become activated solely by cytokines, even in the absence of TCR engagement by CD1d. For example, iNKT cell activation during *Pseudomonas aeruginosa* infection is mediated by IL-12 and IL-18 produced by DCs and macrophages respectively. This capacity is due to the expression of IL-12R and IL-18R by some iNKT cells even in the steady state (Kastenmüller et al., 2012).

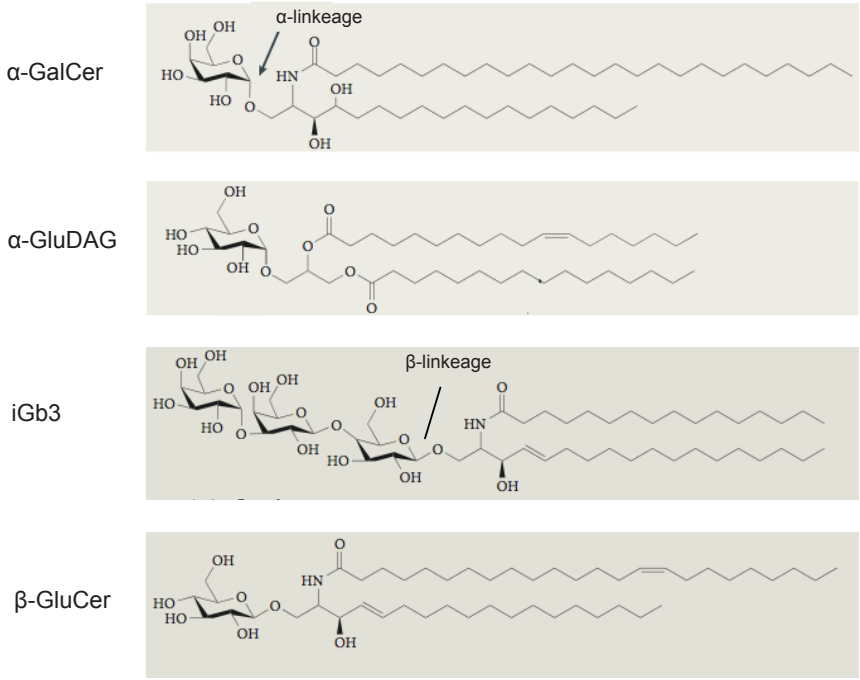

Figure 5.3 iNKT cell lipid antigens

Structures of glycolipids involved or suggested to be involved in iNKT cell activation. The strongest activator of iNKT cells is α-Galactosylceramide (α-GalCer). Some pathogens also contain α-glycolipids, such as α-Glucosyldiacylglycerol (α-GluDAG) present in the cell wall of *Streptococcus p*neumoniae. The initial candidates for endogenous ligands isoglobotrihexosylceramide (iGb3) and β-Glucosylceramide (β-GluCer) are also shown. Structures extracted from (Brennan, Brigl and Brenner, 2013).

All these different mechanisms of activation and their strategic location in the peripheral and secondary lymphoid organs allow iNKT cells to rapidly respond to a variety of pathogenic threats.

5.1.3 Outcome of iNKT cell activation: NKT cell effector subsets

iNKT cells can recognise glycolipids present in the cell wall of Gram positive and negative bacteria and even in the absence of exogenous glycolipids, they can detect specific cytokines or endogenous lipids produced by microbe-activated antigen presenting cells. All these different mechanisms of activation allow them to respond to a broad range of infectious agents and can partially determine the resulting effector outcomes. For example, the activation of iNKT cells with a potent

exogenous glycolipid such as α-GalCer induces the production of IFN-γ and IL-4 whereas the activation through endogenous ligands or cytokines usually leads to IFN-γ production only (Brigl et al., 2003). Regardless of the activation pathway, iNKT cells can differentiate into multiple phenotypically different subsets and modulate the activity of other immune cell types.

iNKT cell subsets are defined by the transcription factors involved in their differentiation and by the cytokines they produce. Th1-like iNKT cells constitute the majority of iNKT cells in the liver and secondary lymphoid organs. They produce IFN-γ and IL-4, they can be $CD4^+$ or $CD4^-$ and they need PLZF, GATA3 and T-bet for their differentiation. Th2-like iNKT cells are mainly found in the intestine and lungs, they are able to produce IL-4, IL-9, IL-10, IL-13 and GM-CSF after activation, are $CD4^+$ and need PLZF and GATA3 for their generation. Th17-like iNKT cells are $CD4^-$, reside in the LNs, lungs and skin, produce IL-17 and IL-22 and require PLZF, GATA3 and Rorγt for their differentiation (Watarai et al., 2012, Brennan, Brigl and Brenner, 2013). iNKTfh cells, as mentioned in chapter 1, express high levels of PD-1 and CXCR-5, require Bcl6 for their differentiation, produce IL-21 and provide cognate help to B cells for GC formation (Chang et al., 2012, King et al., 2012). Recently, a population of regulatory iNKT cells that produce IL-2 and IL-10 has been described in the adipose tissue. These cells require E4BP4 (E4 promoter-binding protein 4) for their differentiation but not PLZF or Foxp3 (forkhead box P3). Furthermore, they induce an anti-inflammatory phenotype in adipose-tissue resident macrophages and enhance the suppressor activity of regulatory T cells (Lynch et al., 2012, 2015).

5.1.4 iNKT cell functions and interaction with other immune cells

The production of cytokines by iNKT cells and the interaction with their CD1d-expressing cognate partners defines the ability of iNKT cells to control immune responses to a diverse spectrum of pathogens. I will discuss here the CD1d-mediated interaction of iNKT cells with different immune cells and the importance of these interactions in the development of an immune response (Figure 5.4).

The first immune cells described to interact with iNKT cells in a CD1d-dependent manner are DCs (Fujii et al., 2004). DCs constitutively express CD1d and they mediate iNKT cell activation in the spleen and lungs after α-GalCer exposure (Scanlon et al., 2011, Barral et al., 2012). In vitro, it has been shown that TLR ligands induce DC-mediated presentation of endogenous lipids and the production of IL-12 to mediate iNKT cell activation (Mattner et al., 2005). The interactions established between DCs and iNKT cells not only involve CD1d-TCR contacts but also CD40—CD40 ligand interactions. Together, this leads to a strong IFN-γ production by iNKT cells and to further IL-12 production by DCs (Kitamura et al., 1999, Fujii et al., 2004). Both IFN-γ and IL-12 induce NK cell transactivation, enhanced responses by conventional $CD4^+$ and $CD8^+$ T cells and the licensing of dendritic cell cross-presentation (Fujii et al., 2003, Hermans et al., 2003, Semmling et al., 2010). Therefore, through bidirectional interactions, iNKT cells and DCs cooperate to amplify innate and adaptive immune responses (Figure 5.4).

iNKT cells also interact with B cells through CD1d. Interestingly, splenic marginal-zone B cells express the highest CD1d levels of all antigen-presenting cells; however, whether these cells contribute to iNKT cell activation during infection remains unclear (Sonoda and Stein-Streilein, 2002). As described in chapter 1, a population of iNKT cells, iNKTfh cells, provide cognate help to B cells after B cell presentation of exogenous glycolipids on CD1d. This interaction results in fast immunoglobulin production and some affinity maturation, but does not lead to the generation of long-term B cell memory. Therefore, iNKT cell cognate-help might be important in enhancing early antibody responses during infection (Barral et al., 2008, Chang et al., 2012, King et al., 2012). Importantly, iNKT cells can provide non-cognate help to B cells through the production of IL-4, IL-5, IL-6, IL-13, IL-21 and CD40 ligand (Coquet et al., 2008) (Figure 5.4).

Macrophages also interact through CD1d with iNKT cells in different organs. In the liver, where iNKT cells represent up to 30% of total T cells, different subsets of macrophages such as Kupffer cells and stellate cells, can present lipid antigens to mediate iNKT cell activation following *Borrelia* sp. Infection (Lee et al., 2010). In the LNs, SCS macrophages can present exogenous lipids on CD1d to resident

iNKT cells following particulate α-GalCer administration (Barral et al., 2010). Moreover, these macrophages can also mediate iNKT cell activation in the LNs through the secretion of IL-18 (Kastenmüller et al., 2012). These interactions are bidirectional, as iNKT cells can modulate the physiology of macrophages. For example, iNKT cell-derived IFN-γ can lead to iNOS production by SCS macrophages and enhanced phagocytosis by pulmonary macrophages (Nieuwenhuis et al., 2002, Kastenmüller et al., 2012). Moreover, iNKT cell-derived IL-10 can polarise macrophages to an anti-inflammatory phenotype in adipose tissue (Lynch et al., 2015) (Figure 5.4).

Neutrophils also express CD1d and can interact with iNKT cells. During inflammation, levels of the acute phase protein SAA1 (serum amyloid A1) increase in the organism and induce the production of IL-10-producing neutrophils. Interestingly, under these conditions, neutrophils can mediate iNKT cell activation through CD1d presentation of endogenous ligands. iNKT cells are able to reverse the suppressive phenotype of these neutrophils and promote IL-12 production, which would be important to balance the frequencies of immunosuppressive neutrophils (De Santo et al., 2010). Moreover, iNKT cells can recruit neutrophils to infected tissues in a CD1d-independent manner through the production of CXCL2 (Nieuwenhuis et al., 2002) (Figure 5.4).

A population of $CD11b^{+}Gr1^{+}$ cells with immunosuppressive characteristics, defined as MDSCs (myeloid derived suppressor cells), also expresses high levels of CD1d. These cells display high-enzymatic activity of iNOS (nitric oxide synthase) and arginase 1, which limits the availability of arginine, and, therefore, T cell proliferation. Following infection, CD1d-mediated interaction of MDSCs with iNKT can counterbalance the suppressive activity of these cells, enhancing the proliferation and formation of antigen-specific T cells (De Santo et al., 2008) (Figure 5.4).

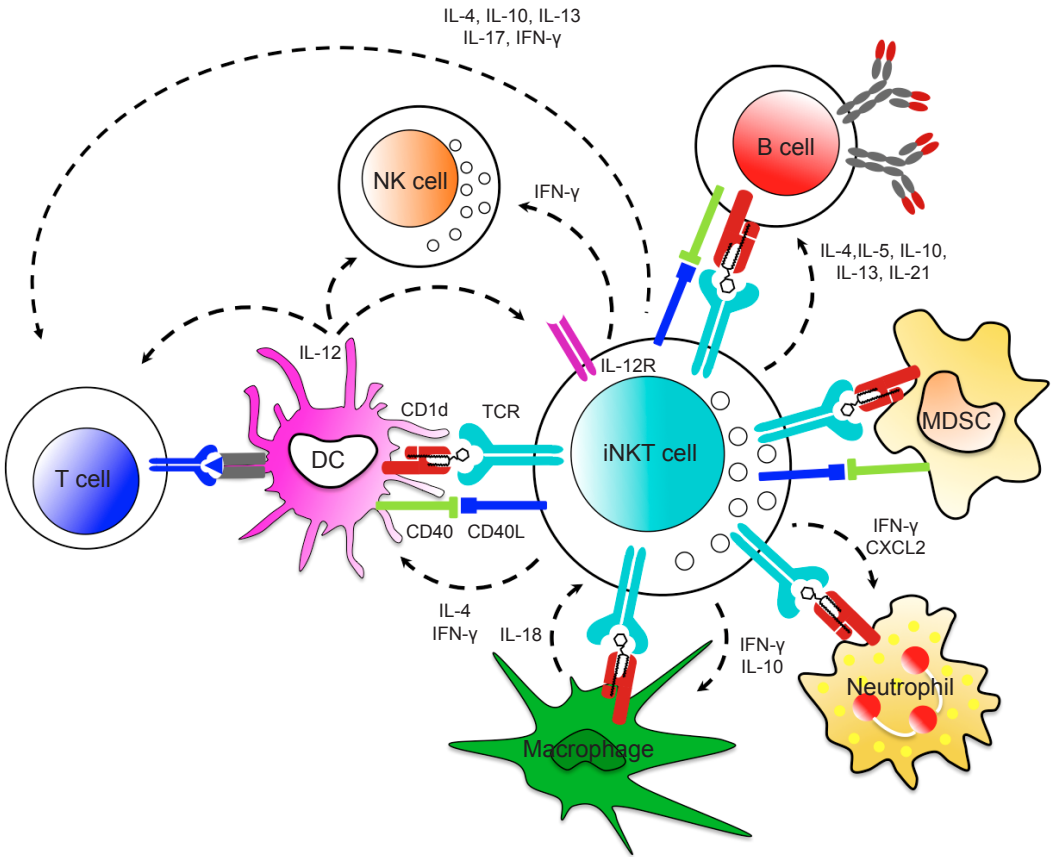

Figure 5.4 Interaction between iNKT cells and other immune cells

The presentation of lipid antigens mediates cognate interactions between iNKT cells and CD1d-expressing cells. These interactions lead to the activation of iNKT cells and reciprocal modulation of CD1d-expressing cell activity through cytokine secretion and/or CD40-CD40L interactions.

NKT cells are now recognised as important participants in the linking of the innate and adaptive immune responses, and have been implicated not only during infection, but also during allergy, asthma, autoimmunity and tumour surveillance (Brennan, Brigl and Brenner, 2013). There are however, essential questions regarding iNKT cell biology that still remain unanswered. For example, which are the roles of the different CD1d expressing cells in the activation of iNKT cells during infection in the absence of exogenous glycolipids? Are iNKT cells able to regulate the antibody response in these situations? In this chapter, through the use of different genetically modified mice, I will attempt to answer these points.

5.2 iNKT cell activation following influenza infection *in vivo* requires MyD88 signalling in DCs

In the last decade, several lines of research explored by different groups have shed light on the iNKT cell biology in the presence of exogenous bacteria-derived glycosphingolipids. However, the vast majority of pathogens, particularly viruses, do not have these special glycolipids on their surface. This led me to investigate the role of iNKT cells in the immune response to pathogens in the absence of exogenous ligands; in particular, how iNKT cells get activated, and their ability to regulate the B cell response.

5.2.1 NKT cell-deficient mice are more susceptible to influenza virus infection

To understand the importance of iNKT cells, I compared the pathology and immune response of wild type and CD1d$^{-/-}$ mice during viral infections. CD1d$^{-/-}$ animals do not have iNKT cells in the periphery because of their impaired selection in the thymus during development (Mendiratta et al., 1997). Therefore, the use of these mice allowed me to understand the role of iNKT cells during an immune response against viral pathogens. Influenza A virus was chosen as an infection model for its importance in the clinic as it is responsible for annual epidemics that cause severe illness in around 5 million people worldwide. Influenza virus clearance from the organism is mainly mediated by cytotoxic CD8^{+} T lymphocytes and by neutralising antibodies secreted by B cells (Waffarn and Baumgarth, 2011). Interestingly, iNKT cells can sustain CD8^{+} T cell response to influenza virus by inhibiting the immunosuppressive activity of lung-resident MDSCs (De Santo et al., 2008). However, the process of iNKT cell activation and the ability of these cells to regulate the B cell response following infection remain largely unknown.

To assess whether iNKT cells play a role in controlling influenza virus infection, wild type and CD1d$^{-/-}$ mice were intranasally infected with a low dose (200 PFU) of influenza virus PR8 (A/Puerto Rico/8/34). After six days of infection, the lungs, mediastinal LNs and spleen were harvested and RNA was extracted from

single cell suspensions to analyse influenza-specific viral RNA expression levels. Real-time RT-PCR was used to quantify the levels of influenza NP (nucleoprotein), using CPH (carboxypeptidase H) gene as a housekeeping gene for normalisation. While NP RNA was detected in the lungs six days after infection, no NP amplification was observed in non-immunised mice (Figure 5.5A). This clearly indicates that the NP primers used for the measurement of influenza virus levels are specific. Moreover, NP was not detected in mediastinal LNs or spleen following infection, indicating that the virus is mainly retained in the lungs (Figure 5.5A). Importantly, the NP RNA levels were significantly higher in the lungs of $CD1d^{-/-}$ mice, suggesting that iNKT cells might play a role in the clearance and protection of mice against influenza virus infection (Figure 5.5A).

During the earliest stages of viral infection, there is a rapid release of IFN-α, IFN-γ, TNF-α, IL-1, IL-6 and IL-18 by innate immune cells such as neutrophils, eosinophils, monocytes, macrophages, DCs and NK cells. The levels of these inflammatory cytokines directly correlate with the magnitude of viral replication (Kaiser, Fritz and Straus, 2001). I therefore wondered whether higher titers of influenza in $CD1d^{-/-}$ mice would alter the cytokine expression pattern following influenza virus infection. To analyse this, wild type and $CD1d^{-/-}$ mice were infected with 200 PFU of influenza A virus, and six days after infection, the levels of several cytokines (IL-2, IL-4, IL-6, IFN-γ, TNF-α, IL-17A and IL-10) were measured in the blood using a cytometric bead array. High levels of IL-6 and IFN-γ were detected in the blood of infected mice while the levels of IL-2, IL-4, TNF-α, IL-17A and IL-10 remained similar to basal levels in most cases (Figure 5.5B). Interestingly, the levels of IFN-γ in the blood were significantly higher in $CD1d^{-/-}$ mice compared to wild type animals (Figure 5.5B). Although, IL-6 levels seemed to be increased in $CD1d^{-/-}$ mice, this difference was not significant. The increase in IFN-γ levels observed in $CD1d^{-/-}$ mice following influenza virus infection was further recapitulated in the lungs by real time RT-PCR (Figure 5.5C). These results indicate that the ineffective clearance of influenza virus from the lungs in the absence of iNKT cells results in high titers of influenza virus and increased production of IFN-γ.

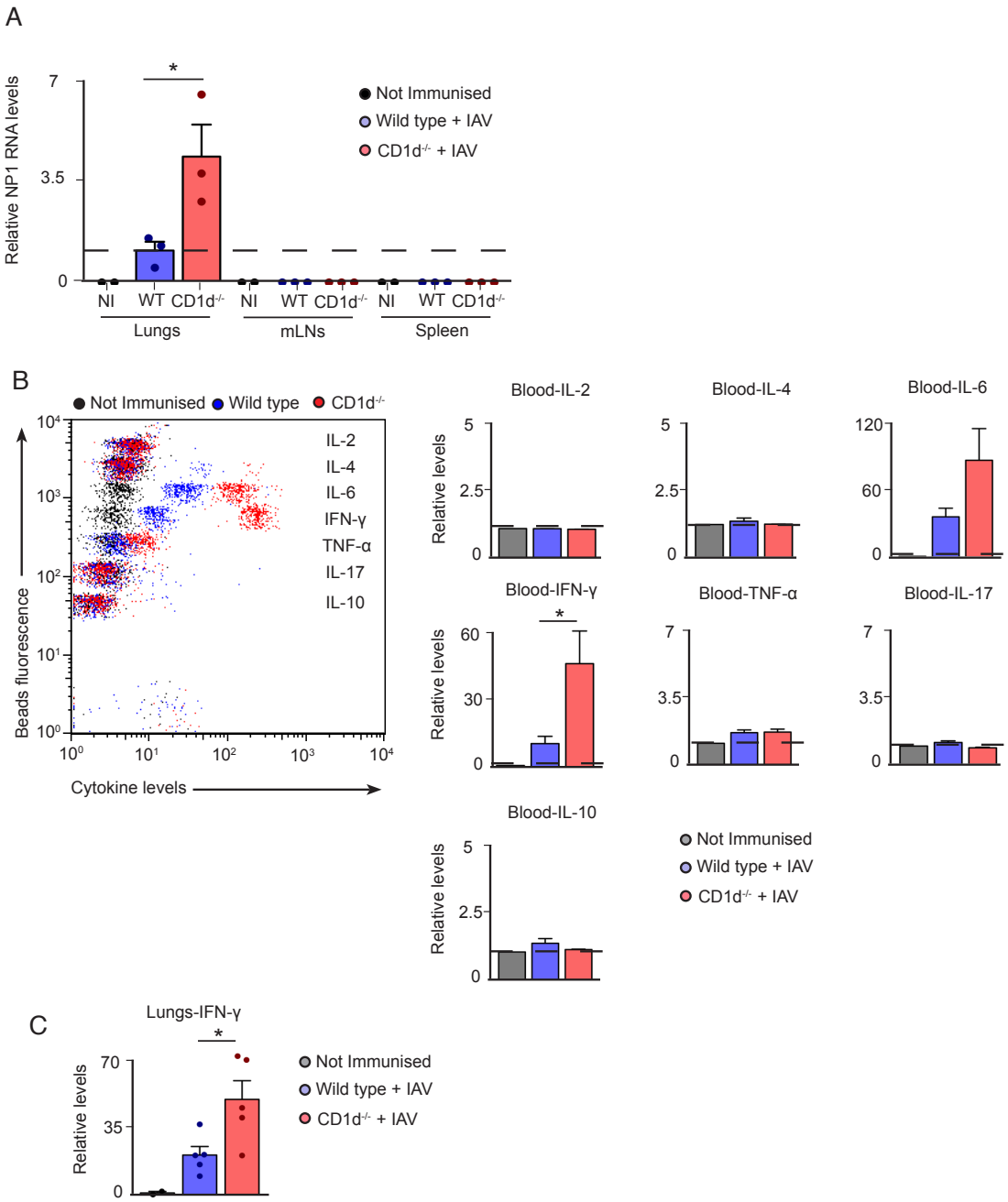

Figure 5.5 CD1d$^{-/-}$ mice are more susceptible to influenza virus infection

(A) RT-PCR analysis of lungs, mediastinal LNs and spleen from wild type and CD1d$^{-/-}$ mice that were infected with 200 PFU of influenza virus 6 days previously or left untreated (not immunised). Relative RNA levels of viral NP1 were normalised to the housekeeping gene CPH and were plotted in the bar charts as expression levels relative to the mean level observed in wild type samples. (B) Cytometric bead array of serum from wild type and CD1d$^{-/-}$ mice treated as in (A). Mean fluorescence intensity for each cytokine was normalised to levels observed in non-immunised samples and plotted in the bar charts. (C) RT-PCR analysis of lungs from mice treated as in (A). Relative RNA levels of IFN-γ were normalised to CPH and plotted as expression levels relative to the mean level observed in non-

immunised samples. Each dot represents a different mouse. Mean± s.e.m. Data are representative of two independent experiments. Student t test, *p<0.05.

5.2.2 iNKT cell activation results in CD69 up regulation and IFN-γ and IL-4 secretion

The previous results indicate that iNKT cells might be important for the regulation of the immune response against influenza virus. I therefore moved on to analyse the signals and components involved in the process of iNKT cell activation following infection. To analyse the kinetics of iNKT cell activation, mice were intranasally infected with 200 PFU of influenza virus and the lungs and mediastinal LNs were harvested after 1 to 6 days of infection. iNKT cells were identified by flow cytometry due to the expression of TCRβ and their ability to bind a PBS-57 loaded CD1d tetramer. PBS-57 is an analog of α-GalCer, a known ligand for iNKT cells (Kawano et al., 1997). Importantly, this $TCR\beta^+$ $tetramer^+$ population is absent in $CD1d^{-/-}$ mice, confirming the specificity of the staining (Figure 5.6A). iNKT cell activation was followed by assessing the levels of the surface activation marker CD69 on the iNKT cell population. The levels of CD69 on iNKT cells increased from day 2 and were maintained at least until day 6 in the lungs and mediastinal LNs (Figure 5.6B). These results indicate that iNKT cells are activated very early during influenza infection.

I further analysed the process of iNKT cell activation by assessing the production of cytokines after 72 hours of infection. For the measurement of intracellular cytokines, single cell suspensions of mediastinal LNs were stimulated *ex vivo* with PMA/ionomycin, and cytokine release was blocked using monensin, a protein transport inhibitor. LN suspensions were then stained with anti-TCRβ and PBS-57 CD1d tetramer, fixed, permeabilised and stained again with labelled antibodies against IFN-γ and IL-4. While IL-4 or IFN-γ production was not detected in iNKT cells from non-immunised mice, influenza infection results in the robust production of IL-4 and IFN-γ by iNKT cells (Figure 5.6C). These results indicate that the early activation of iNKT cells after influenza infection occurs in the lungs and draining mediastinal LNs and results in the up-regulation of CD69 and the production of IFN-γ and IL-4.

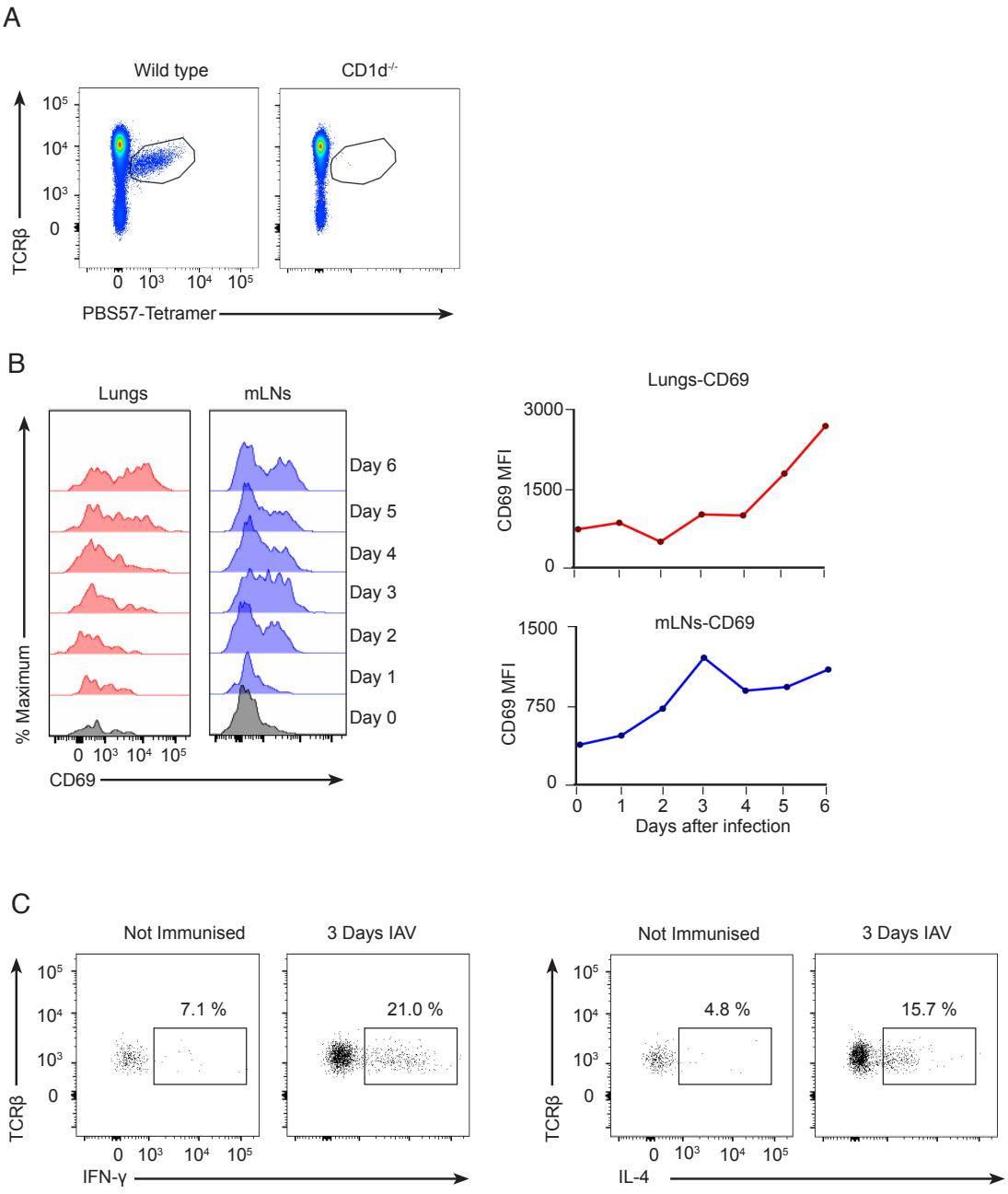

Figure 5.6 Early activation of iNKT cells results in IFN-γ and IL-4 secretion

(A) Flow cytometry analysis of LN cell suspensions from wild type and CD1d$^{-/-}$ mice stained for TCRβ and PBS-57 tetramer. Representative plots are shown. (B) Flow cytometry analysis of lungs and LN cell suspensions from wild type mice infected with 200 PFU of influenza virus 1 to 6 days before. The levels of CD69 on the TCRβ^{+} tetramer^{+} population are shown on the histograms. CD69 MFI (mean fluorescence intensity) in the TCRβ^{+}Tetramer^{+} population was plotted. (C) Flow cytometry analysis of LN cell suspensions from wild type mice infected with 200 PFU of influenza virus 3 days before. The percentage of IFN-γ^{+} and IL-4^{+} cells on

the TCRβ$^+$ tetramer$^+$ population is shown in the dot plots. Data are representative of two independent experiments with three mice per condition.

5.2.3 Differential requirements of MyD88 and TLR7 for iNKT cell activation

As explained before, in the absence of exogenous glycolipids, iNKT cells have the unique ability to recognise lysosomal glycolipids presented on the surface of antigen presenting cells. In vitro studies indicate that the production of these endogenous ligands in response to bacteria requires MyD88-mediated signalling on the presenting cells (Mattner et al., 2005). I therefore wondered whether MyD88-mediated signalling is required for in vivo iNKT cell activation after influenza infection. To this end, wild type and MyD88$^{-/-}$ mice were intranasally infected with 200 PFU of influenza virus, and after 3 days, mediastinal LNs were harvested. iNKT cell activation was assessed by measuring CD69 levels and IFN-γ production as before. CD69 and secreted IFN-γ were up-regulated in iNKT cells from wild type animals in response to influenza infection, however, they were significantly reduced in iNKT cells from MyD88$^{-/-}$ mice (Figure 5.7). These results indicate that iNKT cell activation after influenza infection *in vivo* requires MyD88 signalling.

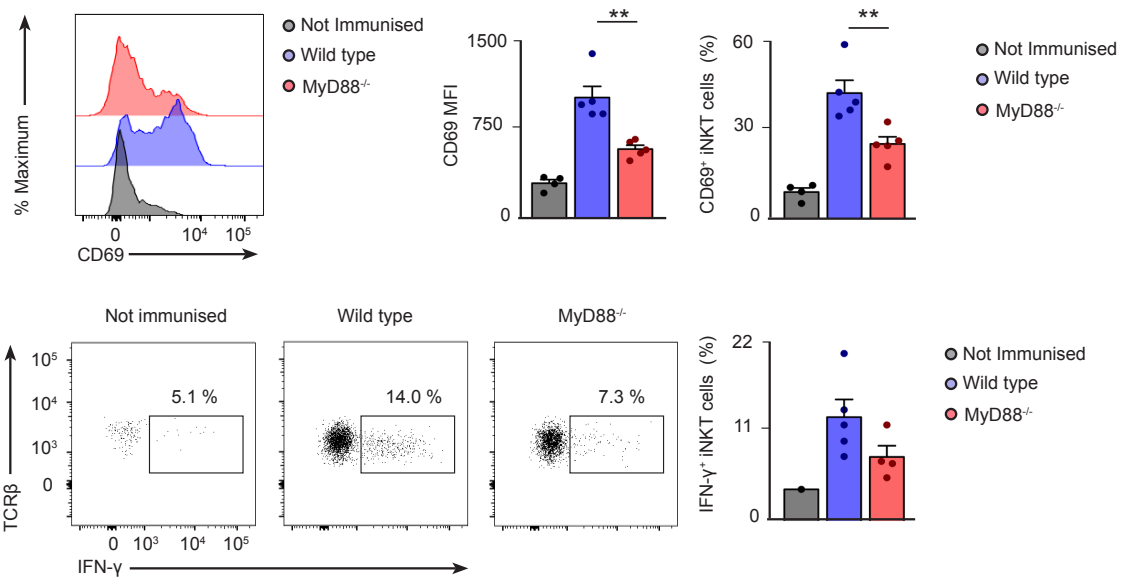

Figure 5.7 iNKT cell activation following influenza infection is MyD88 dependent

Flow cytometry analysis of lymph node cell suspensions from wild type and MyD88$^{-/-}$ mice 3 days after infection with 200 PFU of influenza virus. The levels of CD69 in TCRβ$^+$ tetramer$^+$ cells are shown on the histograms and the percentage of IFN-γ$^+$ iNKT cells is shown in the dot plots. Analysis of CD69 MFI and the percentage of

$CD69^+$ and IFN-γ^+ iNKT cells are shown on the bar charts. Each dot represents a single mouse. Data are representative of two independent experiments. Student t test, **p<0.01.

MyD88 serves as a critical adaptor for signalling induced by TLRs, IL-1R and IL-18R, all of which contain an intracellular homology domain called TIR that recruits MyD88 adaptor for effective signalling (Adachi et al., 1998). As iNKT cell activation requires MyD88-mediated signalling during viral infection, I wondered whether signalling through TLR, IL-1R or IL-18R were involved in this process.

Recognition of influenza single-stranded RNA by immune cells is restricted to TLR7 and TLR8 (Diebold et al., 2004). However, TLR8 is non-functional in mice because it lacks five amino acids, leaving TLR7 as the unique TLR capable of recognising influenza in mice (Kugelberg, 2014). To analyse the role of TLR signalling on NKT cell activation, wild type and $Tlr7^{-/-}$ mice were intranasally infected with 200 PFU of influenza virus, and mediastinal LNs were harvested 3 days afterwards. iNKT cell activation was measured by up regulation of CD69 and secretion of IFN-γ and IL-4. Following infection, mediastinal LNs from $Tlr7^{-/-}$ mice were smaller in size and contained significantly fewer iNKT cells than their wild-type counterparts. Surprisingly, iNKT cells from $Tlr7^{-/-}$ mice up regulate CD69 and secrete IL-4 and IFN-γ to the same extent of iNKT cells from wild type mice (Figure 5.8). This result is key and demonstrates that even though MyD88-mediated signalling is required to activate iNKT cells after viral infection, this process is independent of TLR signalling.

During influenza infection, there is an increased production of IL-1 and IL-18 by lung-resident innate immune cells. This process is dependent on the activation of the inflammasome complex, as mice deficient in Caspase-1 or the adaptor ASC have dramatically reduced levels of IL-1 and IL-18 in the bronchoalveolar lavage (Thomas et al., 2009). As IL-1R and IL-18R signal through the MyD88 adaptor, the potential role of IL-1R and IL-18R on iNKT cell activation in vivo will be addressed in the future. For this, IL-1R and IL-18R-deficient mice were ordered from Jackson Laboratories and as of the time of writing I am still waiting for these strains. If iNKT cell activation were dependent on IL-1 or IL-18, it would be interesting to analyse

the contribution of the inflammasome complex on this process. For that, Caspase-1 and ASC-deficient animals will be used to assess the extent of iNKT cell activation following viral infection.

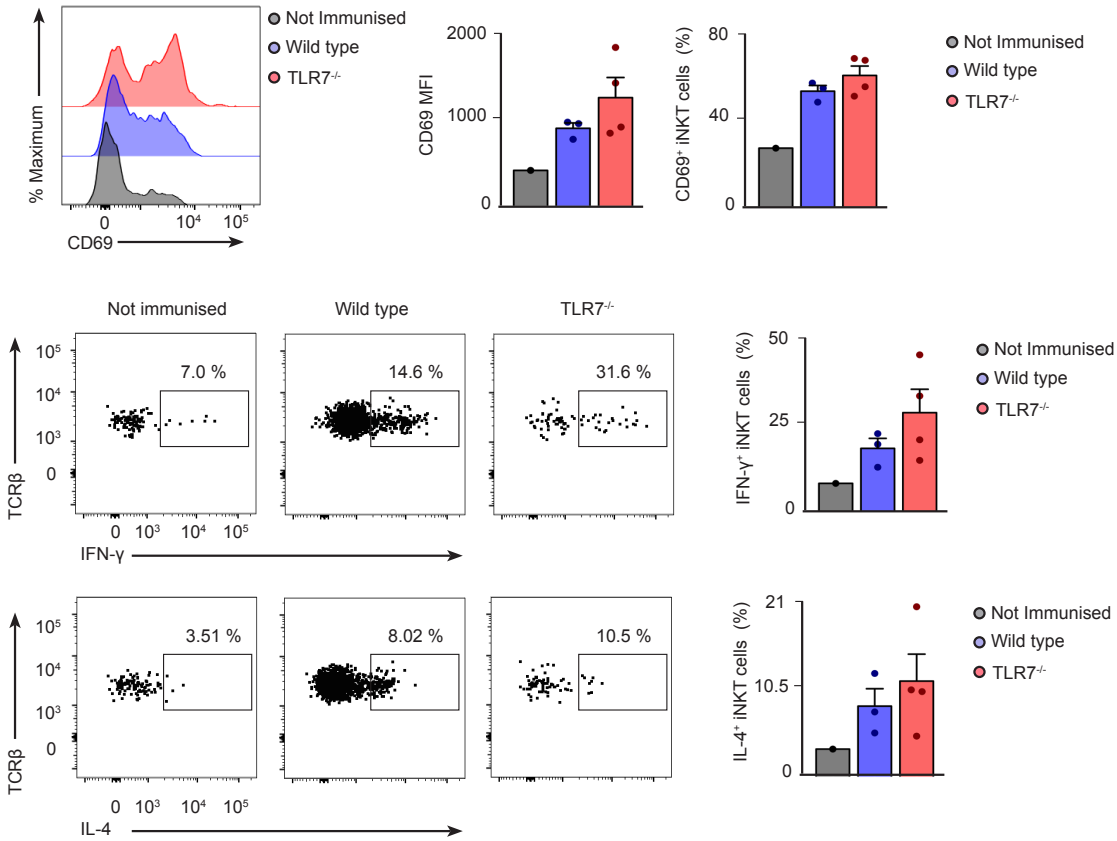

Figure 5.8 iNKT cell activation following influenza infection is TLR7 independent

Flow cytometry analysis of LN cell suspensions from wild type and Tlr7$^{-/-}$ mice 3 days after infection with 200 PFU of influenza virus. The levels of CD69 in TCRβ^{+} tetramer^{+} cells are shown on the histograms and the percentages of IFN-γ^{+} and IL-4^{+} iNKT cells are shown in the dot plots. Analysis of CD69 MFI and the percentage of CD69^{+}, IFN-γ^{+} and IL-4^{+} iNKT cells are shown on the bar charts. Each dot represents a single mouse. Data are representative of two independent experiments.

5.2.4 iNKT cell activation requires MyD88-signalling in DCs

Several immune cell populations in the lungs express MyD88. I therefore went on to analyse in vivo the requirement of MyD88 by different antigen presenting cells to mediate the activation of iNKT cells. For this, MyD88$^{flox/flox}$ mice

were crossed with mice expressing the Cre recombinase under different promoters: CD19, to specifically delete MyD88 on B cells (MyD88$^{flox/flox}$CD19 Cre^{+}), Lyz2 to delete MyD88 on neutrophils (MyD88$^{flox/flox}$Lyz2 Cre^{+}) and CD11c, to delete MyD88 on DCs (MyD88$^{flox/flox}$CD11c Cre^{+}). The analysis of MyD88 deletion in the different strains and immune cell populations was previously shown in Chapter 3. Wild type and these different transgenic mice were infected intranasally with 200 PFU of influenza virus and after 3 days mediastinal LNs were harvested. iNKT cell activation in these transgenic animals was assessed by the measurement of CD69 up regulation and cytokine secretion. Influenza infection induced CD69 up-regulation by iNKT cells to the same extent in wild type, MyD88$^{flox/flox}$CD19 Cre^{+} and MyD88$^{flox/flox}$Lyz2 Cre^{+} mice (Figure 5.9). These results indicate that MyD88-mediated signalling in B cells or neutrophils is not required for the activation of iNKT cells following influenza infection. In contrast, iNKT cells from MyD88$^{flox/flox}$CD11c Cre^{+} mice showed reduced up regulation of CD69 and impaired production of IL-4 and IFN-γ (Figure 5.9). This result demonstrates that iNKT cell activation in vivo following viral infection requires MyD88-mediated signalling in DCs.

I wondered whether iNKT cell activation by DCs in vivo requires the presentation of endogenous lipids in the context of CD1d. To answer this question it would be necessary to specifically delete CD1d on the DC population. However, with the tools available at the initiation of this project, it was not possible to perform this kind of experiment. To address this and many other essential questions in the NKT cell biology, we thought it would be extremely useful to generate CD1d$^{flox/flox}$ mice to delete CD1d on specific immune cell populations.

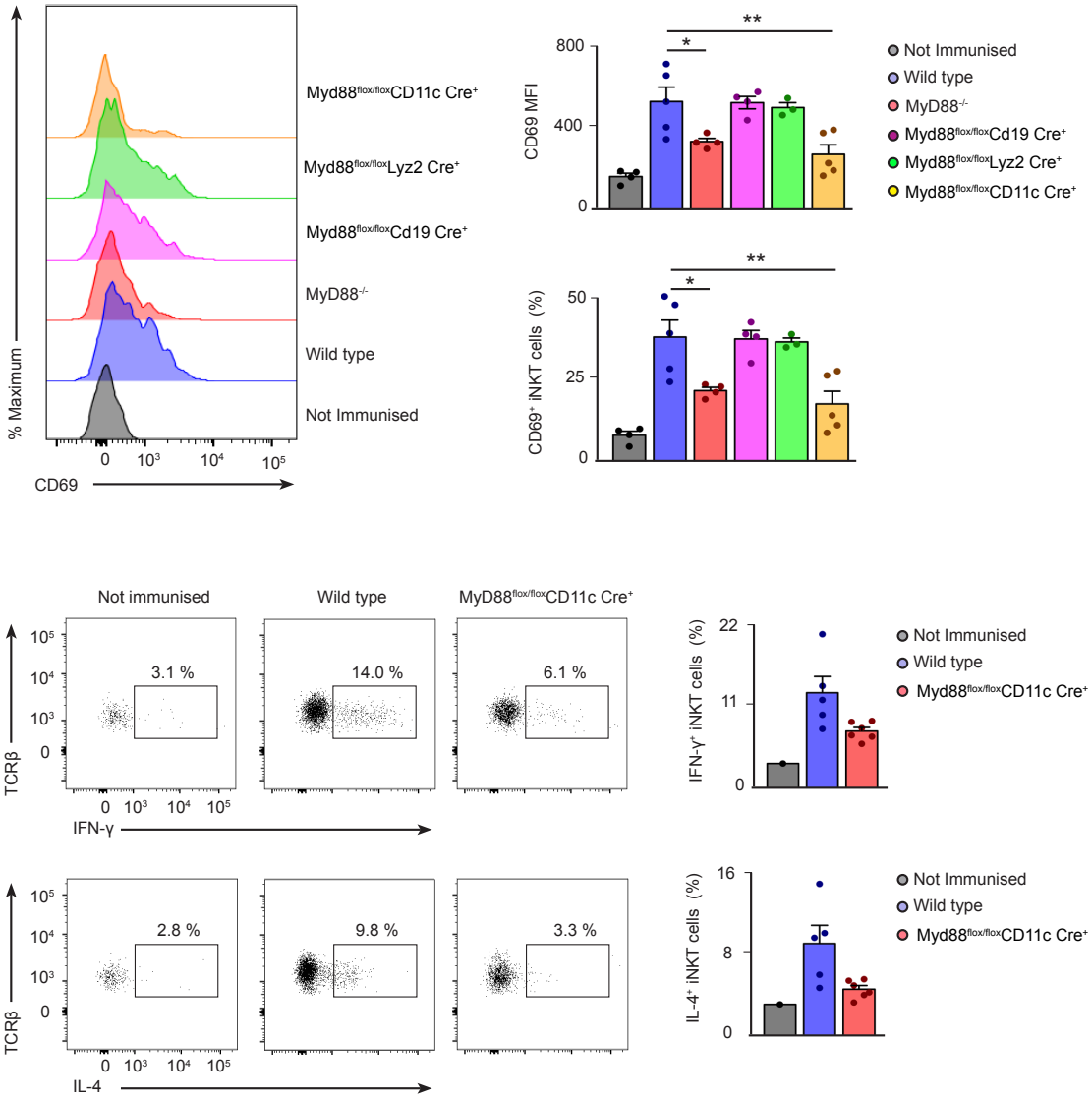

Figure 5.9 iNKT cell activation requires MyD88-mediated signalling in DCs

Flow cytometry analysis of LN cell suspensions from wild type, MyD88$^{-/-}$, MyD88$^{flox/flox}$CD19-Cre^{+}, MyD88$^{flox/flox}$Lyz2-Cre^{+} and MyD88$^{flox/flox}$CD11c-Cre^{+} mice 3 days after infection with 200 PFU of influenza virus. The levels of CD69 in TCRβ^{+} tetramer^{+} cells are shown on the histograms. The percentages of IFN-γ^{+} and IL-4^{+} iNKT cells following infection of wild type and MyD88$^{flox/flox}$CD11c-Cre^{+} mice are shown in the dot plots. Analysis of CD69 MFI and the percentage of CD69^{+}, IFN-γ^{+} and IL-4^{+} iNKT cells are shown on the bar charts. Each dot represents a single mouse. Data are representative of two independent experiments. Student t test, *p<0.05, **p<0.01.

5.3 Generation of CD1d-floxed mice reveals CD1d requirement by DCs to complete iNKT cell activation in vivo

5.3.1 Generation and selection of CD1d-floxed embryonic stem cells

The conditional knockout strategy consists of genetically targeting a gene region of interest with 2 loxP sequences, one on either side. The loxP sites are 34-nucleotide sequences recognised by Cre recombinase, an enzyme that excises any region of DNA placed between two loxP sites. The resulting mice contain the floxed allele (flanked by loxP sites) in all tissues but are phenotypically wild type. By crossing a floxed mouse with a specific Cre-expressing mouse, it is possible to delete the targeted gene only in cells that express Cre (Friedel et al., 2010).

The initial step for the generation of a mouse with a targeted mutation is the construction of an efficient targeting vector. In my case, this vector was generated by Gene Bridges Co and is shown in Figure 5.10A. The two loxP sites (yellow) were inserted flanking exon 3 (blue) of CD1d, as this exon codes for an essential part of the CD1d protein. Both loxP sites were positioned in the introns of CD1d to avoid interference with the coding sequences or the promoter of the gene. A neomycin cassette (orange) surrounded by 2 FRT sites (green) was also added to the construct for future selection of cells that have taken up the vector. Moreover, a continuous length of homologous genomic sequence (6 kb) was added on each sided of the floxed exon to favor homologous recombination. The vector containing the targeted construct was introduced into C57BL/6 mouse ES (embryonic stem) cells by electroporation. Once inside the ES cells, homologous recombination between the mouse genome and the transfected vector occurs in a small percentage of cells. This strategy takes advantage of a cell's own DNA repair machinery to replace a genomic sequence with a targeted genetic locus containing homologous sequences (Friedel et al., 2010). Since the transformation efficiency and the chances of recombination are very low, ES cells were cultured in medium containing Neomycin (a positive selection marker) to enrich clones that have the targeting vector inserted into their genome.

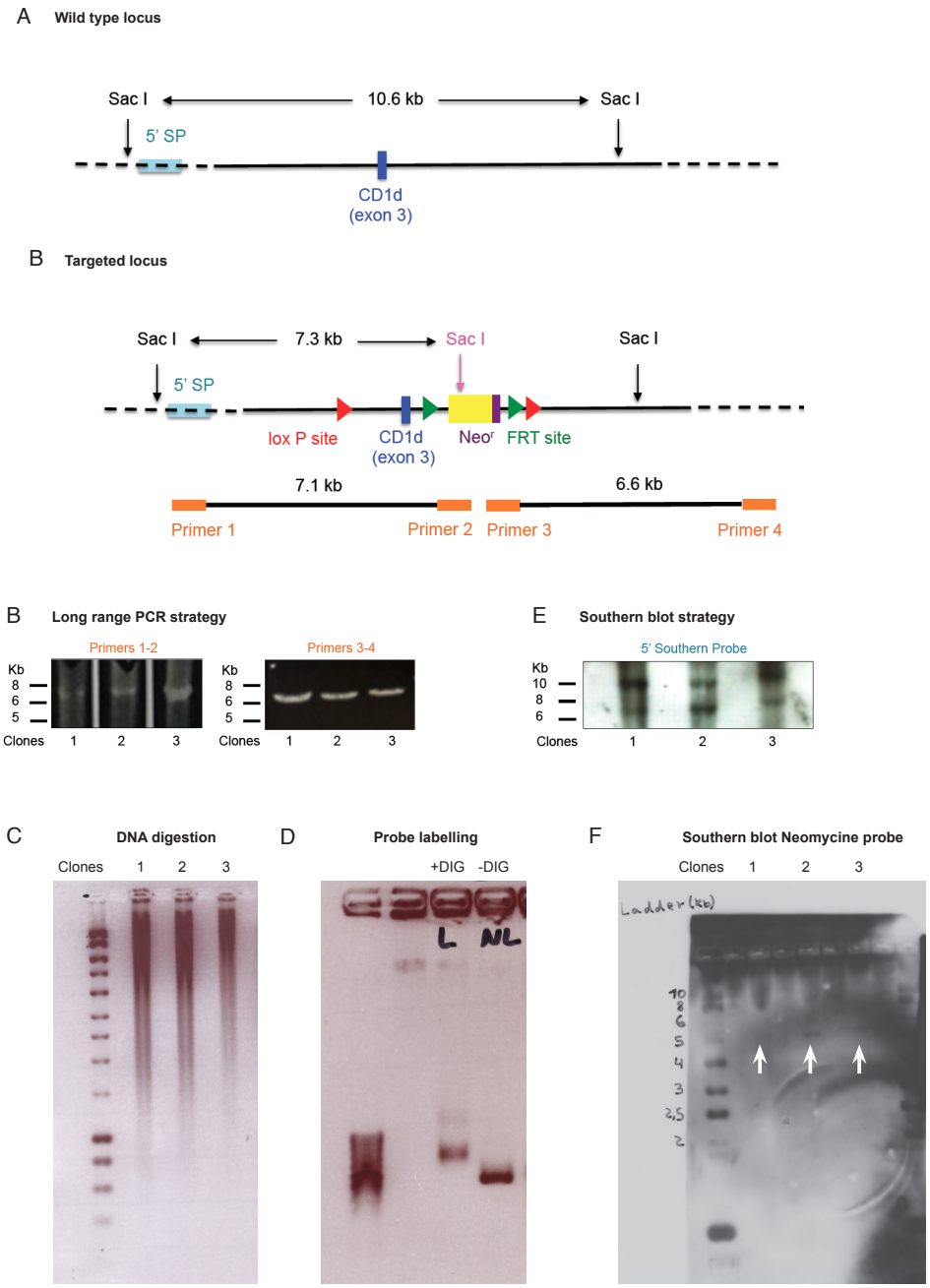

Figure 5.10 Strategy for the generation and selection of CD1d-floxed ES cells

(A) Scheme showing the wild type and targeted CD1d locus containing two loxP sites flanking the exon 3 of CD1d as well as two FRT sites for the removal of the Neomycin resistance cassette. (B) Specific fragments amplified by long-range PCR for the 5' end (7.1kb) and 3' end (6.6kb) of the clones that correctly performed homologous recombination. (C) Electrophoresis gel of digested DNA with SacI restriction enzyme of the three positive clones. (D) Electrophoresis gel of 5' Southern probe labelled with or without with Digoxigenin. (E) Southern blot of the three positive clones performed with the labelled 5' Southern probe. The upper band corresponds to the WT locus (10.6kb) and the lower band to the targeted locus (7.3kb). (F) Southern blot of the three positive clones performed with a

labelled Southern probe against the Neomycin cassette. White arrows indicate the 5.2kb band recognised by this probe.

To identify those ES cell clones that have correctly inserted the targeted locus in the genome, I performed a thorough screening process by long-range PCR of 100 clones. For this strategy, I designed pairs of primers that amplify a fragment from the neomycin cassette to outside the homology arm in the 5' direction (Primers 1-2, 7.1kb fragment) and from the neomycin cassette to outside the homology arm in the 3' direction (primers 3–4, 6.6kb fragment). In this way, only those clones that have the correctly inserted targeted locus in both 5' and 3' directions will generate the 7.1 and 6.6kb fragments after PCR amplification. Only three out of a hundred clones generated these two fragments, indicating correct insertion in the genome (Figure 5.10B). I further confirmed the correct insertion in these three clones by Southern blot. For this, DNA from the three clones was digested with the restriction enzyme SacI. Successful digestion of the DNA was confirmed by electrophoresis, as a smear of DNA is obtained when DNA is properly digested (Figure 5.10C). Digested DNA was subject to Southern blot, where a DIG (digoxigenin)-labelled DNA probe was used for detection. Effective DIG-labeling of the probe was confirmed by a shift in the weight of the DNA probe in the electrophoresis gel (Figure 5.10D). When DNA is digested with SacI, this probe recognises a 10.6kb fragment in the wild type allele and a 7.3kb fragment in the targeted allele due to the insertion of a SacI restriction site in the Neomycin cassette. All these three clones produced the 10.6kb and the 7.3kb bands, confirming the correct insertion of the targeted allele (Figure 5.10E). Moreover, only one insertion event occurred in the genome of these clones as a single band of 5.2kb is obtained when a DIG-labelled probe against the Neomycin cassette is used (Figure 5.10F).

5.3.2 Generation of CD1d-floxed transgenic mice

As the three positive clones have a single correct insertion of the CD1d floxed allele, a karyotype of them was performed to analyse the levels of euploidy. While clone 1 has only 50% of euploidy, clone 2 and 3 had more than 90 % of euploidy. Therefore, clone 1 was discarded, and ES cells from clone 2 and 3 were

used for injection into BALB/C blastocysts and transplanted into surrogate mothers. These C57BL/6 ES cells are totipotent so, when injected into BALB/c blastocysts, they can potentially differentiate into any of the cell types of the resultant chimaeric mouse. When litters were born, only those mice with more than 80% of chimerism, as judge by the coat color, were crossed with C57BL/6 mice. Mice with higher levels of chimerism were used to improve the chances of germ line transmission of the target gene. The black litters from the crosses between chimeras and C57BL/6 mice were genotyped for the neomycin cassette, for detection of mice carrying the targeted gene. Those mice that were positive for the neomycin cassette were then crossed with FLPo mice, which express the flippase recombinase and excise the neomycin cassette flanked by two 34 bp sequences known as FRT sites. The removal of the positive selection marker is necessary to avoid interference with the final mutated gene.

After the removal of the neomycin cassette, mice carrying the flox allele were crossed with mice expressing the Cre recombinase under the following promoters; CD19 and Mb1 to specifically delete CD1d on B cells, Lyz2 to delete CD1d on neutrophils and macrophages, and CD11c to delete CD1d on DCs. Finally, mice were crossed again with the same floxed mice to make them homozygous for the floxed allele. Deletion of CD1d in the different splenic immune cell populations for the different transgenic mice was analysed by flow cytometry. B cells were gated as $B220^{+}TCR\beta^{-}$, DCs were gated as $CD11c^{+}MHCII^{+}$ and further subdivided into $CD11b^{+}$ DCs and $CD8^{+}$ DCs. Macrophages were gated as $CD11b^{int}F4/80^{hi}$ and $CD11b^{hi}F4/80^{int}$. Neutrophils were gated as $CD11b^{hi}F4/80^{-}$ (Figure 5.11A).

In the $CD1d^{flox/flox}CD19\text{-}Cre^{+}$ mice, deletion of CD1d was observed in approximately 80% of B cells (Figure 5.11B). However, in $CD1d^{flox/flox}Mb1\text{-}Cre^{+}$ mice, CD1d deletion in B cells was almost 100% (Figure 5.11C). These results indicate that Mb1-Cre is a more efficient system to delete CD1d in B cells than CD19-Cre. Importantly, no deletion of CD1d was observed in $B220^{-}$ $TCR\beta^{-}$ cells, indicating that CD1d deletion is specific for B cells in these two strains (Figure 5.11B-C).

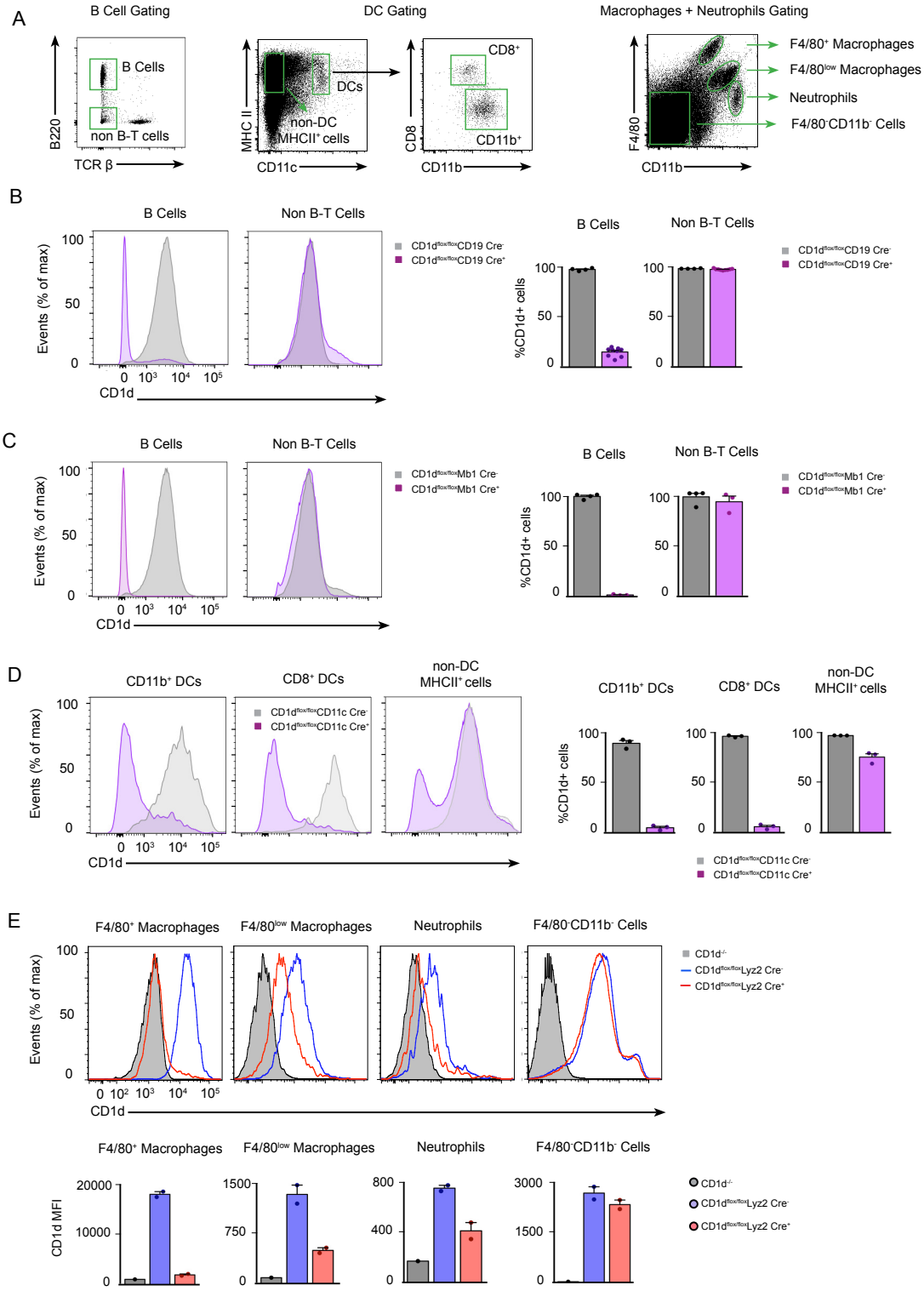

Figure 5.11 Analysis of CD1d deletion in the different immune cell populations

(A) Flow cytometry plots of spleen single cell suspensions showing the gating strategy for B cells ($B220^{+}TCR\beta^{-}$), $CD8^{+}$ DCs ($MHCII^{+}CD11c^{+}CD8^{+}$), $CD11b^{+}$ DCs ($MHCII^{+}CD11c^{+}CD11b^{+}$), $F4/80^{+}$ macrophages ($CD11b^{int}F4/80^{hi}$), $F4/80^{-}$ macrophages ($CD11b^{hi}F4/80^{int}$) and neutrophils ($CD11b^{hi}F4/80^{-}$). (B to E) Histograms displaying the levels of CD1d in WT, $CD1d^{-/-}$ and in the different CD1d-

floxed lines in the populations gated in (A). Bar charts show CD1d deletion efficacy and specificity for the different CD1d-floxed transgenic lines. Each dot represents a single mouse. Data are representative of two independent experiments.

In $CD1d^{flox/flox}$CD11c-Cre^{+} mice, complete deletion of CD1d was observed in both $CD8^{+}$ and $CD11b^{+}$ DCs (Figure 5.11D), showing that CD11c-Cre is an effective tool to delete CD1d from DCs. In this case, CD1d deletion was also observed in around 10% of $MHCII^{+}CD11c^{-}$ cells, indicating that other $MHCII^{+}$ cells, probably splenic macrophages, also deleted CD1d in these mice (Figure 5.11D).

Finally, in $CD1d^{flox/flox}$Lyz2-Cre^{+} mice, CD1d deletion was almost complete in $CD11b^{int}F4/80^{hi}$ macrophages while around 60% deletion was observed in $CD11b^{hi}F4/80^{int}$ macrophages and neutrophils (Figure 5.11E). Almost no deletion was observed in $CD11b^{-}F4/80^{-}$ cells, highlighting the specificity of this Cre-line.

In brief, I was able to generate four different transgenic lines in which CD1d was targeted to different immune cell populations. The generation of these new transgenic tools is of great value for the iNKT cell field as they provide an elegant system to study the role of various immune cells on homeostasis of iNKT cells and their regulation during infection, inflammation or autoimmune diseases.

5.3.3 iNKT cell activation during infection requires CD1d expression on DCs

As I now had these transgenic lines available, I went on to analyse the requirement of CD1d-dependent endogenous ligand presentation for iNKT cell activation in vivo. To analyse this, wild type and the various CD1d-transgenic mice were intranasally infected with 200 PFU of influenza virus. After 3 days of infection, mediastinal LNs were harvested and iNKT cell activation was measured by up-regulation of CD69. Similar levels of CD69 were observed in wild type, $CD1d^{flox/flox}$CD19Cre^{+} and $CD1d^{flox/flox}$Lyz2Cre^{+} mice following infection (Figure 5.12). These results suggest that CD1d is not required on B cells and neutrophils to activate iNKT cells after influenza infection. In contrast, the levels of CD69 in iNKT cells were substantially decreased in $CD1d^{flox/flox}$CD11cCre^{+} mice (Figure 5.12). This result demonstrates that in vivo activation of iNKT cells by DCs requires the

presentation of endogenous lipids in the context of CD1d. In future work, the production of IL-4 and IFN-γ will be assessed in these lines after infection.

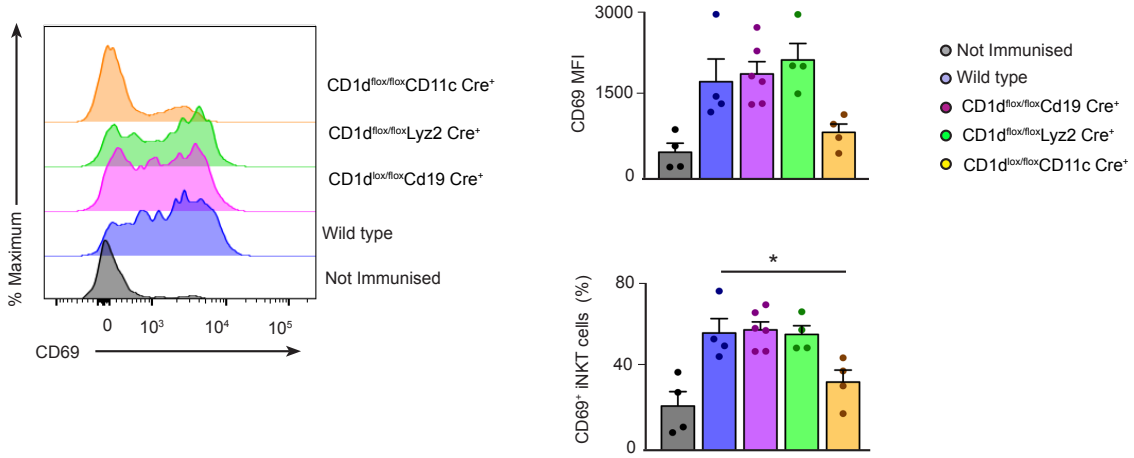

Figure 5.12 CD1d expression by DCs is required to complete iNKT cell activation

Flow cytometry analysis of LN cell suspensions from wild type, CD1d$^{flox/flox}$CD19-Cre^{+}, CD1d$^{flox/flox}$Lyz2-Cre^{+} and CD1d$^{flox/flox}$CD11c-Cre^{+} mice 3 days after infection with 200 PFU of influenza virus. The levels of CD69 in TCRβ^{+} tetramer^{+} cells are shown on the histograms. Analysis of CD69 MFI and the percentage of CD69^{+} iNKT cells are shown on the bar charts. Each dot represents a single mouse. Data are representative of two independent experiments. Student t test, *p<0.05.

5.4 CD103^{+} DCs are essential for iNKT cell activation

During influenza infection, lung-resident DCs up regulate co-stimulatory molecules and cell surface chemokine receptors. In particular, CCR7 up regulation is essential for the migration of lung DCs to mediastinal LNs. Two different subsets of lung-resident DCs have the ability to migrate to draining LNs after infection or inflammation: CD103^{+} DCs and CD11b^{+} DCs. While CD103^{+} DCs are important for the early cross-presentation and priming of CD8^{+} T cell response, CD11b^{+} DCs function as antigen presenting cells for CD4^{+} T cells (del Rio et al., 2007, Neyt and Lambrecht, 2013).

5.4.1 Impaired iNKT cell activation in Batf3$^{-/-}$ and Langerin-DTR mice

iNKT cell activation following influenza infection requires MyD88 and CD1d expression by DCs as shown in the previous paragraphs. For this reason I wanted to find out whether any of these two different subtypes of migratory DCs would preferentially activate iNKT cells following viral infection. CD103^{+} DCs depend on the expression of Batf3 for their development while CD11b^{+} DCs require CSF1 for their development and maintenance (Hildner et al., 2008, Hashimoto et al., 2011, Naik et al., 2015). Making use of this differential requirement for transcription or survival factors, I assessed the relative contribution of these two DC subsets to iNKT cell responses. Batf3$^{-/-}$ mice were used to target CD103^{+} DCs, as these mice lack CD103^{+} DCs in the lungs (Hildner et al., 2008). Moreover, the administration of *Diphteria* toxin to Langerin-DTR mice specifically depletes CD103^{+} DCs from the lungs, while the levels of CD11b^{+} DCs remain unaffected (Helft et al., 2012). Alternatively, MaFIA mice will be used in the future to target CD11b^{+} DCs, as they have an inducible Fas suicide system under the CSF1R promoter that induces apoptosis of CSF1R^{+} cells when AP20187 is administrated (Burnett et al., 2004).

To assess the importance of CD103^{+} DCs on iNKT cell activation, wild type, Batf3$^{-/-}$ and Langerin-DTR mice previously injected i.p. on day -2 and -1 with 200ng of *Diphteria* toxin, were intranasally infected with 200 PFU. After 3 days, mediastinal LNs were harvested and analysis of DC populations and iNKT cell activation was performed by flow cytometry. Migratory DCs were gated as CD11c^{int}MHCII^{hi} and this population was further separated into CD103^{+} and CD11b^{+} populations. Although CD11b^{+} DCs were observed in wild type, Batf3$^{-/-}$ and Langerin-DTR mice, the CD103^{+} population was completely lacking from Batf3$^{-/-}$ and Langerin-DTR mice, indicating that these two transgenic models are suitable for assessing the importance of CD103^{+} DCs *in vivo* (Figure 5.13A). Notably, while iNKT cells from wild type mice secrete high levels of IFN-γ and IL-4, this was dramatically decreased in Batf3$^{-/-}$ and Langerin-DTR mice (Figure 5.13B). This is a key result and demonstrates that CD103^{+} DCs are essential to induce iNKT cell activation in mediastinal LNs following influenza infection. The importance of CD11b^{+} DCs on iNKT cell activation will be addressed in the near future with the help of the MaFIA mice.

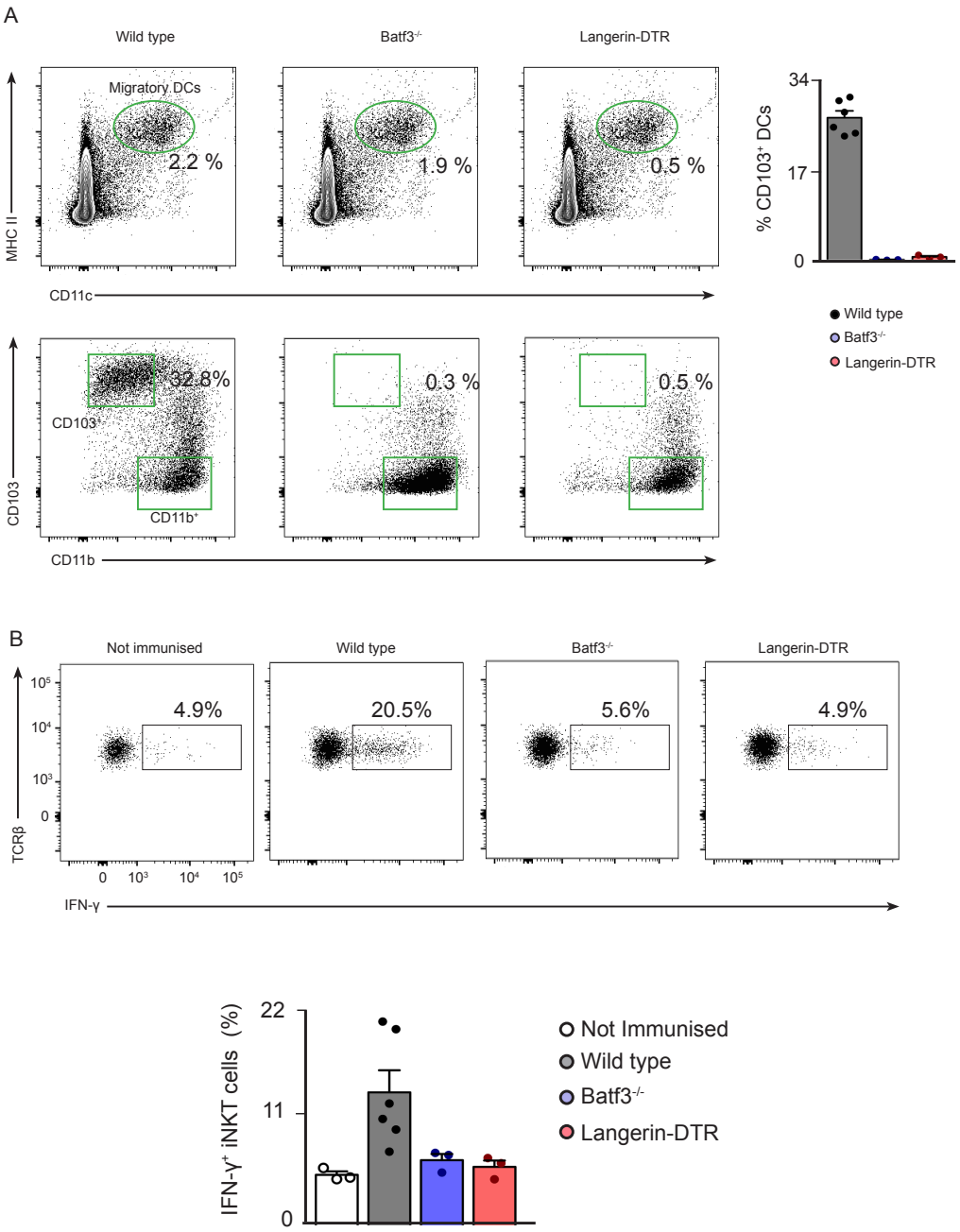

Figure 5.13 CD103^{+} DCs are essential for iNKT cell activation during viral infection

(A) Flow cytometry analysis of LN cell suspensions from wild type, Batf3$^{-/-}$ and Langerin-DTR mice 3 days after infection with 200 PFU of influenza virus. Migratory DCs were gated as MHCII^{hi}CD11c^{int} and further subdivided into CD103^{+} DCs and CD11b^{+} DCs. The percentage of CD103^{+} DCs in each strain is represented in the bar chart. (B) Flow cytometry analysis of IFN-γ secretion by iNKT cells from wild type, Batf3$^{-/-}$ and Langerin-DTR mice treated as in (A). The percentage of IFN-γ^{+} iNKT cells in each strain is shown in the bar chart. Each dot represents a single mouse. Data are representative of two independent experiments.

5.4.2 CD103$^+$ DCs express high levels of IL-12 following infection

I went on to compare different parameters related to iNKT cell activation on CD103$^+$ and CD11b$^+$ DCs to understand why CD103$^+$ DCs are essential for this process. Differential expression of CD1d by CD103$^+$ and CD11b$^+$ seems not to be the reason as flow cytometry analysis indicates that both subsets express similar levels of CD1d on the surface (Figure 5.14A–B). I went on to analyse the expression of the enzymes involved in the production of endogenous glycolipids (Hexb and A3Galt2) in both DC subsets. For this, CD103$^+$ and CD11b$^+$ DCs were sorted from mediastinal LNs 3 days after influenza infection and RNA was extracted from them. Real time RT-PCR showed that the levels of Hexb and A3Galt2 were similar in both subsets (Figure 5.14C). This result indicates that there is no differential transcriptional regulation of the enzymes involved in the production of endogenous glycolipids in CD103$^+$ and CD11b$^+$ DCs. On the other hand, CD103$^+$ DCs express much higher levels of IL-12 p40 compared to CD11b$^+$ DCs (Figure 5.14C). IL-12 has been shown to be necessary for the activation of iNKT cells in the absence of exogenous ligands. Therefore, CD103$^+$ DCs might be essential for the activation of iNKT cells due to their ability to secrete high levels of IL-12.

In the future it will be interesting to test the necessity of having MyD88 and CD1d expressed by CD103$^+$ DCs for the activation of iNKT cells following influenza infection. For this reason, I generated mixed BM chimeras, in which CD45.1 recipient mice were sub-lethally irradiated and received a) 80% Batf3$^{-/-}$ BM + 20% wild type BM, b) 80% Batf3$^{-/-}$ BM + 20% MyD88$^{-/-}$ or c) 80% Batf3$^{-/-}$ BM + 20% CD1d$^{-/-}$ BM. In this way, while most of the immune cells from these three different subsets of chimeras are reconstituted from the Batf3$^{-/-}$ BM, CD103$^+$ DCs are reconstituted from a) wild type BM, b) MyD88$^{-/-}$ BM or c) CD1d$^{-/-}$ BM. Eight weeks after BM transplant, what will be after the submission of this thesis, I will infect these chimeras with 200 PFU of influenza virus and assess iNKT cell activation in mediastinal LNs.

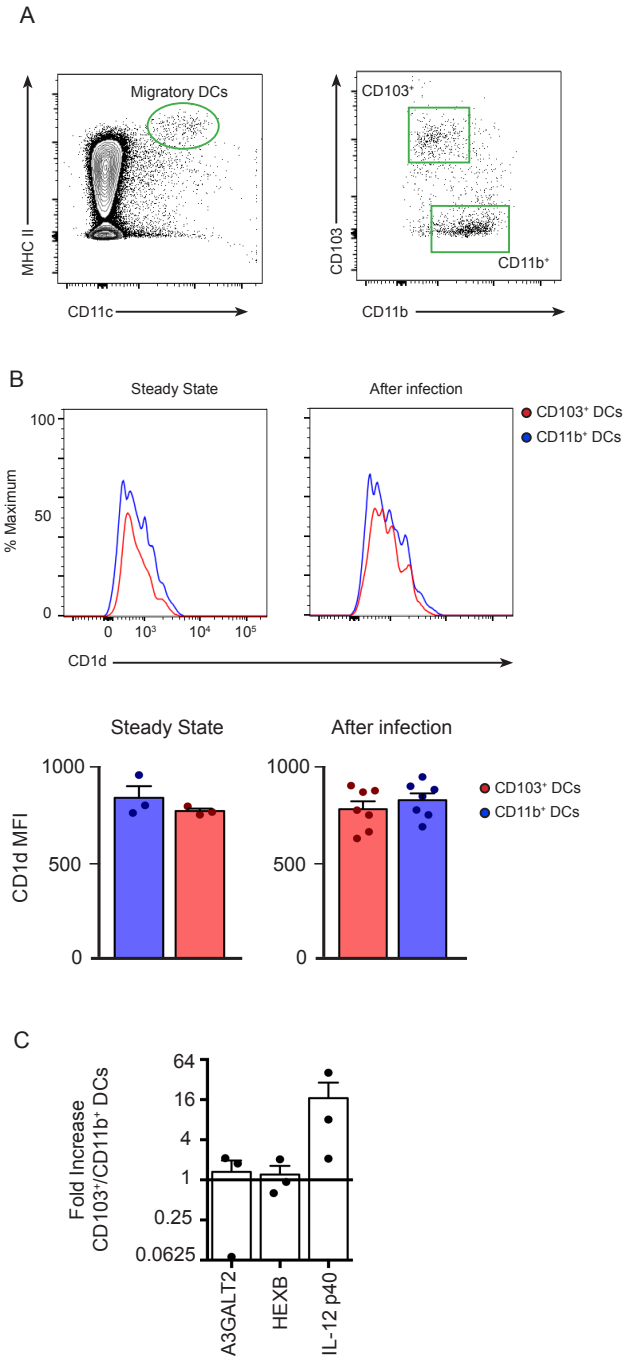

Figure 5.14 CD103$^+$ DCs express high levels of IL-12 p40

(A) Gating strategy for migratory DCs (MHCII^{hi}CD11c^{int}) and further subdivision into CD103$^+$ DCs and CD11b$^+$ DCs. (B) Flow cytometry analysis CD1d expression by CD103$^+$ DCs and CD11b$^+$ DCs before, and 3 days after, infection with 200 PFU of influenza virus. (C) RT-PCR analysis of sorted CD103$^+$ DCs and CD11b$^+$ DCs from mLNs of wild type mice that were infected with 200 PFU of influenza virus 3 days previously. Relative RNA levels of A3GALT2, HEXB and IL-12 p40 were normalised to the housekeeping gene CPH and were plotted in the bar charts as expression levels in CD103$^+$ DCs relative to the mean level observed CD11b$^+$ DCs.

Each dot represents a single mouse. Data are representative of two independent experiments.

In summary, in this first part of the chapter I showed that iNKT cells are important for the effective clearance of influenza virus. Moreover, I demonstrated that iNKT cell activation in vivo requires MyD88-mediated signalling in DCs. Despite being MyD88-dependent, this process is independent of TLR signalling, suggesting a potential role of inflammasome derived IL-1 and IL-18 on this process. By generating new CD1d conditional knock out mice, I was also able to show that *in vivo* iNKT cell activation by DCs requires CD1d-dependent presentation of endogenous lipids. This process might be performed by a particular subset of DCs, $CD103^+$ DCs.

5.5 iNKT cells regulate antiviral GC response

iNKT cells have been shown to regulate the B cell response to sphingolipid-bearing antigens. After immunisation with αGalCer-coated particles, B cells internalise and present these exogenous lipids in the context of CD1d to iNKT cells. iNKT cells then provide the help required for stimulating B cell proliferation and differentiation into extrafollicular plasma cells. These plasma cells mediate the production of high titers of specific IgM and early class-switched antibodies (Barral et al., 2008, Chang et al., 2012). As iNKT cells are essential to induce humoral response in the presence of exogenous glycolipids, I wondered whether they could also regulate the B cell response in the context of viral infections.

5.5.1 iNKT cells are important for GC formation during viral infection

To analyse the role of iNKT cells on the B cell response during viral infection, wild type and $CD1d^{-/-}$ mice were infected with 200 PFU of influenza virus. Nine days after infection, mediastinal LNs were harvested and the differentiation of B cells into GCs and $CD4^+$ T cells into TfH cells were measured by flow cytometry. GC cells were detected as $CD19^+GL\text{-}7^+CD95^+$ cells and T follicular helper cells were recognised as $CD4^+PD\text{-}1^+CXCR\text{-}5^+$ cells. A considerable expansion of these populations was observed in wild type mice following influenza infection compared

to naïve animals (Figure 5.15A). In contrast, the formation of GC cells and Tfh cells were significantly reduced in mediastinal LNs from CD1d$^{-/-}$ animals compared to their wild type counterparts (Figure 5.15A). GC reactions are important for the generation of high-affinity class-switched antibodies specific for invading pathogens (Victora and Nussenzweig, 2012). I therefore went on to measure the levels of influenza-specific IgG levels in the serum of mice 9 days after influenza infection. In line with the impaired formation of GC cells, the blood levels of influenza-specific IgG were significantly reduced in CD1d$^{-/-}$ mice compared to wild type animals (Figure 5.15B). These results demonstrate that iNKT cells are important in the development of the GC response during influenza infection.

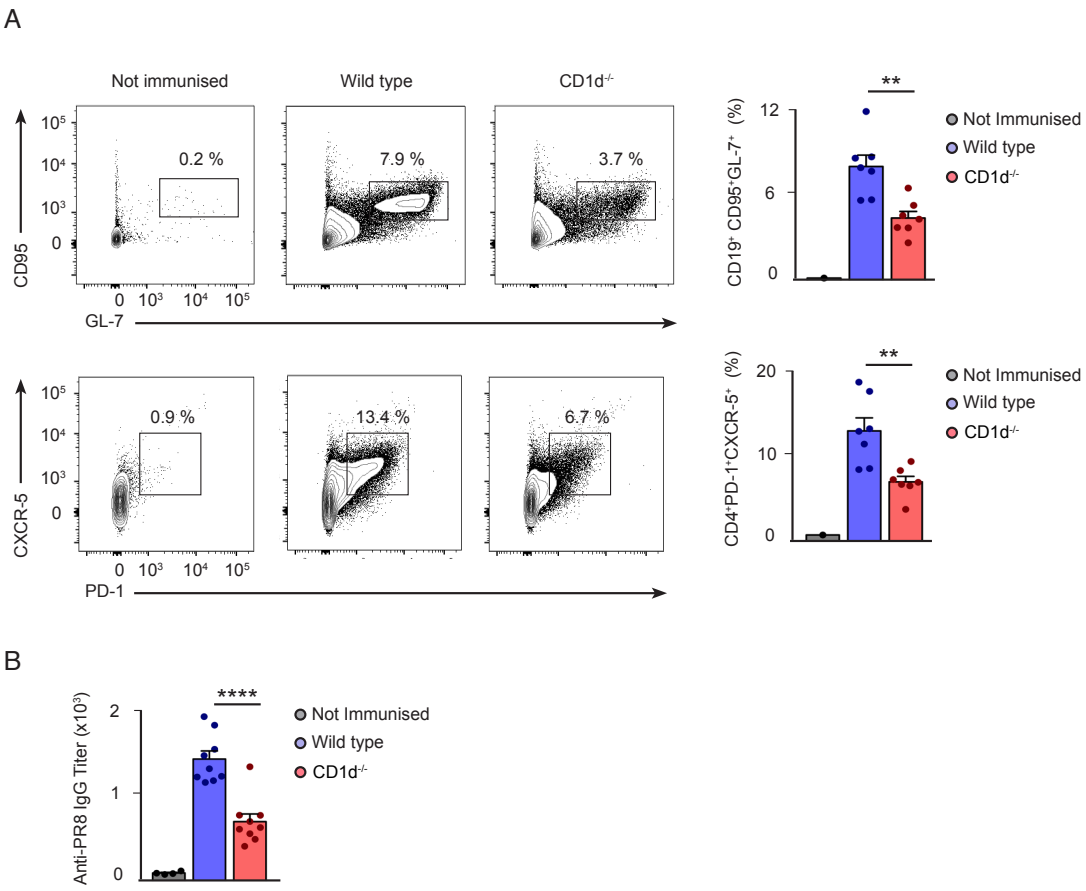

Figure 5.15 CD1d$^{-/-}$ mice have impaired GC formation to influenza infection

(**A**) Flow cytometry analysis of GC and Tfh cell formation in mediastinal LNs of wild type and CD1d$^{-/-}$ mice that were intranasally infected with 200 PFU of influenza virus 9 days before. Representative contour plots display the percentage of B220^{+} cells that are GL-7^{+}Fas^{+} and CD4^{+} T cells that are CXCR-5^{+}PD-1^{+}. Bar charts display the quantification of GC cells and TfH cells in the different mice for a single experiment. (**B**) Serum levels of PR8-specific IgG measured by ELISA in mice treated as in (A). Each dot represents a single mouse. Data are representative of

two independent experiments. Mean ± s.e.m. Student t test, **p<0.01 and ****p<0.0001.

I wondered whether the importance of iNKT cells in the induction of the GC response was specific for the influenza virus or was a general feature of viral infections. I therefore decided to analyse the GC response in wild type and $CD1d^{-/-}$ mice during infection with another type of virus. Vaccinia virus was chosen as an alternative infection model due to its importance in the development of vaccines against smallpox, as immune responses generated from a vaccinia virus infection protects a person against potentially lethal smallpox infections. The vaccinia virus is a member of the Poxviridae family and its genome is comprised of double stranded DNA, very distantly related to single strand RNA viruses such as influenza (Walsh and Dolin, 2011). To this end, wild type and $CD1d^{-/-}$ mice were intranasally infected with 200 PFU of vaccinia virus and after 9 days, mediastinal LNs were harvested. The formation of GCs and TfH cells was assessed by flow cytometry. Following vaccinia virus infection, an expansion of GC and TfH cells was observed in wild type mice compared to non-infected animals (Figure 5.16). However, the formation of GCs was dramatically reduced in CD1d-/- animals compared to wild type animals (Figure 5.16). In this case, TfH cell formation remained unaffected. These results indicate that iNKT cells are general regulators of the GC reaction during viral infections.

The previous results show that in the absence of iNKT cells, the development of the GC reaction during viral infections is compromised. I therefore wondered whether impaired activation of iNKT cells during infection would interfere with the correct development of the GC response. I previously showed that cognate interaction between DCs and iNKT cells is necessary for the complete activation of the later immune cells, as CD69 up regulation by iNKT cells is severely reduced in $CD1d^{flox/flox}$ CD11c-Cre^{+} following influenza infection. To test this, $CD1d^{flox/flox}$ CD11c-Cre^{-} and Cre^{+} mice were intranasally infected with 200 PFU of influenza virus and mediastinal LNs were harvested 9 days later. GC response was analysed as previously by flow cytometry. Although a considerable expansion of GC B cells was observed in $CD1d^{flox/flox}$ CD11c-Cre^{-} mice, the formation of GC cells was significantly decreased in $CD1d^{flox/flox}$ CD11c-Cre^{+} animals (Figure 5.17). This result

shows that impaired activation of iNKT cells during influenza infection interferes with the normal development of the GC response.

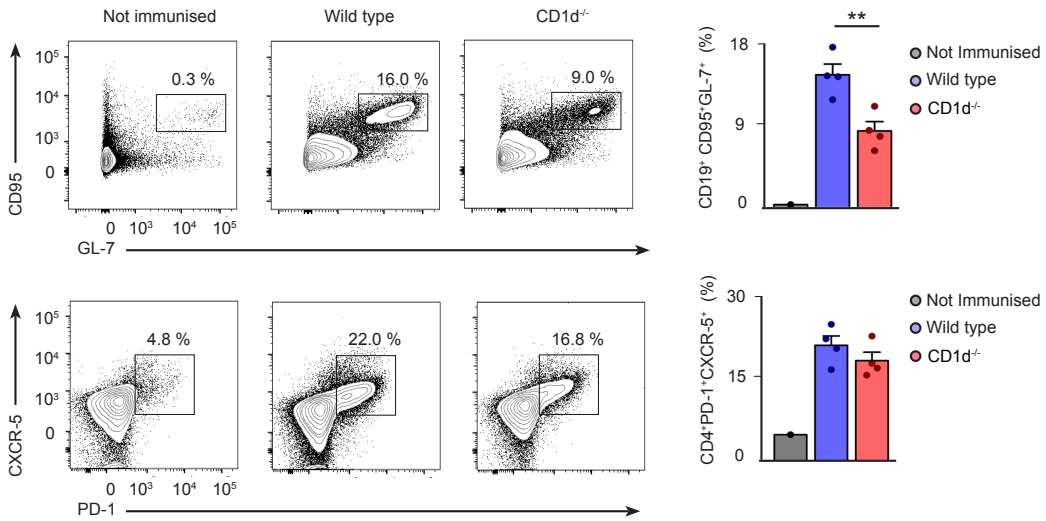

Figure 5.16 CD1d$^{-/-}$ mice have impaired GC formation to vaccinia virus infection

Flow cytometry analysis of GC and TfH cell formation in mediastinal LNs of wild type and CD1d$^{-/-}$ mice that were intranasally infected with 200 PFU of VACV 9 days before. Representative contour plots display the percentage of B220^{+} cells that are GL-7^{+}Fas^{+} and CD4^{+} T cells that are CXCR-5^{+}PD-1^{+}. Bar charts display the quantification of GC B cells and TfH cells for a single experiment. Each dot represents a single mouse. Data are representative of two independent experiments. Mean ± s.e.m. Student t test, **p<0.01.

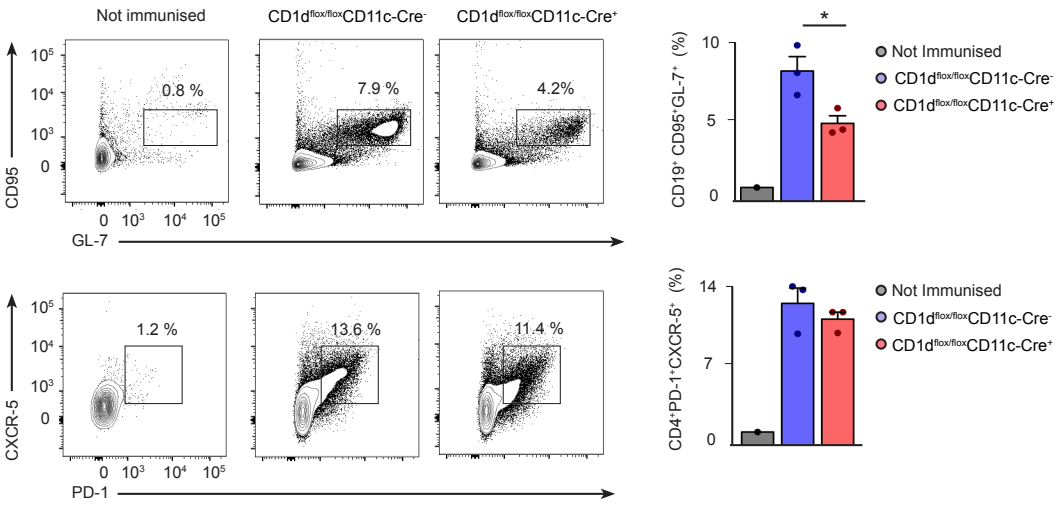

Figure 5.17 CD1d$^{flox/flox}$CD11c-Cre^{+} mice have impaired GC formation

Flow cytometry analysis of GC and TfH cell formation in mediastinal LNs of CD1d$^{flox/flox}$CD11c-Cre^{-} and Cre^{+} mice that were intranasally infected with 200 PFU of influenza virus 9 days before. Representative contour plots display the percentage of B220^{+} cells that are GL-7^{+}Fas^{+} and CD4^{+} T cells that are CXCR-

5^+PD-1^+. Bar charts display the quantification of GC B cells and TfH cells. Each dot represents a single mouse. Data are representative of two independent experiments. Mean ± s.e.m. Student t test, *p<0.05.

5.5.2 Cognate interaction between B cells and iNKTs is dispensable for the GC response during viral infection

The previous data demonstrated that iNKT cells are important players in the GC reaction. How, then, do these innate-like T cells regulate the GC response during a viral infection?

My first hypothesis was that during a viral infection, B cells would detect the presence of influenza virus through TLR-MyD88 and this would induce the presentation of endogenous glycolipids on CD1d. The presentation of endogenous ligands in the context of CD1d would recruit iNKT cells to provide the second signal necessary to complete B cell activation, proliferation and differentiation into GCs. To address whether cognate interaction between B cells and iNKT cells was necessary for GC formation, I prevented this potential interaction by specifically deleting CD1d on the B cell population. This was achieved by crossing $CD1d^{flox/flox}$ mice with mice expressing the Cre recombinase under the promoter of CD19 or Mb1. Wild type, $CD1d^{flox/flox}$ CD19-Cre^+ and $CD1d^{flox/flox}$ Mb1-Cre^+ mice were then intranasally infected with 200 PFU of influenza virus and mediastinal LNs were harvested after 9 days of infection. The formation of GC cells and TfH cells was similar in wild type, $CD1d^{flox/flox}$ CD19-Cre^+ and $CD1d^{flox/flox}$ Mb1-Cre^+ mice (Figure 5.18A-B). This result is key as it demonstrates that cognate interaction between B cells and iNKT cells is not necessary for the GC reaction during viral infection. Therefore, iNKT cells are important in the GC reaction in the presence of pathogen-derived glycolipids (Chang et al., 2012, King et al., 2012) and in the absence of exogenous glycolipids, as shown here. However, the mechanism behind iNKT cell regulation of GC formation is different in both cases. While cognate interaction between B cells and iNKT cells is required for the correct development of GCs in the presence of exogenous glycolipids (Chang et al., 2012, King et al., 2012), this interaction is dispensable during viral infections.

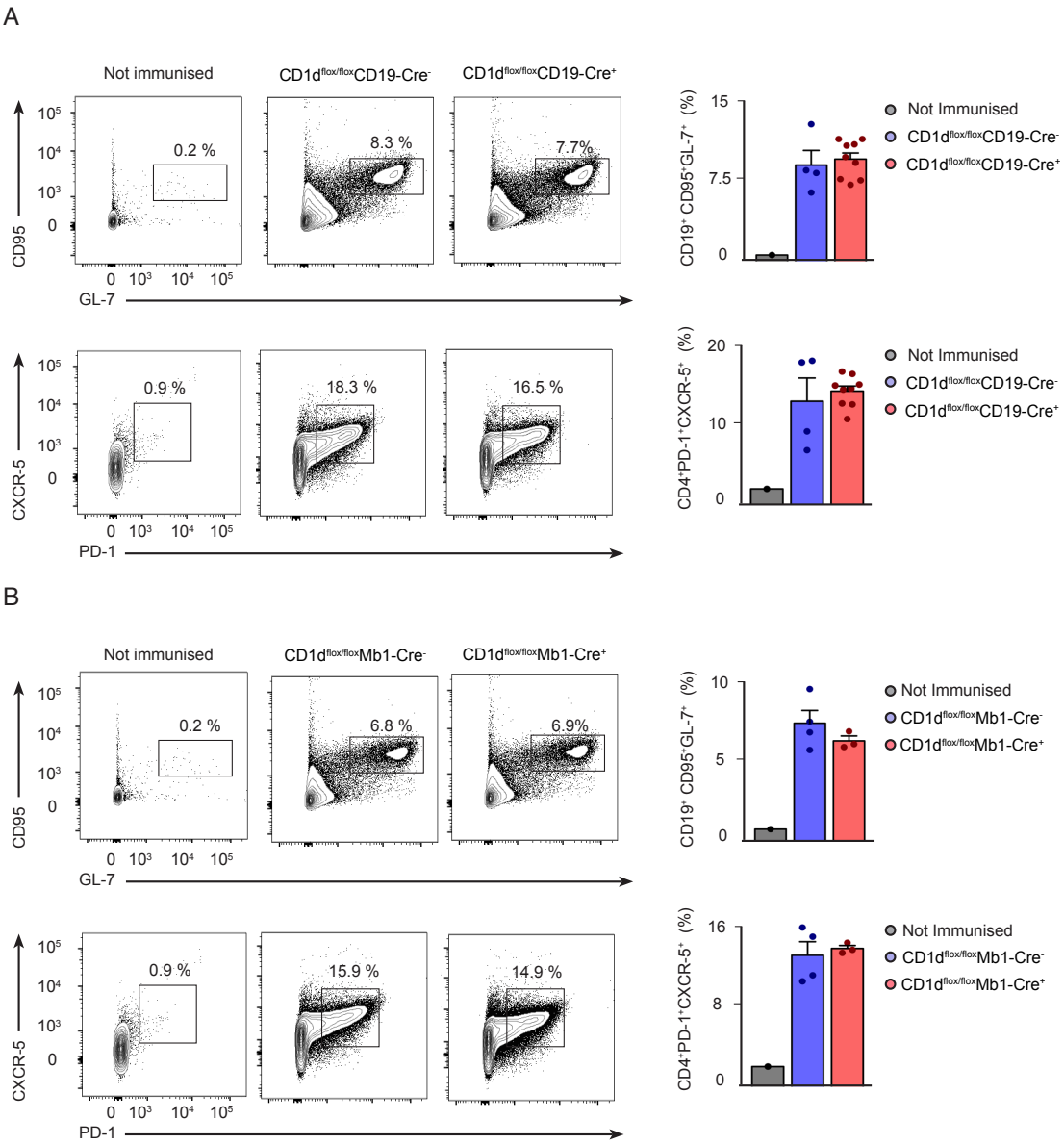

Figure 5.18 CD1d$^{flox/flox}$CD19-Cre^{+} and Mb1-Cre^{+} mice display normal GCs

Flow cytometry analysis of GC and TfHcell formation in mediastinal LNs from (**A**) CD1d$^{flox/flox}$CD19-Cre^{-} and Cre^{+} mice or (**B**) CD1d$^{flox/flox}$Mb1-Cre^{-} and Cre^{+} mice that were intranasally infected with 200 PFU of influenza virus 9 days before. Representative contour plots display the percentage of B220^{+} cells that are GL-7^{+}Fas^{+} and of CD4^{+} T cells that are CXCR-5^{+}PD-1^{+}. Bar charts display the quantification of GC B cells and TfH cells. Each dot represents a single mouse. Data are representative of two independent experiments. Mean ± s.e.m.

5.5.3 Interaction between neutrophils and iNKT cells is dispensable for GC response

During inflammation, neutrophils can mediate iNKT cell activation through CD1d presentation of endogenous ligands. Once activated, iNKT cells are able to induce a pro-inflammatory phenotype on these neutrophils (De Santo et al., 2010). Furthermore, activated neutrophils have been shown to potentiate B cell responses by producing BAFF (B cell activation factor), APRIL (a proliferation-inducing ligand) and IL-21 (Puga et al., 2011). To address whether iNKT-cell mediated activation of neutrophils could regulate GC response, I infected CD1d$^{flox/flox}$ Lyz2-Cre^{-} and Cre^{+} mice with 200 PFU of influenza virus and mediastinal LNs were harvested 9 days later. GC response was analysed by flow cytometry. Surprisingly, a similar expansion of GC B cells and TfH cells was observed in CD1d$^{flox/flox}$ Lyz2-Cre^{-} and Cre^{+} animals (Figure 5.19). This result indicates that cognate interaction between iNKT cells and neutrophils is dispensable for GC formation following influenza infection. iNKT cells therefore seem to promote B cell differentiation independently of neutrophils' regulatory activity.

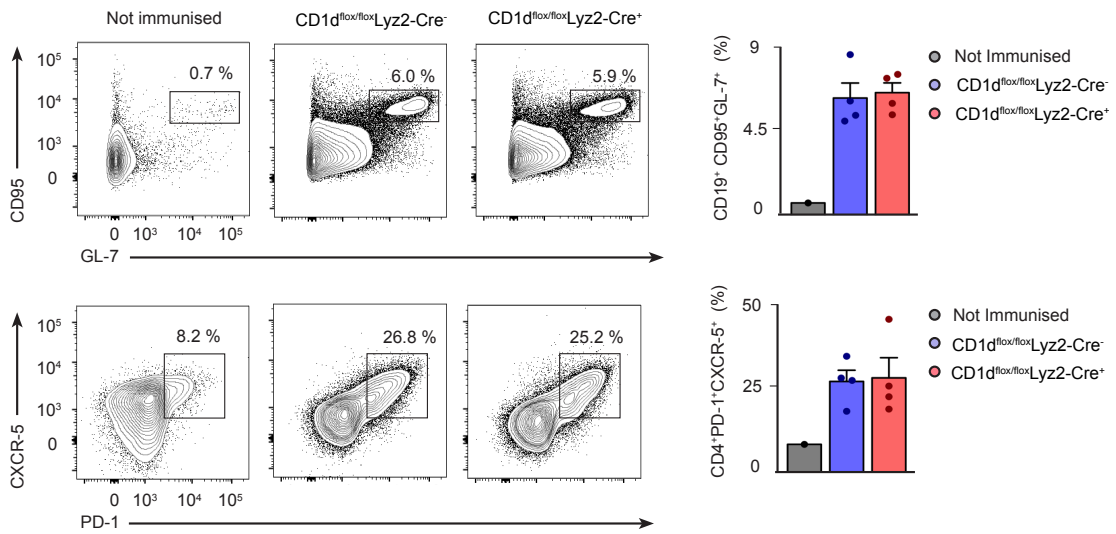

Figure 5.19 CD1d$^{flox/flox}$Lyz2-Cre^{+} mice display normal GCs to influenza infection

Flow cytometry analysis of GC and TfH cell formation in mediastinal LNs from CD1d$^{flox/flox}$Lyz2-Cre^{-} and Cre^{+} mice that were intranasally infected with 200 PFU of influenza virus 9 days before. Representative contour plots display the percentage of B220^{+} cells that are GL-7^{+}Fas^{+} and CD4^{+} T cells that are CXCR-5^{+}PD-1^{+}. Bar charts display the quantification of GC B cells and TfH cells. Each dot represents a

single mouse. Data are representative of two independent experiments. Mean ± s.e.m.

5.5.4 iNKT cells produce high levels of IL-21 during influenza infection

As iNKT cells regulate the GC response during viral infection independently of cognate interaction with B cells or neutrophils, I wondered whether they would help B cells to differentiate into GCs by producing specific cytokines. GC differentiation requires the presence of IL-21 to maintain high-level expression of Bcl-6. IL-21 is usually secreted by T follicular helper cells during an immune response (Zotos et al., 2010). However, when mice are immunised with synthetic glycosphingolipids, 10% of iNKT cells produce IL-21 by day 5 of immunisation (Chang et al., 2012, King et al., 2012). Moreover, when iNKT cells are stimulated in vitro with anti-CD3, anti-CD28 and IL-12, they begin production of IL-21 much faster than conventional CD4+ T cells (Coquet et al., 2007). Therefore I wondered whether iNKT cells produce IL-21 during viral infections and if this production provides the first IL-21 wave to induce GC formation. Wild type mice were intranasally infected with 200 PFU of influenza virus and after 9 days mediastinal LNs were harvested. Single cell suspensions were incubated for 4 hours with PMA/ionomycin at 37^{o}C. Cells were then collected and stained with anti-TCRβ and PBS-57 loaded CD1d tetramer, fixed, permeabilised and intracellularly stained with anti-IL-21 antibody. Flow cytometry analysis revealed that 9 days after influenza infection, around 20% of iNKT cells produce IL-21 (Figure 5.20A). To further confirm the production of IL-21 by iNKT cells, TCRβ^{+} tetramer^{+} cells were sorted from mediastinal LNs 9 days after intranasal administration of PBS (control) or 200 PFU of influenza virus. RNA was extracted from sorted cells and real-time RT-PCR was performed to quantify the levels of IL-21. CPH gene was used as a housekeeping gene for normalisation. RT-PCR analysis revealed that IL-21 production by iNKT cells increases around 16-fold following influenza infection (Figure 5.20B). All together, these results show that iNKT cells produce high levels of IL-21 after viral infection even in the absence of exogenous glycosphingolipids.

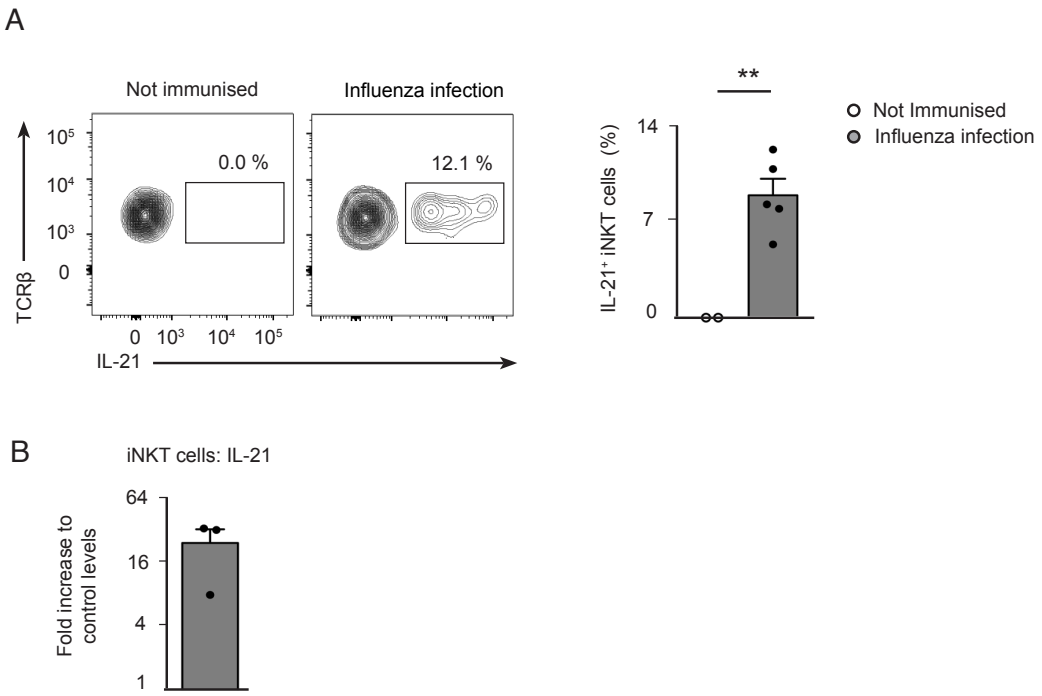

Figure 5.20 iNKT cells secrete IL-21 following influenza infection

(A) Flow cytometry analysis of LN cell suspensions from control mice and mice that were infected with 200 PFU of influenza virus 9 days before. IL-21 secretion by iNKT cells is depicted in the dot plots. The percentage of IL-21$^+$ iNKT cells before and after infection is shown in the bar chart. (B) RT-PCR analysis of sorted iNKT cells from mLNs of wild type mice that were left untreated or infected with 200 PFU of influenza virus 9 days previously. Relative RNA levels of IL-21 were normalised to CPH and were plotted in the bar charts as expression levels relative to the mean level of non-immunised mice. Each dot represents a single mouse. Data are representative of two independent experiments. Mean ± s.e.m. Student t test, *p<0.05.

To analyse whether IL-21 secretion by iNKT cells is necessary for the development of GCs following influenza infection, I went on to generate mixed BM chimeras, where iNKT cells are IL-21$^{-/-}$ while other immune cells are able to produce IL-21. For this, Rag2$^{-/-}$ mice were sub lethally irradiated and injected with: a) 80% Jα18$^{-/-}$ BM + 20% wild type BM or b) 80% Jα18$^{-/-}$ BM + 20% IL-21$^{-/-}$ BM. As Jα18$^{-/-}$ BMs are not able to generate iNKT cells, all the iNKT cells from these chimeras would come from a) wild type or b) IL-21$^{-/-}$ donors. Eight weeks of after reconstitution these mice will be intranasally infected with 200 PFU of influenza and 9 days later the formation of GCs will be assessed in mediastinal LNs. This experimental setup will allow me to dissect the importance of iNKT cell-derived IL-21 on GC formation following viral infection.

5.6 Discussion

iNKT cells influence the activity of many other cell types through the production of a broad range of cytokines, chemokines and surface molecules. Furthermore, the interactions between iNKT cells and their CD1d-expressing partners are at the core of the ability of iNKT cells to orchestrate immune responses (Brennan, Brigl and Brenner, 2013). In this chapter I have shown that iNKT cells are important for the clearance of influenza virus from the lungs. Early iNKT cell activation in mediastinal LNs is mediated by $CD103^+$ DCs, a subset of pulmonary DCs specialised in cross-presentation. This process requires MyD88-signalling in DCs and the subsequent presentation of CD1d-loaded endogenous lipids; however, it does not require TLR recognition of influenza. Importantly, the presence of iNKT cells and their correct activation are necessary to induce GC formation and virus-specific antibodies after infection. Even though this process does not require cognate interaction between B cells and iNKT cells through CD1d, iNKT cells might support the initial development of GCs through the production of IL-21 (Figure 5.21).

The functional plasticity of iNKT cells, combined with their ability to modulate the activation of other immune cell subsets, makes them important in controlling the course of an infection (Juno, Keynan and Fowke, 2012). Here, I showed that iNKT cells are needed for the clearance of influenza virus, as iNKT cell-deficient animals display significantly higher levels of viral NP1 RNA levels in the lungs compared to wild type mice. This inability to control viral replication correlates with high levels of inflammatory cytokines (IFN-γ and IL-6) in the blood and lungs. These observations are in line with previous work by Cerundolo and colleagues, who showed that infection with high doses of influenza virus results in higher viral titres and increased mortality of iNKT cell-deficient animals (De Santo et al., 2008).

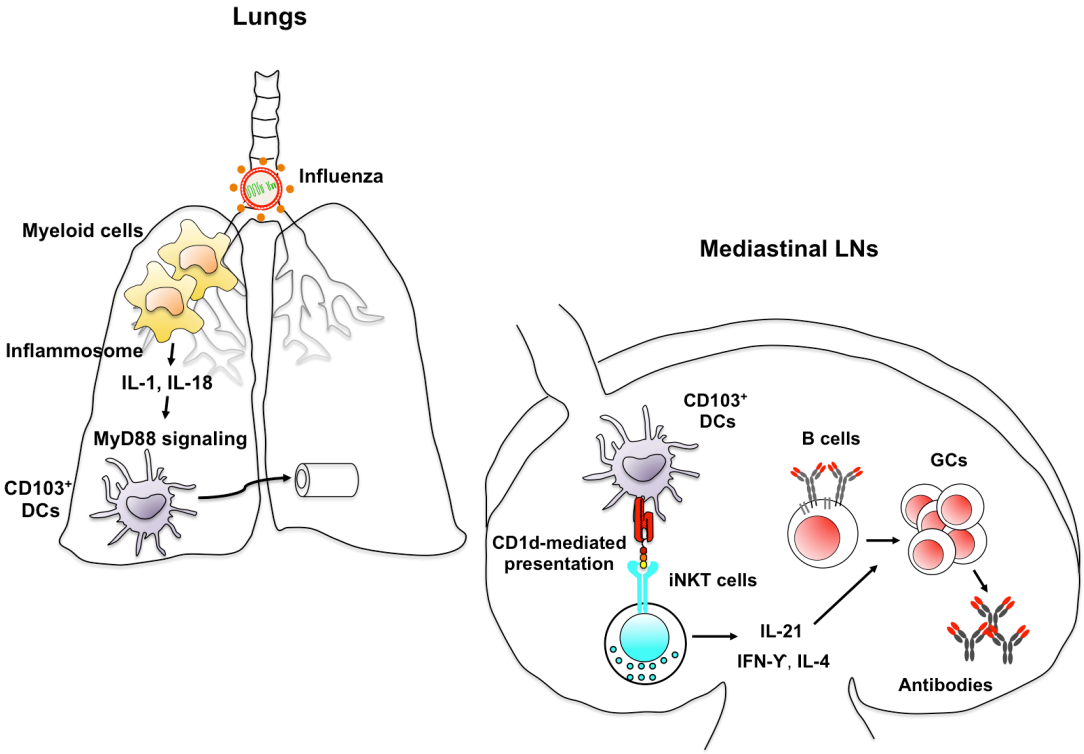

Figure 5.21 iNKT cells: linking innate and adaptive immunity to infection

Proposed model for the activation of iNKT cells in mediastinal LNs by pulmonary DCs and their importance in GC formation and antibody production to viral pathogens.

Due to the essential role of iNKT cells in not only the clearance of influenza but also of HSV (herpes simplex virus), MCMV (mouse cytomegalovirus) and RSV (respiratory syncytial virus) during infection (Juno, Keynan and Fowke, 2012), it is important to define the process of iNKT cell activation during viral challenges. The understanding of this process has been somewhat limited due to the restricted availability of tools to address these types of questions in vivo. I found that iNKT cell activation occurs very early during influenza infection and results in CD69 up-regulation and the secretion of IFN-γ and IL-4. Through the generation of different transgenic lines, I determined that CD1d-mediated presentation of endogenous lipids by DCs is essential for iNKT cell activation in draining LNs. In contrast, CD1d expression by B cells or neutrophils is not necessary for this process. Importantly, the induction of endogenous lipid presentation by DCs requires MyD88-mediated signalling. The general concept is that TLR signalling through MyD88 in antigen presenting cells is necessary to induce iNKT cell activation (Mattner et al., 2005).

However, I found that even though MyD88 expression by DCs is required for iNKT cell activation, TLR recognition of the influenza virus is not necessary. These observations raise the possibility that other receptors that signal through MyD88 might be involved in CD1d-mediated presentation of endogenous lipids in vivo.

As previously mentioned, MyD88 is a common adaptor for TLRs, IL-1R and IL-18R (Adachi et al., 1998). After influenza infection, lung immune and parenchyma cells release high levels of the inflammatory cytokines IL-1 and IL-18 through the activation of the inflammasome complex (Ichinohe et al., 2009, Thomas et al., 2009, Ichinohe, Pang and Iwasaki, 2010). It is conceivable, therefore, that IL-1 or IL-18 signalling on lung-resident DCs may induce CD1d-mediated presentation of endogenous lipids to iNKTs independently of TLR7 recognition of influenza. Interestingly, IL-1R signalling in DCs was shown to replace TLRs in promoting $CD8^+$ T cell responses to the influenza virus (Pang, Ichinohe and Iwasaki, 2013). It is therefore key to analyse iNKT cell activation in the absence of IL-1R and IL-18R signalling to understand their contribution to CD1d-mediated presentation of endogenous lipids by DCs. Furthermore, it would be interesting to analyse iNKT cell activation in the context of defective inflammasome activity in the lungs, which results in the abrogation of IL-1 and IL-18 production after influenza infection (Ichinohe et al., 2009, Thomas et al., 2009). To address these questions, I am in the process of acquiring IL-1R, IL-18R, Caspase-1 and ASC-deficient animals.

After infection with influenza, DCs mediate the cognate activation of iNKT cells in mediastinal LNs. Two main subsets of pulmonary DCs, known as $CD103^+$ and $CD11b^+$ DCs, migrate to mediastinal LNs after influenza infection (Braciale, Sun and Kim, 2012). $CD103^+$ DCs, which reach maximum numbers between two to four days after influenza infection, serve as the most potent antigen presenting cells for $CD8^+$ T cells (Helft et al., 2012). In contrast, $CD11b^+$ DCs reach peak numbers at later time points, between five to seven days after influenza infection, and may act to expand the pool size of previously activated effector $CD8^+$ T cells (Ballesteros-Tato et al., 2010). Both DC subsets also efficiently activate naive virus-specific $CD4^+$ T cells (Braciale, Sun and Kim, 2012). In this chapter, I showed that $CD103^+$ DCs are essential to induce early IFN-γ production by iNKT cells. Importantly, as the transgenic mouse lines used to target $CD103^+$

DCs, Batf3$^{-/-}$ and Langerin-DTR, also affect LN resident CD8^{+} DCs, it will be important for future studies to compare the contribution of migratory CD103^{+} DCs versus resident CD8^{+} DCs. In this case, the use of CCR7$^{-/-}$ mice would be useful to discern the importance of both populations as in the absence of CCR7, CD103^{+} DCs do not migrate to the LNs (Ohl et al., 2004). Furthermore, to analyse the role of CD11b^{+} DCs on iNKT cell activation I will use MaFIA mice, which express an inducible Fas suicide system under the CSF1R promoter that induces apoptosis of CSF1R+ cells (Burnett et al., 2004).

The reason why CD103^{+} DCs play an essential role in iNKT cell activation remains to be investigated; although, it might be due to their early migration to the LNs (Ballesteros-Tato et al., 2010). While this first wave of CD103^{+} DCs arrival is essential for the early activation of iNKT cells, the later arrival of CD11b^{+} DCs might serve to provide further signals and expand the previous pool of cells as occurs with CD8^{+} T cells (Ballesteros-Tato et al., 2010). Furthermore, it could be possible that CD103^{+} DCs are specialised in presenting endogenous lipids on CD1d by expressing high levels of the enzymes involved in their biosynthesis. I measured the RNA levels of different enzymes involved in this process; however, their levels did not differ between CD103^{+} and CD11b^{+} subsets. In the future, it will be interesting to measure the activity of these enzymes in these two subsets and not only their RNA or protein levels. Even though both subsets express the same levels of surface CD1d, CD103^{+} DCs produce higher levels of IL-12 compared to CD11b^{+} DCs. As IL-12 is key for iNKT cell activation in the absence of exogenous glycolipids (Brigl et al., 2003), this would explain why CD103^{+} DCs are so important for iNKT cell activation. Interestingly, CD103^{+} DCs do not express TLR7; the only TLR involved in the recognition of influenza in mice (Diebold et al., 2004). This might explain why iNKT cell activation is independent of TLR signalling after influenza infection. It is then possible that IL-1 and/or IL-18 signalling through MyD88 in CD103^{+} DCs induces the presentation of lipid antigens to iNKT cells in the context of CD1d.

The presence of iNKT cells and their correct activation by DCs in mediastinal LNs are important for B cell formation of GCs and the production of influenza-specific antibodies. Importantly, the ability of iNKT cells to regulate GC

responses is not specific to influenza virus but seems to be a general characteristic of viral infections, as GC formation in response to VACV infection is severally impaired in iNKT cell-deficient mice. Previous studies showed that after immunisation with α-GalCer, iNKT cells support GC development by providing cognate help to B cells through CD1d—TCR direct interaction and the production of IL-21 (Chang et al., 2012, King et al., 2012). However, the help provided by iNKT cells to B cells during influenza infection is non-cognate, as specific deletion of CD1d in B cells does not interfere with the GC development.

The mechanism by which iNKT cells regulate GC development in response to viral infection remains to be defined. I found that iNKT cells produce high levels of IL-21 after influenza infection. As the production of cytokines by iNKT cells is faster than the conventional $CD4^+$ T cells (Coquet et al., 2007), they might provide the first wave of IL-21 to induce B cell differentiation into GCs. Furthermore, it is possible that iNKT cells relocate to GCs after infection, where they might provide surviving signals such as BAFF or APRIL (Coquet et al., 2008) to support the GC response. In fact, a previous study showed the presence of iNKT cells in the GC after immunisation with glycosphingolipids (Chang et al., 2012).

It is also conceivable that iNKT cells regulate GC response in an indirect way. For example, iNKT cells inhibit the suppressor activity of MDSCs after influenza infection, supporting T cell proliferation (De Santo et al., 2008). It is then possible that the inhibition of MDSCs by iNKT cells may also support the high levels of B cell proliferation in the GCs. Furthermore, regulatory iNKT cells have been shown to induce an anti-inflammatory phenotype in adipose tissue-macrophages through the production of IL-10 (Lynch et al., 2015). This anti-inflammatory phenotype includes the production of arginase-1, which resembles the suppressor activity of MDSCs. It might be then possible that the IFN-γ production by iNKT during influenza infection would turn SCS macrophages towards an inflammatory phenotype instead of an anti-inflammatory one. As SCS macrophages are in close contact with B cells, their production of inflammatory signals may support B cell proliferation and differentiation into GCs. In the future, it would be interesting to analyse the regulation of MDSCs and SCS macrophages by iNKT cells and the importance of these axis in the regulation of the B cell response.

Concluding remarks

B cells are key players of the immune system due to their exceptional ability to produce pathogen-specific antibodies. These antibodies mediate the clearance of infectious agents through neutralisation or induction of different effector functions. The activation of B cells and their differentiation into antibody-producing cells are highly regulated processes. Therefore, many factors can shape the outcome of the B cell response during infection.

In the present thesis I found that an intact layer of macrophages at the LN SCS is required to initiate B cell responses after localised infection. Importantly, the integrity of this layer in draining LNs is compromised after primary infection or inflammation, resulting in the impairment of B cells to respond to subsequent incoming pathogens. This temporary shutdown of the B cell response increases the organism's susceptibility to secondary infections. Furthermore, I found that B cell recognition of pathogens through the BCR or TLRs induces the formation of autophagosomes. Interestingly, the induction of this process in B cells is unique, as it is strictly dependent on the PLCγ2 pathway and does not require ULK proteins, as other cell types do. These organelles might play an important role in antigen presentation, as antigen localises in close contact to autophagosomes after internalisation. Finally, I found that iNKT cell activation is required for GC formation and antibody production after respiratory viral infection. Early iNKT cell activation in the LNs is mediated by pulmonary $CD103^+$ DCs, which present CD1d-loaded endogenous lipids to iNKT cells after induction of MyD88-signalling.

I believe that the data presented here contribute to the understanding of how B cells operate *in vivo* during pathogenic challenges.

Reference list

ABTIN, A., JAIN, R., MITCHELL, A.J., ROEDIGER, B., BRZOSKA, A.J., TIKOO, S., CHENG, Q., NG, L.G., CAVANAGH, L.L., ANDRIAN, VON, U.H., HICKEY, M.J., FIRTH, N., and WENINGER, W., 2014. Perivascular macrophages mediate neutrophil recruitment during bacterial skin infection. *Nature immunology*. 15 (1), pp. 45–53.

ACTON, S.E., FARRUGIA, A.J., ASTARITA, J.L., MOURÃO-SÁ, D., JENKINS, R.P., NYE, E., HOOPER, S., VAN BLIJSWIJK, J., ROGERS, N.C., SNELGROVE, K.J., ROSEWELL, I., MOITA, L.F., STAMP, G., TURLEY, S.J., SAHAI, E., and REIS E SOUSA, C., 2014. Dendritic cells control fibroblastic reticular network tension and lymph node expansion. *Nature*. 514 (7523), pp. 498–502.

ADACHI, O., KAWAI, T., TAKEDA, K., MATSUMOTO, M., TSUTSUI, H., SAKAGAMI, M., NAKANISHI, K., and AKIRA, S., 1998. Targeted disruption of the MyD88 gene results in loss of IL-1- and IL-18-mediated function. *Immunity*. 9 (1), pp. 143–150.

ADEREM, A. and UNDERHILL, D.M., 1999. Mechanisms of phagocytosis in macrophages. *Annual review of immunology*.

AGRAWAL, A. and SCHATZ, D.G., 1997. RAG1 and RAG2 form a stable postcleavage synaptic complex with DNA containing signal ends in V(D)J recombination. *Cell*. 89 (1), pp. 43–53.

ALANDER, J.T., KAARTINEN, I., LAAKSO, A., PÄTILÄ, T., SPILLMANN, T., TUCHIN, V.V., VENERMO, M., and VÄLISUO, P., 2012. A review of indocyanine green fluorescent imaging in surgery. *International journal of biomedical imaging*. 2012, p. 940585.

AMIGORENA, S., DRAKE, J.R., WEBSTER, P., and MELLMAN, I., 1994. Transient accumulation of new class II MHC molecules in a novel endocytic compartment in B lymphocytes. *Nature*. 369 (6476), pp. 113–120.

ARAKAWA, H., TAKEDA, S., and TAKEMORI, T., 1996. Early expression of Ig μ chain from a transgene significantly reduces the duration of the pro-B stage but does not affect the small pre-B stage. *International immunology*. 8 (8), pp. 1319–1328.

ASANO, K., NABEYAMA, A., MIYAKE, Y., QIU, C.-H., KURITA, A., TOMURA, M., KANAGAWA, O., FUJII, S.-I., and TANAKA, M., 2011. CD169-positive macrophages dominate antitumor immunity by crosspresenting dead cell-associated antigens. *Immunity*. 34 (1), pp. 85–95.

ASTARITA, J.L., CREMASCO, V., FU, J., DARNELL, M.C., PECK, J.R., NIEVES-BONILLA, J.M., SONG, K., KONDO, Y., WOODRUFF, M.C., GOGINENI, A., ONDER, L., LUDEWIG, B., WEIMER, R.M., CARROLL, M.C., MOONEY, D.J., XIA, L., and TURLEY, S.J., 2015. The CLEC-2-podoplanin axis controls the contractility of fibroblastic reticular cells and lymph node microarchitecture. *Nature immunology*. 16 (1), pp. 75–84.

BALLESTEROS-TATO, A., LEÓN, B., LUND, F.E., and RANDALL, T.D., 2010. Temporal changes in dendritic cell subsets, cross-priming and costimulation via CD70 control CD8(+) T cell responses to influenza. *Nature immunology*. 11 (3), pp. 216–224.

BARNDEN, M.J., ALLISON, J., HEATH, W.R., and CARBONE, F.R., 1998. Defective TCR expression in transgenic mice constructed using cDNA-based

alpha- and beta-chain genes under the control of heterologous regulatory elements. *Immunology and cell biology*. 76 (1), pp. 34–40.
BARRAL, P., ECKL-DORNA, J., HARWOOD, N.E., DE SANTO, C., SALIO, M., ILLARIONOV, P., BESRA, G.S., CERUNDOLO, V., and BATISTA, F.D., 2008. B cell receptor-mediated uptake of CD1d-restricted antigen augments antibody responses by recruiting invariant NKT cell help in vivo. *Proceedings of the National Academy of Sciences of the United States of America*. 105 (24), pp. 8345–8350.
BARRAL, P., POLZELLA, P., BRUCKBAUER, A., VAN ROOIJEN, N., BESRA, G.S., CERUNDOLO, V., and BATISTA, F.D., 2010. CD169(+) macrophages present lipid antigens to mediate early activation of iNKT cells in lymph nodes. *Nature immunology*. 11 (4), pp. 303–312.
BARRAL, P., SÁNCHEZ-NIÑO, M.D., VAN ROOIJEN, N., CERUNDOLO, V., and BATISTA, F.D., 2012. The location of splenic NKT cells favours their rapid activation by blood-borne antigen. *The EMBO journal*. 31 (10), pp. 2378–2390.
BATISTA, F.D. and HARWOOD, N.E., 2009. The who, how and where of antigen presentation to B cells. *Nature reviews Immunology*. 9 (1), pp. 15–27.
BENDELAC, A., LANTZ, O., QUIMBY, M.E., YEWDELL, J.W., BENNINK, J.R., and BRUTKIEWICZ, R.R., 1995. CD1 recognition by mouse NK1+ T lymphocytes. *Science (New York, NY)*. 268 (5212), pp. 863–865.
BENDELAC, A., SAVAGE, P.B., and TEYTON, L., 2007. The biology of NKT cells. *Annual review of immunology*. 25, pp. 297–336.
BENEDICT, C.A., DE TREZ, C., SCHNEIDER, K., HA, S., PATTERSON, G., and WARE, C.F., 2006. Specific remodeling of splenic architecture by cytomegalovirus. *PLoS pathogens*. 2 (3), p. e16.
BENLAGHA, K., WEISS, A., BEAVIS, A., TEYTON, L., and BENDELAC, A., 2000. In vivo identification of glycolipid antigen-specific T cells using fluorescent CD1d tetramers. *The Journal of experimental medicine*. 191 (11), pp. 1895–1903.
BERGTOLD, A., DESAI, D.D., GAVHANE, A., and CLYNES, R., 2005. Cell surface recycling of internalized antigen permits dendritic cell priming of B cells. *Immunity*. 23 (5), pp. 503–514.
BLOMQVIST, M., RHOST, S., TENEBERG, S., LÖFBOM, L., OSTERBYE, T., BRIGL, M., MÅNSSON, J.-E., and CARDELL, S.L., 2009. Multiple tissue-specific isoforms of sulfatide activate CD1d-restricted type II NKT cells. *European journal of immunology*. 39 (7), pp. 1726–1735.
BRACIALE, T.J., SUN, J., and KIM, T.S., 2012. Regulating the adaptive immune response to respiratory virus infection. *Nature reviews Immunology*. 12 (4), pp. 295–305.
BRACK, C., HIRAMA, M., LENHARD-SCHULLER, R., and TONEGAWA, S., 1978. A complete immunoglobulin gene is created by somatic recombination. *Cell*. 15 (1), pp. 1–14.
BRAUN, A., WORBS, T., MOSCHOVAKIS, G.L., HALLE, S., HOFFMANN, K., BÖLTER, J., MÜNK, A., and FÖRSTER, R., 2011. Afferent lymph-derived T cells and DCs use different chemokine receptor CCR7-dependent routes for entry into the lymph node and intranodal migration. *Nature immunology*. 12 (9), pp. 879–887.
BRENNAN, P.J., BRIGL, M., and BRENNER, M.B., 2013. Invariant natural killer T cells: an innate activation scheme linked to diverse effector functions. *Nature reviews Immunology*. 13 (2), pp. 101–117.

BRENNAN, P.J., TATITURI, R.V.V., BRIGL, M., KIM, E.Y., TULI, A., SANDERSON, J.P., GADOLA, S.D., HSU, F.-F., BESRA, G.S., and BRENNER, M.B., 2011. Invariant natural killer T cells recognize lipid self antigen induced by microbial danger signals. *Nature immunology*. 12 (12), pp. 1202–1211.
BRIGL, M., BRY, L., KENT, S.C., GUMPERZ, J.E., and BRENNER, M.B., 2003. Mechanism of CD1d-restricted natural killer T cell activation during microbial infection. *Nature immunology*. 4 (12), pp. 1230–1237.
BROWNE, E.P., 2012. Regulation of B-cell responses by Toll-like receptors. *Immunology*. 136 (4), pp. 370–379.
BRUNDAGE, J.F. and SHANKS, G.D., 2008. Deaths from bacterial pneumonia during 1918-19 influenza pandemic. *Emerging infectious diseases*. 14 (8), pp. 1193–1199.
BRYCESON, Y.T., MARCH, M.E., BARBER, D.F., LJUNGGREN, H.-G., and LONG, E.O., 2005. Cytolytic granule polarization and degranulation controlled by different receptors in resting NK cells. *The Journal of experimental medicine*. 202 (7), pp. 1001–1012.
BURBAGE, M., KEPPLER, S.J., GASPARRINI, F., MARTINEZ-MARTIN, N., GAYA, M., FEEST, C., DOMART, M.-C., BRAKEBUSCH, C., COLLINSON, L., BRUCKBAUER, A., and BATISTA, F.D., 2015. Cdc42 is a key regulator of B cell differentiation and is required for antiviral humoral immunity. *Journal of Experimental Medicine*. 212 (1), pp. 53–72.
BURNETT, S.H., KERSHEN, E.J., ZHANG, J., ZENG, L., STRALEY, S.C., KAPLAN, A.M., and COHEN, D.A., 2004. Conditional macrophage ablation in transgenic mice expressing a Fas-based suicide gene. *Journal of leukocyte biology*. 75 (4), pp. 612–623.
CALADO, D.P., SASAKI, Y., GODINHO, S.A., PELLERIN, A., KÖCHERT, K., SLECKMAN, B.P., DE ALBORÁN, I.M., JANZ, M., RODIG, S., and RAJEWSKY, K., 2012. The cell-cycle regulator c-Myc is essential for the formation and maintenance of germinal centers. *Nature immunology*. 13 (11), pp. 1092–1100.
CARRASCO, Y.R. and BATISTA, F.D., 2007. B cells acquire particulate antigen in a macrophage-rich area at the boundary between the follicle and the subcapsular sinus of the lymph node. *Immunity*. 27 (1), pp. 160–171.
CASTELLO, A., GAYA, M., TUCHOLSKI, J., OELLERICH, T., LU, K.-H., TAFURI, A., PAWSON, T., WIENANDS, J., ENGELKE, M., and BATISTA, F.D., 2013. Nck-mediated recruitment of BCAP to the BCR regulates the PI(3)K-Akt pathway in B cells. *Nature immunology*. 14 (9), pp. 966–975.
CATON, M.L., SMITH-RASKA, M.R., and REIZIS, B., 2007. Notch-RBP-J signaling controls the homeostasis of CD8- dendritic cells in the spleen. *The Journal of experimental medicine*. 204 (7), pp. 1653–1664.
CERUTTI, A., COLS, M., and PUGA, I., 2013. Marginal zone B cells: virtues of innate-like antibody-producing lymphocytes. *Nature reviews Immunology*.
CHANG, P.-P., BARRAL, P., FITCH, J., PRATAMA, A., MA, C.S., KALLIES, A., HOGAN, J.J., CERUNDOLO, V., TANGYE, S.G., BITTMAN, R., NUTT, S.L., BRINK, R., GODFREY, D.I., BATISTA, F.D., and VINUESA, C.G., 2012. Identification of Bcl-6-dependent follicular helper NKT cells that provide cognate help for B cell responses. *Nature immunology*. 13 (1), pp. 35–43.
CHARLES A JANEWAY, J., TRAVERS, P., WALPORT, M., and SHLOMCHIK, M.J., 2001. Principles of innate and adaptive immunity.

CHATURVEDI, A., DORWARD, D., and PIERCE, S.K., 2008. The B cell receptor governs the subcellular location of Toll-like receptor 9 leading to hyperresponses to DNA-containing antigens. *Immunity*. 28 (6), pp. 799–809.
CHEN, G., SHAW, M.H., KIM, Y.-G., and NUÑEZ, G., 2009. NOD-Like Receptors: Role in Innate Immunity and Inflammatory Disease. *Annual Review of Pathology: Mechanisms of Disease*. 4 (1), pp. 365–398.
CHEN, M., HONG, M.J., SUN, H., WANG, L., SHI, X., GILBERT, B.E., CORRY, D.B., KHERADMAND, F., and WANG, J., 2014. Essential role for autophagy in the maintenance of immunological memory against influenza infection. *Nature medicine*. 20 (5), pp. 503–510.
CHEONG, H., LINDSTEN, T., WU, J., LU, C., and THOMPSON, C.B., 2011. Ammonia-induced autophagy is independent of ULK1/ULK2 kinases. *Proceedings of the National Academy of Sciences of the United States of America*. 108 (27), pp. 11121–11126.
CHOWELL, G., BERTOZZI, S.M., COLCHERO, M.A., LOPEZ-GATELL, H., ALPUCHE-ARANDA, C., HERNANDEZ, M., and MILLER, M.A., 2009. Severe respiratory disease concurrent with the circulation of H1N1 influenza. *The New England journal of medicine*. 361 (7), pp. 674–679.
CHRISTIANSEN, D., MILLAND, J., MOUHTOURIS, E., VAUGHAN, H., PELLICCI, D.G., MCCONVILLE, M.J., GODFREY, D.I., and SANDRIN, M.S., 2008. Humans lack iGb3 due to the absence of functional iGb3-synthase: implications for NKT cell development and transplantation. *PLoS biology*. 6 (7), p. e172.
CHTANOVA, T., HAN, S.-J., SCHAEFFER, M., VAN DOOREN, G.G., HERZMARK, P., STRIEPEN, B., and ROBEY, E.A., 2009. Dynamics of T cell, antigen-presenting cell, and pathogen interactions during recall responses in the lymph node. *Immunity*. 31 (2), pp. 342–355.
CHTANOVA, T., SCHAEFFER, M., HAN, S.-J., VAN DOOREN, G.G., NOLLMANN, M., HERZMARK, P., CHAN, S.W., SATIJA, H., CAMFIELD, K., AARON, H., STRIEPEN, B., and ROBEY, E.A., 2008. Dynamics of neutrophil migration in lymph nodes during infection. *Immunity*. 29 (3), pp. 487–496.
CINAMON, G., ZACHARIAH, M.A., LAM, O.M., FOSS, F.W., and CYSTER, J.G., 2008. Follicular shuttling of marginal zone B cells facilitates antigen transport. *Nature immunology*. 9 (1), pp. 54–62.
CLARK, M.R., MASSENBURG, D., and ZHANG, M., 2003. Molecular mechanisms of B cell antigen receptor trafficking. *Annals of the New …*.
CLARK, S.L., 1962. The reticulum of lymph nodes in mice studied with the electron microscope. *The American journal of anatomy*. 110, pp. 217–257.
CLAUSEN, B.E., BURKHARDT, C., REITH, W., RENKAWITZ, R., and FÖRSTER, I., 1999. Conditional gene targeting in macrophages and granulocytes using LysMcre mice. *Transgenic research*. 8 (4), pp. 265–277.
COFFMAN, R.L., 1983. Surface Antigen Expression and Immunoglobulin Gene Rearrangement During Mouse pre-B Cell Development. *Immunological reviews*. 69 (1), pp. 5–23.
COLINO, J., SHEN, Y., and SNAPPER, C.M., 2002. Dendritic cells pulsed with intact Streptococcus pneumoniae elicit both protein- and polysaccharide-specific immunoglobulin isotype responses in vivo through distinct mechanisms. *The Journal of experimental medicine*. 195 (1), pp. 1–13.
COOMBES, J.L., HAN, S.-J., VAN ROOIJEN, N., RAULET, D.H., and ROBEY, E.A., 2012. Infection-induced regulation of natural killer cells by macrophages and collagen at the lymph node subcapsular sinus. *Cell reports*. 2 (1), pp. 124–

135.
COQUET, J.M., CHAKRAVARTI, S., KYPARISSOUDIS, K., MCNAB, F.W., PITT, L.A., MCKENZIE, B.S., BERZINS, S.P., SMYTH, M.J., and GODFREY, D.I., 2008. Diverse cytokine production by NKT cell subsets and identification of an IL-17-producing CD4-NK1.1- NKT cell population. *Proceedings of the National Academy of Sciences*. 105 (32), pp. 11287–11292.
COQUET, J.M., KYPARISSOUDIS, K., PELLICCI, D.G., BESRA, G., BERZINS, S.P., SMYTH, M.J., and GODFREY, D.I., 2007. IL-21 is produced by NKT cells and modulates NKT cell activation and cytokine production. *Journal of immunology (Baltimore, Md : 1950)*. 178 (5), pp. 2827–2834.
CYSTER, J.G. and GOODNOW, C.C., 1995. Pertussis toxin inhibits migration of B and T lymphocytes into splenic white pulp cords.
CYSTER, J.G., ANSEL, K.M., NGO, V.N., HYMAN, P.L., LUTHER, S.A., FÖRSTER, R., SEDGWICK, J.D., BROWNING, J.L., and LIPP, M., 2000. A chemokine-driven positive feedback loop organizes lymphoid follicles
. *Nature*. 406 (6793), pp. 309–314.
DARMOISE, A., TENEBERG, S., BOUZONVILLE, L., BRADY, R.O., BECK, M., KAUFMANN, S.H.E., and WINAU, F., 2010. Lysosomal alpha-galactosidase controls the generation of self lipid antigens for natural killer T cells. *Immunity*. 33 (2), pp. 216–228.
DAS, R., SANT'ANGELO, D.B., and NICHOLS, K.E., 2010. Transcriptional control of invariant NKT cell development. *Immunological reviews*. 238 (1), pp. 195–215.
DAVID, M.Z. and DAUM, R.S., 2010. Community-associated methicillin-resistant Staphylococcus aureus: epidemiology and clinical consequences of an emerging epidemic. *Clinical microbiology reviews*. 23 (3), pp. 616–687.
DE SANTO, C., ARSCOTT, R., BOOTH, S., KARYDIS, I., JONES, M., ASHER, R., SALIO, M., MIDDLETON, M., and CERUNDOLO, V., 2010. Invariant NKT cells modulate the suppressive activity of IL-10-secreting neutrophils differentiated with serum amyloid A. *Nature immunology*. 11 (11), pp. 1039–1046.
DE SANTO, C., SALIO, M., MASRI, S.H., LEE, L.Y.-H., DONG, T., SPEAK, A.O., PORUBSKY, S., BOOTH, S., VEERAPEN, N., BESRA, G.S., GRÖNE, H.-J., PLATT, F.M., ZAMBON, M., and CERUNDOLO, V., 2008. Invariant NKT cells reduce the immunosuppressive activity of influenza A virus-induced myeloid-derived suppressor cells in mice and humans. *The Journal of clinical investigation*. 118 (12), pp. 4036–4048.
DEEKS, S.G., TRACY, R., and DOUEK, D.C., 2013. Systemic effects of inflammation on health during chronic HIV infection. *Immunity*. 39 (4), pp. 633–645.
DEL RIO, M.L., RODRIGUEZ-BARBOSA, J.I., KREMMER, E., and FÖRSTER, R., 2007. CD103- and CD103+ Bronchial Lymph Node Dendritic Cells Are Specialized in Presenting and Cross-Presenting Innocuous Antigen to CD4+ and CD8+ T Cells. *The Journal of Immunology*. 178 (11), pp. 6861–6866.
DELEMARRE, F.G., KORS, N., KRAAL, G., and VAN ROOIJEN, N., 1990. Repopulation of macrophages in popliteal lymph nodes of mice after liposome-mediated depletion. *Journal of leukocyte biology*. 47 (3), pp. 251–257.
DELVES, P.J. and ROITT, I.M., 2000. The immune system. First of two parts. *The New England journal of medicine*. 343 (1), pp. 37–49.
DIAS, J.C.P., 2006. The Treatment of Chagas Disease (South American Trypanosomiasis). *Annals of Internal Medicine*. 144 (10), p. 772.

DIEBOLD, S.S., KAISHO, T., HEMMI, H., AKIRA, S., and REIS E SOUSA, C., 2004. Innate antiviral responses by means of TLR7-mediated recognition of single-stranded RNA. *Science (New York, NY)*. 303 (5663), pp. 1529–1531.
DINARELLO, C.A., 1998. Interleukin-1beta, Interleukin-18, and the Interleukin-1beta Converting Enzymea. *Annals of the New York Academy of Sciences*. 856 (1 MOLECULAR MEC), pp. 1–11.
DUDZIAK, D., KAMPHORST, A.O., HEIDKAMP, G.F., BUCHHOLZ, V.R., TRUMPFHELLER, C., YAMAZAKI, S., CHEONG, C., LIU, K., LEE, H.-W., PARK, C.G., STEINMAN, R.M., and NUSSENZWEIG, M.C., 2007. Differential antigen processing by dendritic cell subsets in vivo. *Science (New York, NY)*. 315 (5808), pp. 107–111.
ECKL-DORNA, J. and BATISTA, F.D., 2009. BCR-mediated uptake of antigen linked to TLR9 ligand stimulates B-cell proliferation and antigen-specific plasma cell formation. *Blood*. 113 (17), pp. 3969–3977.
FACCIOTTI, F., RAMANJANEYULU, G.S., LEPORE, M., SANSANO, S., CAVALLARI, M., KISTOWSKA, M., FORSS-PETTER, S., NI, G., COLONE, A., SINGHAL, A., BERGER, J., XIA, C., MORI, L., and DE LIBERO, G., 2012. Peroxisome-derived lipids are self antigens that stimulate invariant natural killer T cells in the thymus. *Nature immunology*. 13 (5), pp. 474–480.
FARR, A.G., CHO, Y., and DE BRUYN, P.P., 1980. The structure of the sinus wall of the lymph node relative to its endocytic properties and transmural cell passage. *The American journal of anatomy*. 157 (3), pp. 265–284.
FOSSUM, S., 1980. The architecture of rat lymph nodes. IV. Distribution of ferritin and colloidal carbon in the draining lymph nodes after foot-pad injection. *Scandinavian journal of immunology*. 12 (5), pp. 433–441.
FÖRSTER, R., DAVALOS-MISSLITZ, A.C., and ROT, A., 2008. CCR7 and its ligands: balancing immunity and tolerance. *Nature reviews Immunology*. 8 (5), pp. 362–371.
FÖRSTER, R., SCHUBEL, A., BREITFELD, D., KREMMER, E., RENNER-MÜLLER, I., WOLF, E., and LIPP, M., 1999. CCR7 coordinates the primary immune response by establishing functional microenvironments in secondary lymphoid organs. *Cell*. 99 (1), pp. 23–33.
FRIEDEL, R.H., WURST, W., WEFERS, B., and KÜHN, R., 2010. Generating Conditional Knockout Mice. In: *… Mouse Methods and Protocols*. Totowa, NJ: Humana Press. pp. 205–231.
FUJII, S.-I., LIU, K., SMITH, C., BONITO, A.J., and STEINMAN, R.M., 2004. The Linkage of Innate to Adaptive Immunity via Maturing Dendritic Cells In Vivo Requires CD40 Ligation in Addition to Antigen Presentation and CD80/86 Costimulation.
FUJII, S.-I., SHIMIZU, K., SMITH, C., BONIFAZ, L., and STEINMAN, R.M., 2003. Activation of natural killer T cells by alpha-galactosylceramide rapidly induces the full maturation of dendritic cells in vivo and thereby acts as an adjuvant for combined CD4 and CD8 T cell immunity to a coadministered protein. *The Journal of experimental medicine*. 198 (2), pp. 267–279.
GARCIA, Z., LEMAÎTRE, F., VAN ROOIJEN, N., ALBERT, M.L., LEVY, Y., SCHWARTZ, O., and BOUSSO, P., 2012. Subcapsular sinus macrophages promote NK cell accumulation and activation in response to lymph-borne viral particles. *Blood*. 120 (24), pp. 4744–4750.
GARSIDE, P., INGULLI, E., MERICA, R.R., JOHNSON, J.G., NOELLE, R.J., and JENKINS, M.K., 1998. Visualization of specific B and T lymphocyte interactions

in the lymph node. *Science (New York, NY)*. 281 (5373), pp. 96–99.
GAYA, M., CASTELLO, A., MONTANER, B., ROGERS, N., REIS E SOUSA, C., BRUCKBAUER, A., and BATISTA, F.D., 2015. Host response. Inflammation-induced disruption of SCS macrophages impairs B cell responses to secondary infection. *Science (New York, NY)*. 347 (6222), pp. 667–672.
GEISSMANN, F., CAMERON, T.O., SIDOBRE, S., MANLONGAT, N., KRONENBERG, M., BRISKIN, M.J., DUSTIN, M.L., and LITTMAN, D.R., 2005. Intravascular Immune Surveillance by CXCR6 + NKT Cells Patrolling Liver Sinusoids. *PLoS biology*. 3 (4), p. e113.
GERNER, M.Y., KASTENMÜLLER, W., IFRIM, I., KABAT, J., and GERMAIN, R.N., 2012. Histo-cytometry: a method for highly multiplex quantitative tissue imaging analysis applied to dendritic cell subset microanatomy in lymph nodes. *Immunity*. 37 (2), pp. 364–376.
GITLIN, A.D., MAYER, C.T., OLIVEIRA, T.Y., SHULMAN, Z., JONES, M.J.K., KOREN, A., and NUSSENZWEIG, M.C., 2015. HUMORAL IMMUNITY. T cell help controls the speed of the cell cycle in germinal center B cells. *Science (New York, NY)*. 349 (6248), pp. 643–646.
GITLIN, A.D., SHULMAN, Z., and NUSSENZWEIG, M.C., 2014. Clonal selection in the germinal centre by regulated proliferation and hypermutation. *Nature*. 509 (7502), pp. 637–640.
GONZALEZ, S.F., LUKACS-KORNEK, V., KULIGOWSKI, M.P., PITCHER, L.A., DEGN, S.E., KIM, Y.-A., CLONINGER, M.J., MARTINEZ-POMARES, L., GORDON, S., TURLEY, S.J., and CARROLL, M.C., 2010. Capture of influenza by medullary dendritic cells via SIGN-R1 is essential for humoral immunity in draining lymph nodes. *Nature immunology*. 11 (5), pp. 427–434.
GOODNOW, C.C., 1992. Transgenic mice and analysis of B-cell tolerance. *Annual review of immunology*.
GOODNOW, C.C., CROSBIE, J., ADELSTEIN, S., LAVOIE, T.B., SMITH-GILL, S.J., BRINK, R.A., PRITCHARD-BRISCOE, H., WOTHERSPOON, J.S., LOBLAY, R.H., and RAPHAEL, K., 1988. Altered immunoglobulin expression and functional silencing of self-reactive B lymphocytes in transgenic mice. *Nature*. 334 (6184), pp. 676–682.
GRAY, E.E., FRIEND, S., SUZUKI, K., PHAN, T.G., and CYSTER, J.G., 2012. Subcapsular sinus macrophage fragmentation and CD169+ bleb acquisition by closely associated IL-17-committed innate-like lymphocytes. *PLoS ONE*. 7 (6), pp. e38258–e38258.
GRETZ, J.E., ANDERSON, A.O., and SHAW, S., 1997. Cords, channels, corridors and conduits: critical architectural elements facilitating cell interactions in the lymph node cortex. *Immunological reviews*. 156, pp. 11–24.
GRIEWANK, K., BOROWSKI, C., RIETDIJK, S., WANG, N., JULIEN, A., WEI, D.G., MAMCHAK, A.A., TERHORST, C., and BENDELAC, A., 2007. Homotypic interactions mediated by Slamf1 and Slamf6 receptors control NKT cell lineage development. *Immunity*. 27 (5), pp. 751–762.
HABS, H., 1982. *[Immunological concepts in Thucydides' works].* Zentralblatt für Bakteriologie, Mikrobiologie und Hygiene. 1. Abt. Originale A, Medizinische Mikrobiologie, Infektionskrankheiten und Parasitologie = International journal of microbiology and hygiene. A, Medical microbiology, infectiousdiseases, parasitology.
HAMMAD, H. and LAMBRECHT, B.N., 2008. Dendritic cells and epithelial cells: linking innate and adaptive immunity in asthma. *Nature reviews Immunology*. 8

(3), pp. 193–204.
HARWOOD, N.E. and BATISTA, F.D., 2009. Early Events in B Cell Activation. *dx.doi.org*.
HASHIMOTO, D., CHOW, A., GRETER, M., SAENGER, Y., KWAN, W.-H., LEBOEUF, M., GINHOUX, F., OCHANDO, J.C., KUNISAKI, Y., VAN ROOIJEN, N., LIU, C., TESHIMA, T., HEEGER, P.S., STANLEY, E.R., FRENETTE, P.S., and MERAD, M., 2011. Pretransplant CSF-1 therapy expands recipient macrophages and ameliorates GVHD after allogeneic hematopoietic cell transplantation. *Journal of Experimental Medicine*. 208 (5), pp. 1069–1082.
HE, Y., 1985. Scanning Electron Microscope Studies of the Rat Mesenteric Lymph Node with Special Reference to High-Endothelial Venules and Hitherto Unknown Lymphatic Labyrinth. *Archives of Histology and Cytology*. 48 (1), pp. 1–15.
HEESTERS, B.A., MYERS, R.C., and CARROLL, M.C., 2014. Follicular dendritic cells: dynamic antigen libraries. *Nature reviews Immunology*. 14 (7), pp. 495–504.
HEIKENWALDER, M., POLYMENIDOU, M., JUNT, T., SIGURDSON, C., WAGNER, H., AKIRA, S., ZINKERNAGEL, R., and AGUZZI, A., 2004. Lymphoid follicle destruction and immunosuppression after repeated CpG oligodeoxynucleotide administration. *Nature medicine*. 10 (2), pp. 187–192.
HELFT, J., MANICASSAMY, B., GUERMONPREZ, P., HASHIMOTO, D., SILVIN, A., AGUDO, J., BROWN, B.D., SCHMOLKE, M., MILLER, J.C., LEBOEUF, M., MURPHY, K.M., GARCÍA-SASTRE, A., and MERAD, M., 2012. Cross-presenting CD103+ dendritic cells are protected from influenza virus infection. *The Journal of clinical investigation*. 122 (11), pp. 4037–4047.
HEMMI, H., KAISHO, T., TAKEDA, K., and AKIRA, S., 2003. The roles of Toll-like receptor 9, MyD88, and DNA-dependent protein kinase catalytic subunit in the effects of two distinct CpG DNAs on dendritic cell subsets. *Journal of immunology (Baltimore, Md : 1950)*. 170 (6), pp. 3059–3064.
HEMMI, H., TAKEUCHI, O., KAWAI, T., KAISHO, T., SATO, S., SANJO, H., MATSUMOTO, M., HOSHINO, K., WAGNER, H., TAKEDA, K., and AKIRA, S., 2000. A Toll-like receptor recognizes bacterial DNA. *Nature*. 408 (6813), pp. 740–745.
HERMANS, I.F., SILK, J.D., GILEADI, U., SALIO, M., MATHEW, B., RITTER, G., SCHMIDT, R., HARRIS, A.L., OLD, L., and CERUNDOLO, V., 2003. NKT cells enhance CD4+ and CD8+ T cell responses to soluble antigen in vivo through direct interaction with dendritic cells. *Journal of immunology (Baltimore, Md : 1950)*. 171 (10), pp. 5140–5147.
HICKMAN, H.D., 2015. Immunology. There goes the macrophage neighborhood. *Science (New York, NY)*. 347 (6222), pp. 609–610.
HILDNER, K., EDELSON, B.T., PURTHA, W.E., DIAMOND, M., MATSUSHITA, H., KOHYAMA, M., CALDERON, B., SCHRAML, B.U., UNANUE, E.R., DIAMOND, M.S., SCHREIBER, R.D., MURPHY, T.L., and MURPHY, K.M., 2008. Batf3 deficiency reveals a critical role for CD8alpha+ dendritic cells in cytotoxic T cell immunity. *Science (New York, NY)*. 322 (5904), pp. 1097–1100.
HOBEIKA, E., THIEMANN, S., STORCH, B., JUMAA, H., NIELSEN, P.J., PELANDA, R., and RETH, M., 2006. Testing gene function early in the B cell lineage in mb1-cre mice. *Proceedings of the National Academy of Sciences of the United States of America*. 103 (37), pp. 13789–13794.

HORCHER, M., SOUABNI, A., and BUSSLINGER, M., 2001. Pax5/BSAP maintains the identity of B cells in late B lymphopoiesis. *Immunity*. 14 (6), pp. 779–790.
HOU, B., REIZIS, B., and DEFRANCO, A.L., 2008. Toll-like receptors activate innate and adaptive immunity by using dendritic cell-intrinsic and -extrinsic mechanisms. *Immunity*. 29 (2), pp. 272–282.
HOU, H., ZHANG, Y., HUANG, Y., YI, Q., LV, L., ZHANG, T., CHEN, D., HAO, Q., and SHI, Q., 2012. Inhibitors of phosphatidylinositol 3'-kinases promote mitotic cell death in HeLa cells. *PLoS ONE*. 7 (4), p. e35665.
HØYER-HANSEN, M., BASTHOLM, L., SZYNIAROWSKI, P., CAMPANELLA, M., SZABADKAI, G., FARKAS, T., BIANCHI, K., FEHRENBACHER, N., ELLING, F., RIZZUTO, R., MATHIASEN, I.S., and JÄÄTTELÄ, M., 2007. Control of macroautophagy by calcium, calmodulin-dependent kinase kinase-beta, and Bcl-2. *Molecular cell*. 25 (2), pp. 193–205.
IANNACONE, M., MOSEMAN, E.A., TONTI, E., BOSURGI, L., JUNT, T., HENRICKSON, S.E., WHELAN, S.P., GUIDOTTI, L.G., and ANDRIAN, VON, U.H., 2010. Subcapsular sinus macrophages prevent CNS invasion on peripheral infection with a neurotropic virus. *Nature*. 465 (7301), pp. 1079–1083.
ICHINOHE, T., LEE, H.K., OGURA, Y., FLAVELL, R., and IWASAKI, A., 2009. Inflammasome recognition of influenza virus is essential for adaptive immune responses.
ICHINOHE, T., PANG, I.K., and IWASAKI, A., 2010. Influenza virus activates inflammasomes via its intracellular M2 ion channel. *Nature immunology*. 11 (5), pp. 404–410.
IMPAGLIAZZO, A., MILDER, F., KUIPERS, H., WAGNER, M., ZHU, X., HOFFMAN, R.M.B., VAN MEERSBERGEN, R., HUIZINGH, J., WANNINGEN, P., VERSPUIJ, J., DE MAN, M., DING, Z., APETRI, A., KUKRER, B., SNEEKES-VRIESE, E., TOMKIEWICZ, D., LAURSEN, N.S., LEE, P.S., ZAKRZEWSKA, A., DEKKING, L., TOLBOOM, J., TETTERO, L., VAN MEERTEN, S., YU, W., KOUDSTAAL, W., GOUDSMIT, J., WARD, A.B., MEIJBERG, W., WILSON, I.A., and RADO EVI, K., 2015. A stable trimeric influenza hemagglutinin stem as a broadly protective immunogen. *Science (New York, NY)*.
INABA, K., 1992. Generation of large numbers of dendritic cells from mouse bone marrow cultures supplemented with granulocyte/macrophage colony-stimulating factor. *Journal of Experimental Medicine*. 176 (6), pp. 1693–1702.
IRELAND, J.M. and UNANUE, E.R., 2011. Autophagy in antigen-presenting cells results in presentation of citrullinated peptides to CD4 T cells. *The Journal of experimental medicine*. 208 (13), pp. 2625–2632.
IROH TAM, P.-Y., DELAIR, S.F., and OBARO, S.K., 2015. Neonatal group B streptococcus disease in developing countries: are we ready to deploy a vaccine? *Expert review of vaccines*. pp. 1–3.
ITANO, A.A., MCSORLEY, S.J., REINHARDT, R.L., EHST, B.D., INGULLI, E., RUDENSKY, A.Y., and JENKINS, M.K., 2003. Distinct dendritic cell populations sequentially present antigen to CD4 T cells and stimulate different aspects of cell-mediated immunity. *Immunity*. 19 (1), pp. 47–57.
ITO, S., KOSHIKAWA, N., MOCHIZUKI, S., and TAKENAGA, K., 2007. 3-Methyladenine suppresses cell migration and invasion of HT1080 fibrosarcoma cells through inhibiting phosphoinositide 3-kinases independently of autophagy

inhibition. *International journal of oncology*. 31 (2), pp. 261–268.
IWASAKI, A. and MEDZHITOV, R., 2010. Regulation of adaptive immunity by the innate immune system. *Science (New York, NY)*.
JACOB, J., KELSOE, G., RAJEWSKY, K., and WEISS, U., 1991. Intraclonal generation of antibody mutants in germinal centres. *Nature*. 354 (6352), pp. 389–392.
JAKOB, T. and UDEY, M.C., 1998. Regulation of E-Cadherin-Mediated Adhesion in Langerhans Cell-Like Dendritic Cells by Inflammatory Mediators That Mobilize Langerhans Cells In Vivo. *The Journal of Immunology*.
JAMIESON, A.M., PASMAN, L., YU, S., GAMRADT, P., HOMER, R.J., DECKER, T., and MEDZHITOV, R., 2013. Role of tissue protection in lethal respiratory viral-bacterial coinfection. *Science (New York, NY)*. 340 (6137), pp. 1230–1234.
JAMIESON, A.M., YU, S., ANNICELLI, C.H., and MEDZHITOV, R., 2010. Influenza virus-induced glucocorticoids compromise innate host defense against a secondary bacterial infection. *Cell host & microbe*. 7 (2), pp. 103–114.
JANEWAY, C.A., TRAVERS, P., WALPORT, M., and SHLOMCHIK, M.J., 2001. Antigen recognition by B-cell and T-cell receptors.
JENKINS, S.J., RUCKERL, D., COOK, P.C., JONES, L.H., FINKELMAN, F.D., VAN ROOIJEN, N., MACDONALD, A.S., and ALLEN, J.E., 2011. Local macrophage proliferation, rather than recruitment from the blood, is a signature of TH2 inflammation. *Science (New York, NY)*. 332 (6035), pp. 1284–1288.
JIA, W. and HE, Y.-W., 2011. Temporal regulation of intracellular organelle homeostasis in T lymphocytes by autophagy. *Journal of immunology (Baltimore, Md : 1950)*. 186 (9), pp. 5313–5322.
JUNO, J.A., KEYNAN, Y., and FOWKE, K.R., 2012. Invariant NKT cells: regulation and function during viral infection. *PLoS pathogens*. 8 (8), p. e1002838.
JUNT, T., MOSEMAN, E.A., IANNACONE, M., MASSBERG, S., LANG, P.A., BOES, M., FINK, K., HENRICKSON, S.E., SHAYAKHMETOV, D.M., DI PAOLO, N.C., VAN ROOIJEN, N., MEMPEL, T.R., WHELAN, S.P., and ANDRIAN, VON, U.H., 2007. Subcapsular sinus macrophages in lymph nodes clear lymph-borne viruses and present them to antiviral B cells. *Nature*. 450 (7166), pp. 110–114.
JUNT, T., SCANDELLA, E., and LUDEWIG, B., 2008. Form follows function: lymphoid tissue microarchitecture in antimicrobial immune defence. *Nature reviews Immunology*. 8 (10), pp. 764–775.
KAIN, L., COSTANZO, A., WEBB, B., HOLT, M., BENDELAC, A., SAVAGE, P.B., and TEYTON, L., 2015. Endogenous ligands of natural killer T cells are alpha-linked glycosylceramides. *Molecular immunology*.
KAIN, L., WEBB, B., ANDERSON, B.L., DENG, S., HOLT, M., COSTANZO, A., CONSTANZO, A., ZHAO, M., SELF, K., TEYTON, A., EVERETT, C., KRONENBERG, M., ZAJONC, D.M., BENDELAC, A., SAVAGE, P.B., and TEYTON, L., 2014. The identification of the endogenous ligands of natural killer T cells reveals the presence of mammalian α-linked glycosylceramides. *Immunity*. 41 (4), pp. 543–554.
KAISER, L., FRITZ, R.S., and STRAUS, S.E., 2001. Symptom pathogenesis during acute influenza: Interleukin-6 and Other cytokine responses. *Journal of medical ….*
KARRER, U., ALTHAGE, A., and ODERMATT, B., 1997. On the key role of secondary lymphoid organs in antiviral immune responses studied in

alymphoplastic (aly/aly) and spleenless (Hox11−/−) mutant mice. *The Journal of …*.
KASTENMÜLLER, W., BRANDES, M., WANG, Z., HERZ, J., EGEN, J.G., and GERMAIN, R.N., 2013. Peripheral prepositioning and local CXCL9 chemokine-mediated guidance orchestrate rapid memory CD8+ T cell responses in the lymph node. *Immunity*. 38 (3), pp. 502–513.
KASTENMÜLLER, W., TORABI-PARIZI, P., SUBRAMANIAN, N., LÄMMERMANN, T., and GERMAIN, R.N., 2012. A spatially-organized multicellular innate immune response in lymph nodes limits systemic pathogen spread. *Cell*. 150 (6), pp. 1235–1248.
KAWAI, T. and AKIRA, S., 2011. Toll-like receptors and their crosstalk with other innate receptors in infection and immunity. *Immunity*. 34 (5), pp. 637–650.
KAWANO, T., CUI, J., KOEZUKA, Y., TOURA, I., KANEKO, Y., MOTOKI, K., UENO, H., NAKAGAWA, R., SATO, H., KONDO, E., KOSEKI, H., and TANIGUCHI, M., 1997. CD1d-restricted and TCR-mediated activation of valpha14 NKT cells by glycosylceramides. *Science (New York, NY)*. 278 (5343), pp. 1626–1629.
KIM, J., KUNDU, M., VIOLLET, B., and GUAN, K.-L., 2011. AMPK and mTOR regulate autophagy through direct phosphorylation of Ulk1. *Nature Cell Biology*. 13 (2), pp. 132–141.
KING, I.L., FORTIER, A., TIGHE, M., DIBBLE, J., WATTS, G.F.M., VEERAPEN, N., HABERMAN, A.M., BESRA, G.S., MOHRS, M., BRENNER, M.B., and LEADBETTER, E.A., 2012. Invariant natural killer T cells direct B cell responses to cognate lipid antigen in an IL-21-dependent manner. *Nature immunology*. 13 (1), pp. 44–50.
KINJO, Y., ILLARIONOV, P., VELA, J.L., PEI, B., GIRARDI, E., LI, X., LI, Y., IMAMURA, M., KANEKO, Y., OKAWARA, A., MIYAZAKI, Y., GÓMEZ-VELASCO, A., ROGERS, P., DAHESH, S., UCHIYAMA, S., KHURANA, A., KAWAHARA, K., YESILKAYA, H., ANDREW, P.W., WONG, C.-H., KAWAKAMI, K., NIZET, V., BESRA, G.S., TSUJI, M., ZAJONC, D.M., and KRONENBERG, M., 2011. Invariant natural killer T cells recognize glycolipids from pathogenic Gram-positive bacteria. *Nature immunology*. 12 (10), pp. 966–974.
KINJO, Y., TUPIN, E., WU, D., FUJIO, M., GARCIA-NAVARRO, R., BENHNIA, M.R.-E.-I., ZAJONC, D.M., BEN-MENACHEM, G., AINGE, G.D., PAINTER, G.F., KHURANA, A., HOEBE, K., BEHAR, S.M., BEUTLER, B., WILSON, I.A., TSUJI, M., SELLATI, T.J., WONG, C.-H., and KRONENBERG, M., 2006. Natural killer T cells recognize diacylglycerol antigens from pathogenic bacteria. *Nature immunology*. 7 (9), pp. 978–986.
KINJO, Y., WU, D., KIM, G., XING, G.-W., POLES, M.A., HO, D.D., TSUJI, M., KAWAHARA, K., WONG, C.-H., and KRONENBERG, M., 2005. Recognition of bacterial glycosphingolipids by natural killer T cells. *Nature*. 434 (7032), pp. 520–525.
KISSENPFENNIG, A., HENRI, S., DUBOIS, B., LAPLACE-BUILHÉ, C., PERRIN, P., ROMANI, N., TRIPP, C.H., DOUILLARD, P., LESERMAN, L., KAISERLIAN, D., SAELAND, S., DAVOUST, J., and MALISSEN, B., 2005. Dynamics and function of Langerhans cells in vivo: dermal dendritic cells colonize lymph node areas distinct from slower migrating Langerhans cells. *Immunity*. 22 (5), pp. 643–654.
KITAMURA, D., ROES, J., KÜHN, R., and RAJEWSKY, K., 1991. A B cell-deficient

mouse by targeted disruption of the membrane exon of the immunoglobulin mu chain gene. *Nature*. 350 (6317), pp. 423–426.
KITAMURA, H., IWAKABE, K., YAHATA, T., NISHIMURA, S., OHTA, A., OHMI, Y., SATO, M., TAKEDA, K., OKUMURA, K., VAN KAER, L., KAWANO, T., TANIGUCHI, M., and NISHIMURA, T., 1999. The natural killer T (NKT) cell ligand alpha-galactosylceramide demonstrates its immunopotentiating effect by inducing interleukin (IL)-12 production by dendritic cells and IL-12 receptor expression on NKT cells. *The Journal of experimental medicine*. 189 (7), pp. 1121–1128.
KJER-NIELSEN, L., PATEL, O., CORBETT, A.J., LE NOURS, J., MEEHAN, B., LIU, L., BHATI, M., CHEN, Z., KOSTENKO, L., REANTRAGOON, R., WILLIAMSON, N.A., PURCELL, A.W., DUDEK, N.L., MCCONVILLE, M.J., O'HAIR, R.A.J., KHAIRALLAH, G.N., GODFREY, D.I., FAIRLIE, D.P., ROSSJOHN, J., and MCCLUSKEY, J., 2012. MR1 presents microbial vitamin B metabolites to MAIT cells. *Nature*.
KOCH, M., STRONGE, V.S., SHEPHERD, D., GADOLA, S.D., MATHEW, B., RITTER, G., FERSHT, A.R., BESRA, G.S., SCHMIDT, R.R., JONES, E.Y., and CERUNDOLO, V., 2005. The crystal structure of human CD1d with and without alpha-galactosylceramide. *Nature immunology*. 6 (8), pp. 819–826.
KONDO, M., WEISSMAN, I.L., and AKASHI, K., 1997. Identification of clonogenic common lymphoid progenitors in mouse bone marrow. *Cell*. 91 (5), pp. 661–672.
KONI, P.A., SACCA, R., LAWTON, P., BROWNING, J.L., RUDDLE, N.H., and FLAVELL, R.A., 1997. Distinct roles in lymphoid organogenesis for lymphotoxins alpha and beta revealed in lymphotoxin beta-deficient mice. *Immunity*. 6 (4), pp. 491–500.
KOVALOVSKY, D., UCHE, O.U., ELADAD, S., HOBBS, R.M., YI, W., ALONZO, E., CHUA, K., EIDSON, M., KIM, H.-J., IM, J.S., PANDOLFI, P.P., and SANT'ANGELO, D.B., 2008. The BTB-zinc finger transcriptional regulator PLZF controls the development of invariant natural killer T cell effector functions. *Nature immunology*. 9 (9), pp. 1055–1064.
KUGELBERG, E., 2014. Innate immunity: Making mice more human the TLR8 way. *Nature reviews Immunology*. 14 (1), p. 6.
KUIDA, K., LIPPKE, J.A., KU, G., HARDING, M.W., LIVINGSTON, D.J., SU, M.S., and FLAVELL, R.A., 1995. Altered cytokine export and apoptosis in mice deficient in interleukin-1 beta converting enzyme. *Science (New York, NY)*. 267 (5206), pp. 2000–2003.
KUMAR, H., KAWAI, T., and AKIRA, S., 2011. Pathogen Recognition by the Innate Immune System. *International Reviews of Immunology*. 30 (1), pp. 16–34.
KUMAR, V., SCANDELLA, E., DANUSER, R., ONDER, L., NITSCHKÉ, M., FUKUI, Y., HALIN, C., LUDEWIG, B., and STEIN, J.V., 2010. Global lymphoid tissue remodeling during a viral infection is orchestrated by a B cell-lymphotoxin-dependent pathway. *Blood*. 115 (23), pp. 4725–4733.
KUNDU, M., LINDSTEN, T., YANG, C.-Y., WU, J., ZHAO, F., ZHANG, J., SELAK, M.A., NEY, P.A., and THOMPSON, C.B., 2008. Ulk1 plays a critical role in the autophagic clearance of mitochondria and ribosomes during reticulocyte maturation. *Blood*. 112 (4), pp. 1493–1502.
KURIOKA, A., USSHER, J.E., COSGROVE, C., and CLOUGH, C., 2015. MAIT cells are licensed through granzyme exchange to kill bacterially sensitized targets. *Mucosal …*.

KUROSAKI, T., KOMETANI, K., and ISE, W., 2015. Memory B cells. *Nature reviews Immunology*. 15 (3), pp. 149–159.
KWON, D.S., GREGORIO, G., BITTON, N., HENDRICKSON, W.A., and LITTMAN, D.R., 2002. DC-SIGN-mediated internalization of HIV is required for trans-enhancement of T cell infection. *Immunity*. 16 (1), pp. 135–144.
LANIER, L.L., 2013. Shades of grey--the blurring view of innate and adaptive immunity. *Nature reviews Immunology*. 13 (2), pp. 73–74.
LANZAVECCHIA, A., 1985. Antigen-specific interaction between T and B cells. *Nature*. 314 (6011), pp. 537–539.
LÄMMERMANN, T. and SIXT, M., 2008. The microanatomy of T-cell responses. *Immunological reviews*. 221, pp. 26–43.
LEADBETTER, E.A., BRIGL, M., ILLARIONOV, P., COHEN, N., LUTERAN, M.C., PILLAI, S., BESRA, G.S., and BRENNER, M.B., 2008. NK T cells provide lipid antigen-specific cognate help for B cells. *Proceedings of the National Academy of Sciences of the United States of America*. 105 (24), pp. 8339–8344.
LEE, E.-J. and TOURNIER, C., 2011. The requirement of uncoordinated 51-like kinase 1 (ULK1) and ULK2 in the regulation of autophagy. *Autophagy*. 7 (7), pp. 689–695.
LEE, W.-Y., MORIARTY, T.J., WONG, C.H.Y., ZHOU, H., STRIETER, R.M., VAN ROOIJEN, N., CHACONAS, G., and KUBES, P., 2010. An intravascular immune response to Borrelia burgdorferi involves Kupffer cells and iNKT cells. *Nature immunology*. 11 (4), pp. 295–302.
LEVINE, B., MIZUSHIMA, N., and VIRGIN, H.W., 2011. Autophagy in immunity and inflammation. *Nature*. 469 (7330), pp. 323–335.
LIMON, J.J. and FRUMAN, D.A., 2012. Akt and mTOR in B cell activation and differentiation. *Frontiers in immunology*.
LIN, Y., WONG, K., and CALAME, K., 1997. Repression of c-myc transcription by Blimp-1, an inducer of terminal B cell differentiation. *Science (New York, NY)*. 276 (5312), pp. 596–599.
LINDQUIST, R.L., SHAKHAR, G., DUDZIAK, D., WARDEMANN, H., EISENREICH, T., DUSTIN, M.L., and NUSSENZWEIG, M.C., 2004. Visualizing dendritic cell networks in vivo. *Nature immunology*. 5 (12), pp. 1243–1250.
LIU, Y.J., MALISAN, F., DE BOUTEILLER, O., GURET, C., LEBECQUE, S., BANCHEREAU, J., MILLS, F.C., MAX, E.E., and MARTINEZ-VALDEZ, H., 1996. Within germinal centers, isotype switching of immunoglobulin genes occurs after the onset of somatic mutation. *Immunity*. 4 (3), pp. 241–250.
LODER, B.F., MUTSCHLER, B., RAY, R.J., PAIGE, C.J., SIDERAS, P., TORRES, R., LAMERS, M.C., and CARSETTI, R., 1999. B Cell Development in the Spleen Takes Place in Discrete Steps and Is Determined by the Quality of B Cell Receptor-Derived Signals. *Journal of Experimental Medicine*. 190 (1), pp. 75–90.
LÖFFERT, D., EHLICH, A., MÜLLER, W., and RAJEWSKY, K., 1996. Surrogate light chain expression is required to establish immunoglobulin heavy chain allelic exclusion during early B cell development. *Immunity*. 4 (2), pp. 133–144.
LU, T.T. and CYSTER, J.G., 2002. Integrin-mediated long-term B cell retention in the splenic marginal zone. *Science (New York, NY)*.
LUND, J.M., ALEXOPOULOU, L., SATO, A., KAROW, M., ADAMS, N.C., GALE, N.W., IWASAKI, A., and FLAVELL, R.A., 2004. Recognition of single-stranded RNA viruses by Toll-like receptor 7. *Proceedings of the National Academy of Sciences of the United States of America*. 101 (15), pp. 5598–5603.

LÜTHJE, K., KALLIES, A., SHIMOHAKAMADA, Y., BELZ, G.T., LIGHT, A., TARLINTON, D.M., and NUTT, S.L., 2012. The development and fate of follicular helper T cells defined by an IL-21 reporter mouse. *Nature immunology*. 13 (5), pp. 491–498.
LYNCH, L., MICHELET, X., ZHANG, S., BRENNAN, P.J., MOSEMAN, A., LESTER, C., BESRA, G., VOMHOF-DEKREY, E.E., TIGHE, M., KOAY, H.-F., GODFREY, D.I., LEADBETTER, E.A., SANT'ANGELO, D.B., ANDRIAN, VON, U., and BRENNER, M.B., 2015. Regulatory iNKT cells lack expression of the transcription factor PLZF and control the homeostasis of T(reg) cells and macrophages in adipose tissue. *Nature immunology*. 16 (1), pp. 85–95.
LYNCH, L., NOWAK, M., VARGHESE, B., CLARK, J., HOGAN, A.E., TOXAVIDIS, V., BALK, S.P., O'SHEA, D., O'FARRELLY, C., and EXLEY, M.A., 2012. Adipose tissue invariant NKT cells protect against diet-induced obesity and metabolic disorder through regulatory cytokine production. *Immunity*. 37 (3), pp. 574–587.
LYNCH, L., O'SHEA, D., WINTER, D.C., GEOGHEGAN, J., DOHERTY, D.G., and O'FARRELLY, C., 2009. Invariant NKT cells and CD1d(+) cells amass in human omentum and are depleted in patients with cancer and obesity. *European journal of immunology*. 39 (7), pp. 1893–1901.
MA, C.S., DEENICK, E.K., BATTEN, M., and TANGYE, S.G., 2012. The origins, function, and regulation of T follicular helper cells. *Journal of Experimental Medicine*. 209 (7), pp. 1241–1253.
MAARTENS, G., CELUM, C., and LEWIN, S.R., 2014. HIV infection: epidemiology, pathogenesis, treatment, and prevention. *Lancet (London, England)*. 384 (9939), pp. 258–271.
MACLENNAN, I. and TOELLNER, K.M., 2003. Extrafollicular antibody responses. *Immunological …*.
MARSHAK-ROTHSTEIN, A., 2006. Toll-like receptors in systemic autoimmune disease. *Nature reviews Immunology*. 6 (11), pp. 823–835.
MARSHAK-ROTHSTEIN, A. and RIFKIN, I.R., 2007. Immunologically active autoantigens: the role of toll-like receptors in the development of chronic inflammatory disease. *Annual review of immunology*. 25, pp. 419–441.
MATTNER, J., DEBORD, K.L., ISMAIL, N., GOFF, R.D., CANTU, C., ZHOU, D., SAINT-MEZARD, P., WANG, V., GAO, Y., YIN, N., HOEBE, K., SCHNEEWIND, O., WALKER, D., BEUTLER, B., TEYTON, L., SAVAGE, P.B., and BENDELAC, A., 2005. Exogenous and endogenous glycolipid antigens activate NKT cells during microbial infections. *Nature*. 434 (7032), pp. 525–529.
MCKEE, S.J., MATTAROLLO, S.R., and LEGGATT, G.R., 2014. Immunosuppressive roles of natural killer T (NKT) cells in the skin. *Journal of leukocyte biology*. 96 (1), pp. 49–54.
MCLEOD, I.X., JIA, W., and HE, Y.-W., 2012. The contribution of autophagy to lymphocyte survival and homeostasis. *Immunological reviews*. 249 (1), pp. 195–204.
MEBIUS, R.E., HENDRIKS, H.R., BREVÉ, J., and KRAAL, G., 1990. Macrophages and the activity of high endothelial venules. The effect of interferon-gamma. *European journal of immunology*. 20 (7), pp. 1615–1618.
MEBIUS, R.E., STREETER, P.R., BREVÉ, J., DUIJVESTIJN, A.M., and KRAAL, G., 1991. The influence of afferent lymphatic vessel interruption on vascular addressin expression. *The Journal of cell biology*. 115 (1), pp. 85–95.
MENDIRATTA, S.K., MARTIN, W.D., HONG, S., BOESTEANU, A., JOYCE, S.,

and VAN KAER, L., 1997. CD1d1 mutant mice are deficient in natural T cells that promptly produce IL-4. *Immunity*. 6 (4), pp. 469–477.
MIAO, E.A., LEAF, I.A., TREUTING, P.M., MAO, D.P., and DORS, M., 2010. Caspase-1-induced pyroptosis is an innate immune effector mechanism against intracellular bacteria. *Nature*.
MIRASTSCHIJSKI, U., HAAKSMA, C.J., TOMASEK, J.J., and AGREN, M.S., 2004. Matrix metalloproteinase inhibitor GM 6001 attenuates keratinocyte migration, contraction and myofibroblast formation in skin wounds. *Experimental cell research*. 299 (2), pp. 465–475.
MIYAKE, Y., ASANO, K., KAISE, H., UEMURA, M., NAKAYAMA, M., and TANAKA, M., 2007. Critical role of macrophages in the marginal zone in the suppression of immune responses to apoptotic cell-associated antigens. *The Journal of clinical investigation*. 117 (8), pp. 2268–2278.
MIZUSHIMA, N., 2007. Autophagy: process and function. *Genes & Development*. 21 (22), pp. 2861–2873.
MIZUSHIMA, N. and YOSHIMORI, T., 2007. How to interpret LC3 immunoblotting. *Autophagy*. 3 (6), pp. 542–545.
MIZUSHIMA, N., YAMAMOTO, A., MATSUI, M., YOSHIMORI, T., and OHSUMI, Y., 2004. In vivo analysis of autophagy in response to nutrient starvation using transgenic mice expressing a fluorescent autophagosome marker. *Molecular biology of the cell*. 15 (3), pp. 1101–1111.
MIZUSHIMA, N., YOSHIMORI, T., and LEVINE, B., 2010. Methods in Mammalian Autophagy Research. *Cell*. 140 (3), pp. 313–326.
MOON, J.J., CHU, H.H., PEPPER, M., MCSORLEY, S.J., JAMESON, S.C., KEDL, R.M., and JENKINS, M.K., 2007. Naive CD4(+) T cell frequency varies for different epitopes and predicts repertoire diversity and response magnitude. *Immunity*. 27 (2), pp. 203–213.
MOSEMAN, E.A., IANNACONE, M., BOSURGI, L., TONTI, E., CHEVRIER, N., TUMANOV, A., FU, Y.-X., HACOHEN, N., and ANDRIAN, VON, U.H., 2012. B cell maintenance of subcapsular sinus macrophages protects against a fatal viral infection independent of adaptive immunity. *Immunity*. 36 (3), pp. 415–426.
MUELLER, S.N., HOSIAWA-MEAGHER, K.A., KONIECZNY, B.T., SULLIVAN, B.M., BACHMANN, M.F., LOCKSLEY, R.M., AHMED, R., and MATLOUBIAN, M., 2007. Regulation of homeostatic chemokine expression and cell trafficking during immune responses. *Science (New York, NY)*. 317 (5838), pp. 670–674.
MURAMATSU, M., KINOSHITA, K., FAGARASAN, S., YAMADA, S., SHINKAI, Y., and HONJO, T., 2000. Class switch recombination and hypermutation require activation-induced cytidine deaminase (AID), a potential RNA editing enzyme. *Cell*. 102 (5), pp. 553–563.
MURPHY, M.A., SCHNALL, R.G., VENTER, D.J., BARNETT, L., BERTONCELLO, I., THIEN, C.B., LANGDON, W.Y., and BOWTELL, D.D., 1998. Tissue hyperplasia and enhanced T-cell signalling via ZAP-70 in c-Cbl-deficient mice. *Molecular and cellular biology*. 18 (8), pp. 4872–4882.
NAIK, S., BOULADOUX, N., LINEHAN, J.L., HAN, S.-J., HARRISON, O.J., WILHELM, C., CONLAN, S., HIMMELFARB, S., BYRD, A.L., DEMING, C., QUINONES, M., BRENCHLEY, J.M., KONG, H.H., TUSSIWAND, R., MURPHY, K.M., MERAD, M., SEGRE, J.A., and BELKAID, Y., 2015. Commensal-dendritic-cell interaction specifies a unique protective skin immune signature. *Nature*. 520 (7545), pp. 104–108.

NEMAZEE, D. and BUERKI, K., 1989. Clonal deletion of autoreactive B lymphocytes in bone marrow chimeras. *Proceedings of the National Academy of Sciences of the United States of America*. 86 (20), pp. 8039–8043.
NEYT, K. and LAMBRECHT, B.N., 2013. The role of lung dendritic cell subsets in immunity to respiratory viruses. *Immunological reviews*. 255 (1), pp. 57–67.
NIEUWENHUIS, E.E.S., MATSUMOTO, T., EXLEY, M., SCHLEIPMAN, R.A., GLICKMAN, J., BAILEY, D.T., CORAZZA, N., COLGAN, S.P., ONDERDONK, A.B., and BLUMBERG, R.S., 2002. CD1d-dependent macrophage-mediated clearance of Pseudomonas aeruginosa from lung. *Nature medicine*. 8 (6), pp. 588–593.
NOSSAL, G.J., ABBOT, A., MITCHELL, J., and LUMMUS, Z., 1968. Antigens in immunity. XV. Ultrastructural features of antigen capture in primary and secondary lymphoid follicles. *The Journal of experimental medicine*. 127 (2), pp. 277–290.
NUTT, S.L., HODGKIN, P.D., and TARLINTON, D.M., 2015. The generation of antibody-secreting plasma cells. *Nature Reviews …*.
O'BRIEN, T.F., GORENTLA, B.K., XIE, D., SRIVATSAN, S., MCLEOD, I.X., HE, Y.-W., and ZHONG, X.-P., 2011. Regulation of T-cell survival and mitochondrial homeostasis by TSC1. *European journal of immunology*. 41 (11), pp. 3361–3370.
ODERMATT, B., EPPLER, M., LEIST, T.P., HENGARTNER, H., and ZINKERNAGEL, R.M., 1991. Virus-triggered acquired immunodeficiency by cytotoxic T-cell-dependent destruction of antigen-presenting cells and lymph follicle structure. *Proceedings of the National Academy of Sciences of the United States of America*. 88 (18), pp. 8252–8256.
OHL, L., HENNING, G., KRAUTWALD, S., LIPP, M., HARDTKE, S., BERNHARDT, G., PABST, O., and FÖRSTER, R., 2003. Cooperating mechanisms of CXCR5 and CCR7 in development and organization of secondary lymphoid organs. *The Journal of experimental medicine*. 197 (9), pp. 1199–1204.
OHL, L., MOHAUPT, M., CZELOTH, N., HINTZEN, G., KIAFARD, Z., ZWIRNER, J., BLANKENSTEIN, T., HENNING, G., and FÖRSTER, R., 2004. CCR7 governs skin dendritic cell migration under inflammatory and steady-state conditions. *Immunity*. 21 (2), pp. 279–288.
OLSZAK, T., NEVES, J.F., DOWDS, C.M., BAKER, K., GLICKMAN, J., DAVIDSON, N.O., LIN, C.-S., JOBIN, C., BRAND, S., SOTLAR, K., WADA, K., KATAYAMA, K., NAKAJIMA, A., MIZUGUCHI, H., KAWASAKI, K., NAGATA, K., MÜLLER, W., SNAPPER, S.B., SCHREIBER, S., KASER, A., ZEISSIG, S., and BLUMBERG, R.S., 2014. Protective mucosal immunity mediated by epithelial CD1d and IL-10. *Nature*. 509 (7501), pp. 497–502.
PAGET, C., MALLEVAEY, T., SPEAK, A.O., TORRES, D., FONTAINE, J., SHEEHAN, K.C.F., CAPRON, M., RYFFEL, B., FAVEEUW, C., LEITE DE MORAES, M., PLATT, F., and TROTTEIN, F., 2007. Activation of invariant NKT cells by toll-like receptor 9-stimulated dendritic cells requires type I interferon and charged glycosphingolipids. *Immunity*. 27 (4), pp. 597–609.
PALUDAN, C., SCHMID, D., LANDTHALER, M., VOCKERODT, M., KUBE, D., TUSCHL, T., and MÜNZ, C., 2005. Endogenous MHC class II processing of a viral nuclear antigen after autophagy. *Science (New York, NY)*. 307 (5709), pp. 593–596.
PANG, I.K., ICHINOHE, T., and IWASAKI, A., 2013. IL-1R signaling in dendritic cells replaces pattern-recognition receptors in promoting $CD8^+$ T cell responses

to influenza A virus. *Nature immunology*. 14 (3), pp. 246–253.
PAPE, K.A., CATRON, D.M., ITANO, A.A., and JENKINS, M.K., 2007. The humoral immune response is initiated in lymph nodes by B cells that acquire soluble antigen directly in the follicles. *Immunity*. 26 (4), pp. 491–502.
PARK, C., ARTHOS, J., CICALA, C., and KEHRL, J.H., 2015. The HIV-1 envelope protein gp120 is captured and displayed for B cell recognition by SIGN-R1(+) lymph node macrophages. *eLife*. 4.
PASARE, C. and MEDZHITOV, R., 2005. Control of B-cell responses by Toll-like receptors. *Nature*. 438 (7066), pp. 364–368.
PEAR, W.S., TU, L.L., and STEIN, P.L., 2004. Lineage choices in the developing thymus: choosing the T and NKT pathways. *Current opinion in immunology*.
PENGO, N., SCOLARI, M., OLIVA, L., MILAN, E., MAINOLDI, F., RAIMONDI, A., FAGIOLI, C., MERLINI, A., MARIANI, E., PASQUALETTO, E., ORFANELLI, U., PONZONI, M., SITIA, R., CASOLA, S., and CENCI, S., 2013. Plasma cells require autophagy for sustainable immunoglobulin production. *Nature immunology*. 14 (3), pp. 298–305.
PEREZ-PADILLA, R., LA ROSA-ZAMBONI, DE, D., DE LEON, S.P., HERNANDEZ, M., QUIÑONES-FALCONI, F., BAUTISTA, E., RAMIREZ-VENEGAS, A., ROJAS-SERRANO, J., ORMSBY, C.E., CORRALES, A., HIGUERA, A., MONDRAGON, E., and CORDOVA-VILLALOBOS, J.A., 2009. Pneumonia and respiratory failure from swine-origin influenza A (H1N1) in Mexico. *The New England journal of medicine*. 361 (7), pp. 680–689.
PHAN, T.G., GREEN, J.A., GRAY, E.E., XU, Y., and CYSTER, J.G., 2009. Immune complex relay by subcapsular sinus macrophages and noncognate B cells drives antibody affinity maturation. *Nature immunology*. 10 (7), pp. 786–793.
PHAN, T.G., GRIGOROVA, I., OKADA, T., and CYSTER, J.G., 2007. Subcapsular encounter and complement-dependent transport of immune complexes by lymph node B cells. *Nature immunology*. 8 (9), pp. 992–1000.
PICA, N. and PALESE, P., 2013. Toward a universal influenza virus vaccine: prospects and challenges. *Annual review of medicine*. 64, pp. 189–202.
POLTORAK, A., HE, X., SMIRNOVA, I., LIU, M.Y., and VAN HUFFEL, C., 1998. Defective LPS signaling in C3H/HeJ and C57BL/10ScCr mice: mutations in Tlr4 gene. *Science (New York, NY)*.
PORUBSKY, S., SPEAK, A.O., LUCKOW, B., CERUNDOLO, V., PLATT, F.M., and GRÖNE, H.-J., 2007. Normal development and function of invariant natural killer T cells in mice with isoglobotrihexosylceramide (iGb3) deficiency. *Proceedings of the National Academy of Sciences of the United States of America*. 104 (14), pp. 5977–5982.
PUGA, I., COLS, M., BARRA, C.M., HE, B., CASSIS, L., GENTILE, M., COMERMA, L., CHORNY, A., SHAN, M., XU, W., MAGRI, G., KNOWLES, D.M., TAM, W., CHIU, A., BUSSEL, J.B., SERRANO, S., LORENTE, J.A., BELLOSILLO, B., LLORETA, J., JUANPERE, N., ALAMEDA, F., BARÓ, T., DE HEREDIA, C.D., TORÁN, N., CATALÀ, A., TORREBADELL, M., FORTUNY, C., CUSÍ, V., CARRERAS, C., DIAZ, G.A., BLANDER, J.M., FARBER, C.-M., SILVESTRI, G., CUNNINGHAM-RUNDLES, C., CALVILLO, M., DUFOUR, C., NOTARANGELO, L.D., LOUGARIS, V., PLEBANI, A., CASANOVA, J.-L., GANAL, S.C., DIEFENBACH, A., ARÓSTEGUI, J.I., JUAN, M., YAGÜE, J., MAHLAOUI, N., DONADIEU, J., CHEN, K., and CERUTTI, A., 2011. B cell–helper neutrophils stimulate the diversification and production of immunoglobulin in the marginal zone of the spleen. *Nature immunology*. 13 (2),

pp. 170–180.
QI, H., EGEN, J.G., HUANG, A.Y.C., and GERMAIN, R.N., 2006. Extrafollicular activation of lymph node B cells by antigen-bearing dendritic cells. *Science (New York, NY)*. 312 (5780), pp. 1672–1676.
RANDOLPH, G.J., ANGELI, V., and SWARTZ, M.A., 2005. Dendritic-cell trafficking to lymph nodes through lymphatic vessels. *Nature reviews Immunology*. 5 (8), pp. 617–628.
RANTAKARI, P., AUVINEN, K., JÄPPINEN, N., KAPRAALI, M., VALTONEN, J., KARIKOSKI, M., GERKE, H., IFTAKHAR-E-KHUDA, I., KEUSCHNIGG, J., UMEMOTO, E., TOHYA, K., MIYASAKA, M., ELIMA, K., JALKANEN, S., and SALMI, M., 2015. The endothelial protein PLVAP in lymphatics controls the entry of lymphocytes and antigens into lymph nodes. *Nature immunology*. 16 (4), pp. 386–396.
REIF, K., EKLAND, E.H., OHL, L., NAKANO, H., LIPP, M., FÖRSTER, R., and CYSTER, J.G., 2002. Balanced responsiveness to chemoattractants from adjacent zones determines B-cell position. *Nature*. 416 (6876), pp. 94–99.
RICKERT, R.C., ROES, J., and RAJEWSKY, K., 1997. B lymphocyte-specific, Cre-mediated mutagenesis in mice. *Nucleic acids research*. 25 (6), pp. 1317–1318.
ROOZENDAAL, R., MEMPEL, T.R., PITCHER, L.A., GONZALEZ, S.F., VERSCHOOR, A., MEBIUS, R.E., ANDRIAN, VON, U.H., and CARROLL, M.C., 2009. Conduits mediate transport of low-molecular-weight antigen to lymph node follicles. *Immunity*. 30 (2), pp. 264–276.
RUSSELL, R.C., TIAN, Y., YUAN, H., PARK, H.W., CHANG, Y.-Y., KIM, J., KIM, H., NEUFELD, T.P., DILLIN, A., and GUAN, K.-L., 2013. ULK1 induces autophagy by phosphorylating Beclin-1 and activating VPS34 lipid kinase. *Nature Cell Biology*. 15 (7), pp. 741–750.
SACKS, D.L., 2014. Vaccines against tropical parasitic diseases: a persisting answer to a persisting problem. *Nature immunology*. 15 (5), pp. 403–405.
SASINDRAN, S.J. and TORRELLES, J.B., 2011. Mycobacterium Tuberculosis Infection and Inflammation: what is Beneficial for the Host and for the Bacterium? *Frontiers in microbiology*. 2, p. 2.
SAVAGE, A.K., CONSTANTINIDES, M.G., HAN, J., PICARD, D., MARTIN, E., LI, B., LANTZ, O., and BENDELAC, A., 2008. The transcription factor PLZF directs the effector program of the NKT cell lineage. *Immunity*. 29 (3), pp. 391–403.
SCANDELLA, E., BOLINGER, B., LATTMANN, E., MILLER, S., FAVRE, S., LITTMAN, D.R., FINKE, D., LUTHER, S.A., JUNT, T., and LUDEWIG, B., 2008. Restoration of lymphoid organ integrity through the interaction of lymphoid tissue-inducer cells with stroma of the T cell zone. *Nature immunology*. 9 (6), pp. 667–675.
SCANLON, S.T., THOMAS, S.Y., FERREIRA, C.M., BAI, L., KRAUSZ, T., SAVAGE, P.B., and BENDELAC, A., 2011. Airborne lipid antigens mobilize resident intravascular NKT cells to induce allergic airway inflammation. *The Journal of experimental medicine*. 208 (10), pp. 2113–2124.
SCHATZ, D.G., OETTINGER, M.A., and BALTIMORE, D., 1989. The V(D)J recombination activating gene, RAG-1. *Cell*. 59 (6), pp. 1035–1048.
SCHMID, D., PYPAERT, M., and MÜNZ, C., 2007. Antigen-loading compartments for major histocompatibility complex class II molecules continuously receive input from autophagosomes. *Immunity*. 26 (1), pp. 79–92.
SCHUMANN, K., LÄMMERMANN, T., BRUCKNER, M., LEGLER, D.F., POLLEUX, J., SPATZ, J.P., SCHULER, G., FÖRSTER, R., LUTZ, M.B., SOROKIN, L., and

SIXT, M., 2010. Immobilized chemokine fields and soluble chemokine gradients cooperatively shape migration patterns of dendritic cells. *Immunity*. 32 (5), pp. 703–713.
SCHWICKERT, T.A., LINDQUIST, R.L., SHAKHAR, G., LIVSHITS, G., SKOKOS, D., KOSCO-VILBOIS, M.H., DUSTIN, M.L., and NUSSENZWEIG, M.C., 2007. In vivo imaging of germinal centres reveals a dynamic open structure. *Nature*. 446 (7131), pp. 83–87.
SEILER, M.P., MATHEW, R., LISZEWSKI, M.K., and SPOONER, C.J., 2012. Elevated and sustained expression of the transcription factors Egr1 and Egr2 controls NKT lineage differentiation in response to TCR signaling. *Nature*.
SEMMLING, V., LUKACS-KORNEK, V., THAISS, C.A., QUAST, T., HOCHHEISER, K., PANZER, U., ROSSJOHN, J., PERLMUTTER, P., CAO, J., GODFREY, D.I., SAVAGE, P.B., KNOLLE, P.A., KOLANUS, W., FÖRSTER, I., and KURTS, C., 2010. Alternative cross-priming through CCL17-CCR4-mediated attraction of CTLs toward NKT cell-licensed DCs. *Nature immunology*. 11 (4), pp. 313–320.
SHI, W., LIAO, Y., WILLIS, S.N., TAUBENHEIM, N., INOUYE, M., TARLINTON, D.M., SMYTH, G.K., HODGKIN, P.D., NUTT, S.L., and CORCORAN, L.M., 2015. Transcriptional profiling of mouse B cell terminal differentiation defines a signature for antibody-secreting plasma cells. *Nature immunology*. 16 (6), pp. 663–673.
SHINKAI, Y., RATHBUN, G., LAM, K.P., OLTZ, E.M., STEWART, V., MENDELSOHN, M., CHARRON, J., DATTA, M., YOUNG, F., and STALL, A.M., 1992. RAG-2-deficient mice lack mature lymphocytes owing to inability to initiate V(D)J rearrangement. *Cell*. 68 (5), pp. 855–867.
SHULTZ, L.D., BREHM, M.A., GARCIA-MARTINEZ, J.V., and GREINER, D.L., 2012. Humanized mice for immune system investigation: progress, promise and challenges. *Nature reviews Immunology*. 12 (11), pp. 786–798.
SHULTZ, L.D., LYONS, B.L., BURZENSKI, L.M., GOTT, B., CHEN, X., CHALEFF, S., KOTB, M., GILLIES, S.D., KING, M., MANGADA, J., GREINER, D.L., and HANDGRETINGER, R., 2005. Human lymphoid and myeloid cell development in NOD/LtSz-scid IL2R gamma null mice engrafted with mobilized human hemopoietic stem cells. *Journal of immunology (Baltimore, Md : 1950)*. 174 (10), pp. 6477–6489.
SIEGRIST, C.A., 2008. Vaccine immunology. *Vaccines Saunders*.
SIXT, M., KANAZAWA, N., SELG, M., SAMSON, T., ROOS, G., REINHARDT, D.P., PABST, R., LUTZ, M.B., and SOROKIN, L., 2005. The conduit system transports soluble antigens from the afferent lymph to resident dendritic cells in the T cell area of the lymph node. *Immunity*. 22 (1), pp. 19–29.
SONODA, K.-H. and STEIN-STREILEIN, J., 2002. CD1d on antigen-transporting APC and splenic marginal zone B cells promotes NKT cell-dependent tolerance. *European journal of immunology*. 32 (3), pp. 848–857.
STACKER, S.A., WILLIAMS, S.P., KARNEZIS, T., SHAYAN, R., FOX, S.B., and ACHEN, M.G., 2014. Lymphangiogenesis and lymphatic vessel remodelling in cancer. *Nature reviews. Cancer*. 14 (3), pp. 159–172.
SUNG, J.H., ZHANG, H., MOSEMAN, E.A., ALVAREZ, D., IANNACONE, M., HENRICKSON, S.E., LA TORRE, DE, J.C., GROOM, J.R., LUSTER, A.D., and ANDRIAN, VON, U.H., 2012. Chemokine guidance of central memory T cells is critical for antiviral recall responses in lymph nodes. *Cell*. 150 (6), pp. 1249–1263.

SUTTON, J.S. and WEISS, L., 1966. Transformation of monocytes in tissue culture into macrophages, epithelioid cells, and multinucleated giant cells an electron microscope study. *The Journal of cell biology*.

SZAKAL, A.K., HOLMES, K.L., and TEW, J.G., 1983. Transport of immune complexes from the subcapsular sinus to lymph node follicles on the surface of nonphagocytic cells, including cells with dendritic morphology. *Journal of immunology (Baltimore, Md : 1950)*. 131 (4), pp. 1714–1727.

TAKATA, M., HOMMA, Y., and KUROSAKI, T., 1995. Requirement of phospholipase C-gamma 2 activation in surface immunoglobulin M-induced B cell apoptosis. *The Journal of experimental medicine*. 182 (4), pp. 907–914.

THAUNAT, O., GRANJA, A.G., BARRAL, P., FILBY, A., MONTANER, B., COLLINSON, L., MARTINEZ-MARTIN, N., HARWOOD, N.E., BRUCKBAUER, A., and BATISTA, F.D., 2012. Asymmetric segregation of polarized antigen on B cell division shapes presentation capacity. *Science (New York, NY)*. 335 (6067), pp. 475–479.

THOMAS, P.G., DASH, P., ALDRIDGE, J.R., and ELLEBEDY, A.H., 2009. The Intracellular Sensor NLRP3 Mediates Key Innate and Healing Responses to Influenza A Virus via the Regulation of Caspase-1. *Immunity*.

TOOZE, S.A. and YOSHIMORI, T., 2010. The origin of the autophagosomal membrane. *Nature Cell Biology*. 12 (9), pp. 831–835.

TPW, J.G., PHIPPS, R.P., and MANDEL, T.E., 1980. The Maintenance and Regulation of the Humoral Immune Response: Persisting Antigen and the Role of Follicular Antigen-Binding Dendritic Cells as Accessory Cells. *Immunological reviews*.

ULVMAR, M.H., WERTH, K., BRAUN, A., KELAY, P., HUB, E., ELLER, K., CHAN, L., LUCAS, B., NOVITZKY-BASSO, I., NAKAMURA, K., RÜLICKE, T., NIBBS, R.J.B., WORBS, T., FÖRSTER, R., and ROT, A., 2014. The atypical chemokine receptor CCRL1 shapes functional CCL21 gradients in lymph nodes. *Nature immunology*. 15 (7), pp. 623–630.

VAN BLIJSWIJK, J., SCHRAML, B.U., and REIS E SOUSA, C., 2013. Advantages and limitations of mouse models to deplete dendritic cells. *European journal of immunology*. 43 (1), pp. 22–26.

VAN DE VEERDONK, F.L., NETEA, M.G., DINARELLO, C.A., and JOOSTEN, L.A.B., 2011. Inflammasome activation and IL-1β and IL-18 processing during infection. *Trends in Immunology*. 32 (3), pp. 110–116.

VAN ROOIJEN, N., SANDERS, A., and VAN DEN BERG, T.K., 1996. Apoptosis of macrophages induced by liposome-mediated intracellular delivery of clodronate and propamidine. *Journal of immunological methods*. 193 (1), pp. 93–99.

VANHAESEBROECK, B., LEEVERS, S.J., AHMADI, K., TIMMS, J., KATSO, R., DRISCOLL, P.C., WOSCHOLSKI, R., PARKER, P.J., and WATERFIELD, M.D., 2001. Synthesis and function of 3-phosphorylated inositol lipids. *Annual review of biochemistry*. 70, pp. 535–602.

VANTOUROUT, P. and HAYDAY, A., 2013. Six-of-the-best: unique contributions of γδ T cells to immunology. *Nature reviews Immunology*. 13 (2), pp. 88–100.

VICTORA, G.D. and NUSSENZWEIG, M.C., 2012. Germinal Centers. *Annual review of immunology*. 30 (1), pp. 429–457.

VICTORA, G.D., SCHWICKERT, T.A., FOOKSMAN, D.R., KAMPHORST, A.O., MEYER-HERMANN, M., DUSTIN, M.L., and NUSSENZWEIG, M.C., 2010. Germinal center dynamics revealed by multiphoton microscopy with a photoactivatable fluorescent reporter. *Cell*. 143 (4), pp. 592–605.

VIDARSSON, G., DEKKERS, G., and RISPENS, T., 2014. IgG subclasses and allotypes: from structure to effector functions. *Frontiers in immunology*.
WAFFARN, E.E. and BAUMGARTH, N., 2011. Protective B cell responses to flu--no fluke! *Journal of immunology (Baltimore, Md : 1950)*. 186 (7), pp. 3823–3829.
WALSH, S.R. and DOLIN, R., 2011. Vaccinia viruses: vaccines against smallpox and vectors against infectious diseases and tumors. *Expert review of vaccines*. 10 (8), pp. 1221–1240.
WARDEMANN, H., YURASOV, S., SCHAEFER, A., YOUNG, J.W., MEFFRE, E., and NUSSENZWEIG, M.C., 2003. Predominant autoantibody production by early human B cell precursors. *Science (New York, NY)*. 301 (5638), pp. 1374–1377.
WATANABE, K., ICHINOSE, S., HAYASHIZAKI, K., and TSUBATA, T., 2008. Induction of autophagy by B cell antigen receptor stimulation and its inhibition by costimulation. *Biochemical and biophysical research communications*. 374 (2), pp. 274–281.
WATARAI, H., SEKINE-KONDO, E., SHIGEURA, T., MOTOMURA, Y., YASUDA, T., SATOH, R., YOSHIDA, H., KUBO, M., KAWAMOTO, H., KOSEKI, H., and TANIGUCHI, M., 2012. Development and Function of Invariant Natural Killer T Cells Producing T H 2- and T H 17-Cytokines. *PLoS biology*. 10 (2), p. e1001255.
WEBER, M., TREANOR, B., DEPOIL, D., SHINOHARA, H., HARWOOD, N.E., HIKIDA, M., KUROSAKI, T., and BATISTA, F.D., 2008. Phospholipase C- 2 and Vav cooperate within signaling microclusters to propagate B cell spreading in response to membrane-bound antigen. *Journal of Experimental Medicine*. 205 (4), pp. 853–868.
WEI, D.G., CURRAN, S.A., SAVAGE, P.B., TEYTON, L., and BENDELAC, A., 2006. Mechanisms imposing the Vbeta bias of Valpha14 natural killer T cells and consequences for microbial glycolipid recognition. *The Journal of experimental medicine*. 203 (5), pp. 1197–1207.
WONG, C.H.Y., JENNE, C.N., LEE, W.-Y., LÉGER, C., and KUBES, P., 2011. Functional innervation of hepatic iNKT cells is immunosuppressive following stroke. *Science (New York, NY)*. 334 (6052), pp. 101–105.
WU, Y., WANG, C., SUN, H., LEROITH, D., and YAKAR, S., 2009. High-efficient FLPo deleter mice in C57BL/6J background. *PLoS ONE*. 4 (11), p. e8054.
WUCHERPFENNIG, K.W., GAGNON, E., CALL, M.J., HUSEBY, E.S., and CALL, M.E., 2010. Structural biology of the T-cell receptor: insights into receptor assembly, ligand recognition, and initiation of signaling. *Cold Spring Harbor perspectives in biology*. 2 (4), p. a005140.
WURSTER, A.L., RODGERS, V.L., WHITE, M.F., ROTHSTEIN, T.L., and GRUSBY, M.J., 2002. Interleukin-4-mediated protection of primary B cells from apoptosis through Stat6-dependent up-regulation of Bcl-xL. *The Journal of biological chemistry*. 277 (30), pp. 27169–27175.
WYKES, M., POMBO, A., JENKINS, C., and MACPHERSON, G.G., 1998. Dendritic cells interact directly with naive B lymphocytes to transfer antigen and initiate class switching in a primary T-dependent response. *Journal of immunology (Baltimore, Md : 1950)*. 161 (3), pp. 1313–1319.
YAMAMOTO, M., SATO, S., HEMMI, H., HOSHINO, K., KAISHO, T., SANJO, H., TAKEUCHI, O., SUGIYAMA, M., OKABE, M., TAKEDA, K., and AKIRA, S., 2003. Role of adaptor TRIF in the MyD88-independent toll-like receptor

signaling pathway. *Science (New York, NY)*. 301 (5633), pp. 640–643.
YAMAMOTO, M., YAGINUMA, K., TSUTSUI, H., SAGARA, J., GUAN, X., SEKI, E., YASUDA, K., YAMAMOTO, M., AKIRA, S., NAKANISHI, K., NODA, T., and TANIGUCHI, S., 2004. ASC is essential for LPS-induced activation of procaspase-1 independently of TLR-associated signal adaptor molecules. *Genes to cells : devoted to molecular & cellular mechanisms*. 9 (11), pp. 1055–1067.
YAMAZAKI, T., TAKEDA, K., GOTOH, K., TAKESHIMA, H., AKIRA, S., and KUROSAKI, T., 2002. Essential immunoregulatory role for BCAP in B cell development and function. *The Journal of experimental medicine*. 195 (5), pp. 535–545.
YEN, J.-H., KHAYRULLINA, T., and GANEA, D., 2008. PGE2-induced metalloproteinase-9 is essential for dendritic cell migration. *Blood*. 111 (1), pp. 260–270.
ZEPP, F., 2010. Principles of vaccine design—Lessons from nature. *Vaccine*.
ZHOU, D., MATTNER, J., CANTU, C., SCHRANTZ, N., YIN, N., GAO, Y., SAGIV, Y., HUDSPETH, K., WU, Y.-P., YAMASHITA, T., TENEBERG, S., WANG, D., PROIA, R.L., LEVERY, S.B., SAVAGE, P.B., TEYTON, L., and BENDELAC, A., 2004. Lysosomal glycosphingolipid recognition by NKT cells. *Science (New York, NY)*. 306 (5702), pp. 1786–1789.
ZIPFEL, P.F. and SKERKA, C., 2009. Complement regulators and inhibitory proteins. *Nature reviews Immunology*.
ZOTOS, D., COQUET, J.M., ZHANG, Y., LIGHT, A., D'COSTA, K., KALLIES, A., CORCORAN, L.M., GODFREY, D.I., TOELLNER, K.M., SMYTH, M.J., NUTT, S.L., and TARLINTON, D.M., 2010. IL-21 regulates germinal center B cell differentiation and proliferation through a B cell-intrinsic mechanism. *Journal of Experimental Medicine*. 207 (2), pp. 365–378.

Publications

The work presented in this thesis has contributed to the following publications:

GAYA, M., CASTELLO, A., MONTANER, B., ROGERS, N., REIS E SOUSA, C., BRUCKBAUER, A., and BATISTA, F.D., 2015. Host response. Inflammation-induced disruption of SCS macrophages impairs B cell responses to secondary infection. *Science (New York, NY)*. 347 (6222), pp. 667–672.

BURBAGE, M., KEPPLER, S.J., GASPARRINI, F., MARTINEZ-MARTIN, N., **GAYA, M**., FEEST, C., DOMART, M.-C., BRAKEBUSCH, C., COLLINSON, L., BRUCKBAUER, A., and BATISTA, F.D., 2015. Cdc42 is a key regulator of B cell differentiation and is required for antiviral humoral immunity. *Journal of Experimental Medicine*. 212 (1), pp. 53–72.

CASTELLO, A., **GAYA, M**., TUCHOLSKI, J., OELLERICH, T., LU, K.-H., TAFURI, A., PAWSON, T., WIENANDS, J., ENGELKE, M., and BATISTA, F.D., 2013. Nck-mediated recruitment of BCAP to the BCR regulates the PI(3)K-Akt pathway in B cells. *Nature immunology*. 14 (9), pp. 966–975.